ATS-5 TRILATERATION SUPPORT

FINAL REPORT

12 November 1973 - 31 December 1975

Prepared for

NASA-GODDARD SPACE FLIGHT CENTER
GREENBELT, MARYLAND

Prepared Under

NASA Contract NAS5-20034

Prepared by

Axel F. Brisken
Electronic Equipment Development Branch
Communications Laboratory
Corporate Research and Development
General Electric Company
Schenectady, New York 12301

SRD-76-004

FINAL REPORT

ATS-5 TRILATERATION SUPPORT

12 November 1973 - 31 December 1975

NASA Contract NAS5-20034

Prepared by

General Electric Company
Corporate Research and Development
Schenectady, New York

Project Scientist: Axel F. Brisken
Principal Investigator: Roy E. Anderson

for

NASA-Goddard Space Flight Center
Greenbelt, Maryland

Technical Monitor: Walter K. Allen
Contracting Officer: Robert L. Krenning

TABLE OF CONTENTS

SECTION		PAGE
1	INTRODUCTION AND SUMMARY	1-1
2	OBJECTIVES	2-1
3	PRINCIPLES OF OPERATION	3-1
	3.1 TONE-CODE RANGING TECHNIQUE	3-1
	3.2 SELF CALIBRATION TECHNIQUE	3-4
4	L-BAND TRANSPONDER NETWORK	4-1
	4.1 GEOGRAPHICAL DEPLOYMENT OF TRANSPONDERS	4-1
	4.2 GEOMETRICAL CONSIDERATIONS FOR RANGING PRECISION/ACCURACY	4-3
	4.3 SELECTION OF REMOTE TRANSPONDER SITES	4-6
	4.4 ATS-5 L-BAND SIGNAL CHARACTERISTICS	4-7
	4.5 INTERFERENCE OF ATS-6 BY ATS-5 RANGING	4-13
	4.6 L-BAND/VHF TRANSPONDER	4-14
	4.6.1 L-Band Receiver	4-18
	4.6.2 Responder Unit	4-25
	4.6.3 L-Band Exciter	4-31
	4.6.4 Buenos Aires L-band Power Amplifier	4-31
	4.6.5 Hawaii L-band Power Amplifier	4-35
	4.6.6 Self Calibration System	4-39
	4.6.7 L-Band Diplexer	4-41
	4.7 OBSERVATORY L-BAND SYSTEMS	4-45
	4.7.1 Observatory L-band Receiver	4-45
	4.7.2 Observatory L-band Transmitter	4-48
5	ANALYTICAL TECHNIQUES	5-1
	5.1 THE KEPLER ORBIT	5-1
	5.1.1 Orbit as a Conic Section	5-1
	5.1.2 Areal Velocity	5-3
	5.1.3 Periodicity	5-6
	5.1.4 Orbit Coordinate System	5-6
	5.2 DETERMINATION OF THE KEPLER ORBIT PARAMETERS	5-11
	5.2.1 Inclination Angle i	5-12

SECTION	Table of Contents - 2	PAGE
5	Analytical Techniques (cont'd)	
	5.2.2 Eccentricity ϵ	5-13
	5.2.3 Semimajor Axis a	5-13
	5.2.4 Time of Perifocal Passage T	5-15
	5.2.5 Longitude of Ascending Node Ω	5-15
	5.2.6 Argument of the Perifocus ω	5-16
	5.3 PERTURBATIONS TO THE KEPLER ORBIT	5-16
	5.4 IONOSPHERIC PROPAGATION DELAY	5-17
	5.5 TROPOSPHERIC PROPAGATION DELAY	5-19
6	CALIBRATION PROCEDURES AND RESULTS	6-1
	6-1 L-BAND TRANSPONDER CALIBRATION TECHNIQUES	6-1
	6.1.1 "Satellite Aided" Calibration Technique	6-1
	6.1.2 "In House" Calibration Technique	6-7
	6.1.3 Slant Range Calculation	6-9
	6.2 DIPLEXER TIME DELAY	6-10
	6.3 CALIBRATION OF THE BUENOS AIRES TRANSPONDER	6-11
	6.4 CALIBRATION OF THE HAWAIIAN TRANSPONDER	6-20
	6.5 MEASUREMENT OF RESPONDER OSCILLATOR FREQUENCY	6-29
	6.6 OPERATION CONFIGURATION OF BUENOS AIRES TRANSPONDER (USER #8)	6-33
	6.7 OPERATION CONFIGURATION OF HAWAIIAN TRANSPONDER (USER #11)	6-33
	6.8 INTERNAL TIME DELAY VARIATION VS. RADIO FREQUENCY	6-33
	6.9 ANALYSIS OF L-BAND RANGING PRECISION	6-38
7	OPERATION PROCEDURES	7-1
	7.1 RANGING PROCEDURES	7-1
	7.2 SATELLITE POSITION/POSITION PREDICTION CALCULATION	7-5
	7.3 ATS-5 SATELLITE RANGING SEQUENCES	7-7
8	VERIFICATION OF TRILATERATION POSITION MEASUREMENT AND PREDICTED POSITION ACCURACIES	8-1
	8.1 NETWORK OPERATION	8-1
	8.2 TRILATERATION POSITION ACCURACY	8-6

8	Verification of Trilateration Position Measurements and Predicted Position Accuracies (cont'd)	
	8.3 LONG TERM TRILATERATION ACCURACY	8-14
	8.4 ACCURACY OF PREDICTED SATELLITE POSITIONS	8-23
	8.5 ESTIMATED CONTRIBUTIONS OF FACTORS THAT LIMIT ACCURACY	8-29
	8.6 SLANT RANGE STANDARD DEVIATIONS	8-33
	8.7 SYNCHRONIZATION OF RANGING INTERROGATOR WITH PHASE OF SATELLITE "WINDOW"	8-38
9	CONCLUSIONS	9-1
	9.1 PROGRAM GOALS	9-1
	9.2 L-BAND TRILATERATION ACCURACY AND PRECISION	9-1
	9.3 L-BAND TRILATERATION CAPABILITIES	9-3
10	RECOMMENDATIONS	10-1
	10.1 NETWORK IMPROVEMENTS	10-1
	10.2 FURTHER EXPERIMENTS	10-1
11	PUBLICATIONS	11-1
12	REFERENCES	12-1

LIST OF FIGURES

NO.		PAGE
3.1	Tone-Code Ranging Waveform	3-2
3.2	Basic Tone-Code Transponder	3-3
4.1	Recording of the Beacon Signal Transmitted from the ATS-5 Satellite	4-8
4.2	L-Band/VHF Transponder Configuration	4-17
4.3	L-Band/VHF Transponder in Buenos Aires, Argentina (photograph)	4-19
4.4	L-Band and VHF Transponder Antennas in Buenos Aires, Argentina (photograph)	4-20
4.5	L-Band/VHF Transponder in Hawaii (photograph)	4-21
4.6	L-Band and VHF Transponder antennas in Hawaii (photograph)	4-22
4.7	L-Band Transponder Receiver	4-23
4.8	L-Band Transponder Receiver (photograph)	4-24
4.9	L-Band/VHF Responder (photograph)	4-27
4.10	Responder Functional Diagram	4-28
4.11	L-Band Exciter	4-32
4.12	L-Band Exciter (photograph)	4-33
4.13	L-Band Power Amplifier in Buenos Aires, Argentina	4-34
4-14	L-Band Power Amplifier in Buenos Aires, Argentina (photograph)	4-36
4.15	L-Band Power Amplifier in Hawaii	4-38
4.16	L-Band Transponder Self Calibration Loop	4-40
4.17	Observatory L-Band Self Calibration Loop	4-42
4.18	L-Band Diplexer	4-43
4.19	L-Band Diplexer (photograph)	4-44

NO.	List of Figures - 2	PAGE
4.20	General Electric Radio-Optical Observatory, Schenectady, NY (photograph)	4-46
4.21	Observatory L-Band Receiver	4-47
5.1	Definition of a Conic	5-2
5.2	Definition of Eccentric Anomaly	5-4
5.3	Orbit Coordinate System	5-8
5.4	Orbit Plane Related to Equatorial Coordinate System	5-9
5.5	Determination of Orbit Plane Orientation	5-14
6.1	"Satellite Aided" Calibration of Remote Transponder at Observatory	6-2
6.2	Sources of Remote Transponders Time Delays	6-5
6.3	Equipment Configuration for "In House" Calibration of Buenos Aires Transponder	6-8
6.4	Measurement of Diplexer Time Delay	6-12
6.5	Measurements of Buenos Aires Transponder Internal Time Delay	6-13
6.6	"Satellite Aided" Calibration - Automatic Transponder Equipment Configuration at Observatory	6-14
6.7	Measurements of Observatory Internal Time Delay	6-16
6.8	Variation of User #8 Integer Time Delay vs. Setting of Time Delay Thumbwheels	6-18
6.9	Self Calibration Correction of Buenos Aires Transponder Internal Time Delay, "In House" Test	6-19
6.10	Self Calibration Correction of Buenos Aires Transponder Internal Time Delay, Satellite Test	6-21
6.11	Measurements of Hawaiian Transponder Internal Time Delay	6-22
6.12	"In House" Calibration to Simultaneously Determine Remote Transponder Integer Time Delay and Observatory Internal Time Delay	6-24
6.13	Integer Time Delay vs. Responder 10 MHz Oscillator Frequency	6-25

NO.	List of Figures - 3	PAGE
6.14	Variation of User #11 Integer Time Delay vs. Setting of Time Delay Thumbwheels	6-27
6.15	Self Calibration Correction of Hawaiian Transponder Internal Time Delay, "Satellite Aided" Test	6-28
6.16	Equipment Configuration to Measure Frequency of Remote Transponder 10 MHz Oscillator	6-30
6.17	L-Band Transponder Configuration in Buenos Aires, Argentina: User #8	6-34
6.18	L-Band Transponder Configuration at the U.S. Coast Guard Communication Station near Waihiawa, Hawaii: User #11	6-36
6.19	Apparent Time Delay Change vs. Observatory Receiver Frequency Offset	6-39
6.20	Apparent Time Delay Variation vs. Transponder Receiver Frequency Offset	6-40
6.21	Ranging to Buenos Aires Transponder While at Observatory	6-44
6.22	Range Measurements to Hawaiian Transponder	6-45
6.23	Range Measurements to Buenos Aires Transponder	6-49
7.1	Equipment Configuration for L-Band Ranging	7-2
7.2	Tracing of Chart Recording Showing Ranging Interrogations and Responses	7-4
7.3	Format of Recorded Ranging Data	7-6
8.1	Computer Listing of Trilateration Position of ATS-5 Satellite	8-5
8.2	Differences Between the NASA and GE Positions of the ATS-5 Satellite	8-7
8.3	Variation in Observatory and Remote Transponder Time Delays Resulting from Timing Oscillator Drift	8-9
8.4	Comparison of General Electric Smoothed Satellite Positions for Ranging Period at 0830 GMT, Jan. 26, 1975	8-11
8.5	Comparison of General Electric Smoothed Satellite Positions for Ranging Period at 1230 GMT, Jan. 26, 1975	8-12

NO.	List of Figures - 4	PAGE
8.6	NASA Measured ATS-5-Rosman Ranges Less GE Computed Range	8-16
8.7	NASA Measured ATS-5-Mojave Ranges Less GE Computed Range	8-17
8.8	Comparison of NASA Satellite Ephemerides from Two Different Epoch Dates	8-19
8.9	Differences Between NASA and GE Positions of the ATS-5 Satellite, Dec. 1974 to Feb. 1975	8-21
8.10	Differences Between NASA and GE Positions of the ATS-5 Satellite as Function of Time Since Epoch Date, Dec. 1974 to Feb. 1975	8-22
8.11	Degradation of Predicted Satellite Position vs. Time of Day	8-24
8.12	Degradation of Predicted Satellite Position vs. Orientation of Vector Sum of Moon and Sun Gravitational Vectors	8-26
8.13	ATS-5 Position Prediction Table	8-28

LIST OF TABLES

NO.		PAGE
1.1	Satellite Position Accuracy and Precision	1-3
4.1	Location of General Electric L-Band Trilateration and NASA C-Band Range and Range Rate Ground Stations	4-2
4.2	Positions of Ground Station Antenna Phase Centers on the Modified Mercury Datum 1968	4-4
4.3	ATS-5 Position Error as a Function of Slant Range Error and Station Location Error	4-5
4.4(Pt. 1)	ATS-5 Trilateration Power Budgets, Uplink 1651 MHz	4-10
4.4(Pt. 2)	ATS-5 Trilateration Power Budgets	4-11
4.4(Pt. 3)	ATS-5 Trilateration Power Budgets, Downlink 1551 MHz	4-12
4.5(Pt. 1)	ATS-5/ATS-6 L-Band Interference Power Budget, Uplink	4-15
4.5(Pt. 2)	ATS-5/ATS-6 L-Band Interference Power Budget, Downlink	4-16
4.6	L-Band Transponder Receiver Characteristics	4-26
4.7	300-Watt CW L-Band Transmitter	4-37
5.1	Estimated Maximum Predicted Earth Center Distance Errors for Kepler Orbit	5-18
6.1	VHF Satellite Measurement of Responder 10 MHz Oscillator Frequency	6-32
6.2	Effective Transponder Delay, User #8, Buenos Aires	6-35
6.3	Effective Transponder Delay, User #11, Hawaii	6-37
6.4	Theoretical Ranging Resolution at L-Band Due to RF Noise	6-42
6.5	Single Data Point Precision of Two-Way Slant Ranges	6-47
6.6	Contributions to Two-Way Slant Range Standard Deviation, Hawaiian Transponder (User #11), November 26, 1974	6-48
8.1	Two Transponder Ranging Experiments	8-3
8.2	ATS-5 Trilateration Support	8-4

NO.	List of Tables - 2	PAGE
8.3	Disagreement Between Kepler Orbit and Second Order Polynomial Smoothed Ranging Data, Jan. 26-27, 1975	8-13
8.4	NASA Range Measurement Less Computed Range Assuming GE Trilateration Position, ATS-5, Jan. 26-27, 1975	8-15
8.5	Summary of Disagreements Between NASA and GE Positions of ATS-5	8-20
8.6	Observed Maximum Inaccuracies of Predicted Satellite Positions	8-27
8.7	Relative Inaccuracy of Satellite Position from L-Band Trileration	8-30
8.8	Bias Inaccuracy of Satellite Position from L-Band Trilateration	8-31
8.9	Range Measurement Standard Deviation with Respect to Kepler Orbit Model, Jan. 26-27, 1975	8-35
8.10	Range Measurement Standard Deviations with Respect to Kepler Orbit Model, Jan. 9, 1975	8-37
8.11	Responses/No Responses to Ranging Interrogations, Jan. 26-27, 1975	8-39

GLOSSARY OF SYMBOLS

SYMBOL	NAME	SECTION	DESCRIPTION
a	Semimajor Axis	5.1.1	Semimajor axis of ellipse describing Kepler orbit of satellite.
a_e	Equatorial Earth Radius	4.1	-
$A(\theta)$ $A(t)$	Area	5.1.2	Area of sector of ellipse swept out in time t corresponding to values of true anomaly from 0 to θ.
b	Semiminor Axis	5.1.2	Semiminor axis of ellipse.
c	Speed of light	6.5	-
c_1, c_3	Linear Coefficients	5.2	Coefficients relating two satellite position vectors as a linear combination of a third.
C	Constant	5.1.1	Constant of proportionality.
C/N_o	Carrier-to-Noise Ratio	6.9	Carrier-to-Noise density in IF of FM receivers for demodulating ranging tones.
D_A	Propagation Delay	6.1.1	Total one-way atmospheric propagation time delay (ionospheric and tropospheric) between satellite and Observatory.
D'_A	Propagation Delay	6.1.3	Total one-way atmospheric propagation time delay (ionospheric and tropospheric) between satellite and remote transponder.
D_o	Time Delay	6.1.1	Effective Observatory internal time delay.
D'_o	Time Delay	6.1.3	Value of time delay D_o less geometry factor δ_G.
D_R	Time Delay	6.1.1	Total transponder internal time delay.
f	Earth Flattening Factor	4.1	Flattening factor for ellipsoidal model of earth. $f = (a_e - a_p)/a_e$ where a_p is polar radius of earth.

SYMBOL	NAME	SECTION	DESCRIPTION
f_o	Tone Frequency	6.5	Doppler shifted 2.4414 kHz audio frequency tone from remote VHF transponder, relayed through satellite, and detected by Observatory.
f_s	Tone Frequency	6.5	Doppler shifted 2.4414 kHz audio frequency tone generated by remote VHF transponder.
f'_s	Tone Frequency	6.5	2.4414 kHz audio frequency tone as seen by satellite.
GM	Gravitation Constant	5.1.3	Product of universal gravitational constant and mass of earth.
i	Inclination	5.1.4	Inclination of Kepler orbit plane with respect to equatorial plane.
$\hat{i},\hat{j},\hat{k}$	Unit Vectors	5.2	Unit vectors of right-handed coordinate system defining north ($\hat{k}$) and the equatorial plane ($\hat{i},\hat{j}$). $\hat{i}$ is parallel to the Greenwich Meridian.
k	Constant	6.1.1	Constant of proportionality.
n	Digital Plane	4.6.2	Response of remote transponder self calibration phase measurement.
$\hat{N}$	Unit Vector	5.2.6	Unit vector along the line of nodes.
p	Semilatus Rectum	5.1.1	Semilatus rectum of conic section (see Figure 5.1).
$\hat{P}$	Unit Vector	5.2.2	Unit vector in direction of perifocus.
P,P',P'',P'''	Position Vectors	5.1.4	Position vector of satellite relative to respective coordinate system.
P_i	Thumbwheel Setting	6.1.1	Setting of Observatory thumbwheel i, where i = 1,2,3, for adjustment of S_T.
q	Perifocal Distance	5.1.1	Distance between focus and nearest apside of ellipse.

SYMBOL	NAME	SECTION	DESCRIPTION
$\hat{Q}$	Unit Vector	5.2.2	Unit vector perpendicular to $\hat{P}$ and $\hat{W}$ (see Figure 5.3).
Q_i	Thumbwheel Setting	6.1.1	Setting of remote transponder thumbweel i, where i = 1,2,3, for adjustment of S_R.
r	Radial Distance	5.1.1	Radius from focal point to surface of ellipse.
r_i	Radial Distance	5.2	Earth center distance of satellite at position $\vec{r}_i$.
$\vec{r}_i$	Position Vector	5.2	Satellite position at point i.
R	Slant Range	6.1.1	Observatory-satellite slant range.
R_T	Slant Range	6.1.1	Remote transponder-satellite slant range.
S	Auxiliary Constant	5.2.2	Magnitude of cross product of two radial vectors from center of earth to satellite.
S_R	Time Delay	6.1.1	Adjustable portion of remote transponder internal time delay.
S_T	Adjustable Time Delay	6.1.1	Adjustable time delay in starting time interval counter which measures Observatory-satellite-transponder-satellite-Observatory ranging time; contributes to D_o.
t	Event Time	5.1.2	-
T	Tone Duration	6.9	Duration of 256 cycles of ranging tone.
T	Epoch Time	5.1.4	Time of perifocal passage.
T_o	Ranging Time	6.1.1	Observatory-satellite-Observatory ranging time.
T_R	Ranging Time	6.1.1	Observatory-satellite-transponder-satellite-Observatory ranging time.
T'_R	Ranging Time	6.1.1	Observatory-transponder-Observatory ranging time for "in house" calibrations.

SYMBOL	NAME	SECTION	DESCRIPTION
v_o	Velocity	6.5	Velocity of satellite away from Observatory.
v_r	Velocity	6.5	Velocity of satellite away from remote transponder.
$\hat{W}$	Unit Vector	5.2.1	Unit vector perpendicular to the orbit plane.
W_x, W_y, W_z	Components of $\hat{W}$	5.2.5, 5.2.1	Components of unit vector $\hat{W}$ in rectangular Cartesian coordinate system.
$x,y,z;$ $x''',y''',z''';$ $X,Y,Z;$ x_{oi}, y_{oi}	Coordinates	5.1, 5.2, 4.2	Rectangular Cartesian coordinate systems.
α	Auxialiary Angle	5.1.4	Angle relating longitude of ascending node and epoch time to event time.
β	Auxialiary Angle	5.1.4	Angle relating argument of perifocus and true anomaly.
δ_A	Time Delay	6.1.1	Total analog circuits time delay of remote transponder.
δ_C	Time Delay	6.1.1	Effective cable delay in remote transponder.
δ_{CR}	Time Delay	6.1.1	Time delay of RF signal from diplexer to receive cable self calibration reactive signal sampler; contributes to δ_C.
δ_{CT}	Time Delay	6.1.1	Time delay of RF signal from transmit cable reactive signal sampler to diplexer; contributes to δ_C.
δ_{DR}	Time Delay	6.1.1	Time delay of RF signal through receive leg of L-band diplexer; contributes to δ_C.
δ_{DT}	Time Delay	6.1.1	Time delay of RF signal through transmit leg of L-band diplexer; contributes to δ_C.

SYMBOL	NAME	SECTION	DESCRIPTION
δ_G	Geometrical Effect	6.1.1	Difference in transponder-satellite and Observatory-satellite slant range during "satellite aided" calibrations; contributes to D_o.
δ_i	Geocentric Latitude	5.2	Geocentric latitude of satellite position $\vec{r}_i$.
δ_I	Time Delay	6.1.1	Integer time delay of remote transponder, an integer multiple of 102.4 μsec audio frequency tone periods; contributes to δ_A.
δ_L	Time Delay	6.1.1	Fixed portion of remote transponder internal time delay.
δ_M	Time Delay	6.1.2	RF signal time delay through cables for "in house" calibrations.
δ_o	Time Delay	6.1.1	Observatory interrogator-RF-correlator internal time delay, as measured by the Observatory self calibration circuit; contributes to D_o.
δ'_o	Time Delay	6.1.2	Observatory interrogator-correlator internal time delay as measured by the Observatory self calibration circuit, for "in house" calibrations.
δ_P	Time Delay	6.1.1	Phase error time delay of remote transponder, as measured by the transponder self calibration circuits; contributes to δ_A.
δ_R	Time Delay	6.1.1	Effective remote transponder internal time delay.
δ_s	Time Delay	6.1.1	Internal time delay of ATS-5 satellite in repeating a NBFM L-L signal.
δ_{SC}	Phase Measurement	6.1.1	Response of remote transponder self calibration circuit; contributes to δ_P.

SYMBOL	NAME	SECTION	DESCRIPTION
δ_T	Time Delay	6.1.1	Constant time delay in starting time interval counter which measures Observatory-satellite-transponder-satellite-Observatory ranging time; contributes to D_o.
δ'_T	Time Delay	6.1.2	Constant time delay in starting time interval counter which measures Observatory-transponder-Observatory ranging time for "in house" calibrations.
δ_W	Time Delay	6.1.1	Time delay of RF signal from diplexer to surface of 10-foot remote transponder parabolic antenna; contributes to δ_C.
ΔF	Frequency Deviation	6.9	Peak frequency deviation of RF carrier by ranging tones.
ϵ	Eccentricity	5.1.1	Eccentricity of ellipse describing Kepler orbit of satellite.
η	Rotational Speed of Earth	5.1.4	-
θ	True anomaly	5.1.1	Radial distance of point on ellipse from semimajor axis, where angle is measured around focal point of ellipse.
λ_i	Longitude	5.2	Longitude of satellite position $\vec{r}_i$.
σ_{CR}	Standard Deviation	6.9	Contribution to range measurement standard deviation due to round-off of signal time-of-arrival in correlators.
σ_{OS}	Standard Deviation	6.9	Two-way Observatory-satellite range measurement standard deviation.
σ_{RF}	Standard Deviation	6.9	Lower limit on range measurement standard deviation for a frequency modulated carrier.
σ_{TR}	Standard Deviation	6.9	Contribution to range measurement standard deviation due to roundoff in recording of time of ranging interrogation.

SYMBOL	NAME	SECTION	DESCRIPTION
σ_{TS}	Standard Deviation	6.9	Two-way remote transponder-satellite range measurement standard deviation.
τ	Period	5.1.2	Period of satellite in orbit.
Φ	Eccentric Anomaly	5.1.2	Radial distance from semimajor axis along sector of circle of radius a concentric with center of ellipse.
ω	Argument of Perifocus	5.1.4	Angle between the line of nodes and the perifocal direction.
Ω	Longitude of Ascending Node	5.1.4	Angle between the principle direction (x-axis) and the line of nodes (intersection of orbital and equatorial planes).

ACKNOWLEDGMENTS

The author wishes to acknowledge the support and cooperation of the National Aeronautics and Space Administration in making possible the experiments described in this report. The personnel of the Communications and Navigation Division at NASA-Goddard Space Flight Center were especially helpful in program guidance and coordination. NASA's ATS Operations and Control Center personnel, whose assistance and cooperation are extremely valued, provided experimental time on the ATS-1, ATS-3, and ATS-5 satellites. Mr. Edward Doll of the Operations Support Computing Division at NASA-GSFC computed NASA's position of the ATS-5 satellite to provide a standard of comparison.

The Space Communications Group of the General Electric Corporate Research and Development Center expresses its appreciation to the domestic and overseas organizations who graciously acted as hosts for the remote transponders in the General Electric L-band trilateration network. The host organizations housed and activated the transponders so that ranging data could be collected. These organizations are:

United States Coast Guard
U.S.C.G. Communications Station
Waihiawa, Oahu, Hawaii

Fuerza Aerea Argentina (Argentine Air Force)
Comando Regiones Aereas
Dto. Comunicaciones
Buenos Aires, Argentina

Lastly, the author wishes to acknowledge colleagues Roy E. Anderson for program conception and guidance, Richard L. Frey for assembly and testing of RF components and network operation, and James R. Lewis for assembly and testing of logic circuits, computer software, and network operation.

SECTION 1

INTRODUCTION AND SUMMARY

The successful implementation of future maritime and aeronautical satellite surveillance ranging and position fixing operations depends on the systems' ability to determine the positions of reference satellites efficiently and accurately. In view of this real-time satellite position fixing requirement, the National Aeronautics and Space Administration sponsored the development of the General Electric L-band trilateration network. The ATS-6/ATS-5 Position Location and Communication Experiment (PLACE) of NASA and MARAD utilized short term ATS-5 position predictions, based on satellite positions determined while the experiment was in progress. NASA separately provided the position of the ATS-6 satellite.

The objective of the present contract was the development of an L-band trilateration network capable of locating the ATS-5 satellite, determining the satellite's orbital elements, and predicting satellite positions for the next two hours. Predicted positions were sent to the NASA Rosman and MARAD Kings Point ground stations for position location experiments involving the ATS-5 and ATS-6 satellites.

The Applications Technology Satellites of NASA have been used by General Electric since 1968 to test the concept of position location by range measurements from pairs of satellites, to measure the factors that affect position fix accuracy including the propagation delays in the ionosphere, and to test the reliability of voice and digital communications between ground terminals and mobile craft. The work during the first two phases[1] of NASA contract NAS5-11634 was restricted to the use of the VHF transponders on ATS-1 and ATS-3.

Work at L-band using the ATS-5 satellite began with Phase 3[2] of NASA contract NAS5-11634. In 1971 an automatic tone-code ranging transponder was designed, constructed, and used to compare ranging measurements and communications reliability at VHF and L-band, and to measure the performance of the tone-code technique at L-band. A contribution to practical implementation of L-band was made by the development of a solid-state RF power amplifier and receiver. The transponder is equipped for voice communications through the VHF satellite. Voice transmissions, like the tone-code signals, employ narrow band frequency modulation.

Results of the ranging experiments confirmed that ranging resolutions measured in hundreds of feet at VHF and tens of feet at L-band may be achieved within the radio frequency bandwidths used for communications with simple, inexpensive, automatic equipment. The ranging signals can be compatible with communications and the range measurements can be accomplished in a time that is negligibly short compared to the signal durations used for communications.

Experiments conducted by the General Electric Company and Exxon Corporation from mid-1973 to early 1974[3] with the tanker ESSO BAHAMAS demon-

strated near real-time position fixing of NASA's ATS-1 and ATS-3 satellites via a VHF network with remote transponders in Europe, Iceland, North and South America, and Australia. These computed satellite positions were then used immediately to locate the ship.

The L-band/VHF transponder developed under NASA contract NAS5-11634 was installed at a facility of the U.S. Coast Guard near Honolulu, Hawaii. A similar L-band transponder was fabricated and installed at the site of an existing VHF transponder in Buenos Aires, Argentina. The Radio-Optical Observatory of the General Electric Company near Schenectady, New York acts as the master ground station for the L-band trilateration network. The Observatory's facility was upgraded by the addition of an L-band exciter and power amplifier. The L-band transponder network employs the tone-code ranging technique; 9.7656 kHz audio frequency tones frequency modulate the carriers in a 60 kHz RF bandwidth. Correlators in the remote transponders and the Observatory match the phase of the locally generated tone with that received from the satellite. Phase matching is accomplished during 256 tone cycles, thus requiring less than 30 msec for phase matching and correlation.

Self calibration circuits added to the remote transponders and the Observatory provide a measure of the internal time delays on every interrogation. In the remote transponders, reactive signal samplers remove a small fraction of the transmitted signal at the outputs of the L-band power amplifiers. Local oscillators and mixers translate this sampled signal through the same frequency as does the ATS-5 satellite. Similar reactive signal samplers inject the translated signal into the receive line. The transmitted signal is demodulated by the receiver and the phase of the tone at the responder input is compared with the phase at the output. A digital representation of the phase difference is loaded into the data stream following the transponder address code in the tone-code-data response. At the Observatory, the phase differences pass directly to a computer along with the outputs of the time interval counters which measure ranging times. A dipole antenna, a mixer, and a local oscillator at the surface of the 30-foot dish close the self calibration loop at the Observatory. A separate time interval counter measures the total Observatory internal time delay.

The primary method by which the accuracy of the L-band trilateration network was verified is a comparison with NASA's C-band range and range rate measurements to ATS-5 from the NASA Rosman and Mojave tracking stations. During a 24-hour test in which both NASA's C-band range and range rate tracking and General Electric's L-band trilateration were exercised simultaneously, the General Electric positions of ATS-5 showed excellent agreement with the NASA positions, as documented in Table 1.1. The accuracy of the trilateration positions was further verified by computing slant ranges from the ATS-5 satellite to the NASA Rosman and Mojave ground stations and comparing them with the NASA measured slant ranges. The GE computed and NASA measured slant ranges disagreed by 10.0 ± 5.7 meters to the Rosman site and 12.4 ± 12.0 to the Mojave site.

In the period from Dec. 1974 to Feb. 1975, General Electric determined positions of ATS-5 on 17 separate days. A comparison of all General Electric

TABLE 1.1

SATELLITE POSITION ACCURACY

AND PRECISION

	LONGITUDE (degrees)	LATITUDE (degrees)	EARTH CENTER DISTANCE (meters)
Simultaneous NASA/GE tracking disagreement (over 24 hours)	0.00014 ± 0.00012	0.00003 ± 0.00023	18 ± 19
Mean NASA/GE disagreement over three month period	0.00024 ± 0.00033	0.00007 ± 0.00025	4 ± 24
Estimated bias uncertainty	0.00006	0.00011	7
Estimated relative uncertainty	0.00030	0.00032	27
Observed position prediction accuracy after one hour	0.0007	0.0003	180
Limiting accuracy due to range measurement precision (10-minute period)	0.00002	0.00002	1

ATS-5 positions with the NASA predictions generated from bi-weekly range and range rate measurements shows similarly excellent agreement within the bounds of the gradual degradation of the NASA predictions as a function of time since epoch date.

All factors that affect accuracy have been studied and divided into two catagories. Bias errors reflect constant unknowns such as the absolute locations of the trilateration ground stations and the internal time delay of the ATS-5 satellite. Errors due to station location have been minimized by referring all the General Electric trilateration and NASA range and range rate ground stations to a common geocentric coordinate system; the major remaining location error is position accuracy on a local scale. Relative errors encompass diurnal variations in the internal time delays of the remote transponders and the atmospheric propagation time delay and random variations due to modeling in the software algorithms. Table 1.1 also lists the bias and relative position uncertainties.

In support of the two-satellite position fixing experiments of NASA and MARAD, three 10-minute ranging periods separated by one hour defined the orbit of the satellite, from whence position predictions followed for the next two hours. Repeated ranging to the ATS-5 satellite resulted in continued deliverance of satellite position predictions. Observed predicted position uncertainties one hour after the last satellite ranging period are shown in Table 1.1.

Over the period from Dec. 1974 to Feb. 1975, two-way range measurement precisions on the Observatory-ATS-5 link of 0.08 μsec were routinely achieved; for the Observatory-ATS-5-remote transponder link, 0.15 μsec. The corresponding one-way slant range precisions are 12 and 23 meters, respectively, which reduce to mean slant range precisions of one and two meters for 10-minute ranging periods. Range measurement precision does not significantly affect satellite position accuracy.

The ATS-5 Trilateration Support program has resulted in the development of a unique network for accurately and precisely determining satellite positions utilizing inexpensive, remote, automatic transponders. The techniques demonstrated during these experiments have broad applications in position location of satellites, aeronautical or maritime position surveillance, and search and rescue operations. The presently demonstrated accuracy of approximately $\pm$ 0.0002 degrees in latitude and longitude and $\pm$ 20 meters in earth center distance will contribute less than $\pm$ 40 meters error to a remote vehicle line-of-position, 45 degrees from the subsatellite point. Slight improvements to the L-band trilateration network are estimated to decrease this line-of-position error by a factor of four.

SECTION 2

OBJECTIVES

The successful implementation of future maritime and aeronautical satellite ranging and position fixing operations will depend on the systems' ability to efficiently and accurately determine the positions of the reference satellites. In view of this real-time satellite position fixing requirement, the National Aeronautics and Space Administration sponsored the development of the General Electric L-band satellite trilateration network. The L-band trilateration network would support the ATS-6/ATS-5 Position Location and Aircraft Communication Experiments (PLACE) of NASA and MARAD by providing short term position predictions of the ATS-5 satellite, based on ground station-satellite slant range measurements conducted during PLACE operations. NASA would separately provide the positions of the ATS-6 satellite.

The specific objective of this program to provide a trilateration network capable of locating the ATS-5 satellite included the following tasks:

1. Investigate and report on:

   (a) A system of predicting satellite positions using measurements made at short intervals spaced an hour apart and predicting for the next hour.

   (b) A method of verifying prediction capability (precision and accuracy).

   (c) The use of 6-foot diameter versus 10-foot diameter antennas at unmanned remote sites considering gain, beamwidth and pointing errors.

   (d) The recommendation of sites for remote terminals considering available existing equipment, accessibility for maintenance, and costs.

   (e) The hardware design of the trilateration system with particular emphasis on the remote terminals.

   (f) The design of computer software required to determine near real-time satellite positions in latitude, longitude, and earth center distance and to predict satellite position.

   (g) A data interface for transmission of predicted satellite positions via commercial communication channels to the NASA Rosman ground station and the MARAD Kings Point ground station.

2. Install at a remote site the L-band transponder developed under NASA contract NAS5-11634 and provide on a no-cost loan basis a 300-watt L-band power amplifier.

3. Design and manufacture one L-band transponder and install it at a second remote site. This transponder shall be similar to the L-band transponder developed under NASA contract NAS5-11634 and shall contain the following components:

   (a) An L-band receiver with a balanced limiter discriminator specially designed to reduced variations in the received signal time delay as a function of signal amplitude.

   (b) A tone-code responder with a built-in setable time delay to anticipate the range time and thus match the "window" of the spinning ATS-5 satellite.

   (c) An L-band exciter.

   (d) An existing engineering prototype 300-watt solid state L-band power amplifier.

   (e) An antenna with an adjustable mount.

4. Install an L-band exciter and a 100-watt L-band power amplifier at the master ground station of the trilateration network, the General Electric Radio Optical Observatory.

5. Develop computer software to determine the near real-time satellite position in latitude, longitude, and earth center distance. The software will also compute the orbital elements of the satellite, range measurement standard deviation, and short term predictions of satellite position.

6. Conduct cooperative experiments with NASA using ATS-5. These tests will accomplish the following:

   (a) An exercise of real-time satellite trilateration ranging, position and predicted position computation, and data transmission to NASA and MARAD.

   (b) Establish basis for predicting satellite positions up to several hours. The prediction will be an extrapolation based on Kepler's laws from a sequence of trilateration positions.

   (c) Verify the accuracy of trilateration position measurements and predicted positions.

SECTION 3

PRINCIPLES OF OPERATION

3.1 TONE-CODE RANGING TECHNIQUE

Range measurements to satellites are made by measuring the radio propagation time of a signal from a ground station to the satellite and return. Following corrections for the propagation delay of the ionosphere and internal time delays in the satellite and ground station, the ranging time can be converted into a slant range by relating it to the known speed of light. Propagation time is measured by placing a time marker in the form of a tone-code interrogation (Figure 3.1) on the transmitted signal and observing the two-way transit time of the tone-coded signal. As used in this experiment, the interrogation signal consists of a short audio frequency tone followed by a digital synchronization and address code in which an audio cycle is inhibited for "0" and transmitted for "1".

A master ground station can determine the slant range from itself to the satellite by the above mentioned technique. The slant range from the satellite to any number of other remote ground stations can be determined if the ground stations are equipped to acknowledge and retransmit the tone-code interrogation after a precisely determined time delay. The other ground stations are fully automatic transponders.

A unique digital address code identifies each remote transponder. When the satellite-transponder slant range is to be determined, the ground station transmits a tone burst followed by the transponder address code. The satellite repeats the tone-code interrogation and all remote transponders within the satellite line-of-sight receive the retransmission. Only the transponder which recognizes its address code will retransmit the tone-code after a precise delay. The satellite repeats the transponder's response, but automatic muting prevents the transponder from acknowledging reception upon the second repetition of its address code by the satellite. The master ground station recognizes the address code as the one it sent, and records the master ground station-satellite two-way propagation time and the master ground station-satellite-transponder two-way propagation time. To obtain measurements of the slant ranges from the satellite to several transponders, the master ground station will interrogate them in sequence.

The basic tone-code transponder configuration is depicted in Figure 3.2. When a transponder receives the tone cycles from the satellite in its receiver, they are applied to the phase matching circuit even though they may be part of an interrogation for another transponder. A locally generated tone of the same frequency and with a stability better than one part in 10^6 is also applied to the phase matcher, which adjusts the phase of the locally generated tone such that it corresponds to the phase of the received tone. Phase matching is accomplished by averaging over 256 cycles. The averaging process improves the timing accuracy by the square root of the number of cycles averaged.

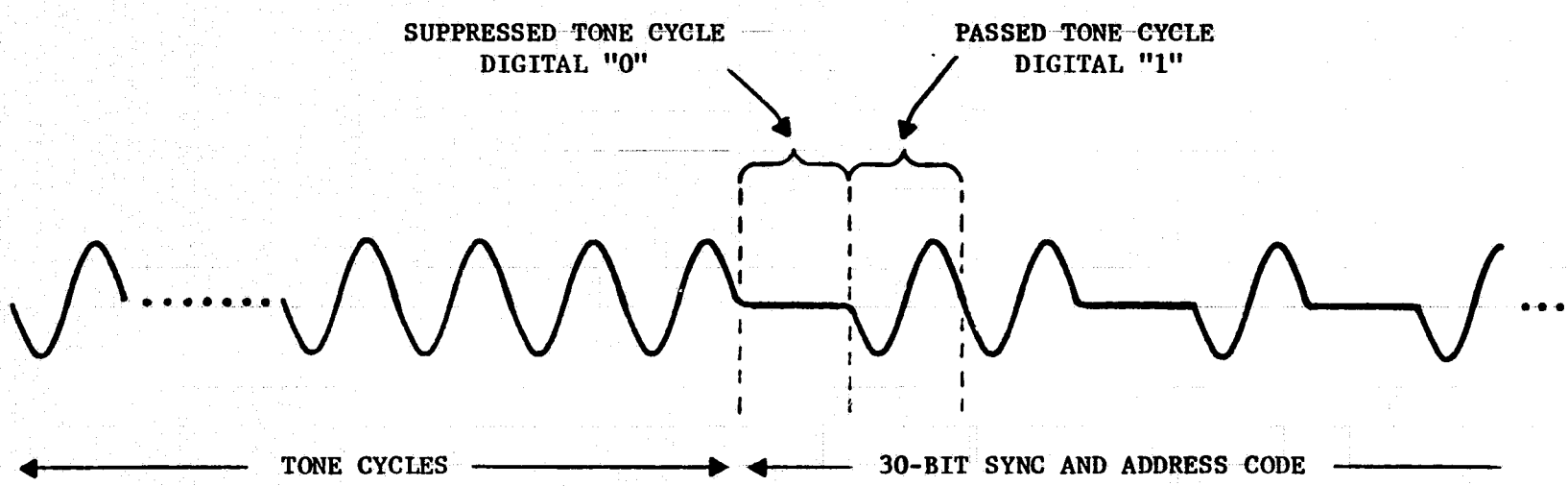

FIGURE 3.1 TONE-CODE RANGING WAVEFORM

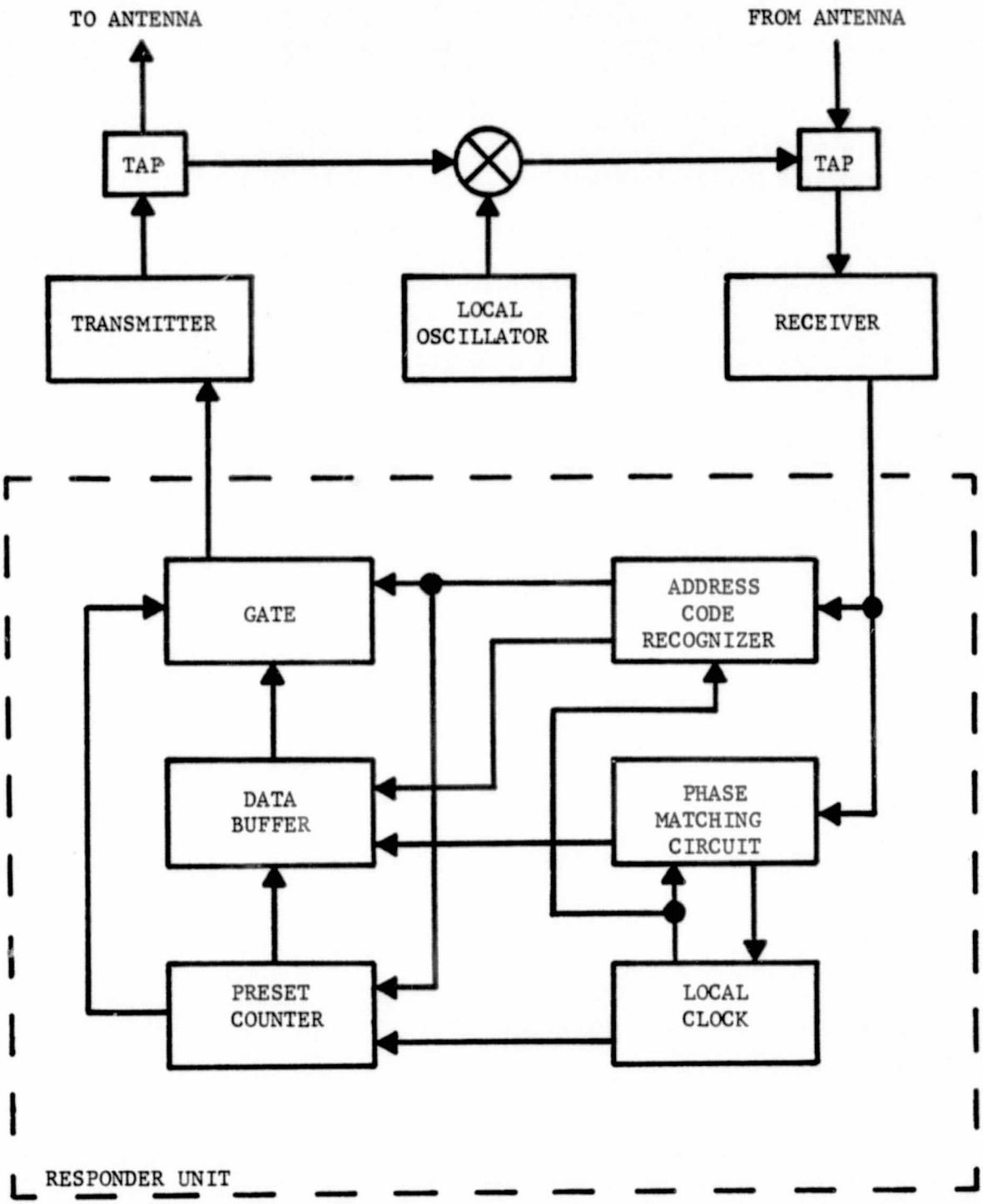

FIGURE 3.2 BASIC TONE-CODE TRANSPONDER

The phase matched locally generated tone clocks the received interrogation signal into an address code recognizer consisting of a shift register with summing circuits prewired to correspond to the unique digital address code of the transponder. When the sequence of pulses representing the transponder address code is loaded into the recognizer and acknowledged by the transponder, the recognition circuit produces a single, unambiguous output pulse which simultaneously keys the transmitter and starts a counter which measures out a precise number of locally generated tone cycles. Clock pulses reapplied to the shift register cause the address code to be clocked out to the transmitter following a preset number of tone cycles. In this way the transponder transmits its unique address code after a precisely measured time delay following correlation.

At the master ground station, the receiver output is applied to an address code recognizer similar to that in the transponder. Prior to the interrogation of an individual transponder, the taps of the summing circuit are switched to correspond to the address code of the intended transponder. When the address code is received from a satellite, a single output clock pulse occurs at the output of the summing circuit.

The L-band trilateration network described in this report consists of the master ground station at the General Electric Radio Optical Observatory near Schenectady, New York, and two remote transponders in Waihiawa, Oahu, Hawaii and Buenos Aires, Argentina. An audio frequency tone of 9.7656 kHz frequency modulates a carrier at 1651.475 MHz with an RF bandwidth of 60 kHz. The downlink signal is received from the satellite at 1550.455 MHz. Demodulated tones pass through tuned circuits with bandwidths of approximately 470 Hz before being applied to the phase matching circuits.

Both remote transponders and the Observatory are equipped to operate at VHF frequencies in addition to L-band. At VHF, an audio frequency tone of 2.4414 kHz frequency modulates 149.195 MHz (F1), 149.220 MHz (F2), or 149.245 MHz (F3). The downlink signal is received from the satellite at 135.575 MHz (F1), 135.600 MHz (F2), or 135.625 MHz (F3). The transponder in Buenos Aires operates at VHF on F1 only. Demodulated tones pass through tuned circuits with bandwidths of approximately 120 Hz before being compared with the locally generated tones.

Improved performance at low signal levels would result from the use of phase shift keying. As one L-band frequency modulation transponder had already been successfully demonstrated under NASA contract NAS5-11634, FM was chosen for the second transponder and the Observatory as the performance fulfilled the requirements of this experiment.

3.2 SELF CALIBRATION TECHNIQUE

The transponders at Buenos Aires and Hawaii and the master ground station at Schenectady are equipped with unique devices which measure the internal time delay each time a range measurement is made. The re-

mote transponders transmit their measured internal delays as digital messages following each tone-code response. Time delay measurements from the remote transponder and Observatory are automatically entered into a computer at the Observatory and used to correct the range measurements.

The internal time delay calibration includes all components which have a significant effect on the measurement process. Ideally, this would include all components through which the ranging signal passes from the time the received signal arrives at the antenna until the transmitted signal leaves the antenna. Practically, however, some components are excluded from the self-calibration loop because their time delays can be measured prior to installation and because their delays are not expected to vary beyond the anticipated accuracy limits of the range measurements. These components include the receive and transmit cables, the diplexer, the low noise receiver preamplifier, and the antenna feed assembly.

Variations in the transponder time delays occur in the logic sections of the responder or in the analog and RF circuits to and from the responder logic sections. A variation in the frequency of the 10 MHz responder oscillator through 1 Hz results in a range measurement error of approximately 8 meters. Heating or cooling of the tuned circuits of the responder through $\pm$ 15°C results in a range measurement error of approximately 150 meters. Variations in the local environment can be expected to contribute additional range measurement errors due to the RF component changes.

As sketched in Figure 3.2, the L-band transponders contain reactive signal samplers which remove a small fraction of the transponder's response transmission from the output of the L-band power amplifier. A double-balanced mixer and local oscillator translate this sample of the transmitted signal through the same frequency difference as the satellite converts the uplink frequency to the downlink frequency. A second reactive signal sampler injects the self calibration loop signal (appears identical to satellite downlink) into the transponder receiver. The receiver demodulates the mixed transmitted signal and passes the audio tone-code to the responder. The total L-band signal delay from the output of the responder back through its input is typically 140 μsec, slightly more than one complete tone cycle.

After a preset period of time sufficient to allow the self calibration signal to settle in the tuned circuits of the responder, the phase measuring gate is opened. The responder will compare the phase of the next 256 tone cycles with the phase of the tone being transmitted and will load the resulting phase measurement into a data buffer. The operation of the self calibration circuit within the responder proceeds with no checks on signal presence or quality. If the self calibration loop is not installed or if the RF signal levels are inadequate, phase measurement will proceed on noise and an erroneous value will result. These values must be detected and discarded in data processing.

Following transmission of the tone-code signal, the responder sends 48 digital bits of data to the master ground station. Digital data include the number of received address code bits in error at correlation, the setting of the manually adjustable responder thumbwheel switches which govern the number of transmitted tone cycles before code, and a representation of self calibration signal phase difference. Three tone cycles represent a "1" while three suppressed tone cycles represent a "0".

SECTION 4

L-BAND TRANSPONDER NETWORK

4.1 GEOGRAPHICAL DEPLOYMENT OF TRANSPONDERS

The General Electric L-band trilateration network consists of the Radio-Optical Observatory near Schenectady, New York, and two remote transponders located near Waihiawa, Oahu, Hawaii, and in Buenos Aires, Argentina.

Elevation angles to the ATS-5 satellite from these sites all range between 26 to 32 degrees. For a trilateration network designed to yield a two-way range measurement accuracy of $\pm$ 0.1 μsec, the ground station locations must be correspondingly accurate to within $\pm$ 17 meters and their altitudes to within $\pm$ 30 meters. Table 4.1 gives the locations of the antenna phase centers for each ground station, the estimated position accuracy, and the reference.

The Aero Services Corporation of Philadelphia, Pennsylvania, used aerial photographs to determine the location of the Radio-Optical Observatory radome containing the 30-foot dish antenna. They assume a maximum error of $\pm$ 3 meters, this being due entirely to the precision achievable in stereoscopic measurements of photographic plates. A $\pm$ 0.1 meter error due to shrinkage in the photographic emulsion can be ignored. Second order U.S. Coast and Geodetic Survey triangulation stations were referenced. These in turn are referenced to the 1927 North American Datum and use the 1866 Clarke ellipsoid (equatorial radius of earth a_e = 6378206.400 meters and flattening factor 1/f = 294.97869823). The altitude of the Observatory was read from a topographical map of the U.S. Coast and Geodetic Survey showing elevation contours for every 10 feet. Bench marks located within 1200 feet of the Observatory and at approximately the same altitude verify the accuracy of the elevation contour lines.

The L-band transponder antenna in Hawaii is located on a building of the U.S. Coast Guard Communication Station within the U.S. Navy Communication Station, three miles north of Waihiawa, Oahu, Hawaii. A U.S. Air Force survey team referenced a 1962 radio triangulation station of the U.S. Coast and Geodetic Survey to fix the location of an antenna on the northwest corner of the Coast Guard building. The L-band antenna is mounted approximately 40 meters due south of the Air Force antenna, and 90 meters from the USCGS triangulation station. The $\pm$ 0.1" error quoted for the latitude and longitude thus represents primarily the round-off error in the quoted position. The position of the antenna was verified by careful measurements from a USGS quadrangle map covering 7.5' on a 1:24,000 scale. The USCGS triangulation station references the Old Hawaiian Datum which assumes the 1866 Clarke ellipsoid.

TABLE 4.1

LOCATION OF GENERAL ELECTRIC L-BAND TRILATERATION AND NASA C-BAND RANGE AND RANGE RATE GROUND STATION ANTENNA PHASE CENTERS

STATION	LOCATION* Geodetic Latitude Longitude Height	REFERENCE
GE Radio-Optical Observatory near Schenectady, New York	42° 50' 53.67" ± 0.10" -74° 04' 13.34" ± 0.13" 414.5 ± 1.7 meters	Survey by Aero Services, Corp., of Philadelphia, Pa.; USGS topographical map, 1:24000; North American Datum of 1927.
GE Remote Transponder (User Code 11), U.S. Coast Guard Communication Station, Waihiawa, Oahu, Hawaii	21° 31' 25.3" ± 0.1" -157° 59' 56.5" ± 0.1" 393.3 ± 1.0 meters	Antenna mounted within 270 feet of USCGS Triangulation Station; USGS topographical map, 1:24000; Old Hawaiian Datum.
GE Remote Transponder (User Code 08), Argentine Air Force Buenos Aires, Argentina	-34° 35' 07.00" ± 0.50" -58° 22' 12.69" ± 0.60" 40.0 ± 1.0 meters	Carta Topografica de la Republica Argentina, 1:50000; Argentine Datum.
NASA 85-foot dish #2 (S85 2), NASA Rosman Tracking Station, Rosman, North Carolina	35° 11' 55.677" ± 0.130" 277° 07' 27.451" ± 0.160" 894 ± 1 meters	"NASA Directory of Observation Station Locations," (4) North American Datum of 1927.
NASA 40-foot dish (S40 5), NASA Mojave Tracking Station Goldstone, California	35° 19' 53.970" ± 0.130" 243° 06' 47.762" ± 0.160" 918 ± 3 meters	"NASA Directory of Observation Station Locations," (4) North American Datum of 1927.

*Accuracies with respect to datum origin.

The L-band transponder antenna in Buenos Aires is located on the roof of a 13-floor building of the Argentine Air Force. The building is within sight of the Rio de la Plata, slightly above sea level. The height of the building thus represents a good estimate of the antenna altitude. The building latitude and longitude were read directly from a topographical map of the City of Buenos Aires (Ejercito Argentina - Instituto Geografico Militar, Carta Topografica de la Republica Argentina) covering 10' on a 1:50,000 scale. The chart references the Argentine Datum which uses the 1910 International Ellipsoid of Hayford (a_e = 6378388.0 meters, 1/f = 297.0).

The accurate location of a satellite with respect to these three sites requires them to be on some common coordinate system. The Modified Mercury Datum of 1968 was selected; all data and satellite positions quoted within this report reference the Modified Mercury Datum. The "NASA Directory of Observation Station Locations"[4] gives shifts from the North American Datum of 1927 and the Old Hawaiian Datum to the Modified Mercury Datum. For conversion of the Buenos Aires position, datum tilt requires that the altitudes of positions in the Buenos Aires area must first be increased by 1.5 meters before translating a position in the Argentine Datum to a position in the South American Datum of 1969 (ΔX = -83 meters, ΔY = 130 meters, and ΔZ = 120 meters)[5] . The NASA Directory gives the shifts from the South American Datum to the Modified Mercury Datum. Table 4.2 presents the positions of the L-band trilateration antenna phase centers on the Modified Mercury Datum in geocentric and geodetic coordinates.

Tables 4.1 and 4.2 also list the estimated positions of the phase centers of the 85-foot dish #2 (S85 2) at the NASA Rosman Tracking station at Rosman, North Carolina and the 40-foot dish (S40 5) at the NASA Mojave Tracking Station at Goldstone, California. NASA uses range and range rate measurements from these two stations to determine the position of the ATS-5 satellite. Any comparison of the NASA position and the General Electric position requires both networks to reference the same coordinate system. NASA further utilizes the S40 5 antenna at Rosman as the primary ground facility of the PLACE experiment. The computer software which provides ATS-5 ephemeris also tabulates the slant range from the satellite to this antenna.

4.2 GEOMETRICAL CONSIDERATIONS FOR RANGING PRECISION/ACCURACY

Analytic equations generate satellite positions based on measured slant ranges to three known locations on the earth. No simple analtyic expressions exist, however, which evaluate the error in satellite position as a function of slant range error or station location error. Satellite position errors can be computed by defining slant ranges and station locations, and then varying each parameter separately and noting the effect on the defined position of the satellite. Table 4.3 lists the results of

TABLE 4.2

POSITIONS OF GROUND STATION ANTENNA
PHASE CENTERS ON THE
MODIFIED MERCURY DATUM 1968

	Geocentric Coordinates X (meters) Y (meters) Z (meters)	Geodetic Coordinates latitude (°,',") longitude(°,',") height (meters)
GE Radio-Optical Observatory, Schenectady, NY	1285500.7 -4503862.5 4315420.1	42 50 53.457 285 55 47.650 379.5
GE Remote Transponder, Waihiawa, HA	-5504120.1 -2224223.0 2325246.1	21 31 13.667 202 00 13.341 385.1
GE Remote Transponder, Buenos Aires, Argentina	2756736.8 -4475926.4 -3600082.4	-34 35 05.396 301 37 44.554 50.7
NASA 85-Foot Dish #2, (S85 2), Rosman, NC	647203.9 -5178155.4 3656426.2	35 11 56.232 277 07 27.491 856.3
NASA 40-Foot Dish, (S40 5), Goldstone (Mojave), CA	-2356174.3 -4646758.2 3668472.0	35 19 53.843 243 06 44.510 901.9

TABLE 4.3

ATS-5 POSITION ERROR AS A FUNCTION OF SLANT RANGE ERROR AND STATION LOCATION ERROR

	ATS-5 POSITION ERROR		
	LATITUDE (degrees)	LONGITUDE (degrees)	EARTH CENTER DISTANCE (meters)
One-Way Slant Range Error (1 μsec)			
Observatory	-0.00227	-0.00159	41.3
Hawaii	0.000368	0.00211	128.
Buenos Aires	0.00190	-0.000540	133.
Station Altitude Error (1 meter)			
Observatory	-0.00000399	-0.00000276	0.0726
Hawaii	0.000000547	0.00000314	0.191
Buenos Aires	0.00000287	-0.000000815	0.201
Station Latitude Error (1 second)			
Observatory	0.000149	0.000103	- 2.71
Hawaii	-0.00000910	-0.0000516	- 3.14
Buenos Aires	0.0000823	-0.0000234	5.75
Station Longitude Error (1 second)			
Observatory	-0.000131	-0.0000669	1.76
Hawaii	-0.0000305	-0.000175	-10.6
Buenos Aires	0.000127	-0.0000361	8.89

such a calculation, where the triad of stations consisted of the Observatory, Hawaii, and Buenos Aires. From Table 4.3, decreasing the internal time delay of the Buenos Aires transponder by 0.1 μsec, for example, would have the effect of moving the satellite 0.00019 degrees further north, 0.000054 degrees further west, and 13.3 meters higher in altitude.

Range measurement and station location accuracies and precisions can be converted to satellite position accuracy and precision by use of Table 4.3. If more than one component is varied, the resultant satellite position deviation is the square root of the sum of squares.

Assuming station locations to be known to within one second in latitude and longitude (approximately 30 meters) and 10 meters in altitude, the net position inaccuracy in the location of ATS-5 is as follows:

$\pm$ 0.000256°, latitude

$\pm$ 0.000228°, longitude

$\pm$ 15.9 meters, earth center distance.

The above inaccuracies are roughly equivalent to 85 nanosecond inaccuracies on all slant ranges, corresponding to 0.17 μsec two-way range measurement inaccuracies.

4.3 SELECTION OF REMOTE TRANSPONDER SITES

The General Electric Company operates a VHF trilateration network with the master ground station near Schenectady, New York, and with remote transponders in Europe, Iceland, North and South America, and Australia. Only two of the transponder sites within view of the ATS-5 satellite, however, provide a baseline from Schenectady of more than several hundred miles. Either of these sites, Daytona Beach, Florida or Buenos Aires, Argentina, would be useful in providing a north-south baseline for trilaterating ATS-5.

The transponder site in Buenos Aires, Argentina, is under the control of the Department of Communications of the Argentine Air Force. Past experience has shown them to be able to provide not only capable operators but also experienced electronics maintenance personnel. The Earth Stations Department of the General Electric Company maintains and operates the VHF transponder in Daytona Beach, Florida. This organization has a long history of excellent participation with the Corporate Research and Development Center in space communications projects. Both sites, consequently, are more than technically adequate to support an L-band transponder.

The long Schenectady-Buenos Aires baseline provides better satellite position precision and accuracy than the shorter Schenectady-Daytona Beach baseline. Assuming the same ranging errors for Daytona Beach and Buenos Aires, the earth center distance, latitude, and longitude errors

can be reduced by factors of 5.4, 3.3, and 1.6, respectively. This significant reduction in satellite position error justified the installation of the L-band transponder in Buenos Aires.

The lack of existing transponder sites west of the Schenectady, New York-Daytona Beach, Florida-Buenos Aires, Argentina, meridian necessitated the establishment of a new transponder site with candidate locations being Hawaii or the west coast of the continental United States. Placing a transponder in Hawaii results in an east-west baseline roughly twice as long as the west coast - Schenectady baseline without significantly increasing shipping costs or entering foreign territory. Furthermore, the satellite earth center distance, latitude, and longitude errors would be factors of 2.3, 1.5, and 1.8 less, respectively, with the transponder in Hawaii than on the west coast of the continental United States.

The final selection of Hawaii and Buenos Aires, Argentina, as L-band transponder sites versus the U. S. west coast and Daytona Beach, Florida, result in improvements in satellite earth center distance, latitude, and longitude by factors of 12, 5, and 3 respectively, having assumed the same ranging precision and accuracy at all sites.

4.4 ATS-5 L-BAND SIGNAL CHARACTERISTICS

The ATS-5 satellite was designed to be stabilized with its L-band antenna pointed toward the earth. A malfunction at orbit injection caused the satellite to spin at a rate of approximately 77 revolutions per minute with its axis of rotation parallel to the earth's axis. The approximately 25-degree wide beam of the L-band antenna rotates with the satellite like a search light beam, pointing to the earth for approximately 100 msec during each 780 msec rotation period. L-band signals can be passed through the satellite antenna "window" only when the antenna beam is pointed toward the earth. Figure 4.1 is a recording of the L-band beacon signal strength as received at the Observatory. The side lobes of the satellite antenna are nominally 15 dB below the peak of the main beam.

The spin of the satellite makes it necessary to provide variable delay timing circuits at the Observatory and in the remote transponders to affect the relay of tone-code ranging signals during the satellite antenna "windows." Timing circuits would not be necessary if the satellite were capable of transmitting signals continuously.

The L-band transponder of the ATS-5 satellite can operate in narrow band (2.5 MHz) or wideband (25 MHz) frequency translation modes. The remote L-band transponders require the reduced satellite noise bandwidth inherent in the narrow band mode. The ATS-5 satellite receives ranging signals at 1651.475 MHz and retransmits them at 1550.455 MHz, a frequency translation of 101.020 MHz. The satellite's L-band transponder has one functioning traveling wave tube power amplifier yielding 12 watts of RF power. The peak effective isotropic radiated power (EIRP) is the product of antenna gain and RF output power, 53.8 dBm.

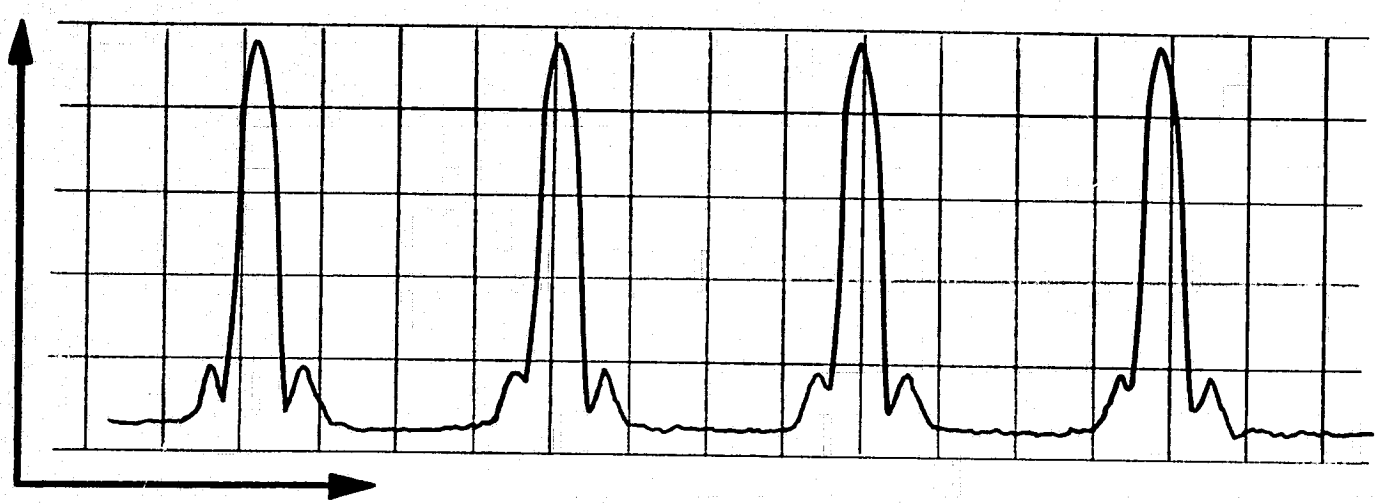

FIGURE 4.1 RECORDING OF THE BEACON SIGNAL TRANSMITTED FROM THE ATS-5 SATELLITE

The noise temperature of the satellite receiver system was 32.5 dB°K prior to launch. When used in the narrow band frequency translation mode, the receiver noise power at the input of its transponder is approximately -102 dBm. The uplink space loss at 1651 MHz is 188.4 dB. With the satellite net receive antenna gain of 14.2 dB, a ground transmitter would have to generate an EIRP of 75.5 dBm to equal the receiver noise. A signal approximately 20 dB stronger than the satellite receiver noise input will capture virtually all of the satellite transmit power. A further increase in ground station EIRP will not improve the signal-to-noise ratio transmitted from the satellite. At this point, the satellite receiver is said to be saturated.

When the signal into the satellite is much below saturation, the downlink signal quality from the satellite is uplink limited. The signal received by the satellite and the satellite receiver noise add together to become the transmitted signal. In this circumstance, the use of a large ground station antenna and a low noise preamplifier do not insure a high signal-to-noise ratio. This is determined at the satellite receiver.

Both remote transponders are equipped with 300-watt solid state L-band power amplifiers and fixed 10-foot parabolic antennas. The Observatory utilizes a 100-watt solid-state L-band power amplifier and a fully steerable 30-foot parabolic antenna. The Observatory 30-foot dish antenna, however, does not exhibit a gain characteristic of this size antenna. It acts much like a 10-foot dish antenna because the L-band feed is mounted off-set from the prime focus and is partially blocked by another feed structure.

Detailed power budgets presented in Table 4.4 relate to ranging interrogations from the Observatory to Buenos Aires, Hawaii, and the Observatory "satellite aided" calibration station (see Section 6.1) and reflect the final operational configurations of the two remote transponders as described in Sections 6.6 and 6.7.

The Observatory 100-watt L-band power amplifier is located in the radio room instead of being mounted near the antenna feed. The Observatory generates a sufficient EIRP to conduct range measurements to ATS-5 and the L-band transponder network in spite of the 100-foot cable between the amplifier and feed. Placing the amplifier behind the feed may increase the EIRP by 2 dB but will only decrease the noise power sharing factor in ATS-5 and consequently increase the signal-to-noise ratio in the transponders by approximately 0.6 dB. The fully steerable Observatory dish antenna can be accurately pointed toward the ATS-5 satellite in a time short compared to the duration of ranging periods. A maximum signal loss of 0.5 dB is anticipated due to pointing errors.

The 10-foot dish antennas at both remote transponder sites represent the optimum sized fixed antennas which can be used for ranging experiments at L-band frequencies with the ATS-5 satellite. A fixed antenna two feet larger in diameter would have approximately 2.0 dB more gain but would suffer more

TABLE 4.4 (PART 1)

ATS-5 TRILATERATION POWER BUDGETS

UPLINK 1651 MHz

	OBSERVATORY 30' (100W)	BUENOS AIRES 10' (300W)	HAWAII 10' (300W)	OBSERVATORY 6' (300W)
GROUND STATION				
Transmit Power (dBm)	50.0	54.3	54.3	54.3
Antenna Gain (dB)	31.7	31.0	31.0	26.5
Maximum Pointing Loss (dB)	- 0.5	- 3.0	- 3.0	- 1.0
Circuit Loss (dB)	- 2.5	- 2.8	- 2.1	- 1.8
EIRP (dBm)	78.7	79.5	80.2	78.0
SPACE LOSS (dB)	-188.4	-188.4	-188.4	-188.4
ATMOSPHERIC LOSS (dB)	- 0.2	- 0.2	- 0.2	- 0.2
ATS-5 SATELLITE				
Effective Receive Antenna Gain (dB)	10.9	10.9	10.9	10.9
Pointing Loss (dB)	- 1.0	- 0.6	- 0.4	- 1.0
TOTAL RECEIVED POWER (dBm)	-100.0	- 98.8	- 97.9	-100.7
RECEIVER NOISE POWER DENSITY (dBm/Hz)	-166.0	-166.0	-166.0	-166.0
SIGNAL-TO-NOISE POWER DENSITY (dBHz)	66.0	67.2	68.1	65.3
SATELLITE NOISE BANDWIDTH (dBHz) (2.5 MHz Bandwidth)	64.0	64.0	64.0	64.0
SIGNAL-TO-NOISE RATIO (dB) (2.5 MHz ATS-5 Bandwidth)	2.0	3.2	4.1	1.3
NOISE POWER SHARING FACTOR (dB)	- 2.1	- 1.7	- 1.4	- 2.4
SIGNAL-TO-NOISE RATIO (dB) (60 kHz Transponder BW)	18.2	19.4	20.3	17.5

TABLE 4.4 (PART 2)

ATS-5 TRILATERATION POWER BUDGETS

ATS-5 Satellite (Uplink)	
Receive Antenna Gain (dB)	15.5
Circuit Loss (dB)	- 1.3
Polarization Loss (dB)	- 0.3
50 msec ATS-5 "Window" (dB)	- 3.0
Effective ATS-5 Receive Antenna Gain (dB)	10.9

ATS-5 Satellite (Downlink)	
Transmit Power (dBm)	40.8
Antenna Gain (dB)	15.0
Circuit Loss (dB)	- 2.0
EIRP (dBm)	53.8
Space Loss (dB)	-187.8
Atmospheric Loss (dB)	- 0.2
Power Incident on Ground Antenna (dBm)	-134.2

EFFECTIVE GROUND STATION ANTENNA GAINS

STATION	OBSERVATORY (30')	BUENOS AIRES	HAWAII	OBSERVATORY (6')
Antenna Gain (dB)	31.2	30.5	30.5	26.0
Polarization Loss (dB)	- 0.2	- 0.2	- 0.2	- 0.2
Circuit Loss (dB)	- 1.2	- 3.3	- 1.2	- 2.3
Pointing Loss (dB)	- 0.5	- 3.0	- 3.0	- 1.0
Off Beam Loss (dB)	- 1.4	- 1.0	- 0.5	- 1.4
50 msec ATS-5 "Window" (dB)	- 3.0	- 3.0	- 3.0	- 3.0
Total Downlink Antenna Gain (dB)	24.9	20.0	22.6	18.1

TABLE 4.4 (PART 3)

ATS-5 TRILATERATION POWER BUDGETS

DOWNLINK 1551 MHz

From To	OBS. (30') OBS. (30')	OBS. (30') BA	OBS. (30') HAW	OBS. (30') OBS. (6')	BA OBS. (30')	HAW OBS. (30')	OBS. (6') OBS. (30')
Power Incident on Antenna (dBm)	-134.2	-134.2	-134.2	-134.2	-134.2	-134.2	-134.2
Effective Antenna Gain (dB)	24.9	20.0	22.6	18.1	24.9	24.9	24.9
Noise Power Sharing at Satellite (dB)	- 2.1	- 2.1	- 2.1	- 2.1	- 1.7	- 1.4	- 2.4
Effective Received Power (dBm)	-111.4	-116.3	-113.7	-118.2	-111.0	-110.7	-111.7
Receiver Noise Power Density (dBm/Hz) (3 dB N.F.)	-171.0	-171.0	-171.0	-171.0	-171.0	-171.0	-171.0
S/N Power Density-Ground (dBHz)	59.6	54.7	57.3	52.8	60.0	60.3	59.3
S/N Power Density-Satellite (dBHz)	66.0	66.0	66.0	66.0	67.2	68.1	65.3
S/N Power Density-Result (dBHz)	58.7	54.4	56.8	52.6	59.2	59.6	58.3
Receiver Noise Bandwidth (dBHz) (60 kHz Bandwidth)	47.8	47.8	47.8	47.8	47.8	47.8	47.8
Signal-to-Noise Ratio (dB)	10.9	6.6	9.0	4.8	11.4	11.8	10.5

than 1.0 dB additional pointing loss at the northern and southern extremes of the satellite orbit. An antenna two feet smaller in diameter would remove 1.0 dB in pointing loss but would have 2.0 dB less gain. If 6-foot antennas were to replace the 10-foot dish antennas, the transponders in Buenos Aires and Hawaii would see the ranging interrogations with signal-to-noise ratios of 4.2 and 6.7 dB, respectively, a drop of roughly 2.4 dB. The Observatory would see the responses from these transponders with signal-to-noise ratios of 10.2 and 10.7 dB, a drop of approximately 1.0 dB. During the "satellite aided" calibrations of both transponders, a 6-foot dish antenna was used. The estimated signal-to-noise ratio in the transponder was 4.8 dB. This compares favorably with a measured signal-to-noise ratio of 4.5 dB at the output of the transponder receiver 60 kHz bandpass filter. The responders correlated on approximately 90 percent of the interrogations under optimum conditions and on approximately 10 percent under poor conditions. The marginal operations at the Observatory with a 6-foot antenna would become unacceptable at the Buenos Aires site.

The ATS-5 L-band antenna sweeps past the earth once every 780 msec with a 100 msec "window", as sketched in Figure 4.1. The antenna beamwidths at the -1.0 and -3.0 dB points are 22 msec and 52 msec, respectively. The complete ranging interrogation (phase matching and correlation) requires approximately 29 msec. An additional 20 to 30 msec is required to allow the tuned circuits of the responder to settle. The entire ranging interrogation can thus pass through the narrow "window" of the spinning satellite. Furthermore, proper phase synchronization of the Observatory interrogator with the satellite "window" will allow the ranging interrogation to pass between the -3.0 dB points of the satellite antenna pattern. The power budgets of Table 4.4 reflect the maximum gains of the satellite antenna with appropriate "window" losses.

The ranging interrogation and response signal-to-noise ratios in the satellite range between 1.3 and 4.1 dB. This assumes the minimum satellite RF bandwidth of 2.5 MHz, as compared to the 60 kHz RF bandwidth employed by the Observatory and remote transponders. The last line of Table 4.4, Part 1, lists the signal-to-noise ratios that would be obtained in a 60 kHz satellite transponder bandwidth.

4.5 INTERFERENCE OF ATS-6 BY ATS-5 RANGING

The real-time ATS-5/ATS-6 position fixing experiments prompted development of the ATS-5 trilateration network. The uplink ranging frequency from the Observatory and remote transponders falls within the narrow bandwidth L-band receiver of the ATS-6 satellite, located on the equator 10° east of ATS-5. Furthermore, the downlink frequency from ATS-6 overlaps the downlink from ATS-5. The General Electric trilateration support will be the only user of the ATS-5 L-band transponder during scheduled ranging periods, but several other experimenters may be using the L-band receiver and/or transmitter of ATS-6 at the same time.

Table 4.5 represents the uplink and downlink power budgets, respectively, in this interference problem, where the characteristics of the various ATS-6 experiments have been taken from the "Integrated Test Plan for ATS-F L-band Experiment", vol. 1.[6] It will be noticed from Table 4.5 that none of the ATS-6 experiments have uplink transmissions spilling over into ATS-5 with powers greater than approximately 25 dB below the tone-code ranging, thus minimizing interference and removing all possibility of power sharing. The ranging tones, however, spill into ATS-6 and share a significant amount of power with most of the ATS-6 experimenters, the only exception being NASA's trilateration of ATS-6. This occurs in spite of the more than 30 dB reduction in signal strength to ATS-6 when the Observatory 30-foot dish antenna is pointed toward ATS-5 and a corresponding 20 dB reduction for the 10-foot dish antennas at the remote transponders. Reduction of the Observatory transmit power by 6 dB results in a slight reduction of power sharing by the ATS-6 users while reducing the signal strength to the remote transponders to a marginal level. The ranging code, however, has a duration of only 50 ms every 780 ms and thus probably does no more damage than occasional "clicks" in ATS-6 experimenters' signals.

The downlink transmission power budgets of Table 4.5 Part 2 show no significant problem area. Signals from ATS-6 appear to be 20 dB weaker at the Observatory and remote transponders than those from ATS-5. Furthermore, ATS-5 does not interfere with the ATS-6 downlink. ATS-5 signals appear to be more than 17 dB weaker, in all cases, than ATS-6 transmissions.

No tests have been conducted to date to verify the degree of interference and/or power sharing of signals to/from ATS-5 and ATS-6. General Electric trilateration tone-code transmissions have been detected by the ATS-6 satellite, however, while ATS-6 was being illuminated by no other experimenter.

4.6 L-BAND/VHF TRANSPONDER

The remote L-band transponders assembled under this contract should perhaps be called L-band/VHF transponders as both the Buenos Aires and Hawaii transponder are capable of L-band and VHF ranging and VHF voice communications. As shown in Figure 4.2, the L-band and VHF RF sections are entirely independent but use the same responder unit. The L-band/VHF transponder is designed to receive at L-band or VHF and to respond automatically at both frequencies simultaneously with coherent baseband signals. Turning off the appropriate transmitter disables the L-band or VHF response. The L-band system utilizes a ranging tone of 9.7656 kHz to insure that 256 tone cycles can be passed through the 50 msec "window" of the ATS-5 satellite. The VHF transponders utilize a ranging tone of 2.4414 kHz. The "Final Report on Phases 1 and 2, VHF Ranging and Position Fixing Experiments Using ATS Satellites"[1], NASA Contract NAS5-11634, fully describes the operation of the VHF transponders.

TABLE 4.5 (PART 1)

ATS-5/ATS-6 L-BAND INTERFERENCE POWER BUDGET

UPLINK

Ground Station	OBSERVATORY	REMOTE GE TRANSPONDER	KC-135 AIRCRAFT	ESRO BUOY	NASA TRILAT.	DOT/USCG	ESRO SHIP
Antenna	30' dish	10' dish	dipole	omni	15' dish	high gain	CP
Power	100W	300W	100W	20W	100W	10W	40W
Assigned Satellite	ATS-5	ATS-5	ATS-6	ATS-6	ATS-6	ATS-6	ATS-6
Frequency (MHz)	1651.475	1651.475	1650.	1655.	1650.	1650.	1650.
Bandwidth (MHz)	0.60	0.60					
Station Transmit Power (dBm)	50.0	54.3	50.0	43.0	50.0	40.0	46.0
Circuit Loss (dB)	- 2.5	- 2.5	- 1.3	- 2.5	- 1.0	- 1.5	- 1.5
Antenna Gain (dB)	31.7	31.0	3.0	3.0	35.0	12.0	12.0
EIRP (dBm)	79.2	82.8	51.7	43.5	84.0	50.5	56.5
Space Loss (dB)	-188.4	-188.4	-188.4	-188.4	-188.4	-188.4	-188.4
Atmospheric Loss (dB)	- 0.2	- 0.2	- 0.2	- 0.2	- 0.2	- 0.2	- 0.2
Polarization Loss (dB)	- 0.3	- 0.3	- 0.3	- 0.3	- 0.3	- 0.3	- 0.3
Multipath Loss (dB)	0.0	0.0	- 0.5	- 6.0	0.0	- 1.0	- 6.0
Power into Isotropic Satellite Antenna (dBm)	-109.7	-106.1	-137.7	-151.4	-104.9	-139.4	-138.4
ATS-5 Satellite							
Pointing Loss (dB)	- 0.5	- 3.0	0.0	0.0	- 30.0	- 1.0	- 1.0
Off-Beam Loss (dB)	- 1.0	- 0.5	- 1.2	- 1.5	- 1.0	- 1.5	- 1.5
Satellite Antenna Gain (dB)	14.2	14.2	14.2	14.2	14.2	14.2	14.2
Signal into Satellite (dBm)	- 97.0	- 95.4	-124.7	-138.7	-121.7	-127.7	-126.7
ATS-6 Fan Beam							
Pointing Loss (dB)	- 30.0	- 20.0	0.0	0.0	- 0.5	0.0	0.0
Off Beam Loss (dB)	- 6.0	- 25.0	- 3.0	- 3.0	- 22.0	- 3.0	- 3.0
Satellite Antenna Gain (dB)	29.0	29.0	29.0	29.0	29.0	29.0	29.0
Signal into Satellite (dBm)	-116.7	-122.1	-111.7	-125.4	- 98.4	-113.4	-112.4

TABLE 4.5 (PART 2)

ATS-5/ATS-6 L-BAND INTERFERENCE POWER BUDGET

DOWNLINK

Satellite	ATS-5	ATS-6 FAN BEAM
Transmit Power (dBm)	40.8	46.0
Antenna Gain (dB)	15.0	28.5
Circuit Loss (dB)	- 2.0	- 2.0
EIRP (dBm)	53.8	72.5
Space Loss (dB)	-187.8	-187.8
Atmospheric Loss (dB)	- 0.2	- 0.2
Polarization Loss (dB)	- 0.2	- 0.2
Effective Power into Isotropic Ground Antenna (dBm)	-134.4	-115.7

Ground Station	OBSERVATORY	REMOTE GE TRANSPONDERS	KC-135 AIRCRAFT	DOT/USCG AND ESRO SHIP	NASA TRILAT.
Frequency (MHz)	1550.455	1550.455	1550.	1550.	1550.
Bandwidth (MHz)	0.060	0.060			
Antenna	30' dish	10' dish	dipole	CP	15' dish
Assigned Satellite	ATS-5	ATS-5	ATS-6	ATS-6	ATS-6
Signals from ATS-5					
Incident Power (dBm)	-134.4	-134.4	-134.4	-134.4	-134.4
Satellite Pointing Loss (dB)	- 1.4	- 1.0	- 1.5	- 1.5	- 1.0
Ground Antenna Pointing Loss (dB)	- 0.5	- 3.0	0.0	- 2.0	- 30.0
Antenna Gain (dB)	31.2	30.5	3.0	12.0	35.0
Received Power (dBm)	-105.1	-107.9	-132.9	-125.9	-130.4
Signals from ATS-6 Fan Beam					
Incident Power (dBm)	-115.7	-115.7	-115.7	-115.7	-115.7
Satellite Pointing Loss (dB)	- 10.0	- 25.0	- 3.0	- 3.0	- 22.0
Ground Antenna Pointing Loss (dB)	- 30.0	- 20.0	0.0	0.0	- 0.5
Antenna Gain (dB)	31.2	30.5	3.0	12.0	35.0
Received Power (dBm)	-124.5	-130.2	-115.7	-106.7	-103.2

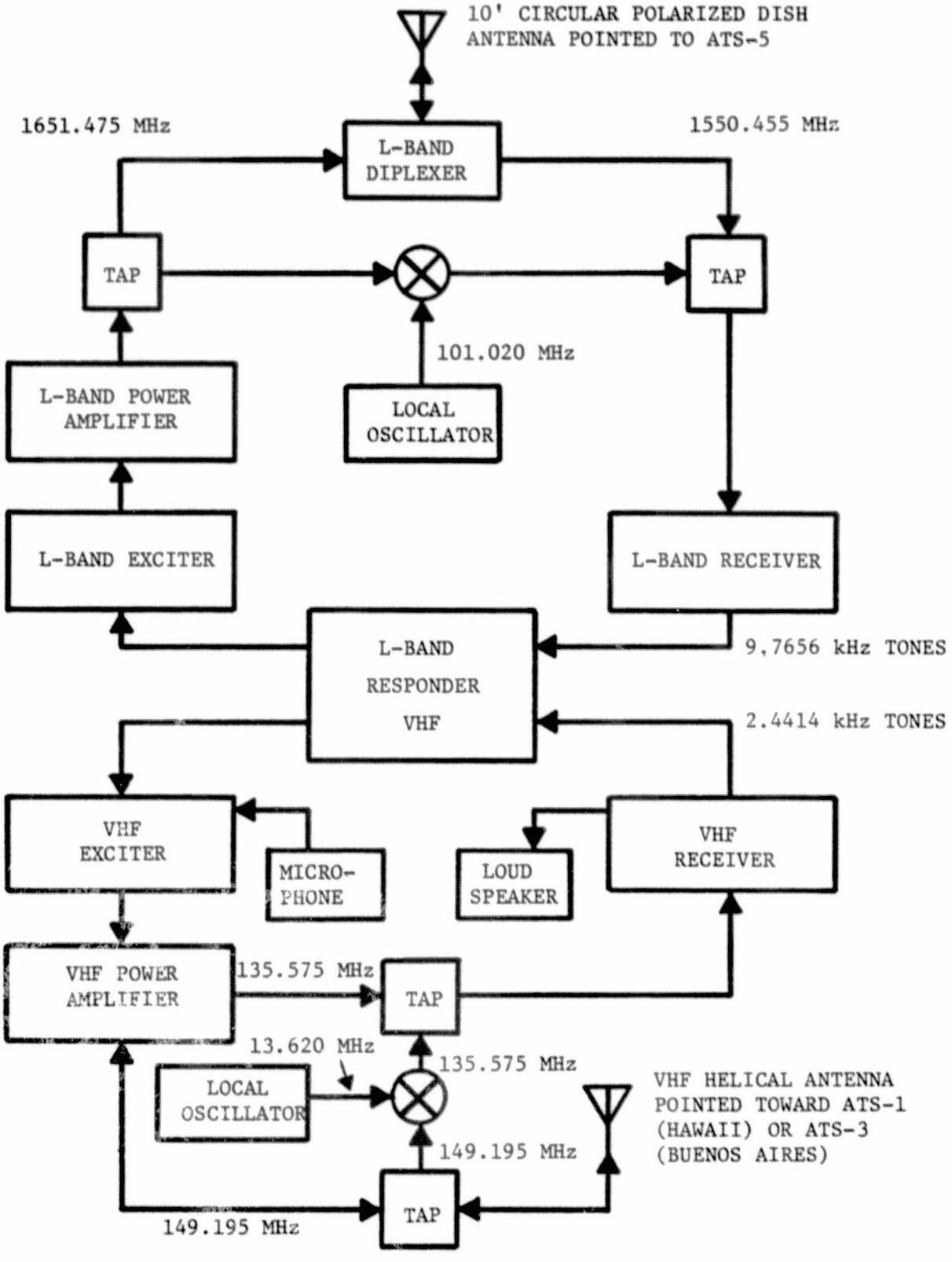

FIGURE 4.2 L-BAND/VHF TRANSPONDER CONFIGURATION

The existing site in Buenos Aires, Argentina, consisted of a complete VHF transponder including transmitter, power amplifier, receiver with specially designed limiter-discriminator circuits, responder, and an 8-turn circularly polarized helical antenna. In addition to the L-band RF equipment, a completely new L-band/VHF responder was shipped to Buenos Aires, replacing the original VHF only responder. Figure 4.3 is a photograph inside the radio room at the Buenos Aires site, showing the entire L-band/VHF transponder with the exception of the antennas. Figure 4.4 details the antennas on the roof of the "Condor" building in Buenos Aires.

The entire L-band/VHF transponder developed under Phase 3 of NASA Contract NAS5-11634[2] was shipped to Hawaii, making the Hawaiian transponder site identical to the Buenos Aires system with the following exceptions: a 4-turn VHF helical antenna instead of an 8-turn helical antenna, a complete VHF self-calibration loop, and a second generation prototype L-band solid state power amplifier. Figure 4.5 is a photograph of the L-band/VHF transponder (less antennas) at the U.S. Coast Guard Communication Station in Hawaii. Figure 4.6 details the antennas on the roof of the USCG building.

In addition to being particularly useful in passing schedule information and discussing operational procedures, the VHF communication channel can be exploited to check out most of the responder circuits. With the exception of the analog input and output circuits, the responder uses the same logic functions for both L-band and VHF, at 9.7656 kHz and 2.4414 kHz, respectively.

The following subsections describe individual components of the L-band/VHF transponders in more detail.

4.6.1 L-Band Receiver

The L-band receivers in both remote transponders are of modular construction as shown schematically in Figure 4.7 and photographically in Figure 4.8. The receivers are designed for a fixed frequency of 1550.455 MHz. A temperature compensated crystal oscillator operating as the first local oscillator at 1520.000 MHz insures receiver frequency stability to within one part in 10^6. The second local oscillator at 30.000 MHz is also crystal controlled.

The effective noise figure of approximately 4 dB of the receiver as referenced to the antenna feed is determined primarily by the low noise (< 3.0 dB) transistorized preamplifier mounted in the diplexer housing near the antenna feed. A low-loss (0.6 dB) RF bandpass filter between the diplexer and preamplifier limits the RF bandwidth to 50 MHz. An IF preamplifier with a bandwidth of 10 MHz follows the 1-2 GHz balanced mixer. A tuning range of 1550 ± 5 MHz can be achieved by exchanging the crystal in the second local oscillator. The second IF bandwidth of 60 kHz centered at 455 kHz is chosen to accommodate the ranging signal modulation format. Specially designed balanced limiter-discriminator circuits yield a minimum variation in the phase of the audio signal as a function of RF signal strength.

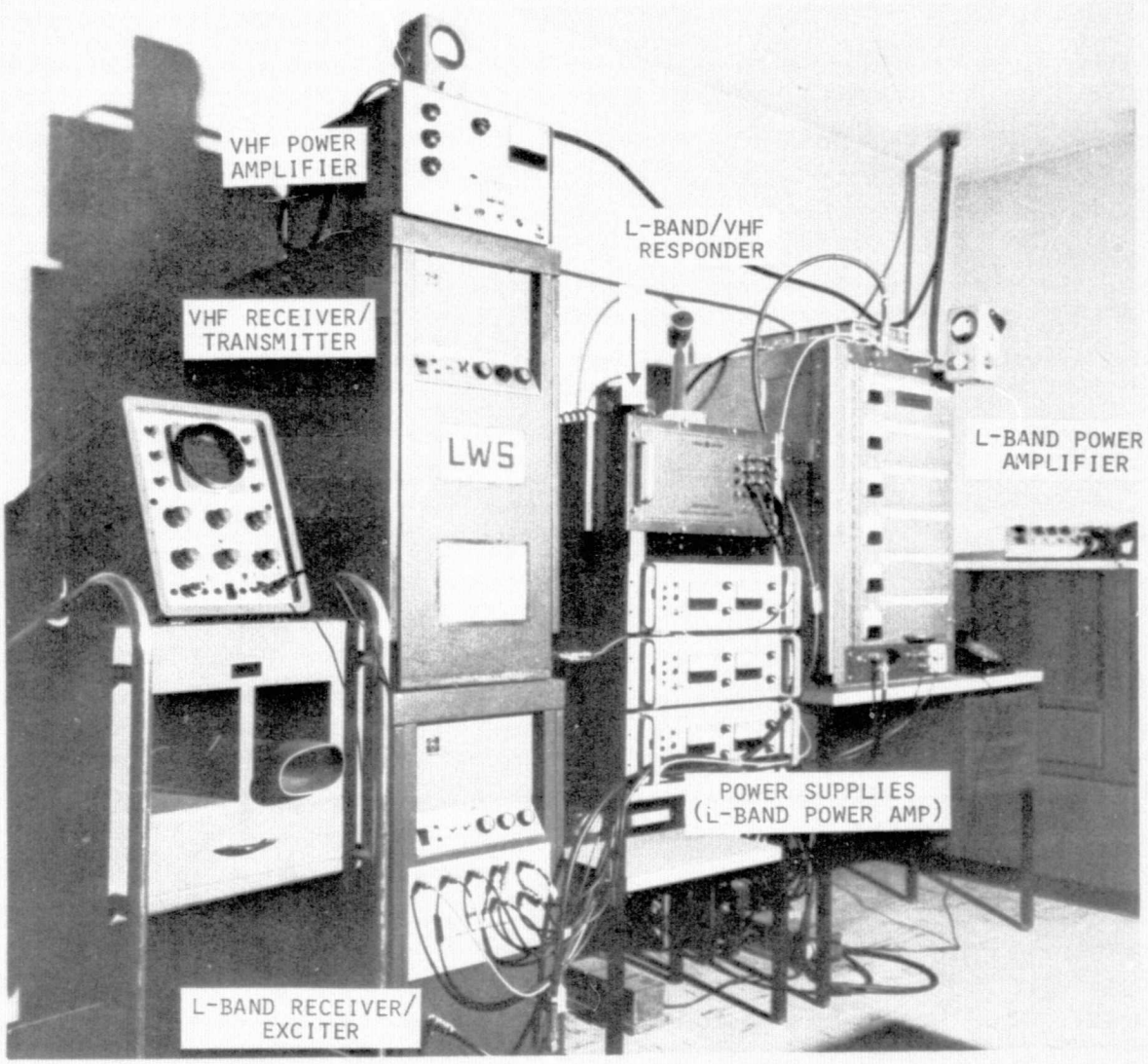

FIGURE 4.3 L-BAND/VHF TRANSPONDER IN BUENOS AIRES, ARGENTINA

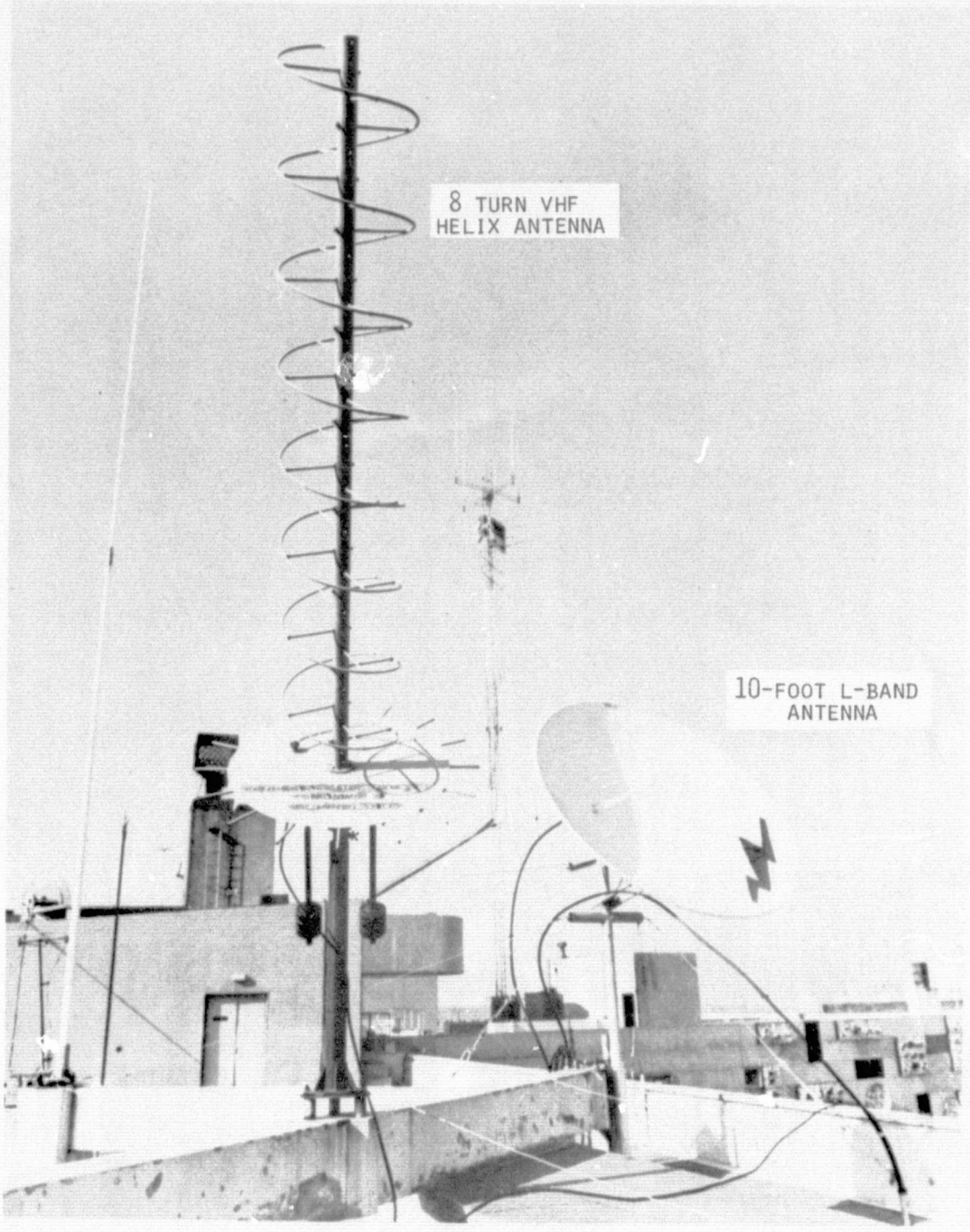

FIGURE 4.4 L-BAND AND VHF TRANSPONDER ANTENNAS IN BUENOS AIRES, ARGENTINA

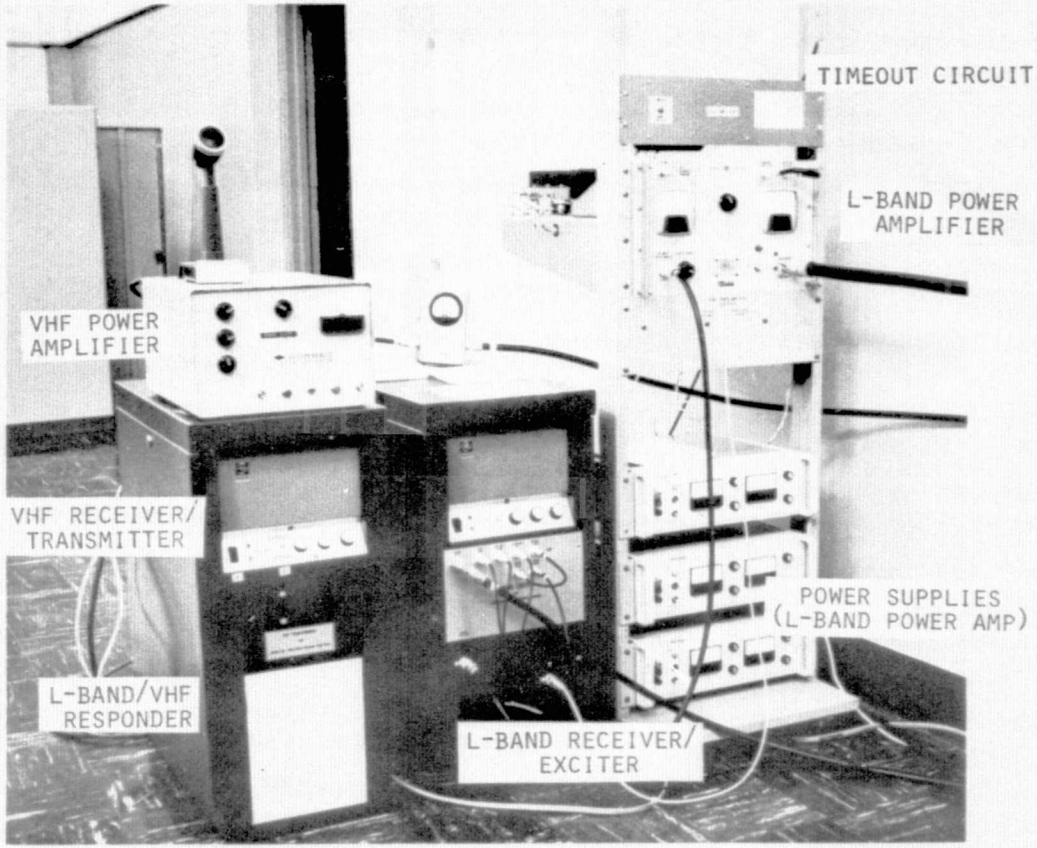

FIGURE 4.5 L-BAND/VHF TRANSPONDER IN HAWAII

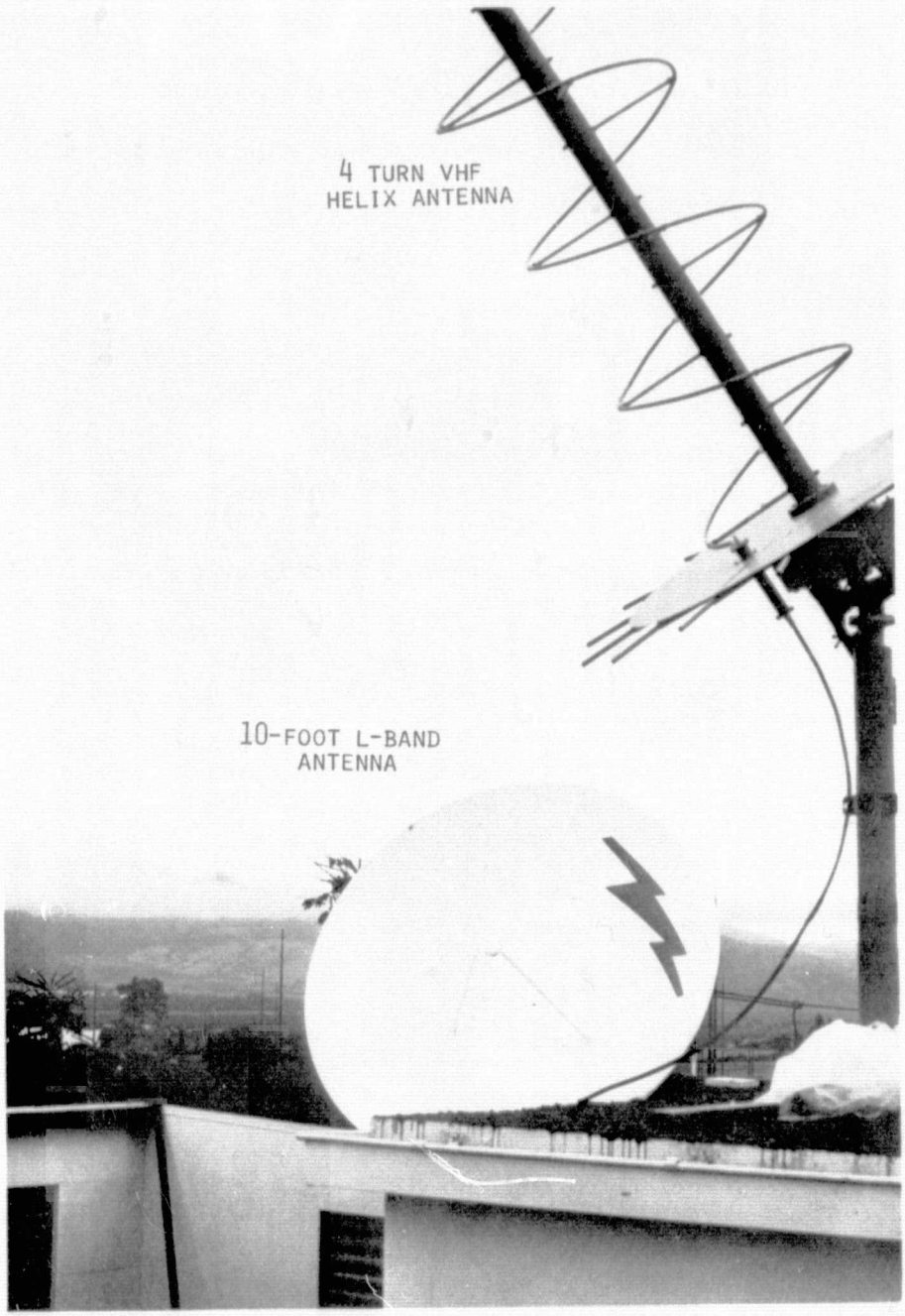

FIGURE 4.6 L-BAND AND VHF TRANSPONDER ANTENNAS IN HAWAII

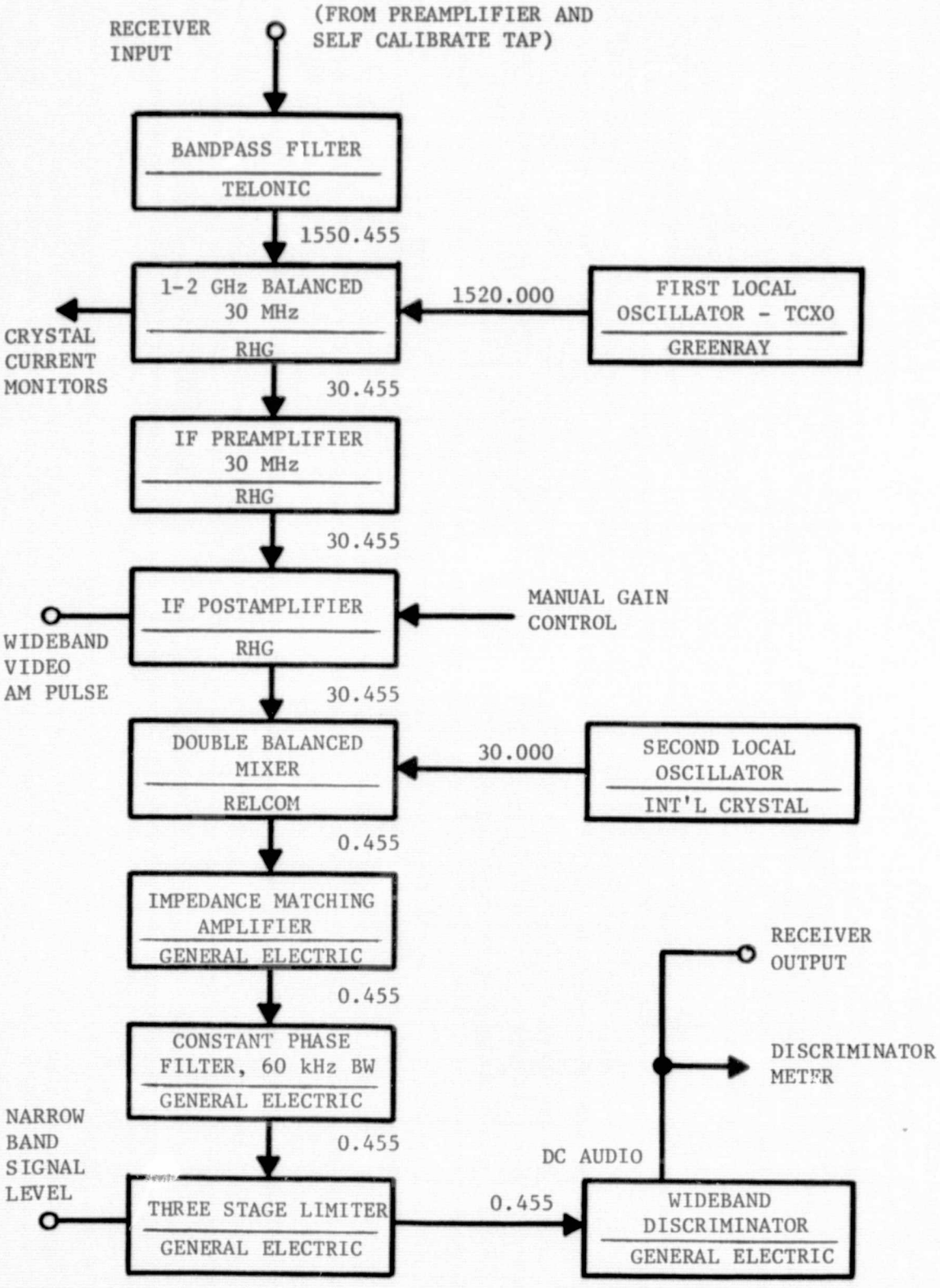

FIGURE 4.7 L-BAND TRANSPONDER RECEIVER

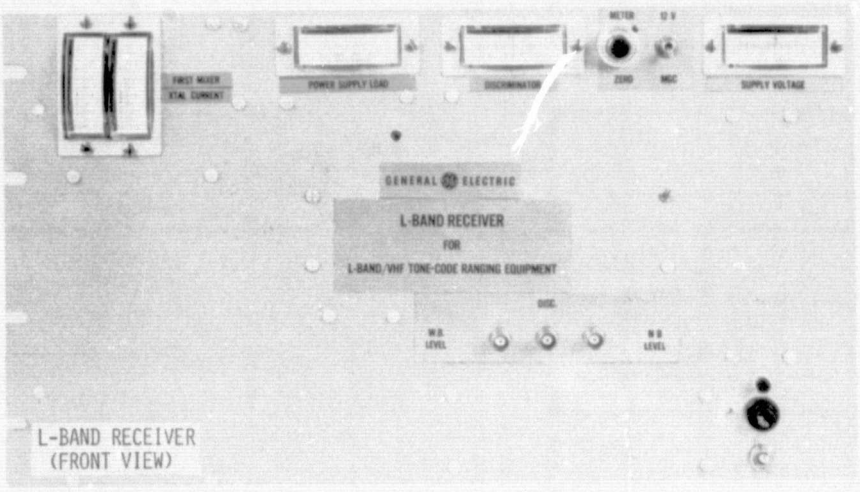

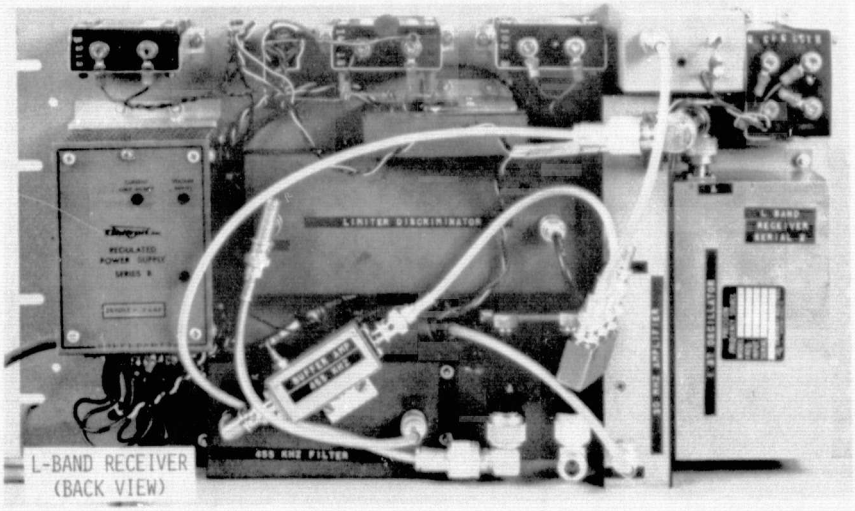

FIGURE 4.8 L-BAND TRANSPONDER RECEIVER
(Top photograph is front view; bottom photograph is back view with back cover removed)

Modules making up the receiver have not been individually tested to determine whether or not they conform to the manufacturer's specifications. The receiver has been tested as a whole to determine if overall system performance is acceptable. Essential receiver characteristics are tabulated in Table 4.6.

4.6.2 Responder Unit

The responder unit shown in the photographs of Figure 4.9 is the digital logic center of the L-band/VHF transponder and performs the functions of automatic response to tone-code interrogations, timing control, and data readout. It accepts audio frequency signals from the L-band and VHF receivers and operates in the following sequential manner:

- matches the phase of a locally generated tone with the phase of the received tone,
- recognizes its unique digital address code and subsequently generates a response at L-band and VHF,
- performs necessary timing functions to match the response delay with the "window" of the spinning ATS-5 satellite, and
- digitizes the manual settings of the delay thumbwheel switches, the number of address code bits in error at correlation, and the responder internal time delay allowing them to be transmitted as digital data following the tone-code ranging response.

A detailed description of the operation of the responder may be found in the "Operation and Maintenance Manual, L-Band/VHF Transponder."[7]

The L-band/VHF responder is designed to respond at both L-band and VHF after either L-band or VHF correlation has occurred. Disabling the appropriate transmitter will prevent unwanted RF transmission. Audio tone frequencies of 9.7656 kHz and 2.4414 kHz are used at L-band and VHF, respectively.

Many of the responder processes are the same for L-band and VHF, so that the following description applies to either frequency band unless otherwise specified. Figure 4.10 depicts a simplified block diagram of the responder.

The audio output of the receiver passes through the appropriate low pass and bandpass filters which reduce noise that may be present on the received signal. The audio frequency tone is applied to a zero crossing detector and to a tone recognition circuit. The zero crossing detector hard limits the signal accurately about its zero crossings producing a square wave with precisely defined rise and fall times corresponding to the zero crossings of the input audio frequency tone. The tone recognition

TABLE 4.6

L-BAND TRANSPONDER RECEIVER CHARACTERISTICS

Received Center Frequency	-	1550.455 MHz fixed
Stability	-	0.0001%
RF Bandwidth	-	50 MHz at 3 dB
First IF Bandwidth	-	10 MHz at 3 dB
Second IF Bandwidth	-	60 kHz
Sensitivity	-	-171.6 dBm/Hz
Detection	-	FM
Audio Output	-	0.06V peak/kHz deviation
Auxiliary Outputs	-	30 MHz Wideband video (AM) detector 0.455 Narrowband AM (envelope) detector (signal level)

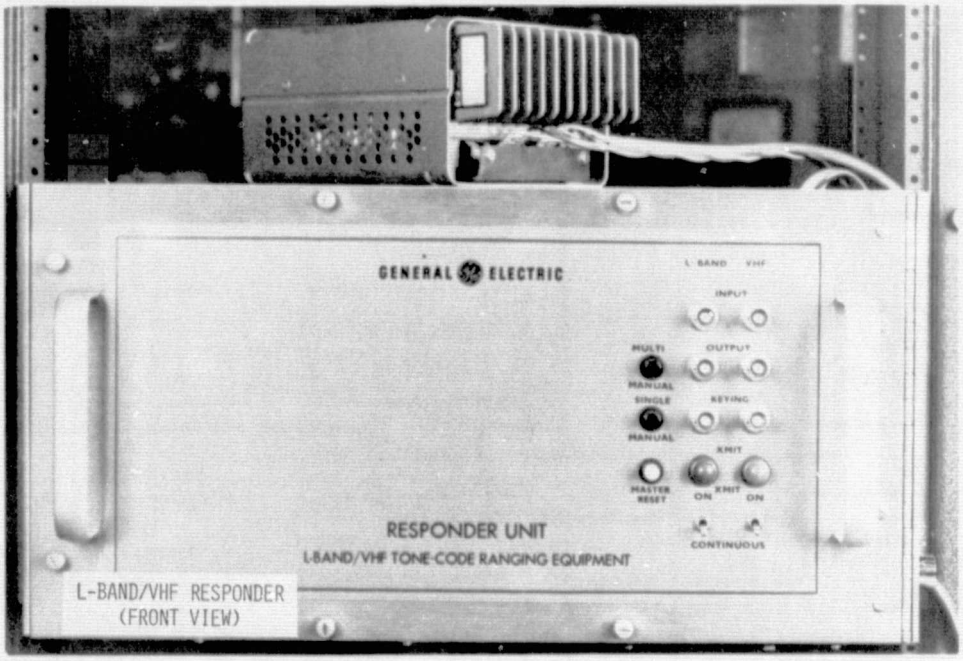

L-BAND/VHF RESPONDER
(FRONT VIEW)

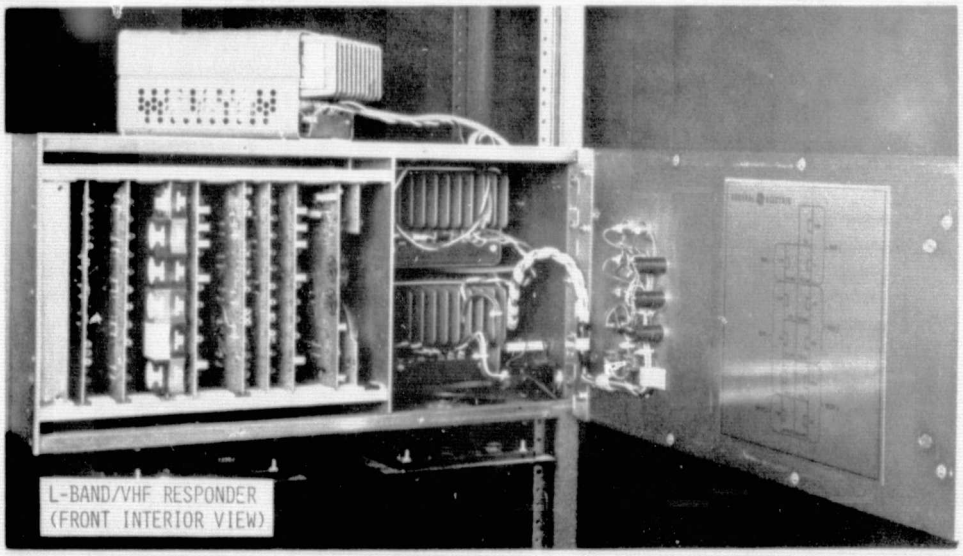

L-BAND/VHF RESPONDER
(FRONT INTERIOR VIEW)

FIGURE 4.9 L-BAND/VHF RESPONDER

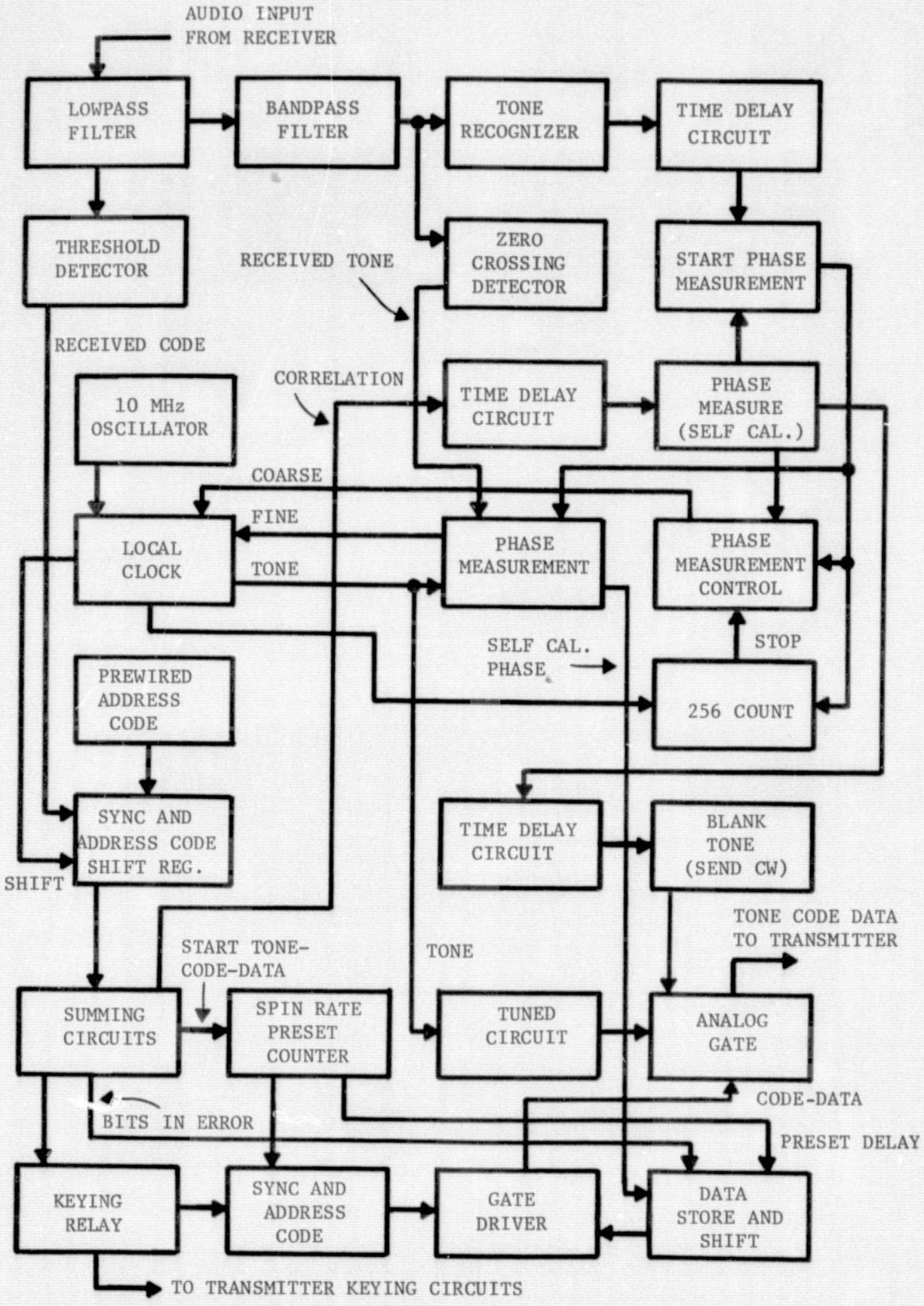

FIGURE 4.10 RESPONDER FUNCTIONAL DIAGRAM

circuit consists of a narrow bandwidth filter and switching circuit that produces a zero output under no-tone conditions and positive output when tone is present. Interlocking the L-band and VHF tone recognition circuits causes selection of the first received tone in circumstances where tones are detected in both receivers.

Applying the output of the tone recognition circuit to a time delay circuit insures that the phase measurement process does not start before the filters have arrived at a steady state. The time delay is 20-30 msec at L-band and 200-300 msec at VHF.

When tone has been recognized and the time delay circuit has allowed sufficient time for the steady state phase to be reached, a start pulse stops the responder clock. The 10 MHz oscillator drives this clock which generates the local 9.7656 kHz and 2.4414 kHz tones. The clock is restarted on the next zero crossing of the received waveform, making a coarse adjustment in the setting of the clock such that the received and locally generated tone phases are within $\pm$ 5 μsec. The received and locally generated tones are in the form of square waves from the zero crossing detector and the clock, respectively.

Fine phase matching continues through the next 256 audio tone cycles. Counters accumulate the phase differences between the rising and falling edges of each cycle of the received tone and locally generated tone. A fine adjustment in the setting of the responder clock is based on the mean phase difference over 256 cycles. Averaging over 256 cycles instead of relying on a single comparison reduces the phase matching error due to phase jitter on the received tone by a factor of 16.

Following completion of phase matching, the receiver output signal is passed through a lowpass filter, on to a threshold detector for code, and to a 30-bit synchronization and address code shift register. In the event that the received address code matches that prewired into the responder, correlation occurs and control circuits initiate a ranging response. As the output of the threshold detectors is hard limited, the random nature of noise may sometimes generate a sequence of 1's and 0's that correspond to the unique digital address code of the responder. Correlation would thus occur prematurely. Noise may also precipitate the exchange of 1's and 0's in the received address code. Correlation may only occur in an adjustable 10 to 30 msec code "window" which is opened immediately following fine phase matching. Preadjustment of the responders allows correlation to occur with up to two bits in error.

A preset counter with three octal (0-7) thumbwheel switches controls the number of tone cycles sent to the L-band transmitter before the responder sends the sync word and address code, thus providing for passage of the ranging response through the "window" of the spinning ATS-5 satellite. The position of each switch is stored as a digital number in a data buffer. The prewired minimum number of tone cycles is 3956, corresponding to 405094.4 μsec. Adjusting the thumbwheel switches can increase this delay in increments

of 409.6 μsec. The present counter controlling the number of VHF tone cycles is prewired for a delay of 577945.6 μsec.

Upon correlation, the responder counts down from both preset counters while generating 9.7656 kHz and 2.4414 kHz audio frequency tones in phase with the received tone. When the appropriate counter has reached 174, the 15-bit synchronization word and 15-bit digital address code are transmitted. When the counter has reached 144, data is transmitted; when the counter has reached 0, the ranging response has been completed and transmission ceases.

During tone transmission, reactive signal samplers on both the L-band and VHF transmit cables remove small fractions of RF power. Mixers translate these RF signals by the same amount that they would be translated in the satellites (101.020 MHz for L-band and 13.620 MHz for VHF). The resultant transponder self calibration signals are injected into the appropriate receive cables by the same type of reactive signal samplers. If the responder correlated on an L-band ranging interrogation, the phase of the L-band self calibration tone is compared against the phase of the tone transmitted at L-band. VHF phase comparison is not allowed even if the VHF transmitter were enabled. The reverse would occur for a VHF correlation.

The self calibration phase measurement sequence starts exactly 135 msec after correlation. The phase measurement gate is reopened starting the 256 tone cycle counter and clearing the phase measurement register. Over 256 cycles, the average of the time differences between the received and transmitted rising edge and between the received and transmitted falling edge is divided by 256 and accumulated in the phase measurement register. An increasing count in the phase measurement register from 0000 to "n" indicates that the received tone phase leads the transmitted tone phase by n tenths of microseconds, where n is an octal number. A decreasing count in the phase measurement register from 4096 (0000) to "n" indicates that the received tone phase lags the transmitted tone phase by 4096-n tenths of microseconds.

The operation of the responder self calibration circuits is hardware controlled; no checks on tone presence or quality are made. If the responder correlated on an L-band interrogation, it will compare 256 cycles of phase of any signal at the L-band input with the phase of the outgoing L-band tone. If the self calibration RF loop is not installed or if the self calibration RF power is inadequate or noisy, phase measurement will still proceed on noise and a meaningless value of phase will appear in the phase measurement register. Data processing systems must be capable of distinguishing between acceptable and meaningless self calibration measurements; erroneous values must be discarded.

The number of received address code bits in error during correlation, the settings of the manually adjustable thumbwheels specifying the responder time delay, and the self calibration phase measurement are saved as digital

numbers in a data buffer. The response ranging tone is applied through a lowpass filter converting the square waveform to a sinusoidal waveform for frequency modulation on the appropriate carriers. When the address code is to be transmitted, the sequence of 30 binary numbers is shifted synchronously with the audio tone cycles to suppress one audio cycle for a "0" and to transmit one audio cycle for a "1". 48 bits representing the stored data on bits in error, the setting of the thumbwheel switches, and the self calibration phase measurement, are clocked into the gating circuit at one-third the clock rate to suppress three consecutive audio tone cycles for a logical "0" and allow the transmission of three consecutive tone cycles for a logical "1". The divide by three circuit is adequate for the transmitted data rate, the lower rate insuring that the received data will have a low bit error rate.

Following completion of the tone-code-data transmission, the responder is muted for 0.35 seconds to prevent the tone recognition circuits from initiating a response on the satellite return of the transponder's response. At the end of the muting period, the responder is ready for the next interrogation.

4.6.3 L-Band Exciter

The remote L-band transponders and the Observatory utilize the same type of L-band exciter, as sketched in Figure 4.11 and as photographed in Figure 4.12. The main component of the exciter is a commercial UHF base station transmitter operating at 412.869 MHz with a frequency stability of $\pm$ 0.0002%. Either the 9.7656 kHz audio frequency output tone of the responder or a voice channel frequency modulates the transmitter through a maximum 5 kHz deviation. A passive varactor 4X frequency multiplier generates the L-band transmit frequency of 1651.475 MHz and thereby increases the effective modulation index of the transmitter to approximately 2. Spurious sideband output signals from the frequency multiplier are at least 30 dB below the center frequency power and are further reduced by a bandpass filter on the output of the exciter. A nominal power level of 0.3 to 0.5 watts at 1651 MHz drives the L-band power amplifiers at the remote sites. The L-band exciter output frequency can be changed over a limited range by exchanging the crystal in the UHF transmitter.

4.6.4 Buenos Aires L-band Power Amplifier

The L-band power amplifier stationed in Buenos Aires is a first generation engineering prototype 300-watt solid state device developed by the Heavy Military Electronic Systems Products Department (HMED) of the General Electric Company in Syracuse, New York. The amplifier as sketched in Figure 4.13 develops the prescribed gain and power output by using a total compliment of 122 transistors. Individual transistors are conservatively rated at 5 watts CW output each and are combined in pairs via -3 dB quadrature hybrids. The high power level is achieved by combining appropriate numbers of dual transistor modules. The photograph of Figure

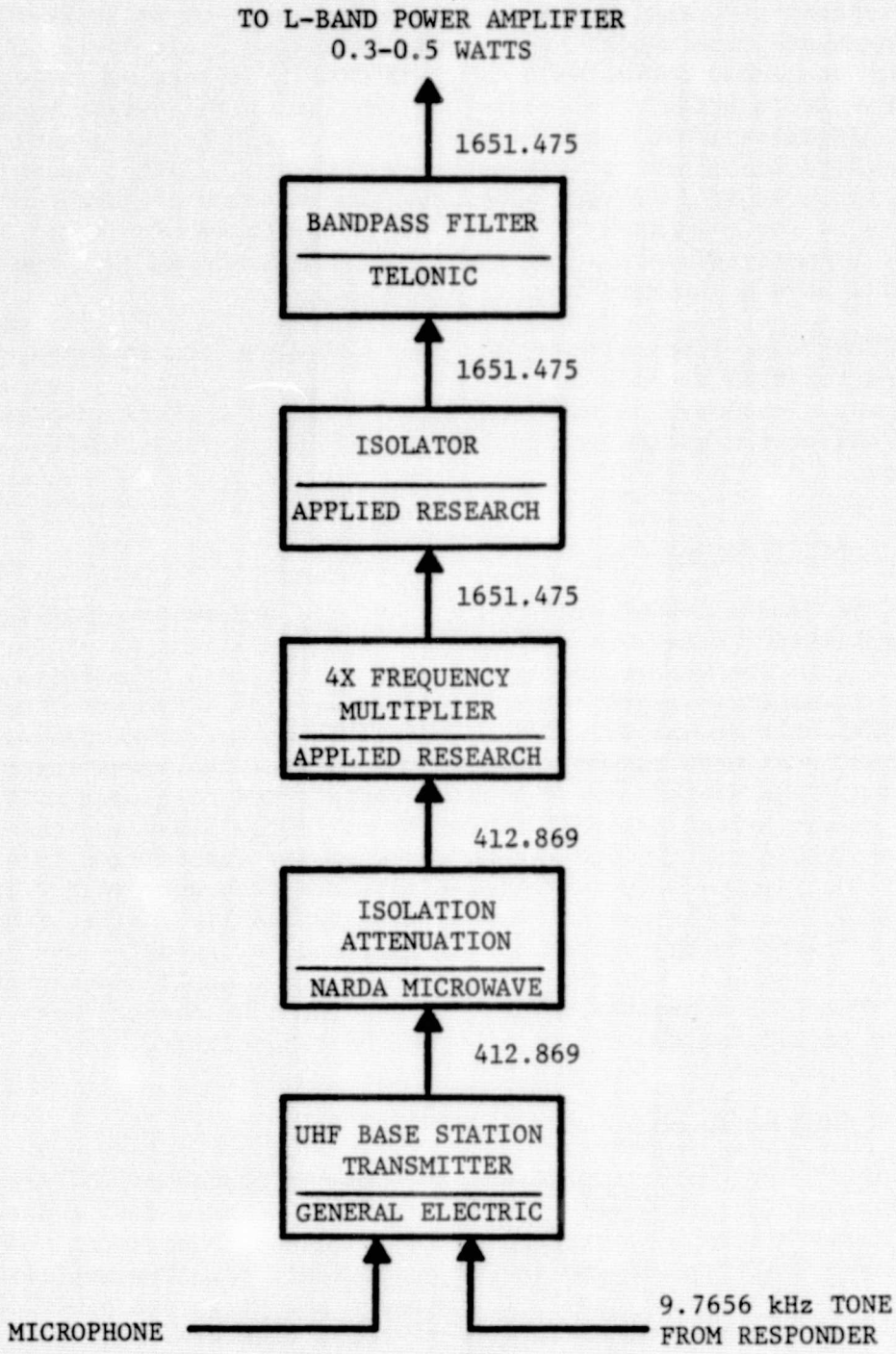

FIGURE 4.11 L-BAND EXCITER

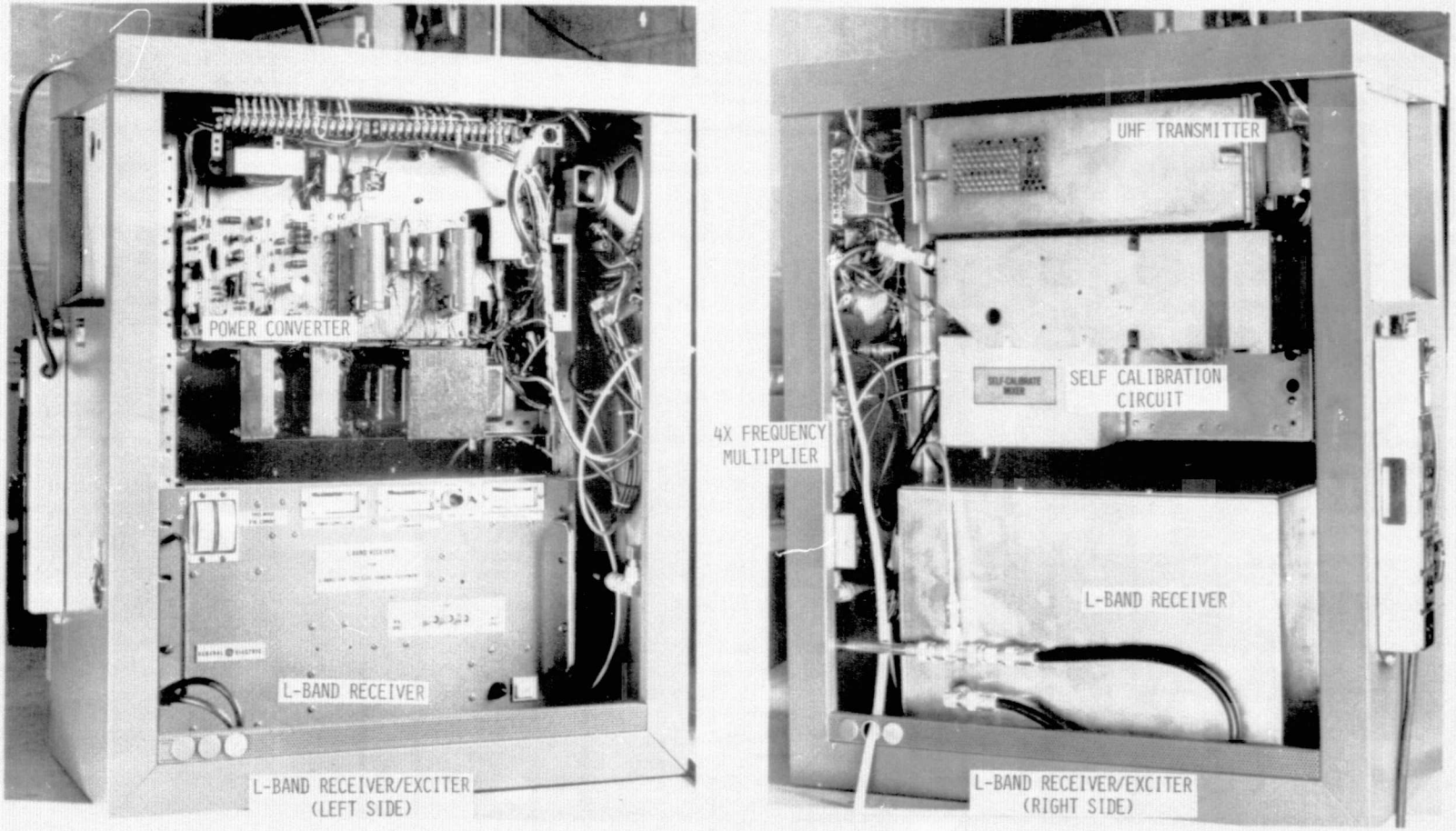

FIGURE 4.12 L-BAND EXCITER

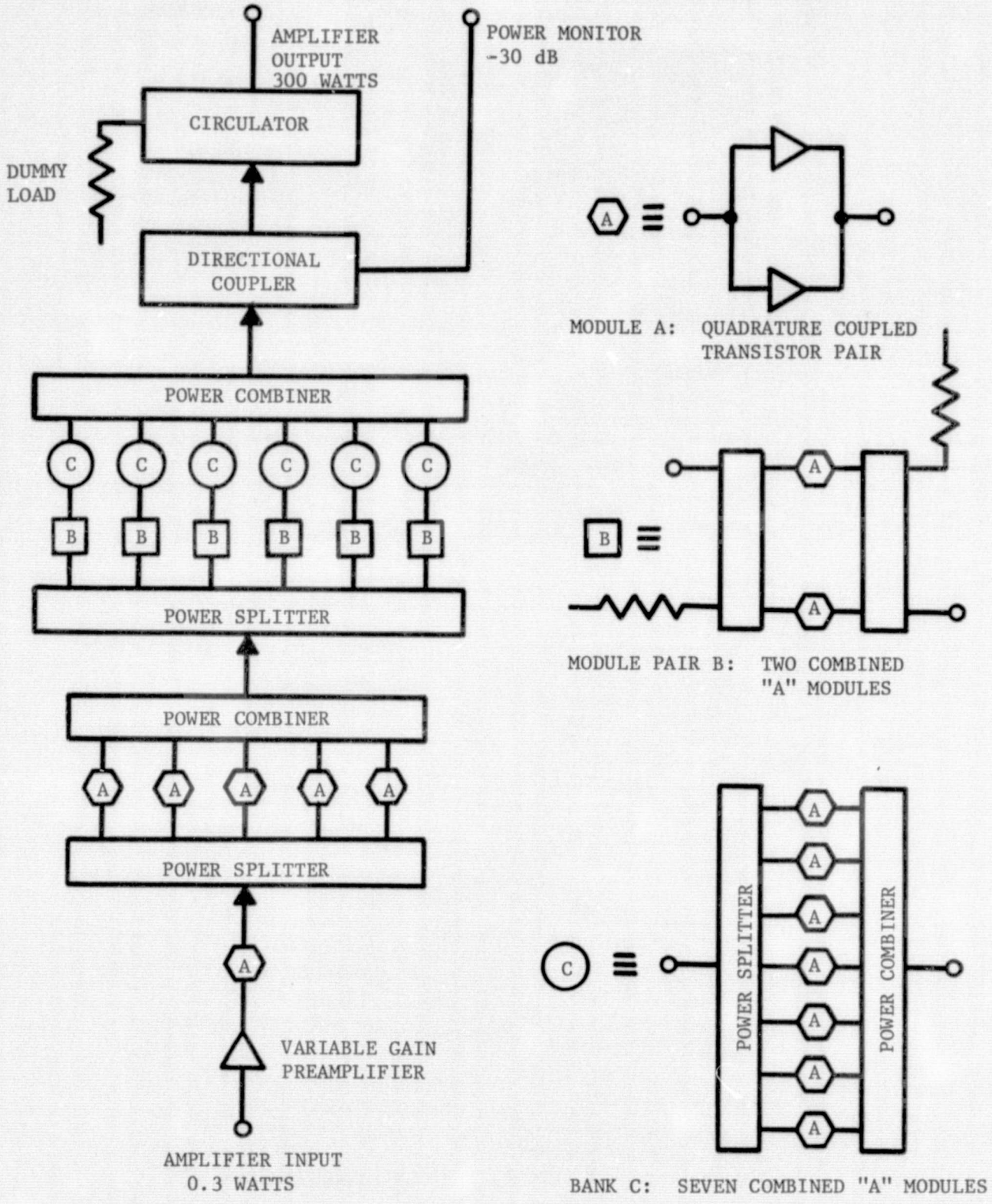

FIGURE 4.13 L-BAND POWER AMPLIFIER IN BUENOS AIRES, ARGENTINA

4.14 shows the various stages of the power amplifier from the input variable gain preamplifier through the intermediate and driver amplifiers to the final output power banks. Table 4.7 lists the performance specifications for this amplifier.

The final output stage contains 84 transistors combined in six banks of 14 transistors (seven modules of two transistors each). At this level, the banks are combined with their own drivers, each driver consisting of a pair of modules (four transistors). Input drive power to the combination of six driver/banks is approximately 32 watts. Ten combined transistors (five combined modules) driven by a single module, develop this intermediate power level. The first stage variable gain module is the only one which differs from the others. Power output control of the amplifier is accomplished by varying the collector supply voltage and thus limiting the saturated power output of this module. The first stage is capable of a maximum two watts output. This amplifier requires a nominal input power level of 0.3 watts.

The collector current of each transistor in the final output stage can be separately monitored. If an individual transistor in the final output stage fails, the output power of the amplifier will be reduced by approximately 0.05 dB. Consequently, failure of many output transistors will not seriously affect the performance of the amplifier. Should a single transistor in a driver for an output power bank fail, all transistors in the bank will show an approximate 3 dB reduction in output power. Should a single transistor in the intermediate bank of five modules fail, the entire amplifier will show an approximate 5 dB reduction in output power. If a transistor in the second stage module fails, the amplifier will generate no RF output power. Each of these three failures, however, can be immediately rectified by substituting a good module from the final output stage for the defective module, thus incurring only a 0.05 dB power loss instead of those stated above. As the first stage module is different from all others, it must be repaired should a failure occur. The amplifier is thus seen to have a graceful degradation. Totally disabling failures are very unlikely.

An RF output power monitor (30 dB below the main RF power) on the front panel of the amplifier provides an indication of overall amplifier performance. A circulator in the main output line protects the unit against short periods of high VSWR. A timer connected to the amplifier keying circuit will automatically turn off the transmitter after five minutes of CW. This protects the ATS-5 satellite from accidentally being saturated during non trilateration schedules.

4.6.5 Hawaii L-Band Power Amplifier

The L-band power amplifier stationed in Hawaii is a second generation prototype 300-watt solid state device developed by HMED and is on loan to NASA for the duration of the ATS-5 Trilateration Support program. As sketched in Figure 4.15, the amplifier develops the prescribed gain and power output

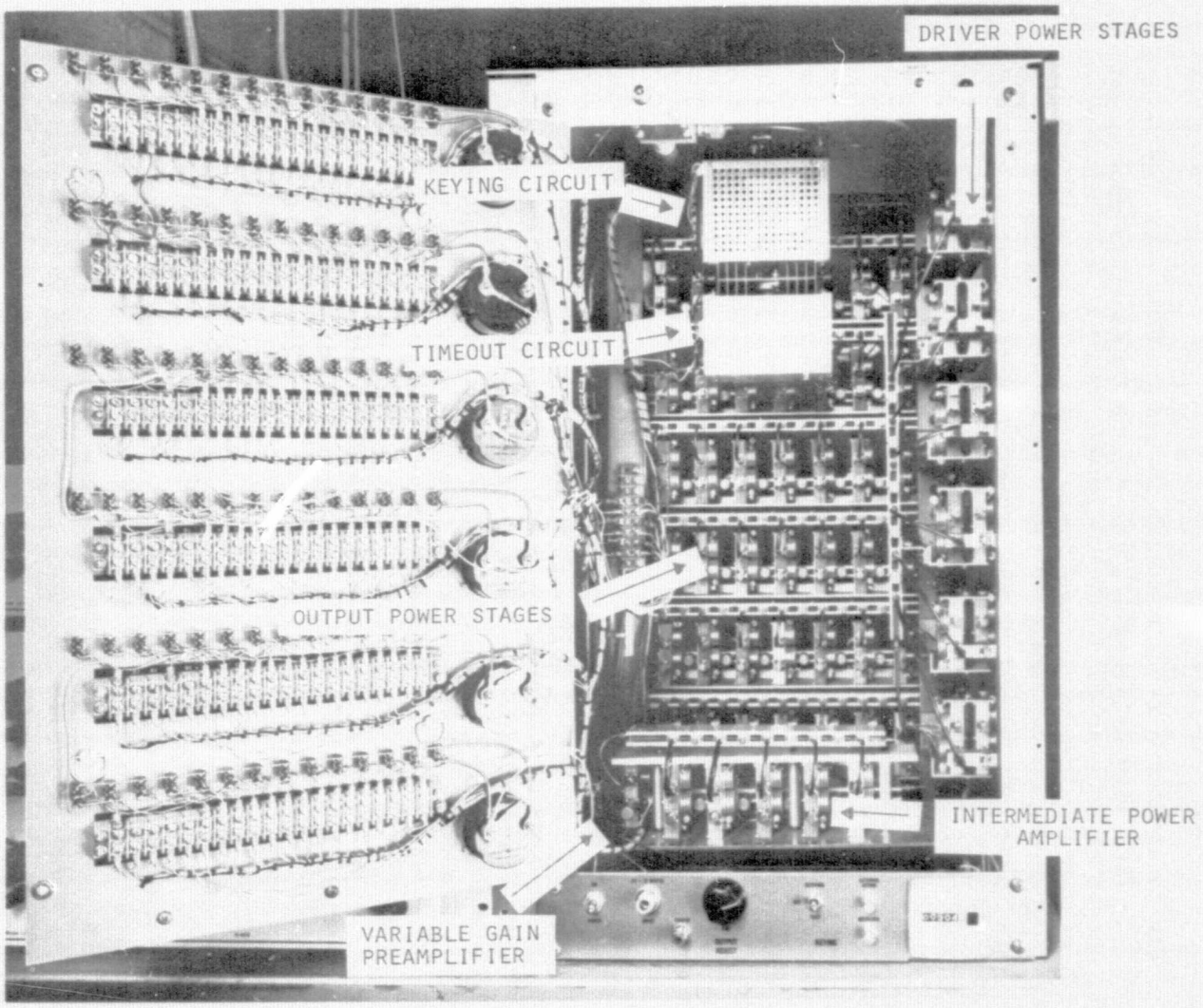

Figure 4.14 L-Band Power Amplifier in Buenos Aires, Argentina

TABLE 4.7

300-WATT CW L-BAND TRANSMITTER

Output Power	300 Watts CW
Frequency	1650 MHz
Bandwidth	~50 MHz (-1 dB points)
Gain	30 dB Minimum
Efficiency	30% Minimum (DC to RF)
Input VSWR	1.2:1
Load VSWR	Will tolerate short circuit to open circuit
Operating Temperature	40^{o}F to 100^{o}F
Noise Figure	20 dB
Supply Voltage	+26V DC
Current per Transistor	< 0.62 amps at 5 watts out
Physical Configuration	19" Rack mounted
Cooling	Forced air ventilation

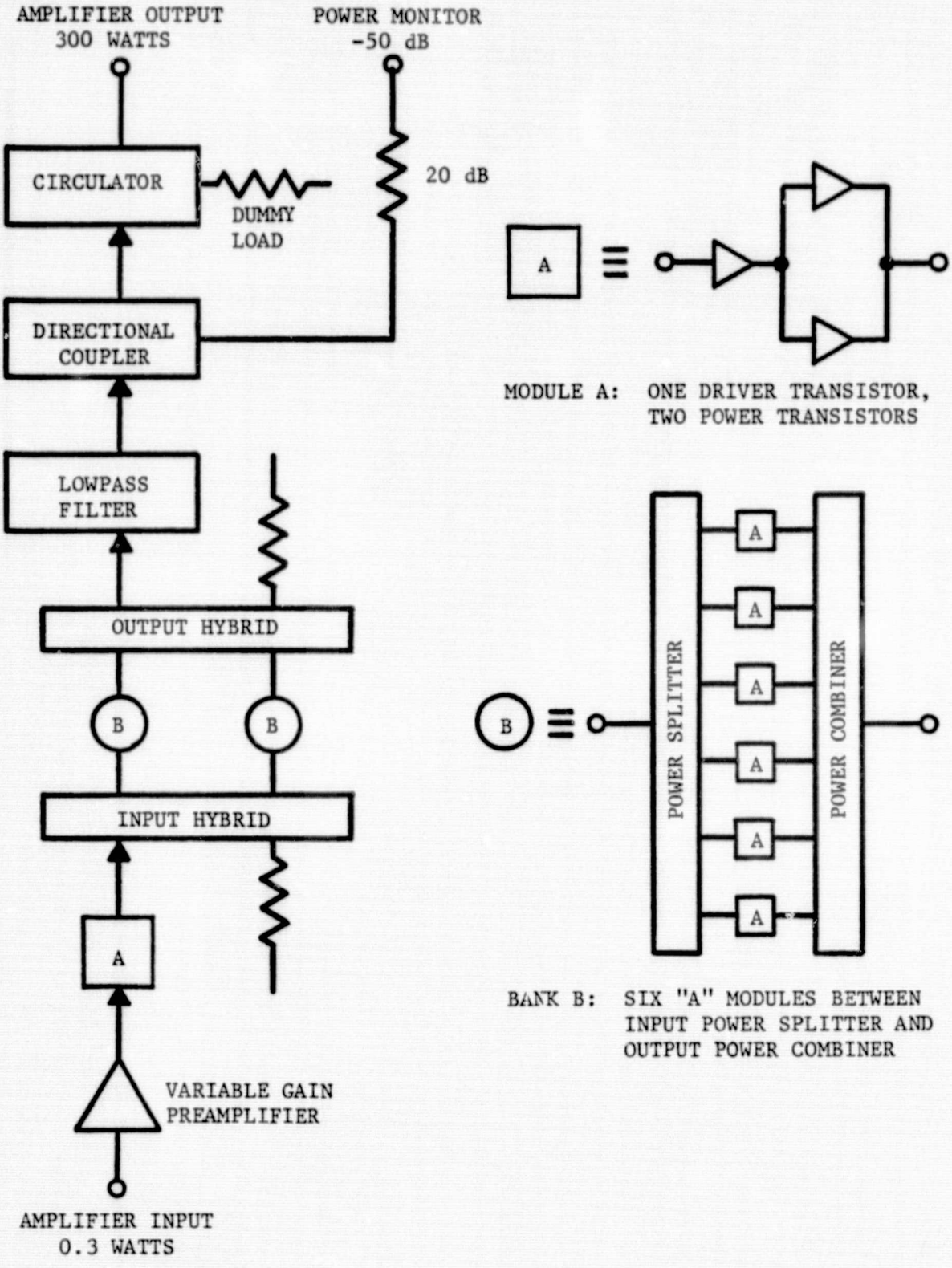

FIGURE 4.15 L-BAND POWER AMPLIFIER IN HAWAII

by using a total compliment of 41 transistors. The output power transistors are conservatively rated at 15 watts CW output each. The performance of this amplifier is similar to that of the first prototype unit, as listed in Table 4.7.

This amplifier contains 13 identical power modules, one operating as a driver and the remainder operating as output power devices. These modules contain two output power transistors and a single input driver transistor. The driver transistor requires two watts of RF power to produce a saturated output power of approximately 25 watts. Varying the collector supply voltage to the first stage dual transistor preamplifier provides power output control by limiting the saturated power output of the module. The first stage is capable of a maximum two watts output; the nominal input power level is 0.3 watts.

The current drawn by each of the 13 power modules can be separately monitored. If an individual final output transistor in one of the 12 output modules fails, a power loss of 0.2 dB will result. If the driver transistor in the module fails, the entire module produces no significant power. A measurement of the current drawn by each module thus provides an indication to the performance of the transistors. As with the power amplifier stationed in Buenos Aires, a failure in the driver module can be immediately rectified by exchanging any output power module for the defective driver module, thus affecting only a 0.4 dB power loss instead of a complete outage. The amplifier is thus expected to provide a useful service even with several of its transistors inoperative.

An RF output power monitor (50 dB below the main RF power) on the front panel of the amplifier provides an indication of overall amplifier performance. A circulator in the main output line protects the unit against short periods of high VSWR. A timer connected to the amplifier keying circuit will automatically turn off the amplifier if CW transmissions exceed five minutes, thus protecting the ATS-5 satellite from being accidentally saturated during non trilateration schedules.

4.6.6 Self Calibration System

The purpose of the self calibration system is to provide a measure of the internal time delay experienced by the ranging signal as it passes through the transponder. The tuned circuits in the responder and various components of the RF sections may change the time delay of the ranging signal as a function of the environment or cable length.

The circuit sketched in Figure 4.16 depicts the RF sections of the L-band transponder self calibration system. A reactive signal sampler on the transmit line removes approximately 12 dBm from the 300-watt transmitted signal. This 1651.475 MHz signal is mixed with 101.020 MHz to yield 1550.455 MHz which is injected into the receive line at a level of approximately -90 dBm, thus appearing similar to the downlink from the ATS-5 satellite after the downlink has been preamplified.

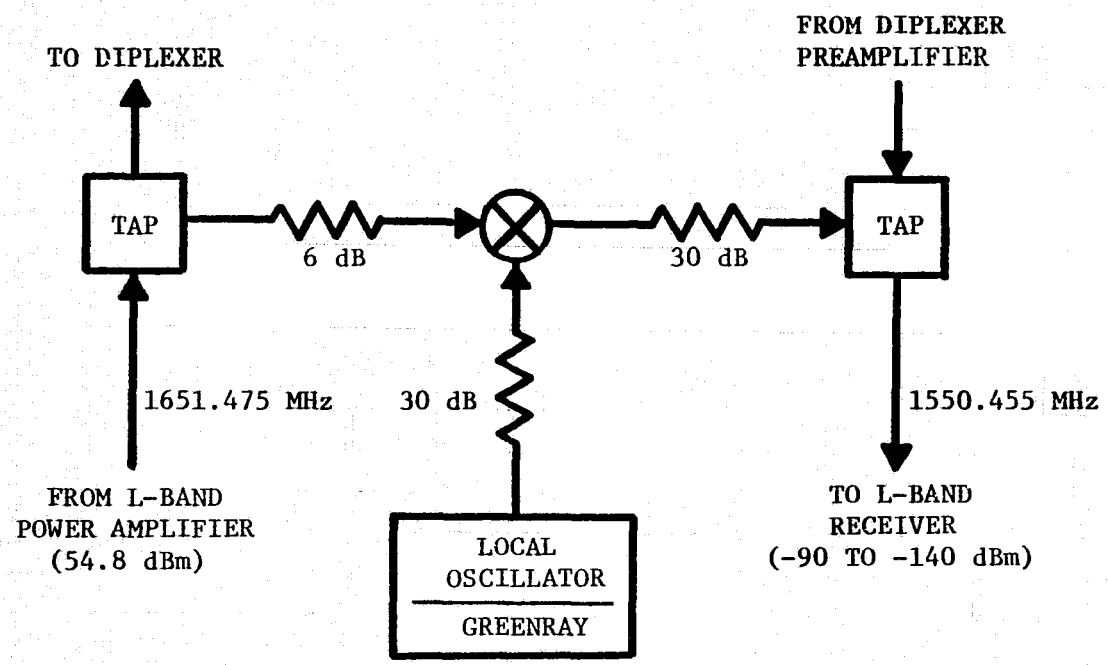

FIGURE 4.16 L-BAND TRANSPONDER SELF CALIBRATION LOOP

When the responder transmits its ranging response, approximately 5000 cycles of tone precede the code and data. The responder sees this tone via the RF self calibration loop and compares the phase of the tone at the input of the responder with that being transmitted. A counter preset at 409.6 μsec counts down the phase difference and loads the phase measurement as a digital number into the data buffer. A typical response of 370.0 μsec indicates a phase difference of 39.6 μsec.

The measured phase difference may vary through ± 2 μsec for temperature extremes in the transponder, or it may vary approximately 0.13 μsec for each 100 feet of cable length variation in the installation of the transponder and within the self calibration loop.

The self calibration loop does not measure the absolute signal delay through the transponder, only the phase difference. The absolute delay, however, can be easily determined by initial calibration measurements.

The Observatory self calibration system is similar to that employed at the two remote transponders with the exception that the RF signals are sampled and injected at the surface of the 30-foot parabolic antenna via a dipole antenna rather than at the transmit and receive cables via reactive signal samplers. As sketched in Figure 4.17, one port of a single balanced mixer is connected to a dipole antenna mounted on the surface of the 30-foot dish and the second to a local oscillator generating 101.020 MHz. The dipole antenna receives a 1651.475 MHz signal from the spiral feed of the 30-foot dish antenna and transmits 1550.455 MHz back into the spiral feed.

The Observatory receiver demodulates the self calibration signal and feeds it to the correlator which measures the ranging signal propagation time from the interrogator to the correlator. Referencing the signal propagation time to the surface of the antenna is particularly useful as it allows variations to be made in the entire RF/audio system without necessitating a remeasurement of cable length, etc. The Observatory is self-calibrated on every ranging interrogation.

4.6.7 L-Band Diplexer

The use of a diplexer instead of a transmit/receive switching relay at the antenna greatly increases the reliability of the L-band transponders. Furthermore, use of a diplexer at the Observatory facilitates the use of the surface of the 30-foot parabolic antenna as the reference point for the Observatory self calibration system.

The diplexer as sketched in Figure 4.18 and photographed in Figure 4.19 is used in the remote transponders and at the Observatory. The filter on the diplexer transmit leg is a notch filter at the receive frequency; on the receive leg, a similar filter rejects the transmit frequency. Both filters have a 500 kHz bandwidth at 75 dB rejection. The combiner which connects both filters to the antenna provides the proper transmission line lengths from the filters to the antenna; the line to the receive leg filter appears as an open circuit to the transmitter and vice versa. The 50 MHz wide band-

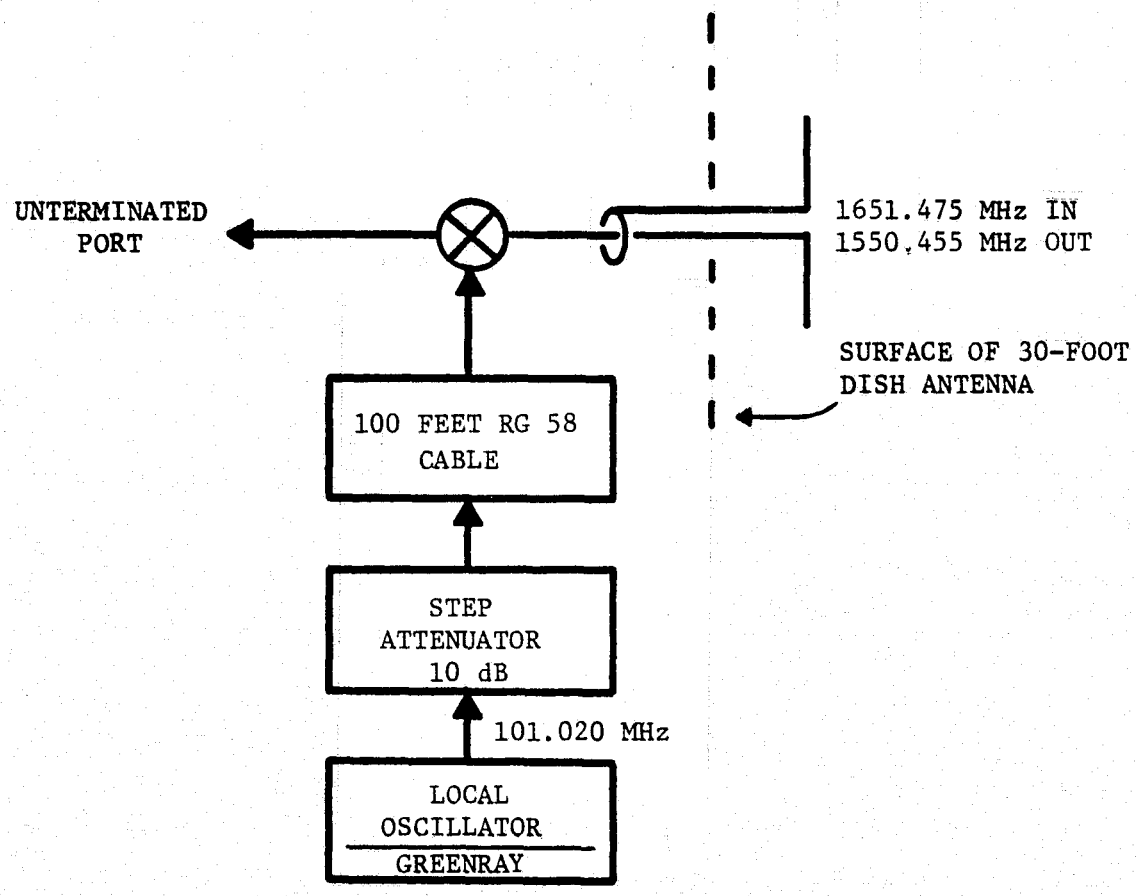

FIGURE 4.17 OBSERVATORY L-BAND SELF CALIBRATION UNIT

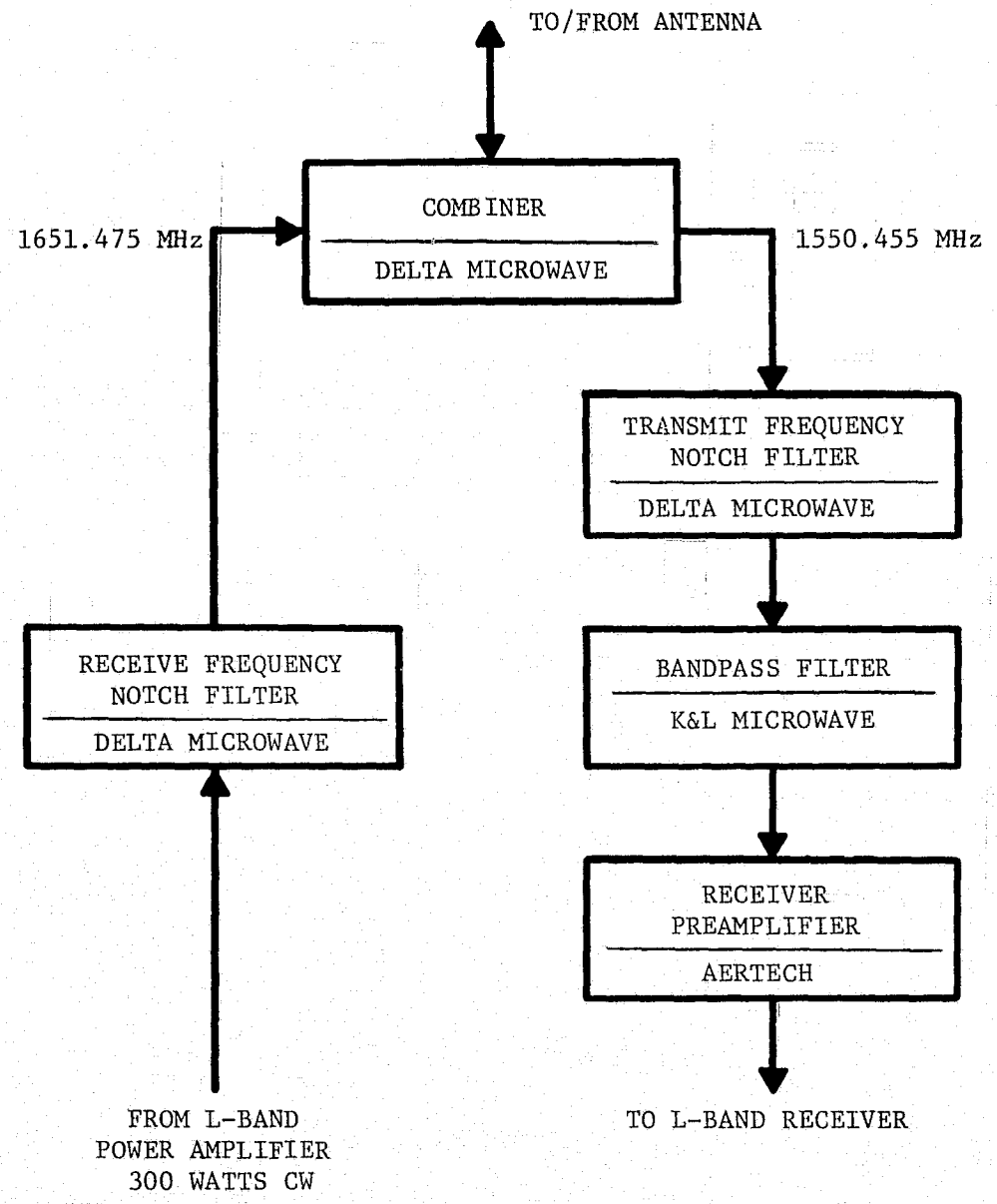

FIGURE 4.18 L-BAND DIPLEXER

FIGURE 4.19 L-BAND DIPLEXER

pass filter behind the receive leg notch filter prevents desensitization of the broadband preamplifier due to spurious emissions from the power amplifier or from sources outside the transponder. The solid state preamplifier generates approximately 23 dB gain and has a noise figure of less than 3.0 dB.

4.7 OBSERVATORY L-BAND SYSTEMS

The primary ground station for the General Electric L-band trilateration network is the Radio-Optical Observatory near Schenectady, New York, shown in Figure 4.20. The equipment configuration utilized at the Observatory for the operation of the network and the collection of data is detailed in Section 7 of this report.

4.7.1 Observatory L-Band Receiver

The Observatory L-band receiver sketched in Figure 4.21 is built in modular form to retain a capability for a wide variety of applications. After passing through the diplexer/preamplifier mounted behind the feed of the 30-foot dish antenna, L-band signals pass through the tunable bandpass filter of the L-band receiver and are immediately mixed with a locally generated 1520.000 MHz signal to produce the first IF at 30.455 MHz.

A manually controlled VCXO and two frequency multipliers generate the 1520 MHz first local oscillator frequency. A single crystal in the VCXO allows the first local oscillator frequency to be adjusted through tens of kHz. Replacement of the VCXO crystal allows the generation of first local oscillator frequencies over hundreds of MHz, the final frequency being limited only by the appropriate selection of a bandpass filter. Both frequency multipliers are broadband devices and the tunable amplifiers have ranges from 10 to 500 MHz. Consequently, the Observatory L-band receiver is fully tunable over the entire L-band spectrum, limited only by the bandpass filter and notch filter in the diplexer. If the Observatory self calibration system were to be hard mounted to the transmit and receive cables as in the remote transponders, the diplexer could be replaced with a transmit/receive switching relay, thus leaving virtually no limitation on the receive frequency.

The 30.455 MHz first IF passes to the remainder of the IF system and also to a monitor AM receiver. The beat frequency oscillator of the receiver is used to measure the IF frequency. Manual adjustments to the first local oscillator's VCXO are made until the first intermediate frequency is properly centered on frequency. The monitor receiver shows a drift of approximately 2 kHz during the first two hours of operation after turn-on. After two hours, virtually no drift can be seen.

A local oscillator referenced to the Observatory frequency standard generates 30.000 MHz. Mixing this frequency with the first IF produces the second IF of 0.455 MHz. From this point, the receiver consists of specially designed components which reduce the variation of signal phase as a function

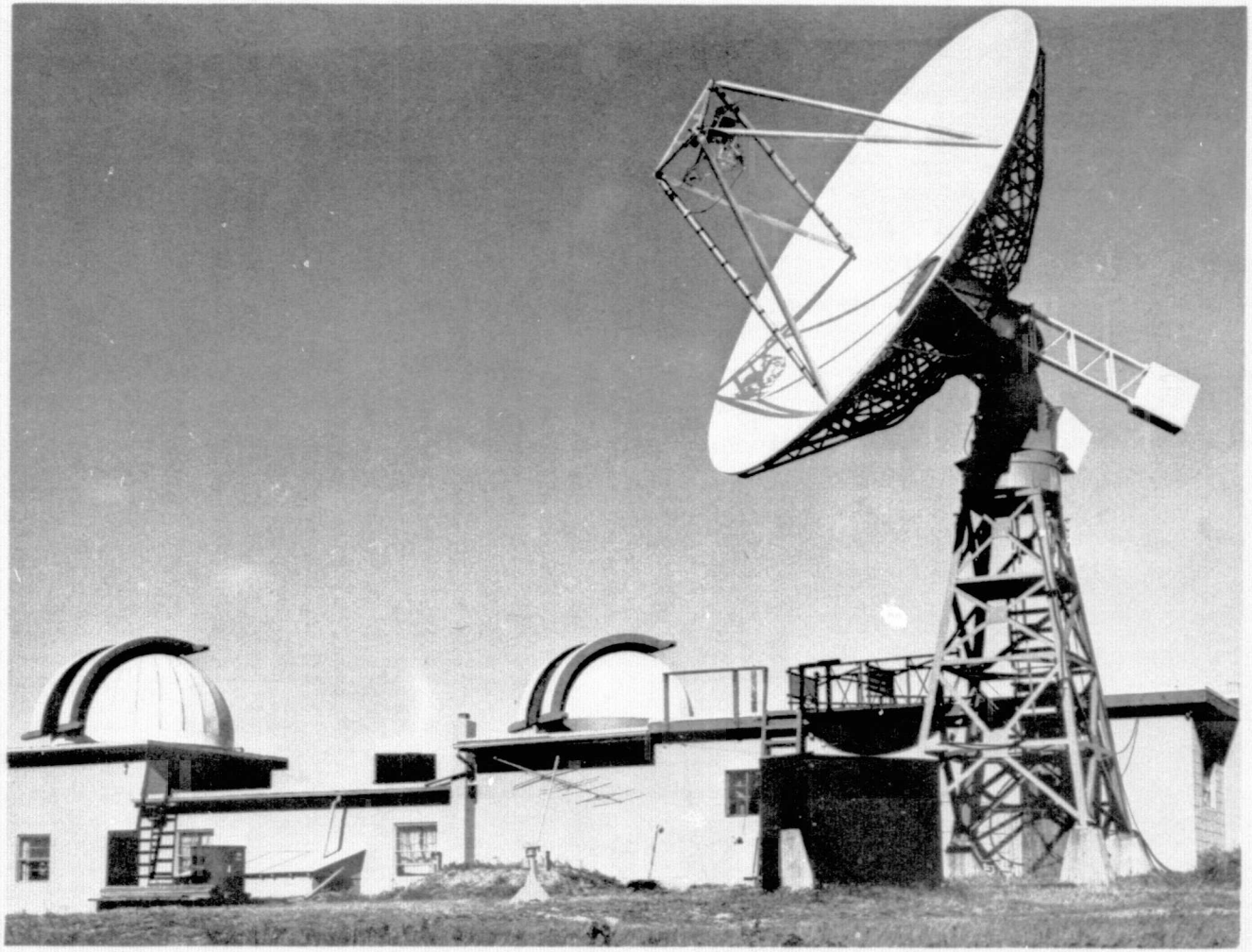

Figure 4.20 General Electric Radio-Optical Observatory, Schenectady, NY

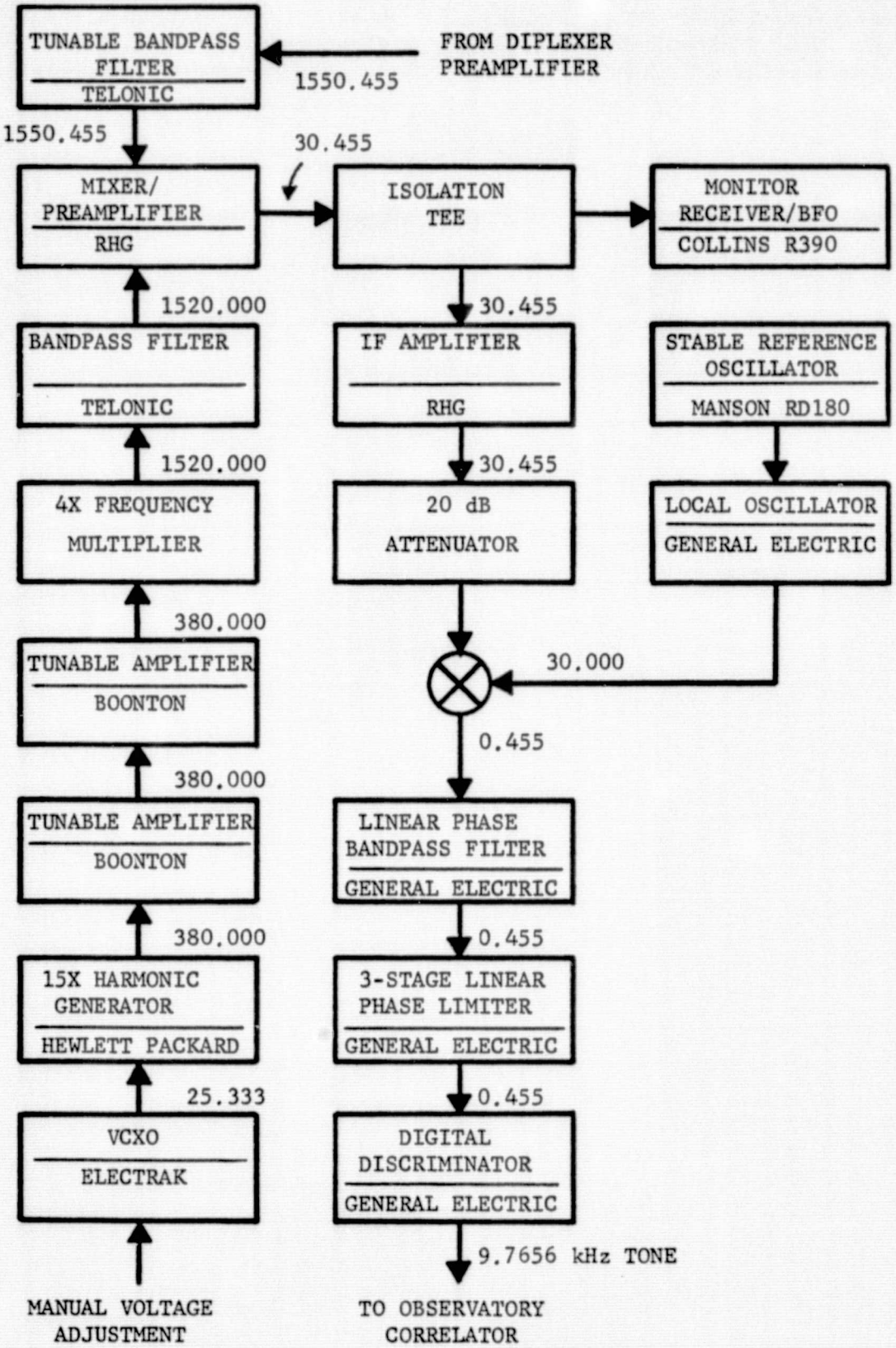

FIGURE 4.21 OBSERVATORY L-BAND RECEIVER

of signal amplitude. The 0.455 MHz second IF with a modulation index of 2 passes through a 60 kHz linear phase bandpass filter, through a three-stage linear phase limiter and lastly into a digital discriminator. The 9.7656 kHz ranging signals are then relayed directly to the Observatory correlator.

4.7.2 Observatory L-Band Transmitter

Audio frequency ranging interrogations from the Observatory tone-code generator pass to an L-band exciter identical to those employed in Buenos Aires and Hawaii (see Section 4.6.3) with the exception of a reduced output power at 0.04 watts. The signal is further attenuated before being passed to the Observatory L-band power amplifier, a commercial unit purchased from Microwave Power Devices. The amplifier develops 100 watts CW output power and has an overall gain of 60 dB.

SECTION 5

ANALYTICAL TECHNIQUES

5.1 THE KEPLER ORBIT

The a priori requirement for a simple model defining the orbital motion of the satellite excludes the consideration of the effects of the moon, sun, and non-spherical shape of the earth. Yet, the simplest of orbit models still utilizes six parameters. The motion of the satellite may be described as that of a freely falling body (Newtonian model) or as that of a body in an elliptical orbit with the gravitating mass at one focal point (Keplerian model). Both models describe the same physical phenomenon. The following discussion describes the motion of the satellite based on Kepler's three laws of planetary motion.

5.1.1 Orbit as a Conic Section

The first of Kepler's empirical laws of planetary motion states that every planet moves in an ellipse with the sun at one focus. Neglecting the influences of the sun, moon, and other planets, the orbit of a satellite about the earth will then, according to Kepler's first law, also be that of an ellipse.

An ellipse is one of the three types of conic sections, where a conic section is defined as the locus of points P for which the distance from P to a fixed point F, the focus, is a constant ratio to the distance from P to a fixed line, the directrix. This constant ratio is defined as the eccentricity ε. Figure 5.1 depicts the geometry defining a conic section.

In Figure 5.1, the x_o axis defines the axis of symmetry, with the origin of the x_o, y_o coordinate system centered at one focus. The angle θ between the radial distance r from the focus to the conic is termed the true anomaly, and p, the value of y_o at $x_o = 0$, is termed the semilatus rectum. The equation of a conic thus becomes

$$p/\varepsilon - r/\varepsilon = x_o = r \cos \theta \ , \tag{5.1}$$

or

$$p = r(1 + \varepsilon \cos \theta) \ . \tag{5.2}$$

Integration of the Newtonian differential equations of motion[8] for a body in an inverse square gravitational field yields the same general relation

$$\frac{1}{C} = r(1 + \varepsilon \cos \theta) \ . \tag{5.3}$$

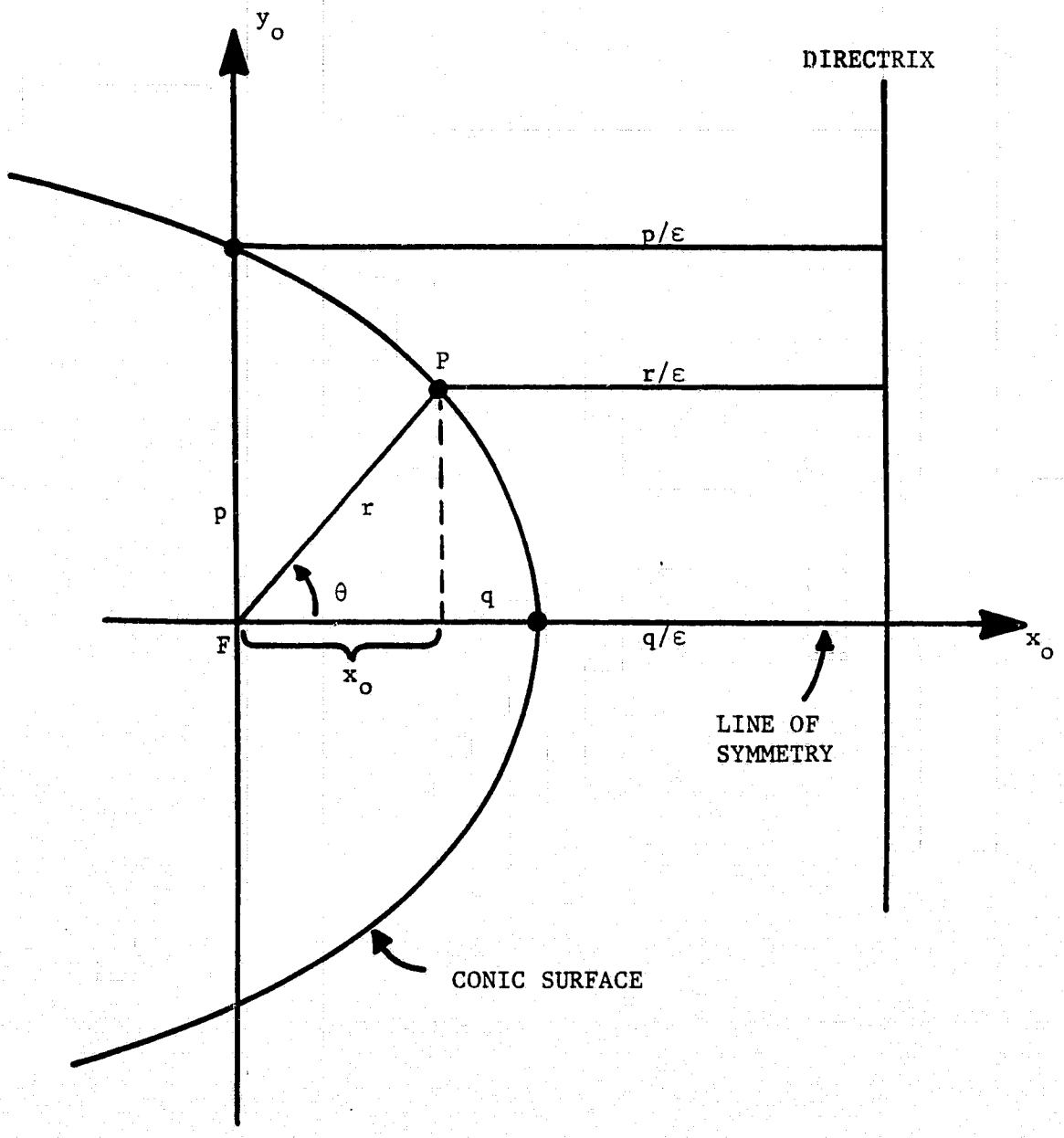

FIGURE 5.1 DEFINITION OF A CONIC

The distance between the intersections (apsides) of the line of symmetry with the conic is the transverse axis, line of apsides, or for an ellipse, the major axis of length 2a. When $\theta = 0$, the conic surface is closest to the focus, and is defined to be at perigee. The positive x_o axis defines the perifocal direction. At perigee, define $r = q$ and

$$p = q(1 + \varepsilon) \quad . \tag{5.4}$$

At apogee, $r = 2a - q$ and

$$p = (2a - q)(1 - \varepsilon) \quad . \tag{5.5}$$

Thus,

$$q = a(1 - \varepsilon) \quad , \tag{5.6}$$

and the distance from the center of the ellipse to the focus becomes $a\varepsilon$. From Equations 5.4, 5.6, and 5.2, it follows that

$$r = \frac{a(1 - \varepsilon^2)}{1 + \varepsilon \cos \theta} \quad . \tag{5.7}$$

5.1.2 Areal Velocity

Kepler's second law states that objects in periodic orbits sweep out equal areas in equal times. Specifically, from Figure 5.1, the area bounded by the semimajor axis, the radius vector r, and the arc defined by the angle θ is directly proportional to time, or

$$A(\theta) = kt \quad . \tag{5.8}$$

There exists no simple expression for A as a function of θ. Consequently, in place of the true anomaly θ, an auxiliary angle Φ, the eccentric anomaly, is defined as shown in Figure 5.2. The point S is the perigee of the orbit, and the direction from O to S the perifocal direction. Arc $\overline{SQ}$ is a sector of a circle of radius a centered at O; arc $\overline{SP}$ is part of the ellipse with focus F. The point Q on the circle is a projection parallel to the y_o axis from point P on the ellipse where

$$x_{oQ} = a \cos \Phi - a\varepsilon \quad , \tag{5.9}$$

$$y_{oQ} = a \sin \Phi \quad , \tag{5.10}$$

$$x_{oP} = r \cos \theta \quad , \tag{5.11}$$

$$y_{oP} = r \sin \theta \quad . \tag{5.12}$$

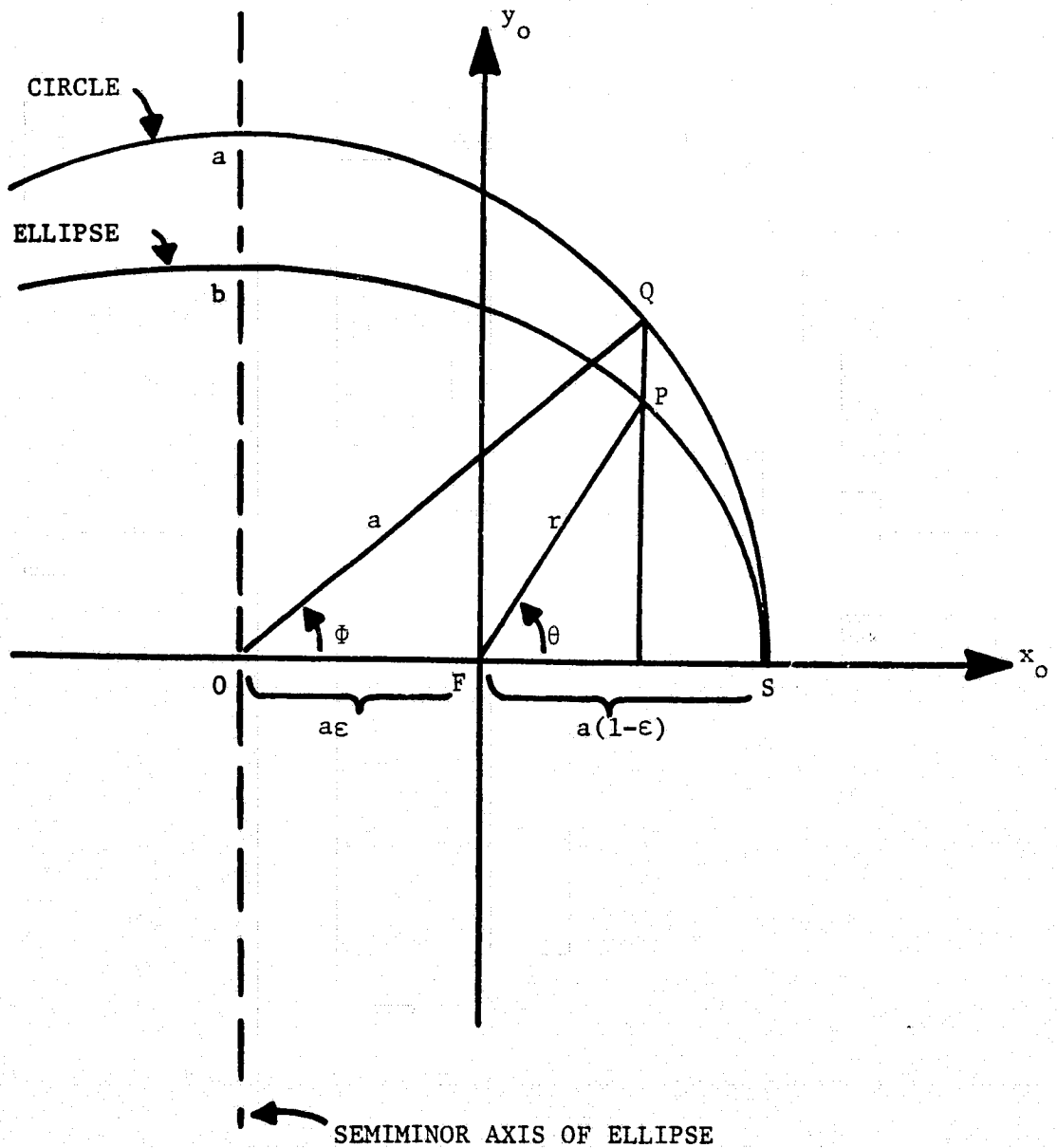

FIGURE 5.2 DEFINITION OF ECCENTRIC ANOMALY

As the geometry of Figure 5.2 is defined such that at all times

$$x_{op} = x_{oQ} \quad , \tag{5.13}$$

substitution of Equations 5.7, 5.9, and 5.11 into Equation 5.13 yields the expression for the eccentric anomaly in terms of the true anomaly and eccentricity.

$$\cos \Phi = \frac{\varepsilon + \cos \theta}{1 + \varepsilon \cos \theta} \quad . \tag{5.14}$$

Other relationships betwee. the true and eccentric anomaly which are of interest are as follows:

$$\sin \Phi = \frac{(1 - \varepsilon^2)^{\frac{1}{2}} \sin \theta}{1 + \varepsilon \cos \theta} \quad , \tag{5.15}$$

$$\cos \theta = \frac{\varepsilon - \cos \Phi}{\varepsilon \cos \Phi - 1} \quad , \tag{5.16}$$

$$\sin \theta = \frac{(1 - \varepsilon^2)^{\frac{1}{2}} \sin \Phi}{1 - \varepsilon \cos \Phi} \quad , \tag{5.17}$$

and

$$1 + \varepsilon \cos \theta = \frac{1 - \varepsilon^2}{1 - \varepsilon \cos \Phi} \quad . \tag{5.18}$$

The radial distance from the planet to the satellite can now also be written in terms of the eccentric anomaly as

$$r = a(1 - \varepsilon \cos \Phi) \quad . \tag{5.19}$$

The facility for computing $A(\theta)$ has now been developed. The differential area of a sector of an ellipse is

$$dA = \tfrac{1}{2} r^2 \, d\theta \quad . \tag{5.20}$$

Integration of Equation 5.20 to an angle θ allows a simple form for $A(\theta)$ in terms of Φ,

$$A(\theta) = \tfrac{1}{2} ab \, (\Phi - \varepsilon \sin \Phi) \quad , \tag{5.21}$$

where b is the semiminor axis of the ellipse given by

$$b = a(1 - \varepsilon^2)^{\frac{1}{2}} \quad , \tag{5.22}$$

and

$$\Phi = \Phi(\varepsilon,\theta) \quad . \tag{5.23}$$

The total area enclosed by an elliptical orbit is

$$A = \pi ab \quad . \tag{5.24}$$

As the area being swept out is proportional to time, Equations 5.8 and 5.24 can be rewritten as

$$A(t) = \pi ab \frac{t}{\tau} \quad , \tag{5.25}$$

where τ is the period of the orbit. Defining t to be zero at the time of the perifocal passage ($\theta = 0$),

$$t = \frac{\tau}{2\pi} \ (\Phi - \varepsilon \sin \Phi). \tag{5.26}$$

Equation 5.26 represents the solution of the differential equations of motion in the sense that it defines Φ as a function of t, and consequently, also θ and r as a function of t.

5.1.3 Periodicity

The third law of Kepler states that the square of the period is proportional to the cube of the semimajor axis. In terms of the universal gravitational constant G and the mass of the earth M, the period becomes

$$\tau = 2\pi a^{3/2} (GM)^{-\frac{1}{2}} \quad , \tag{5.27}$$

where

$$GM = 3.98 \times 10^{14} \ m^3/sec^2 \quad . \tag{5.28}$$

Equation 5.26 then becomes

$$t = \sqrt{\frac{a^3}{GM}} \ (\Phi - \varepsilon \sin \Phi) \quad . \tag{5.29}$$

5.1.4 Orbit Coordinate System

At this point, the orbit has been defined in its own x_o, y_o plane. The orientation of this orbit plane with respect to the equatorial plane must still

be determined. Following a practice frequently used[9], this orientation is defined by the use of 4 parameters as shown in Figure 5.3, where

- i = inclination of orbit plane with respect to the equatorial plane,
- Ω = longitude of the ascending node; the angle between the principle direction (x-axis) and the line of nodes (intersection of the orbital and equatorial planes),
- ω = argument of the perifocus; the angle between the line of nodes and the perifocal direction,
- T = epoch time; time of perifocal passage.

In Figure 5.3, the x-y plane in the right-handed coordinate system defines the equatorial plane, with the z-axis pointed north. The x-axis will be considered as passing through the Greenwich meridian. The vectors $\hat{W}$, $\hat{P}$, and $\hat{Q}$ are unit vectors in the orbit plane with $\hat{W}$ pointing perpendicular to the orbit plane, $\hat{P}$ along the perifocal direction, $\hat{Q}$ along y_o to complete a right-handed coordinate system.

To compensate for the fact that the earth will rotate under the satellite, a new angle α is defined, where

$$\alpha = \Omega - \eta(t-T) \quad , \tag{5-30}$$

and where η is the rotational speed of the earth. Note that the angle α is defined to be Ω when t is T, the epoch time. In like manner, Equation 5.29 is rewritten as

$$(t - T) = \sqrt{\frac{a^3}{GM}} \; (\Phi - \varepsilon \sin \Phi) \quad . \tag{5.31}$$

A second auxiliary angle β is defined, where

$$\beta = \omega + \theta \quad , \tag{5-32}$$

and $\theta = 0$ when $t = T$ such that $r = a(1-\varepsilon)$, the perifocal radius.

It is convenient to express the location of the satellite in terms of the rectangular coordinate system. This can be easily accomplished by rotating the coordinate system, a problem identical to that of using the Euler angles. Defining a position vector in a rectangular coordinate as

$$P = \begin{pmatrix} x \\ y \\ z \end{pmatrix} \quad , \tag{5.33}$$

consider first the satellite to be in the x''', y''', z''' coordinate system at $x''' = r$, as shown in Figure 5.4(A), where the x''', y''' plane is coincident with the orbital plane. Here,

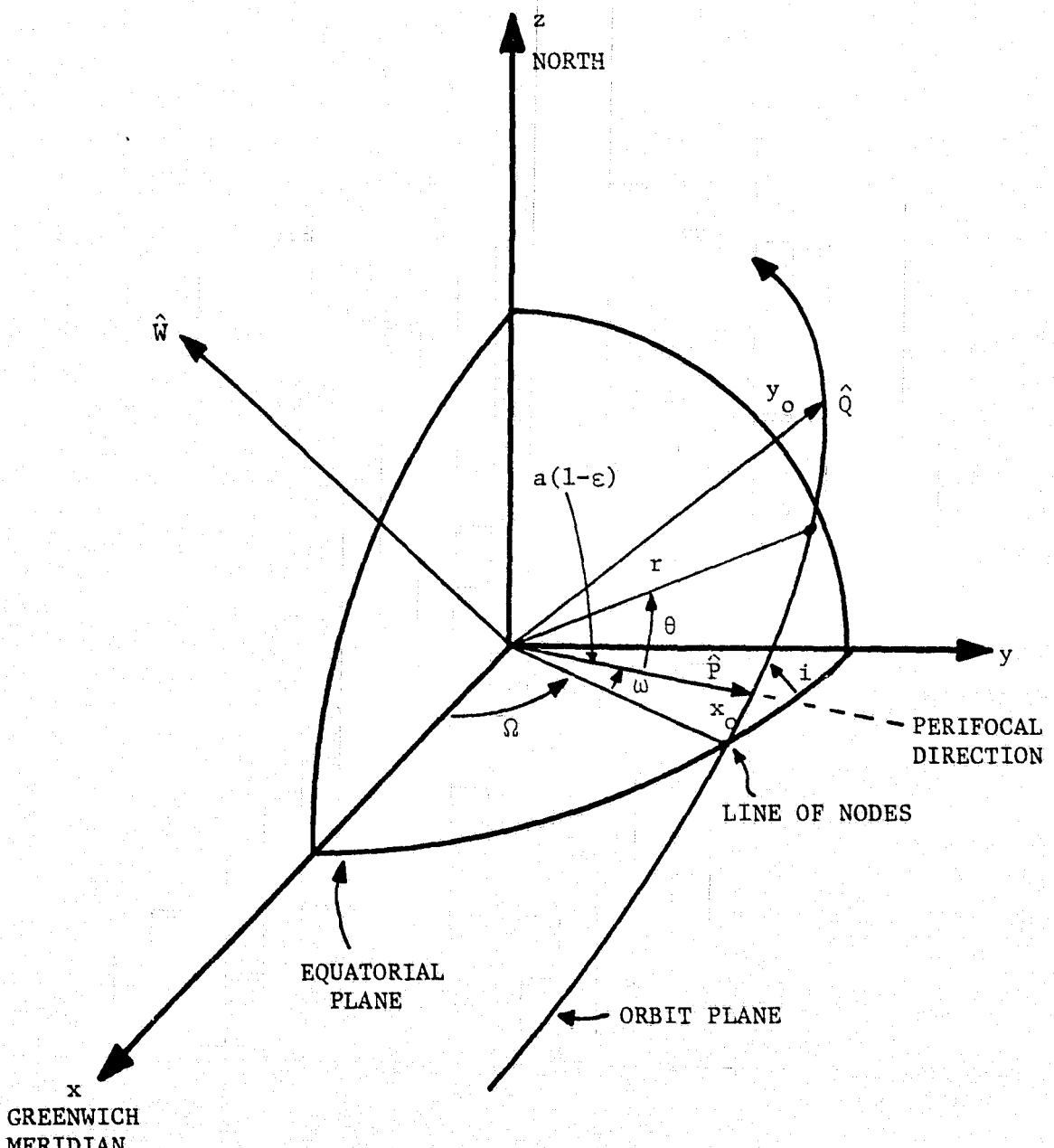

FIGURE 5.3 ORBIT COORDINATE SYSTEM

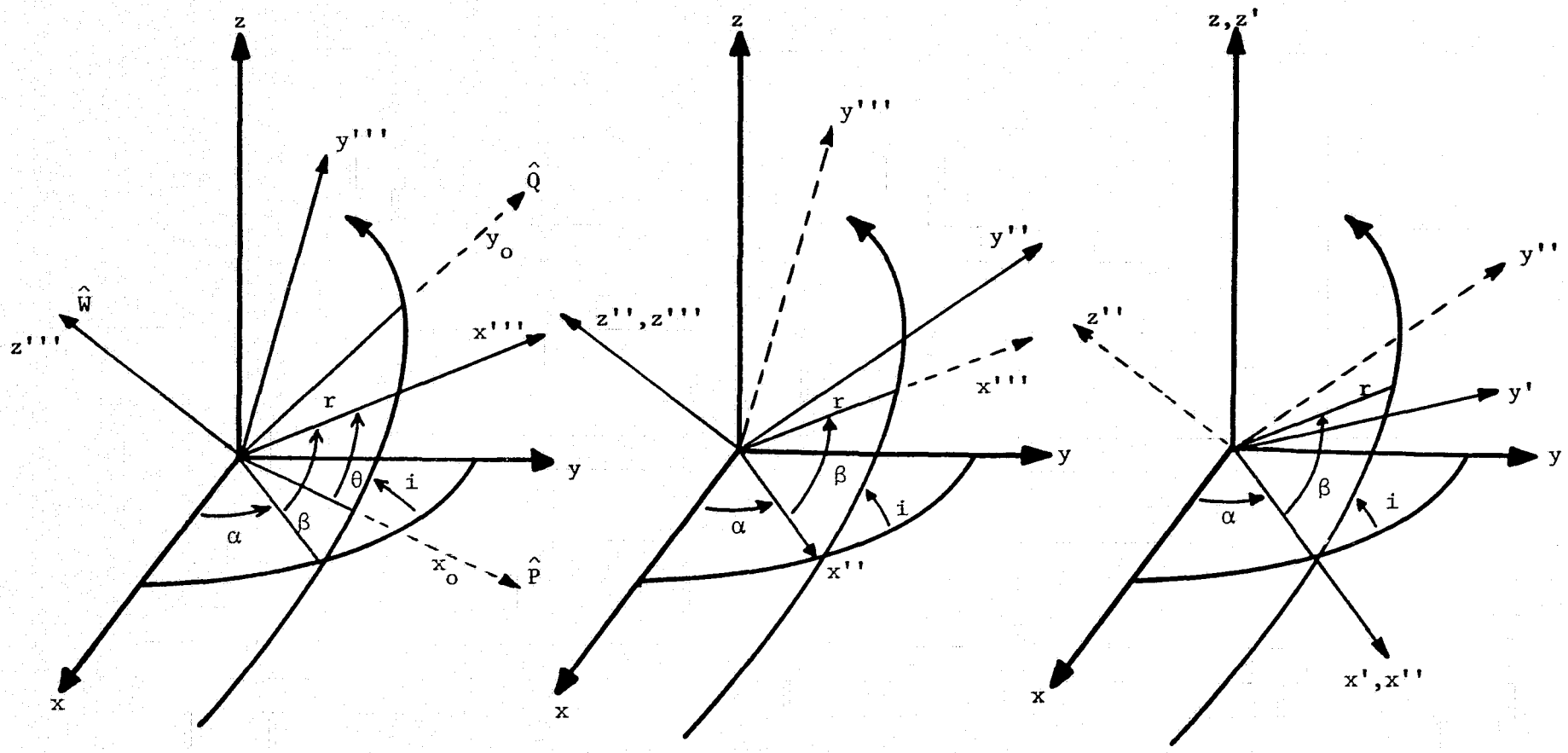

(A) Orbit and Equatorial Coordinate Systems.

(B) Orbit Plane Rotated Through Angle β.

(C) Orbit Plane Rotated Through Inclination i.

FIGURE 5.4 ORBIT PLANE RELATED TO EQUATORIAL COORDINATE SYSTEM

$$P''' = \begin{pmatrix} r \\ 0 \\ 0 \end{pmatrix} , \tag{5.34}$$

Rotating this first coordinate system through an angle β about the z''' axis defines a new coordinate system, shown in Figure 5.4(B), where again the x''', y''' plane lies in the orbital plane. In this system, however, the x''' axis defines the line of nodes and the position of the satellite is given as

$$\begin{aligned} P'' &= \begin{pmatrix} \cos\beta & -\sin\beta & 0 \\ \sin\beta & \cos\beta & 0 \\ 0 & 0 & 0 \end{pmatrix} \begin{pmatrix} r \\ 0 \\ 0 \end{pmatrix} \\ &= \begin{pmatrix} r\cos\beta \\ r\sin\beta \\ 0 \end{pmatrix} . \end{aligned} \tag{5.35}$$

Rotating this second coordinate system about the line of nodes (x''-axis) through the angle i (inclination of the orbit plane with respect to the equatorial plane) generates the coordinate system of Figure 5.4(C), where now the x', y' plane is coincident with the equatorial plane. The position of the satellite now becomes

$$\begin{aligned} P' &= \begin{pmatrix} 1 & 0 & 0 \\ 0 & \cos i & -\sin i \\ 0 & \sin i & \cos i \end{pmatrix} \begin{pmatrix} r\cos\beta \\ r\sin\beta \\ 0 \end{pmatrix} \\ &= \begin{pmatrix} r\cos\beta & \\ r\sin\beta & \cos i \\ r\sin\beta & \sin i \end{pmatrix} . \end{aligned} \tag{5.36}$$

A final rotation of the coordinate system about the z' axis through an angle α generates the coordinate system of Figure 5.3, with the z axis north and the x axis through the Greenwich meridian. The position of the satellite now becomes,

$$\begin{aligned} P &= \begin{pmatrix} \cos\alpha & -\sin\alpha & 0 \\ \sin\alpha & \cos\alpha & 0 \\ 0 & 0 & 1 \end{pmatrix} \begin{pmatrix} r\cos\beta & \\ r\sin\beta\cos i & \\ r\sin\beta\sin i & \end{pmatrix} \\ &= \begin{pmatrix} r\cos\beta\cos\alpha - r\sin\beta\cos i\sin\alpha \\ r\cos\beta\sin\alpha + r\sin\beta\cos i\cos\alpha \\ r\sin\beta\sin i \end{pmatrix} . \end{aligned} \tag{5.37}$$

Summarizing the results of this discussion, the position of the satellite at time t in terms of the 6 orbital parameters a, ε, Ω, ω, i, and T is as follows:

$$x = r \cos \beta \cos \alpha - r \sin \beta \cos i \sin \alpha \quad , \tag{5.38}$$

$$y = r \cos \beta \sin \alpha + r \sin \beta \cos i \cos \alpha \quad , \tag{5.39}$$

$$z = r \sin \beta \sin i \quad ,$$

where

$$\beta = \omega + \theta \quad , \tag{5.40}$$

$$\alpha = \Omega - \eta (t - T) \quad , \tag{5.41}$$

$$r = a(1 - \varepsilon \cos \Phi) \quad , \tag{5.42}$$

$$(t - T) = \sqrt{\frac{a^3}{GM}} (\Phi - \varepsilon \sin \Phi) \quad , \tag{5.43}$$

and where θ and Φ are related by Equations 5.14 through 5.18.

5.2 DETERMINATION OF THE KEPLER ORBIT PARAMETERS

The method of Gibbs lends itself most readily to the solution of the 6 Kepler orbital parameters, given three known positions, $\vec{r}_1$, $\vec{r}_2$, and $\vec{r}_3$, of the satellite. The fact that the three position vectors are coplanar, any one can be expressed as a linear combination of the others, typically

$$\vec{r}_2 = c_1 \vec{r}_1 + c_3 \vec{r}_3 \quad , \tag{5.44}$$

where

$$\vec{r}_i = r_i \{\hat{i} \cos \delta_i \cos \lambda_i + \hat{j} \cos \delta_i \sin \lambda_i + \hat{k} \sin \delta_i\} \quad , \tag{5.45}$$

and where

r_i = earth center distance of position i,

δ_i = latitude of position i,

λ_i = longitude of position i,

$\hat{i}, \hat{j}, \hat{k}$, = unit vectors of right handed coordinate system of Figure 5.3

The solution of Equation 5.44 yields 3 expressions for both c_1 and c_3, two of which are:

$$c_1 = \frac{r_2 \cos \delta_2 \sin (\lambda_3 - \lambda_2)}{r_1 \cos \delta_1 \sin (\lambda_3 - \lambda_1)} \quad , \tag{5.46}$$

$$c_1 = \frac{r_2 (\cos \delta_2 \sin \lambda_2 \sin \lambda_3 - \sin \delta_2 \cos \delta_3 \sin \lambda_3)}{r_1 (\cos \delta_1 \sin \lambda_1 \sin \lambda_3 - \sin \delta_1 \cos \delta_3 \sin \lambda_3)} \quad , \tag{5.47}$$

and

$$c_3 = \frac{r_2 \cos \delta_2 \sin (\lambda_1 - \lambda_2)}{r_3 \cos \delta_3 \sin (\lambda_1 - \lambda_3)} \quad , \tag{5.48}$$

$$c_3 = \frac{r_2 (\cos \delta_2 \sin \lambda_2 \sin \delta_1 - \sin \delta_2 \cos \delta_1 \sin \lambda_1)}{r_3 (\cos \delta_3 \sin \lambda_3 \sin \delta_1 - \sin \delta_3 \cos \delta_1 \sin \lambda_1)} \quad . \tag{5.49}$$

The computational ease of Equations 5.46 and 5.48 is lost when $\lambda_1 = \lambda_3$, forcing the use of Equations 5.47 and 5.49.

From Equation 5.1, the x-coordinates in the orbit plane are:

$$x_{o1} = (p - r_i)/\varepsilon \quad . \tag{5.50}$$

But, from Equation 5.44,

$$x_{o2} = c_1 x_{o1} + c_3 x_{o3} \quad , \tag{5.51}$$

such that the semilatus rectum becomes

$$p = \frac{c_1 r_1 + c_3 r_3 - r_2}{c_1 + c_3 - 1} \quad . \tag{5.52}$$

5.2.1 Inclination Angle i

The unit vector $\hat{W}$ has been defined to be perpendicular to the orbit plane such that the cross product of any two vectors in the orbit plane will yield this direction. Taking the two most widely separated positions,

$$\hat{W} = \vec{r}_1 \times \vec{r}_3 / |\vec{r}_1 \times \vec{r}_3| \quad . \tag{5.53}$$

The angle between $\hat{W}$ and the z-axis is the inclination angle, as shown in Figure 5.5, such that

$$i = \cos^{-1}(W_z) \quad , \tag{5.54}$$

where W_z is the z-component of $\hat{W}$.

5.2.2 Eccentricity ε

The unit vectors defining the orbit coordinate system in Figure 5.3 are orthogonal such that

$$\hat{Q} = \hat{W} \times \hat{P} \quad , \tag{5.55}$$

Defining

$$S = |\vec{r}_1 \times \vec{r}_3| \quad , \tag{5.56}$$

it follows that

$$S\hat{Q} = \vec{r}_3 (\hat{P} \cdot \vec{r}_1) - \vec{r}_1 (\hat{P} \cdot \vec{r}_3) \quad . \tag{5.57}$$

But, from the definition of $\hat{P}$ (Equation 5.1) which specifies $\hat{P}$ to be in the perifocal direction,

$$\hat{P} \cdot \vec{r} = x_o = (p - r)/\varepsilon \quad , \tag{5.58}$$

and

$$\varepsilon\hat{Q} = \left[\vec{r}_3 (p - r_1) - \vec{r}_1 (p - r_3)\right]/S \quad . \tag{5.59}$$

Finally,

$$\varepsilon = (\varepsilon\hat{Q} \cdot \varepsilon\hat{Q})^{1/2} \quad . \tag{5.60}$$

5.2.3 Semimajor Axis a

From Equations 5.5 and 5.6,

$$a = p/(1 - \varepsilon^2) \quad . \tag{5.61}$$

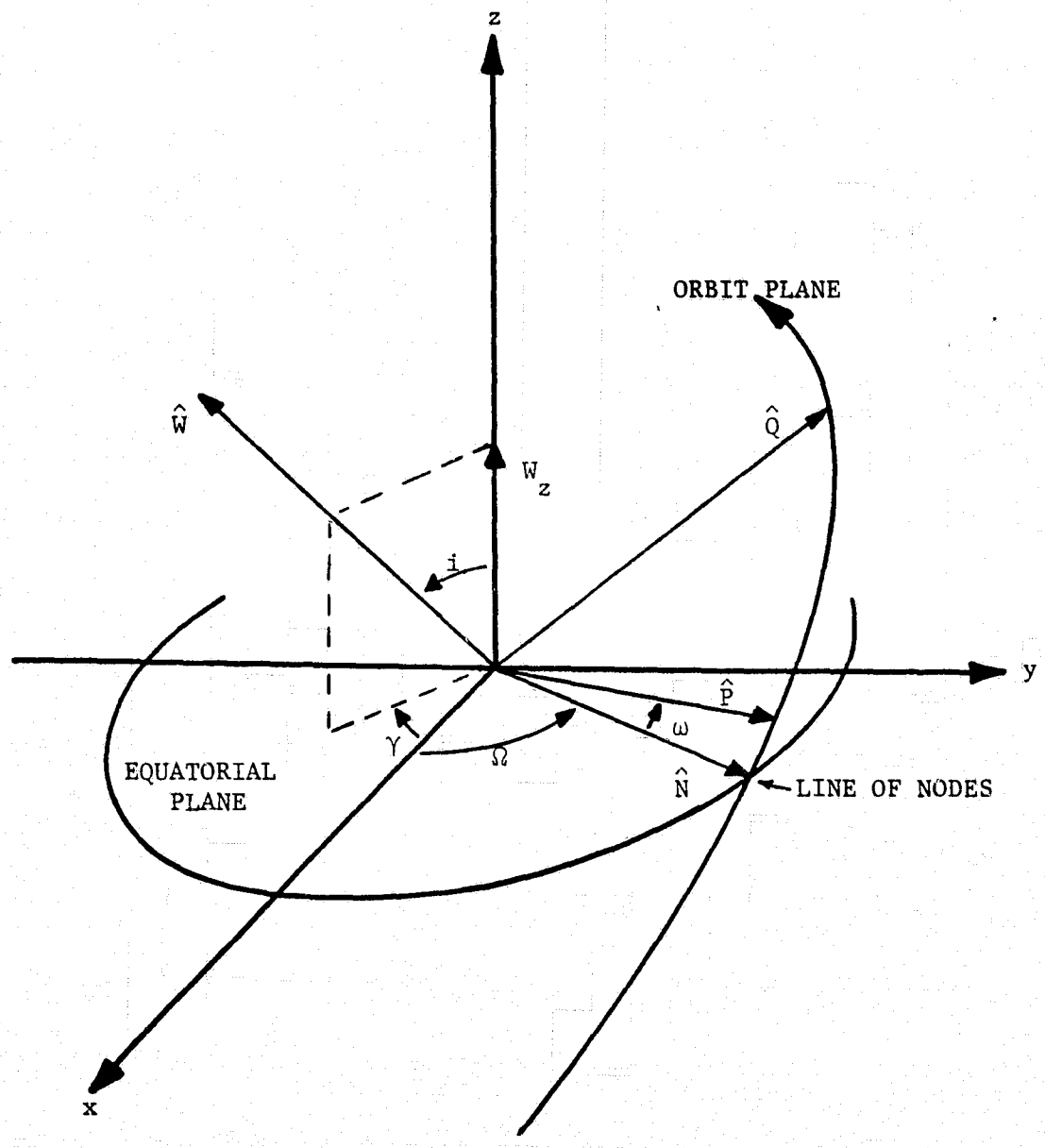

FIGURE 5.5 DETERMINATION OF ORBIT PLANE ORIENTATION

5.2.4 Time of Perifocal Passage T

At some time t_3 corresponding to position $\vec{r}_3$, the eccentric anomaly is given by Equation 5.43 as

$$(t_3 - T) = \sqrt{\frac{a^3}{GM}} \; (\Phi_3 - \varepsilon \sin \Phi_3) \quad . \tag{5.62}$$

Care must be taken to assure the correct quadrant for the solution of Φ_3 before substituting Φ into Equation 5.62 for a value of T. From Equations 5.12, 5.17, and 5.19,

$$y_{o3} = a \; (1 - \varepsilon^2)^{\frac{1}{2}} \sin \Phi_3 \quad . \tag{5.63}$$

Since

$$y_o = \hat{Q} \cdot \vec{r} \quad , \tag{5.65}$$

it follows that

$$\sin \Phi_3 = \frac{\hat{Q} \cdot \vec{r}_3}{a(1 - \varepsilon^2)^{\frac{1}{2}}} \quad . \tag{5.65}$$

Also, from Equations 5.9 and 5.57,

$$x_o = (p - r)/\varepsilon = a \cos \Phi - a\varepsilon \quad , \tag{5.66}$$

such that an unambiguous definition of Φ_3 is completed by

$$\cos \Phi_3 = (1 - \frac{r_3}{a})/\varepsilon \quad . \tag{5.67}$$

Substitution of Φ_3 into Equation 5.62 yields the time of perifocal passage.

5.2.5 Longitude of Ascending Node Ω

The projection of the vector $\hat{W}$ onto the x, y equatorial plane will be at an angle γ with respect to the x-axis, as shown in Figure 5.5. This projection is 90^o removed from the line of nodes (i.e., $\Omega + \gamma = \pi/2$). Taking into account the rotation of the earth, Ω then becomes

$$\Omega = \pi/2 + \tan^{-1} Wy/Wx + (t_3 - T) \quad . \tag{5.68}$$

5.2.6 Argument of the Perifocus ω

Defining $\hat{N}$ as the unit vector along the line of nodes, the argument of the perifocus focus ω is the scalar product of $\hat{N}$ and $\hat{P}$. Since

$$\hat{P} = \hat{Q} \times \hat{W} \quad , \tag{5.69}$$

$$\omega = \cos^{-1}\left[\hat{N} \cdot \hat{Q} \times \hat{W}\right] \quad , \tag{5.70}$$

where

$$\hat{N} = \hat{i} \cos \Omega + \hat{j} \sin \Omega \quad . \tag{5.71}$$

5.3 PERTURBATIONS TO THE KEPLER ORBIT

The presence of the sun and moon and the non-spherical shape of the earth contribute major perturbations to the Kepler model for satellite motion. Solar radiation pressure affects the satellite orbit by more than two orders of magnitude less than the factors mentioned above.

When the satellite is between the earth and the moon, it experiences its greatest non-Keplerian acceleration toward the moon, approximately 8.9×10^{-6} m/sec^2. When the satellite is opposite the moon, the "tidal" gravitational acceleration away from the earth is 6.3×10^{-6} m/sec^2. When the satellite and the earth form the base of an isosceles triangle with the moon, both the earth and satellite have the same gravitational acceleration toward the moon and the effective perturbation to the satellite's Kepler orbit due to the presence of the moon is minimal. As the earth-sun distance is much greater than the earth-moon distance, the satellite will feel roughly the same non-Kepler gravitational acceleration (3.4×10^{-6} m/sec^2) away from the earth when it is between the sun and the earth and when it is opposite the sun.

The assumption of a uniform spherical earth in place of the non-spherical earth results in a gravitational acceleration error which varies through $\pm$ 1.2×10^{-7} m/sec^2 as the satellite moves to latitudes of $\pm$ 2 degrees. This does not represent the strongest perturbation due to the simplifying earth model assumption but is the largest variable component by several orders of magnitude.

The elements of the Kepler orbit which are determined from slant range measurements will reflect an effective gravitational field due to the combination of the non-spherical earth, the moon, the sun, and other lesser sources. The continuously changing gravitational fields due to the non-Keplerian influences cause the effective gravitational field to be invalid except at the time and location for which it was defined. The magnitude of the errors incurred by the assumption of the Kepler orbit may be readily evaluated by assuming the satellite to move about the earth in simple har-

monic motion at synchronous altitudes. The introduction of an external field such as that of the moon or the sun transforms the orbit from circular to elliptical, with the center of the ellipse at the center of the earth. Assuming the use of three satellite positions separated by one hour, Table 5.1 summarizes the peak disagreements between the satellite earth center distances of the Kepler orbit generated from the three positions and of the simple harmonic orbit, as a function of time since the last satellite position. Locating the earth at the center of the elliptical orbit (simple harmonic motion) instead of one focal point (Kepler model) causes the differences of Table 5.1.

From Table 5.1, the Kepler model is estimated to generate satellite ephemeris earth center distances accurate to with approximately 400 meters two hours after the last satellite position measurement. Earth center distance errors have periodicities of approximately 12 hours, with the magnitude of the effect depending on the relative orientation of the moon and sun. The greatest errors occur at 45 degrees from the resultant moon/sun gravitational acceleration vector. Longitudes predicted by the Kepler orbit model are expected to have errors of the same magnitude as for the earth center distance, 45 degrees out of phase. The gravitational acceleration vector component perpendicular to the ecliptic plane will tend to pull the satellite toward the ecliptic plane, thus increasing the orbit eccentricity. This phenomenon generates errors in predicted latitude, with a 24 hour periodicity.

5.4 IONOSPHERIC PROPAGATION DELAY

Electron densities on the order of $10^6/cm^3$ give the ionosphere a different index of refraction than that of free space and affect radio propagation by adding a time delay and by increasing the propagation path length due to refraction.

Unpredictable solar disturbances can affect changes in the ionosphere causing propagation time delays to change by 50 percent over tens of minutes. Two general statements can be made, however. First, on the average the range measurement error is a maximum during the daytime, increasing with lower elevation angles. Second, the error is inversely proportional to the square of the frequency. Assuming the undisturbed daytime and nighttime ionosphere of Millman[10], the one way propagation delays experienced by L-band signals at mid latitudes and at elevation angles between 26 and 32 degrees are 0.030 and 0.007 μsec, respectively, corresponding to apparent slant range increases of 8.9 and 2.0 meters. The computer software which generates satellite positions from slant range measurements assumes ionospheric delays of this magnitude; furthermore, a sinusoidal variation from daytime propagation delays to nighttime propagation delays is assumed.

The different refractive index of the ionosphere causes the elevation angle to a VHF radio source at synchronous altitudes to be incorrect by typically 0.08 degrees, having assumed an initial elevation angle of 20

TABLE 5.1

ESTIMATED MAXIMUM PREDICTED

EARTH CENTER DISTANCE ERRORS

FOR KEPLER ORBIT

TIME SINCE LAST POSITION*	DUE TO MOON	DUE TO SUN	DUE TO NON-SPHERICAL EARTH
(hours)	(meters)	(meters)	(meters)
1	72.	28.	1.0
2	290.	110.	4.0
4	1300.	510.	18.
8	4800.	1900.	65.

* Error model assumes use of three satellite positions, separated by one hour.

degrees. The corresponding L-band elevation angle error is 0.00125 degrees, resulting in an increased path length on the order of fractions of a millimeter. Increased path length errors due to ionospheric refraction are neglected.

5.5 TROPOSPHERIC PROPAGATION DELAY

The index of refraction in the troposphere is a function primarily of meterological variables such as relative humidity, air temperature, and air pressure. Assuming a standard atmosphere model with 100% relative humidity, radio signals at L-band frequencies will suffer propagation delays of 0.020 μsec and 0.016 μsec for transmissions through the atmosphere at elevation angles of 26 and 32 degrees, respectively. Propagation delays are reduced approximately 20 percent in a dry atmosphere.

An error on the order of fractions of a centimeter is generated by the refraction of the radio beam through the troposphere. Slant range errors due to tropospheric refraction are neglected.

SECTION 6

CALIBRATION PROCEDURES AND RESULTS

6.1 L-BAND TRANSPONDER CALIBRATION TECHNIQUES

Uncertainty in the internal time delay of a remote transponder could set a limit on the accuracy of range measurements from the satellite to the transponder. Accurate calibration of the transponder internal time delay eliminates the delay as a significant contribution to range error.

The linearity of the internal time delay devices of the L-band transponders and the absolute transponder delays and stabilities were measured at the Observatory by two independent methods prior to shipment to their remote sites. The first method includes the satellite in its operational configuration, and hence is called the "satellite aided" calibration method. The second relies on devices which simulate the satellite at the Observatory, and is called the "in house" method.

6.1.1 "Satellite Aided" Calibration Technique

The "satellite aided" calibration technique as sketched in Figure 6.1 requires the remote transponder and its antenna to be located at the Observatory. The Observatory's transmission to the satellite is represented by the number 1. Both the Observatory and the remote transponder correlate on the satellite return, number 2. After a precise internal time delay, the remote transponder transmits its response (number 3) to the ranging interrogation and the Observatory correlates on the downlink from the satellite (number 4). The combined two-way ground-satellite ranging time and the satellite internal time delay are measured by the Observatory-satellite link; the Observatory time delay is measured by the Observatory self calibration circuit. All time delays of the four-way link are thus known with the exception of the remote transponder internal time delay. Subtracting the sum of the known time delays from the two-way Observatory-satellite-remote transponder ranging time yields the transponder internal time delay.

Not shown in Figure 6.1 are the self calibration circuits. At the Observatory, a local oscillator, an L-band mixer, and a dipole antenna are mounted on the surface of the 30-foot dish antenna. The Observatory correlates on its own self calibration signal almost immediately after transmission of the ranging interrogation; it correlates on the satellite return approximately 250 msec after transmission, and on the remote transponder return approximately one second after transmission.

The remote transponder self calibration circuits consist of a similar local oscillator and L-band mixer connected to reactive signal samplers on the transponder transmit and receive cables. The responder compares the phase of 256 "self calibration" tone cycles with the phase of the tone being generated for transmission. A digitized value of the phase difference is

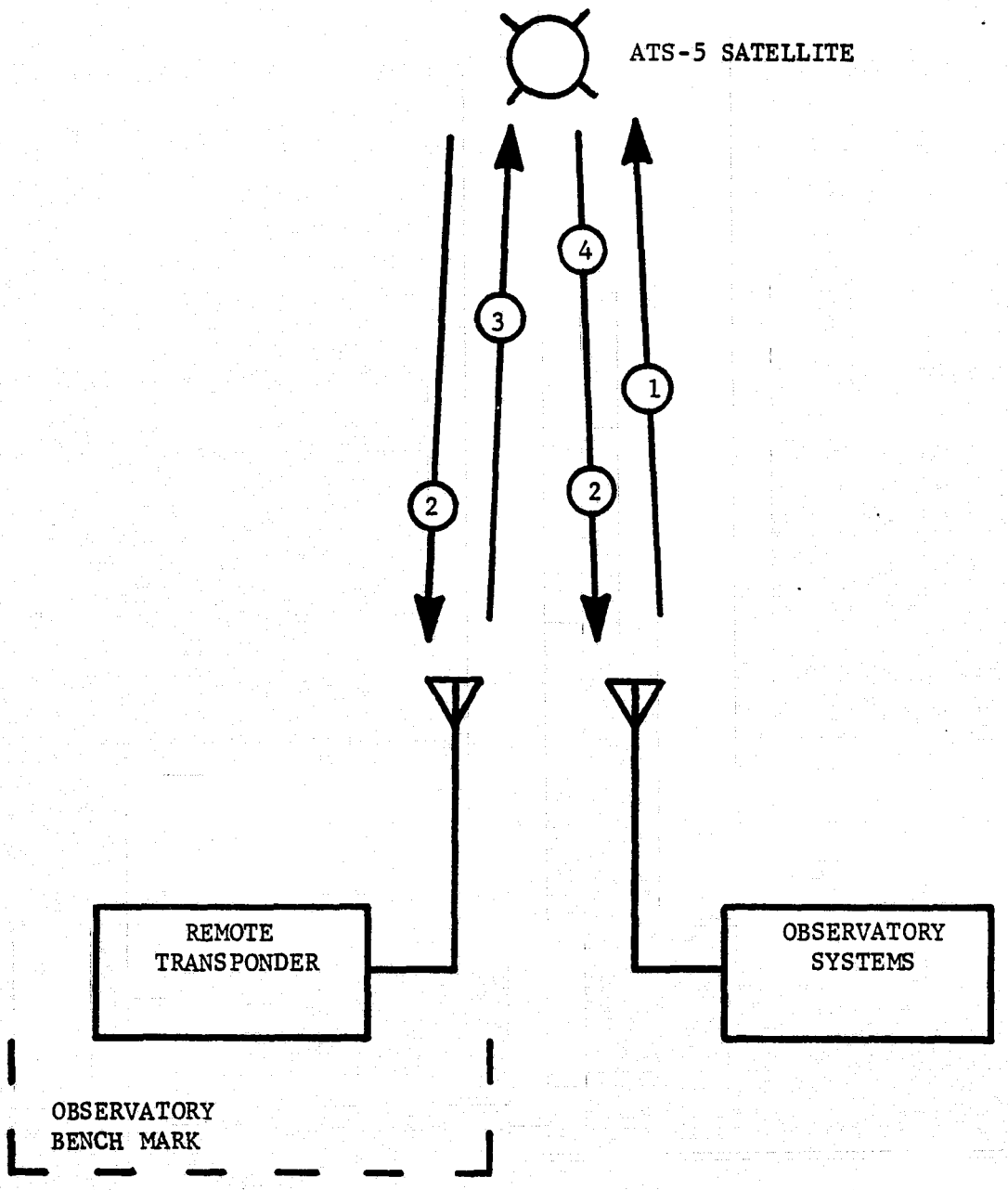

FIGURE 6.1 "SATELLITE AIDED" CALIBRATION OF REMOTE TRANSPONDER AT OBSERVATORY. Numbers on beams indicate sequential signaling order. All slant ranges are the same.

loaded onto the data stream following the address code.

In the "satellite aided" calibration, consider T_R as the four-way ranging time measured at the Observatory. T_R is defined as the sum of all propagation times and time delays; specifically,

$$T_R = 4R + D_o + D_R + 2\delta_s + 4D_A \tag{6.1}$$

where

R = ground-satellite radio propagation time,

D_o = total time delay incurred at the Observatory,

D_R = total time delay at the remote transponder,

δ_s = internal time delay of satellite in repeating a NBFM L-band signal,

D_A = total one-way atmospheric propagation time delay (ionospheric and tropospheric).

The time delay seen at the Observatory can be represented by the expression

$$D_o = \delta_o - \delta_T - S_T + 2\delta_G, \tag{6.2}$$

where

δ_o = actual signal time delay from the Observatory interrogator to the 30-foot dish antenna and back to the Observatory correlator,

δ_T = fixed time delay in starting the time interval counter which measures T_R. For tests through the satellite, δ_T = 39334.3 μsec,

S_T = adjustable time delay in starting the time interval counter,

δ_G = geometrical effect; difference in remote transponder antenna-satellite distance and Observatory antenna-satellite distance, expressed in units of time.

The adjustable time delay, S_T, is set in increments of 409.6 μsec by a group of three octal thumbwheels with settings defined as P_j for thumbwheel j such that

$$S_T = 409.6(P_3 + 8P_2 + 64P_1)\ \mu\text{sec}. \tag{6.3}$$

The Observatory self calibration circuit measures the signal time delay,

δ_o, on every ranging interrogation. Consequently, the total Observatory delay, D_o, is known for each interrogation.

The total time delay of the remote transponder is an accumulation of delays in the various components of the unit, as sketched in Figure 6.2. The delays fall into three general categories; cable delays, analog circuit delays, and logic delays. The cable delay can be represented by δ_C, where

$$\delta_C = \delta_{DR} + \delta_{DT} + 2\delta_W + \delta_{CR} + \delta_{CT}, \tag{6.4}$$

and where

δ_{DR} = signal time delay through receive section of diplexer,

δ_{DT} = signal time delay through transmit section of diplexer,

δ_W = signal time delay from diplexer through antenna feed to 10-foot dish antenna surface,

δ_{CR} = signal time delay through cable from diplexer to receiver self calibration tap,

δ_{CT} = signal time delay through cable from transmitter self calibration tap to diplexer.

Signal propagation velocities through cables are well documented in the literature of the various manufacturers. Furthermore, for cable lengths used in this experiment, these data show insignificant variations in time delays as a function of environmental conditions. The time delays through the receive and transmit sections of the diplexer must be measured. No time delay variations are anticipated as a function of temperature as all diplexer components are broadband devices.

Analog circuit time delays occur in the L-band receiver, the responder input and output sections, and the L-band transmitter. This delay, δ_A, can be broken up into two parts, a delay representing an integer number of tone cycles, δ_I, plus a delay representing a phase error, δ_P, such that

$$\delta_A = \delta_I + \delta_P. \tag{6.5}$$

The responder self calibration circuits measure the phase error by comparing the signal received through the self calibration loop with that being generated by the responder. The responder counts down from 409.6 μsec during phase comparison and sends the phase difference as a digital number following the sync word and address code. Thus, the phase difference is represented by

$$\delta_P = 409.6 - \delta_{SC}, \tag{6.6}$$

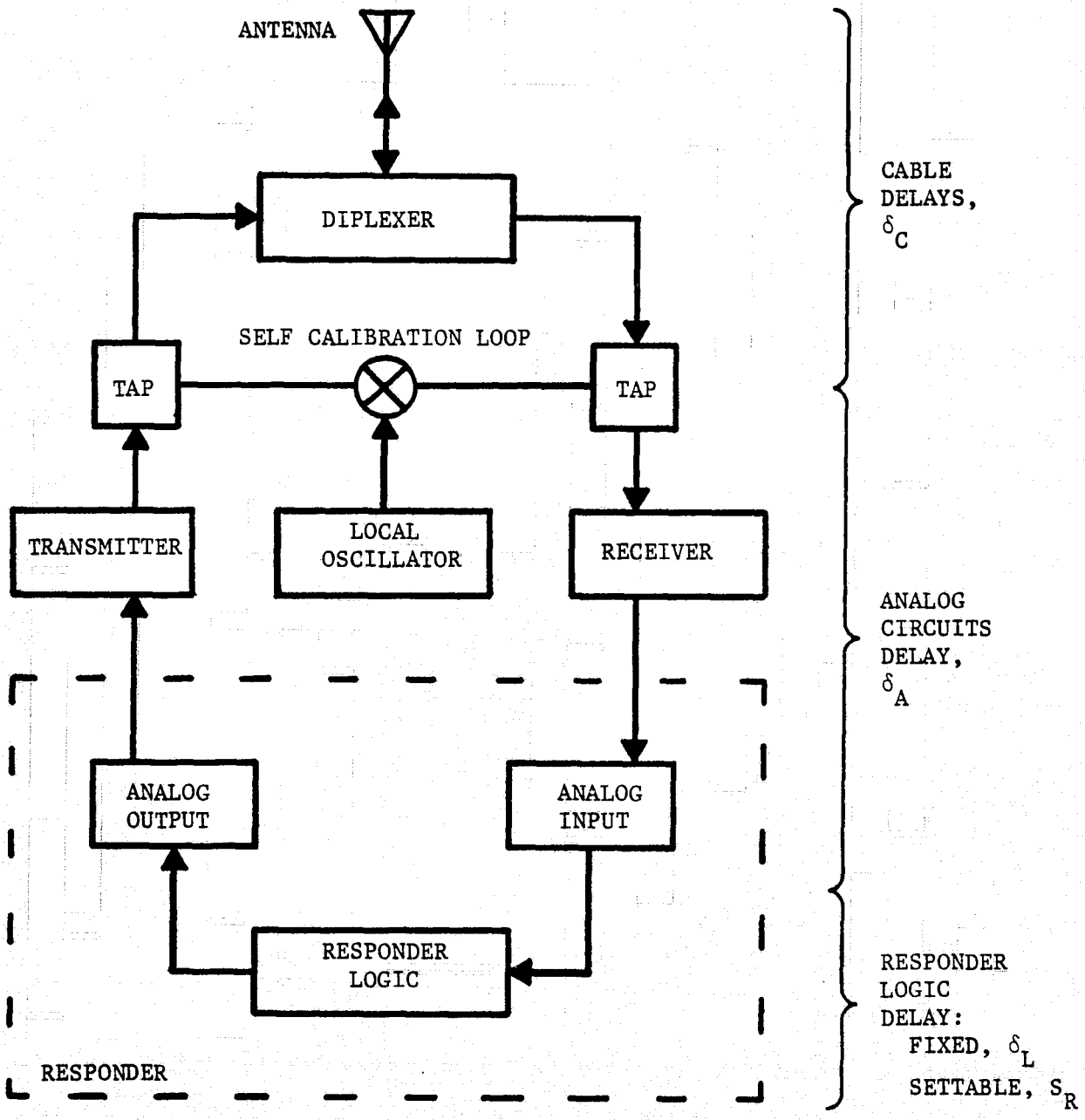

FIGURE 6.2 SOURCES OF REMOTE TRANSPONDER TIME DELAYS

where δ_{SC} is the digital response of the remote transponder self calibration circuit. The greater the internal time delay, the smaller δ_{SC} becomes. Finally,

$$\delta_A = \delta_I + 409.6 - \delta_{SC}. \tag{6.7}$$

The delay from the transmitter self calibration tap through the mixer and on to the receiver self calibration tap is considered negligible. The cable in the self calibration loop is approximately 4 feet long and the mixer is a broad band device. While δ_{SC} is known on every ranging response, δ_I must be determined experimentally. For the L-band responder, a tone cycle has a period of 102.4 μsec. δ_I is thus expected to be an integer multiple of 102.4 μsec.

Following correlation, the responder will automatically count down 3926 cycles while transmitting tone and count down another 30 cycles while transmitting the sync word and address code. Consequently, the fixed delay of the responder, δ_L, is 3956 tone cycles long, or 405094.4 μsec. The fixed time delay is supplemented with a variable time delay (similar to S_T for the Observatory time delay D_Q), adjustable in increments of four tone cycles (409.6 μsec) by a group of three octal thumbwheels with settings defined as Q_j for thumbwheel j. The adjustable time delay is

$$S_R = 409.6(Q_3 + 8Q_2 + 64Q_1) \text{ μsec}. \tag{6.8}$$

Non zero values of Q_j cause the appropriate number of tone cycles to be added in front of the tone generated by the fixed time delay, δ_L. Both δ_L and S_R are known delays.

Combining all components, the total transponder time delay can be written as

$$\begin{aligned} D_R = {} & \delta_{DR} + \delta_{DT} + 2\delta_W + \delta_{CR} + \delta_{CT} && \text{(Cable delays)} \\ & + \delta_I + 409.6 - \delta_{SC} && \text{(Analog delays)} \\ & + \delta_L + S_R . && \text{(Logic delays)} \end{aligned} \tag{6.9}$$

The only value in the above equation which needs to be experimentally determined is δ_I. In the "satellite aided" calibration, it follows that

$$\begin{aligned} \delta_I = {} & T_R - 4R - 2\delta_s - \delta_o + \delta_T + S_T - 2\delta_G - \delta_C + \delta_{SC} \\ & - S_R - 405504.0. \end{aligned} \tag{6.10}$$

A measurement of the Observatory-satellite-Observatory ranging time, T_o, is made on every interrogation of the remote transponder, where

$$T_o = 2R + \delta_s + \delta_o + 2D_A . \qquad (6.11)$$

Substituting the above into Equation 6.10, the integer delay δ_I becomes

$$\delta_I = T_R - 2T_o + \delta_o + \delta_{SC} + S_T - 2\delta_G - \delta_C - S_R - 366169.7. \qquad (6.12)$$

6.1.2 "In House" Calibration Technique

The second calibration technique, as sketched in Figure 6.3, replaces the ATS-5 satellite with mixers and a local oscillator at the satellite translation frequency and replaces the ground-satellite distance with short pieces of cable. Reactive signal samplers tap a small fraction of the transmitted power and feed it into the satellite simulator mixers; the same type of reactive signal samplers then inject the translated signals into the receiver cables of the Observatory and remote transponder. Switching the relay indicated on Figure 6.3 provides a measurement of the Observatory internal time delay. The mixers and attenuators do not contribute significant signal delays due to their broadband nature. Furthermore, cable length differences between the Observatory internal time delay measurement circuit and remote transponder internal time delay measurement circuit are small. Insignificant cable delays result. This calibration scheme can be performed at the Observatory without the use of a satellite and is consequently hereafter referred to as the "in house" calibration.

For the "in house" calibration, consider T'_R as the four-way "ranging time" measured at the Observatory, where

$$T'_R = \delta'_o - \delta'_T - S_T + \delta_M + \delta_I + 409.6 - \delta_{SC} + \delta_L + S_R, \qquad (6.13)$$

and where all symbols remain as previously defined with the following additions:

δ'_o = signal time delay from Observatory interrogator through satellite simulator mixer to Observatory correlator,

δ'_T = constant time delay in starting the time interval counter which measures T'_R. For "in house" tests, δ'_T = 319910.3 μsec.

δ_M = time delay in cables, if any.

From the above, the integer time delay of the remote transponder is given by

$$\delta_I = T'_R - \delta'_o + \delta_{SC} + S_T - S_R - \delta_M - 85593.7, \qquad (6.14)$$

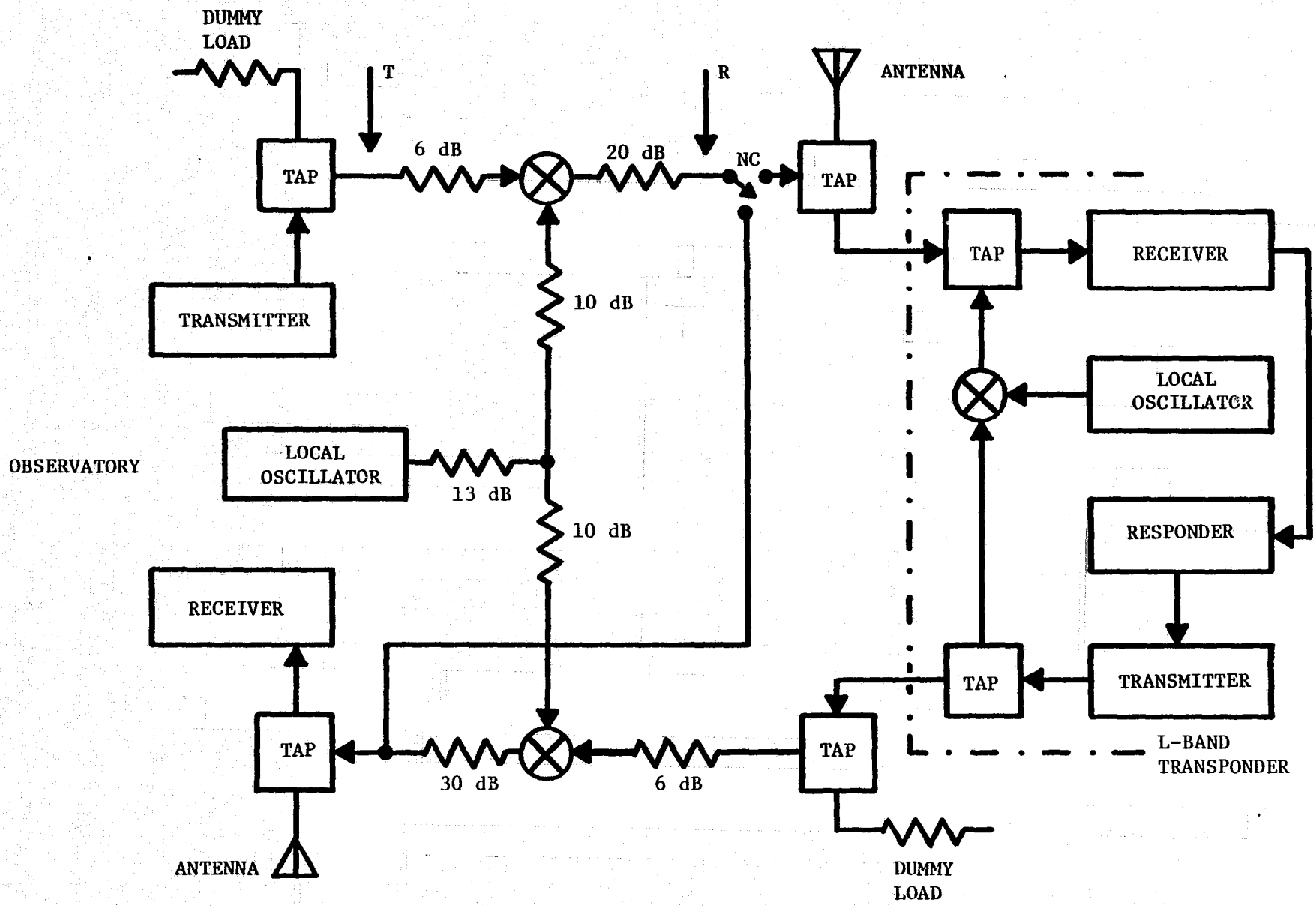

FIGURE 6.3 EQUIPMENT CONFIGURATION FOR "IN HOUSE" CALIBRATION OF BUENOS AIRES TRANSPONDER. T and R refer to insertion points for diplexer time delay measurement.

with all units in μsec.

It is possible with the "in house" calibration technique to inject signals into the receivers with signal-to-noise ratios orders of magnitude greater than those obtainable from the satellite. Each single ranging interrogation and response would thus have a precision orders of magnitude better than through the satellite and orders of magnitude less than the least significant digit of the measurement equipment. The immediate benefit from this approach would be the requirement of only one interrogation to establish internal time delays. This swift calibration, however, limits the range measurement accuracy to the resolution of the time interval counters and correlators. Error bounds on a single data point from a gaussian distribution having a standard deviation much less than the resolution of the measurement device are strictly plus and minus one half the value of the least significant digit in the measurement device. For this experiment, the accuracy would automatically be limited to $\pm$ 0.05 μsec for each correlator and time interval counter.

"In house" calibration precision may be significantly improved by reducing the signal-to-noise ratio such that the standard deviation of the data gaussian distribution is roughly equivalent to the magnitude of the least significant digit of the measurement device. Error bounds are now limited by the number of data points taken. The measurement precision improves as the inverse square root of the number of data points.

When data are grouped into integer sized bins, the measured mean will have its greatest accuracy if the true mean falls in the center of the bin or on the edge; the least accuracy will be achieved at points midway between the middle and edge of the bin. If the physical distribution has a standard deviation greater than 70 percent of the bin size, the measured mean will be in error by less than 5 percent. The inaccuracy of the measured mean decreases with an increase in standard deviation of the physical distribution, provided a sufficient number of data points are collected.

Observed values of range measurement standard deviation are similarly affected. With an increasing standard deviation in the physical distribution, the error in the observed standard deviation decreases. For values of standard deviation of the physical distribution greater than 70 percent of the bin size, the maximum error in the observed standard deviation would be less than 8 percent; for 40 percent, the maximum error is 30 percent. Maximum errors in observed standard deviation occur when the true mean value is centered in the bin.

6.1.3 Slant Range Calculation

From Equation 6.11, the Observatory-satellite slant range is given by

$$R = \tfrac{1}{2} (T_o - \delta_o - \delta_S - 2D_A). \qquad (6.15)$$

Defining R_T as the slant range from the satellite to the remote transponder, Equation 6.1 must be rewritten as follows:

$$T_R = 2R + 2R_T + D_o + D_R + 2\delta_S + 2D_A + 2D'_A, \qquad (6.16)$$

where

D'_A = total one-way atmospheric propagation time delay (ionospheric and tropospheric) between the remote transponder and the satellite.

The slant range R_T thus becomes

$$R_T = \tfrac{1}{2} (T_R - T_o + \delta_o - \delta_S - D'_o - D_R - 2D'_A), \qquad (6.17)$$

where D'_o is D_o less the geometry factor. Recalling the definitions for D_o and D_R^o, the above equation can be rewritten as

$$R_T = \tfrac{1}{2} (T_R - T_o + \delta_{SC} - \delta_R - 2D'_A), \qquad (6.18)$$

where all variables except the effective transponder delay, δ_R, are observables. The effective transponder delay includes delays in the satellite and at the Observatory, and is given by

$$\delta_R = \delta_S - \delta_T - S_T + \delta_I + S_R + \delta_{DR} + \delta_{DT} + 2\delta_W + \delta_{CR} + \delta_{CT} + 405504.0. \qquad (6.19)$$

The value for δ_R is determined prior to all ranging experiments and will not change unless changes are made to the transponder external to the self-calibration loop or unless changes are made to the thumbwheel settings.

6.2 DIPLEXER TIME DELAY

The remote transponder reactive signal samplers which remove a small fraction of the transmitted signal and inject the translated signal into the receiver are located between the diplexer and power amplifier and between the diplexer and receiver (see Figure 6.2). The diplexer is thus excluded from the self-calibration loop. Both the transmit and receive leg rejection filters and the L-band preamplifier are broadband devices. The band pass filter on the diplexer receive leg has the narrowest bandwidth, 50 MHz, at 3 dB down. As stated below, small time delays were observed in the diplexer; variations in time delay as a function of environmental conditions are assumed to be negligible.

The diplexer time delay is best measured by the "in house" calibration technique. The transmit leg of the diplexer is placed in the 1651

MHz line between the Observatory transmit reactive signal sampler and the satellite simulator mixer. Measurements of the Observatory internal time delay follow with and without the diplexer in place. The experiment was repeated with the receive leg of the diplexer in the 1550 MHz line between the satellite simulator mixer and the Observatory receiver. A 23 dB attenuator at the diplexer input compensates for the diplexer preamplifier gain. The symbols "T" and "R" in Figure 6.3 show the insertion points for the transmit leg and receive leg of the diplexer.

The results of an experiment conducted on Dec. 16, 1974, are presented in Figure 6.4. Subtraction of the interpolated Observatory internal time delay without the diplexer in place from the Observatory internal time delay with the diplexer in place determined the time delay through the appropriate diplexer leg. The standard deviations given for measurements do not include an uncertainty due to variations in the Observatory time delay, which changed through 0.03 μsec during this test. Several other tests to determine the diplexer time delay had to be discounted because of unaccountable variations in the Observatory internal time delay.

On the basis of the above experiment, the following values are assumed for the diplexer time delay:

Transmit Leg Time Delay, $\delta_{DT} = 0.016 \pm 0.007$ μsec,

Receiver Leg Time Delay, $\delta_{DR} = 0.084 \pm 0.009$ μsec.

6.3 CALIBRATION OF THE BUENOS AIRES TRANSPONDER

Both "satellite aided" and "in house" calibrations were performed on the Buenos Aires transponder (address code #8) to determine the internal time delay, to verify the accuracy of the self calibration circuits, and to verify the linearity of the adjustable portion of the responder internal time delay. Figure 6.5 shows a summary of these tests, representing data from one "satellite aided" calibration and two "in house" calibrations.

During the "satellite aided" calibration of Aug. 2, 1974, the transponder was operated in a configuration as sketched in Figure 6.6. The diplexer was mounted directly at the output of the L-band power amplifier, with a 6 foot piece of RG214 cable extending to the receiver. The diplexer was connected to the feed of a 6-foot dish antenna via 68 feet of 7/8" air dielectric coaxial cable and 6 feet of ½" foam dielectric coaxial cable. Cable lengths internal to the receive and transmit self calibration taps were not measured as their signal time delays are included in the self calibration response. The total cable delay, δ_C, for this experiement was 0.278 μsec; the geometrical delay, due to the 6-foot antenna being 26.7 feet closer to the satellite than the 30-foot dish antenna, was 0.027 μsec.

The result of the above test is presented in Figure 6.5 in the form of measurements of the responder integer time delay, δ_I. The measured

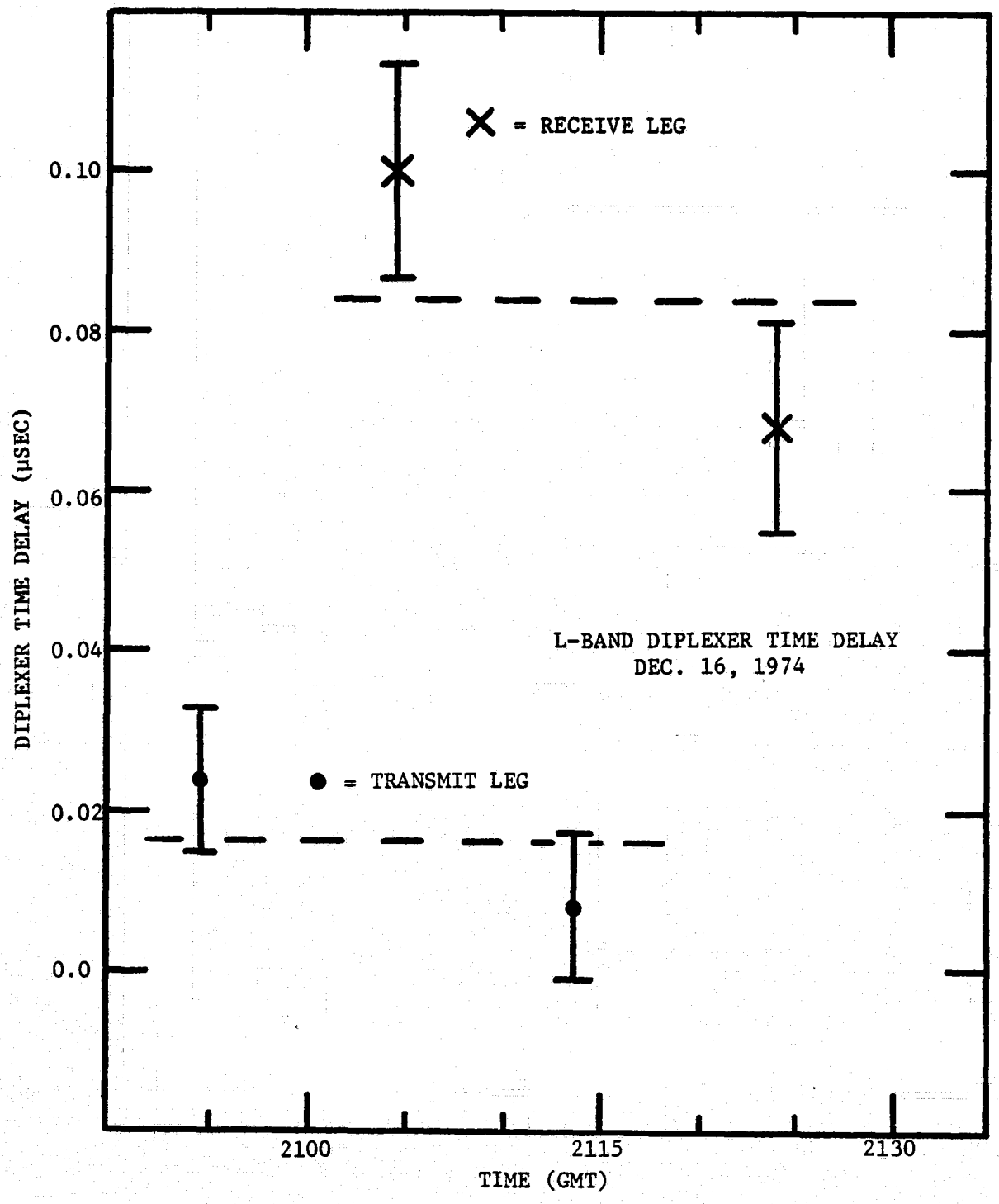

FIGURE 6.4 MEASUREMENT OF DIPLEXER TIME DELAY

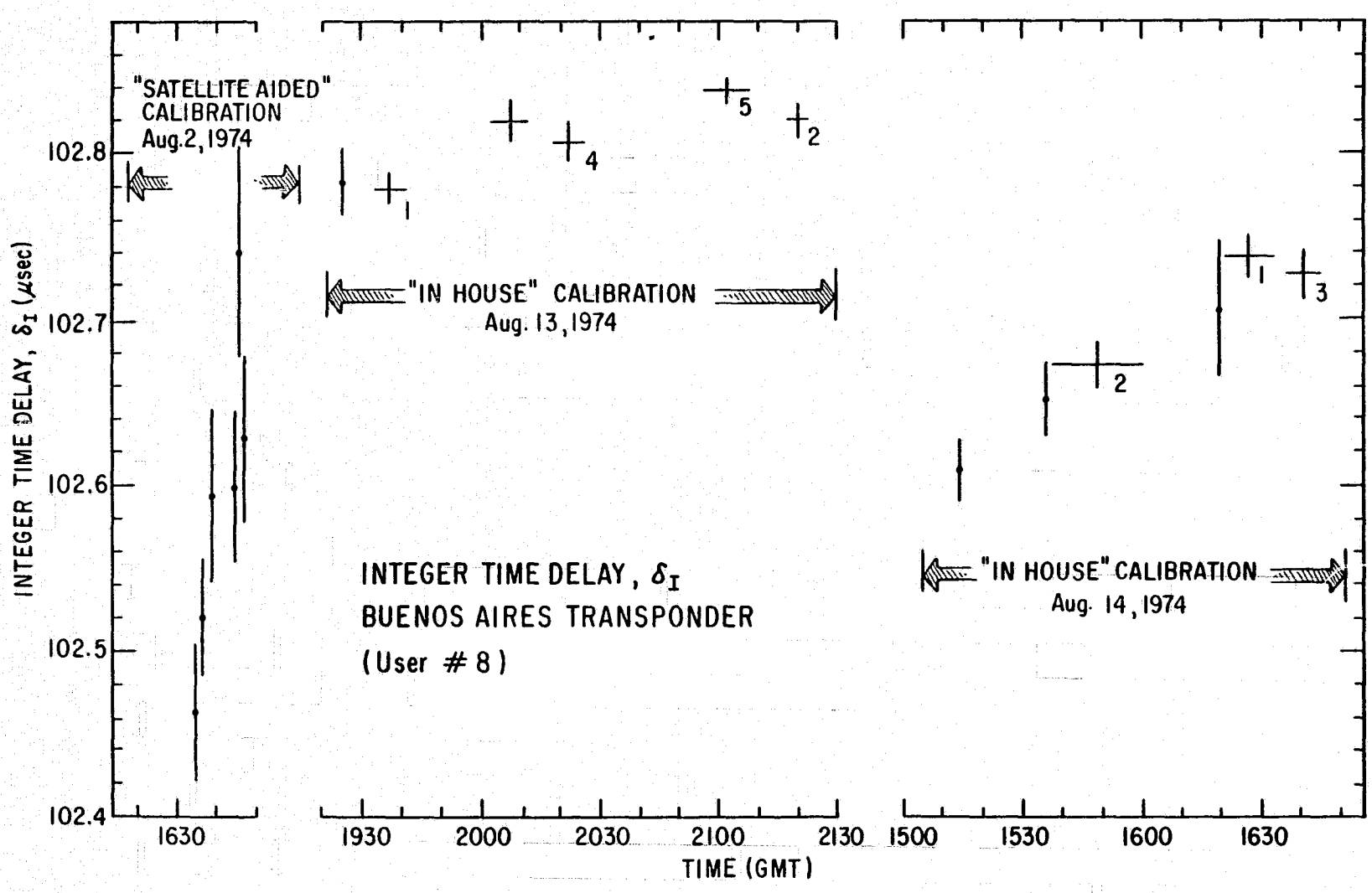

FIGURE 6.5 MEASUREMENTS OF BUENOS AIRES TRANSPONDER INTERNAL TIME DELAY

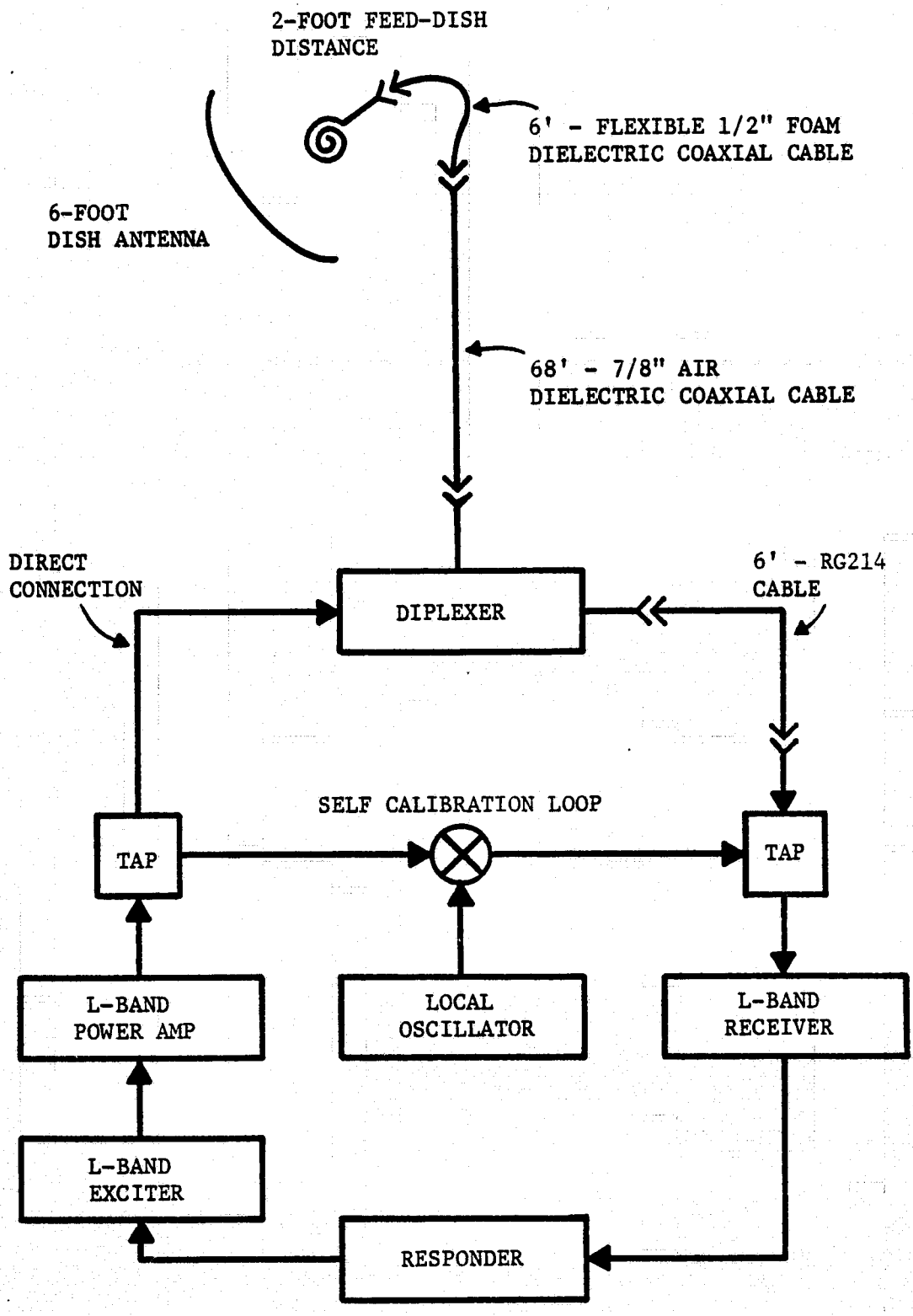

FIGURE 6.6 "SATELLITE AIDED" CALIBRATION - AUTOMATIC TRANSPONDER EQUIPMENT CONFIGURATION AT OBSERVATORY

ranging data have been corrected for the Observatory internal time delay, adjustable and fixed time delays at the responder and Observatory, transponder self calibration response, cable propagation delays, and geometrical effects.

It had been anticipated that the integer time delay would be an integer multiple of 102.4 μsec. Yet, the data suggest an integer time delay of roughly 102.6 μsec; the integer time delay thus appears to be a unit multiple of 102.4 μsec, plus a bias error. The responder has a fixed time delay of 405094.4 μsec, plus an adjustable delay specified by the manual setting of three thumbwheels. During this test, the adjustable delay was 116326.4 μsec, for a total "logic" delay in the responder of 521420.8 μsec. The responder delay is governed entirely by a 10 MHz oscillator, with a specified accuracy of $\pm$ 1 part in 10^6. Over 0.52 seconds, the oscillator could contribute a timing error of $\pm$ 0.52 μsec and still be within specifications. As no simultaneous measurements of oscillator frequency and internal time delay were made, the 0.2 μsec difference between the observed and expected value of the integer time delay is well within the oscillator specification.

At the time of this test only, the Observatory internal time delay was measured using a local oscillator with a frequency approximately 9 kHz lower than the satellite translation frequency. When the Observatory L-band receiver was tuned to the satellite return, the Observatory internal time delay was found to be 0.867 μsec lower than with the receiver tuned to the Observatory self calibration return. The Observatory internal time delay for both receiver tuning positions is sketched in Figure 6.7. The integer time delay data were all corrected for this effect by linear interpolations of the Observatory internal time delay.

Whenever the remote transponder correlates and returns the tone and address code, the self calibration response follows in the data stream. For the test on August 2, 1974, the time of the ranging interrogation and the range measurements were immediately punched on paper tape, while the self calibration data were read by the Observatory PDP-11/20 computer and put on a video display for recording by hand. For subsequent tests, the Observatory computer provided a hard copy of all self calibration data.

The shutdown of the ATS-5 L-band receiver on Aug. 3, 1974, prompted the development of the "in house" calibration technique, exercised on Aug. 13 and Aug. 14, 1974. The data points plotted in Figure 6.5 again represent the integer time delay δ_I. The unnumbered data points of Figure 6.5 were the result of range measurements with the Observatory and transponder systems undisturbed. The numbered data points reflect range measurements under the following conditions:

1. Responder thumbwheels cycled through various positions, thus changing the adjustable time delay of the transponder,

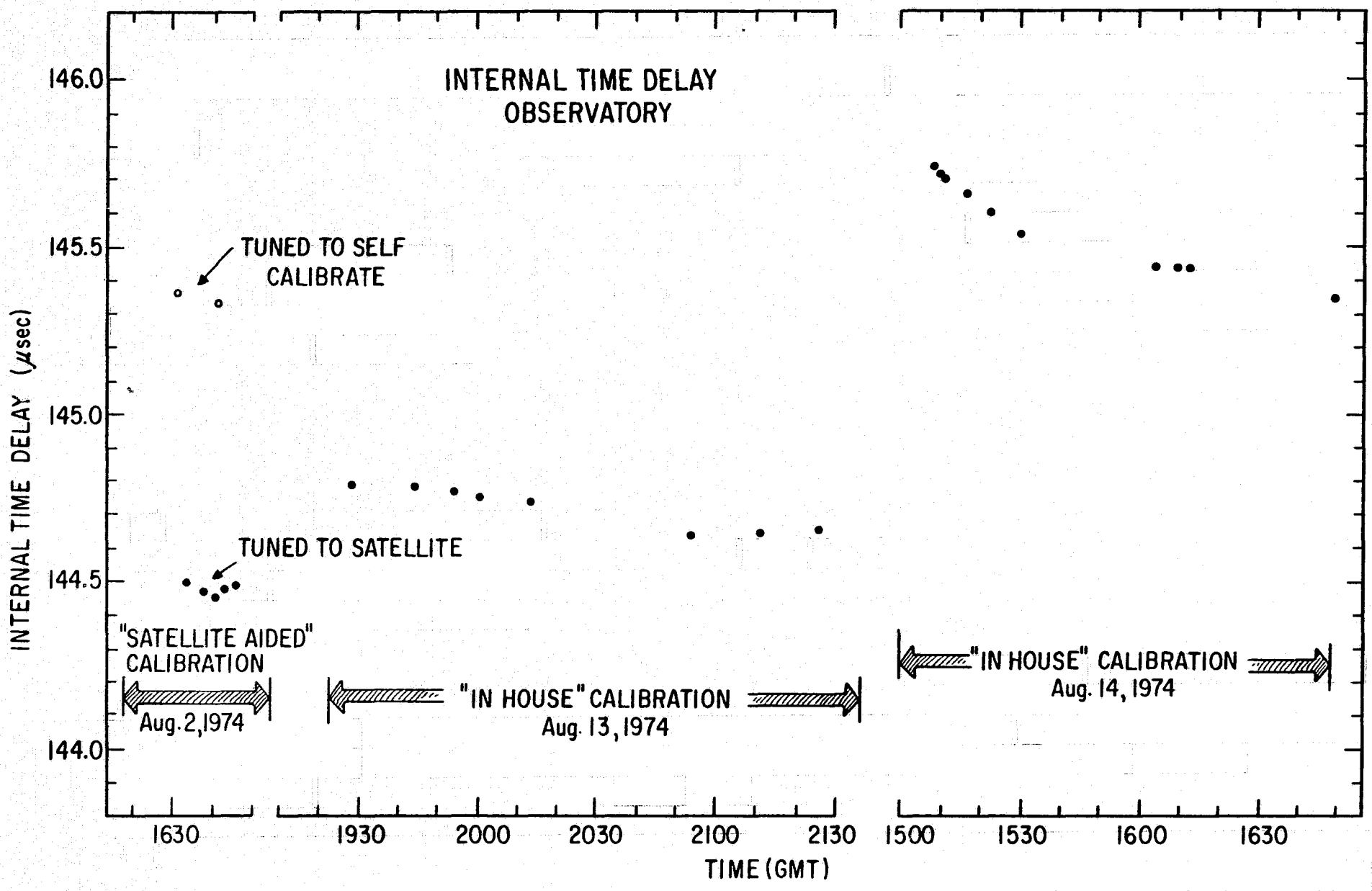

FIGURE 6.7 MEASUREMENTS OF OBSERVATORY INTERNAL TIME DELAY

2. Observatory thumbwheels cycled through various positions, thus changing the starting time of the time interval counter which measures the two-way Observatory-satellite-remote transponder ranging time,

3. Observatory and responder thumbwheels simultaneously cycled through the same settings thus affecting off-setting changes in the observed ranging time,

4. Responder tuned circuits subjected to heat,

5. Responder tuned circuits subjected to complete hot-cold cycle.

The data in Figure 6.5 show the ability to compute the variable time delay as determined by the responder and Observatory thumbwheels and also point out the corrective ability of the self calibration circuits as the responder tuned circuits are temperature cycled.

Figure 6.8 is an expansion of the single data point at 1628 GMT on Aug. 14, 1974, of Figure 6.5 and demonstrates the stability of the responder integer time delay as the variable portion of the responder time delay is adjusted through several settings of the three thumbwheels. Individual data points have standard deviations of typically 0.04 to 0.06 μsec. In the figure, each digit of the three digit number refers to the setting of one of the corresponding three thumbwheel switches which adjust the delay. The gradual drift of data points to a lower value for δ_I with an increase in time is probably due to over compensation of the Observatory time delay, δ'_o. During this test, no means existed for the simultaneous recording of δ'_o and the ranging time to the transponder. An interpolated value of δ'_o was subtracted from each ranging data point. The variation of the Observatory time delay is seen in Figure 6.7.

Individual ranging time measurements which contributed to the data point at 2102 GMT on Aug. 13, 1974, of Figure 6.5 are plotted in Figure 6.9, along with the response of the self calibration circuit and the individual values for the integer time delay. During this experiment, the tuned circuits of the responder were heated to approximately 80°C causing the ranging time to the transponder, T'_R, to drop approximately 4.5 μsec. The response of the self calibration circuit rose by the same amount such that the sum of the ranging time and the self calibration response remained a constant, as reflected by a constant value, plus statistical noise, for the integer time delay, δ_I. The responder tuned circuits were allowed to cool off naturally until 21:03:30, at which time they were cooled further to approximately -40°C by a spray of freon. Again, the change in the ranging time was matched by an equivalent and opposite change in the self calibration response.

A similar experiment conducted on July 30, 1974, verified the compensating action of the self calibration circuit while ranging through ATS-5. For "satellite aided" tests, the motion of the satellite will

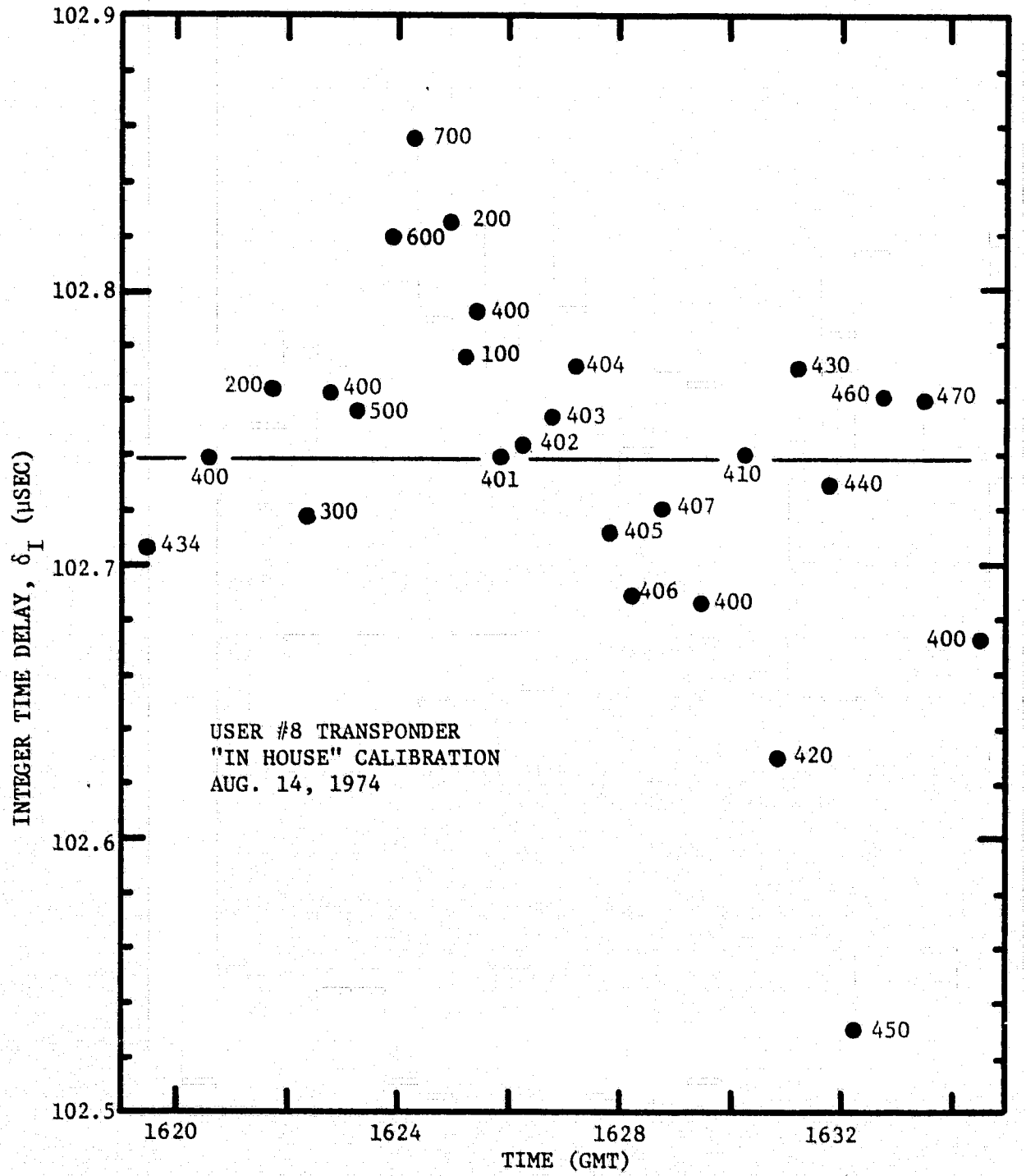

FIGURE 6.8 VARIATION OF USER #8 INTEGER TIME DELAY VS SETTING OF TIME DELAY THUMBWHEELS

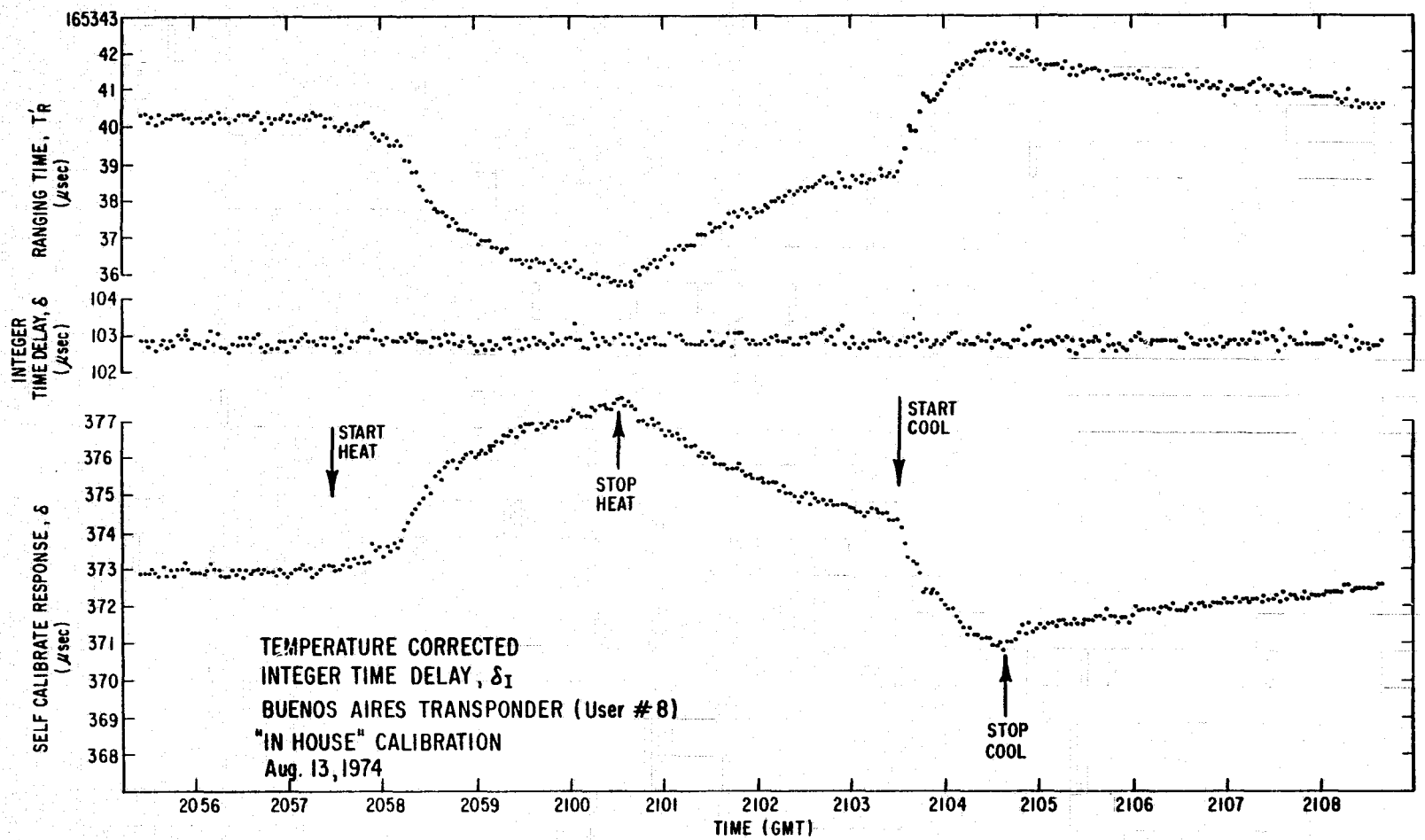

FIGURE 6.9 SELF CALIBRATION CORRECTION OF BUENOS AIRES TRANSPONDER INTERNAL TIME DELAY, "IN HOUSE" TEST

cause large changes in the ranging time. Consequently, the uncorrected relative internal time delay of the responder plotted in Figure 6.10 represents the two-way Observatory-ATS-5-transponder ranging time less twice the two-way Observatory-ATS-5 ranging time. The Observatory internal time delay was not measured during this experiment making it impossible to compute the integer time delay, δ_I. The relative internal time delay plotted in Figure 6.10 is the sum of the uncorrected relative internal time delay and the self calibration response. As the tuned circuits were heated in this experiment, the responder again showed a drop in internal time delay of roughly 4.0 μsec, equivalent to approximately 600 meters in slant range.

The data points of Figure 6.5 appear to follow trends consistent only for the particular day on which the experiment was conducted. There remain marked differences in the integer time delay as measured by the two "in house" calibrations and the "satellite aided" calibration. It is most significant that all the trends appear to be monotonically increasing. It has been pointed out that a change in the integer time delay of $\pm$0.52 μsec is consistent with the 10 MHz responder oscillator specification over a 0 to 50°C temperature range. The monotonically increasing values for the integer time delays are thus interpreted to be due to the warm-up of the 10 MHz oscillator. The equipment on each of the three days was turned on at approximately 1300 GMT, 1400 GMT, and 1400 GMT. On Aug. 13, 1974, the integer time delay was more stable than on the other days because the oscillator had been turned on more than 5 hours before the test.

Based primarily on the experiment conducted on Aug. 13, 1974, a value of 102.8 μsec is adopted for the integer time delay of the Buenos Aires transponder.

During all of the calibration experiments, the self calibration response was approximately 374.0 μsec due to the measurement of 35.6 μsec phase errors. The total analog delay of the transponder thus becomes 138.0 μsec. The Observatory analog time delay is typically 145.0 μsec. The Observatory receiver is conceptually the same as those in the remote transponders but contains more stages. Also, cables carrying the 9.7656 kHz tone at the Observatory are considerably longer than those in the transponders thus changing the characteristics of the Observatory interrogator/correlator tuned circuits. The lower analog delay of the transponder is thus entirely reasonable.

6.4 CALIBRATION OF THE HAWAIIAN TRANSPONDER

The transponder scheduled for operation in Hawaii (address code #11) was calibrated in a manner similar to that utilized for the Buenos Aires transponder. Figure 6.11 shows a summary of these calibrations, pointing out which were accomplished via the "satellite aided" or "in house" technique.

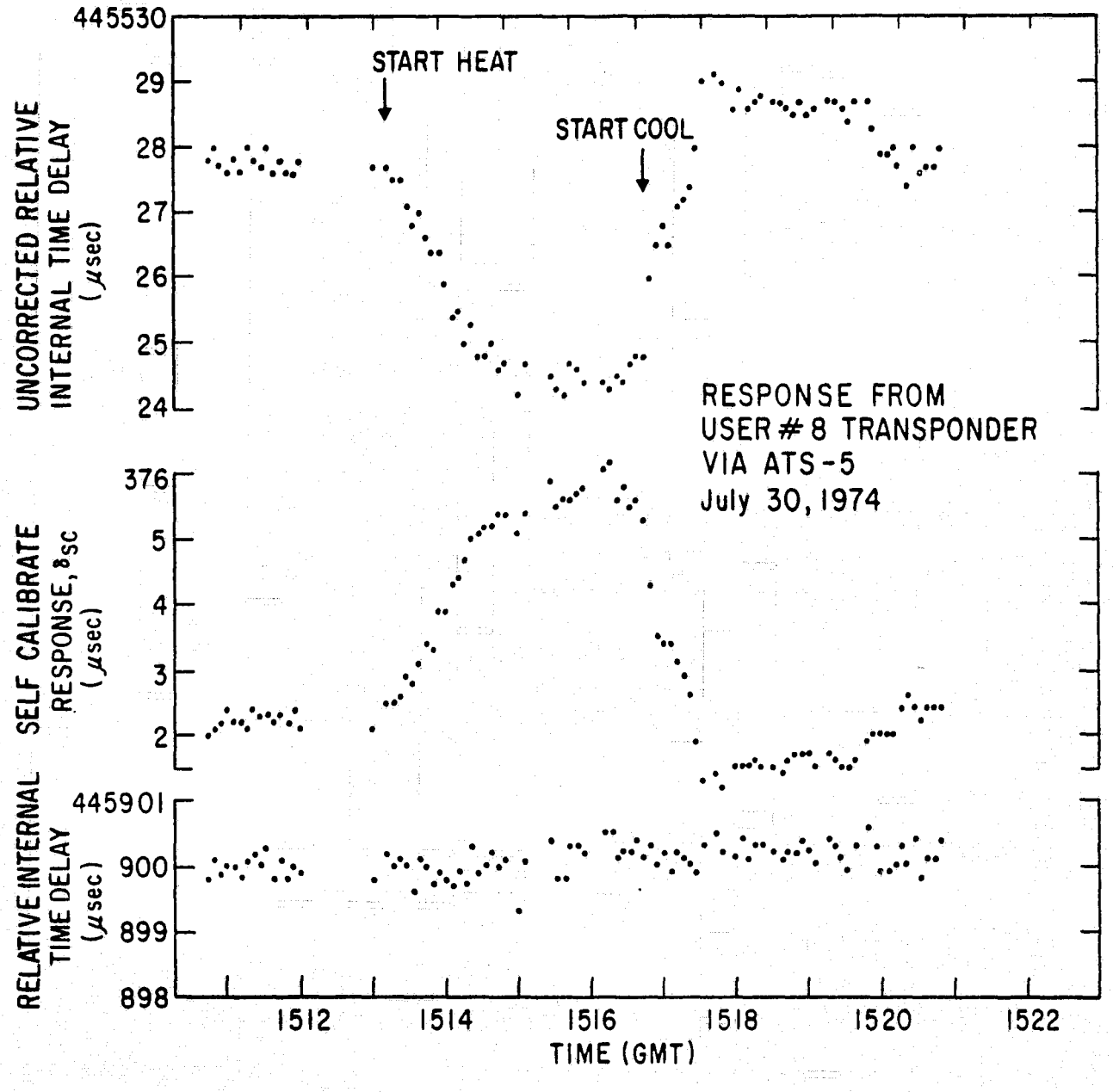

FIGURE 6.10 SELF CALIBRATION CORRECTION OF BUENOS AIRES TRANSPONDER INTERNAL TIME DELAY, SATELLITE TEST

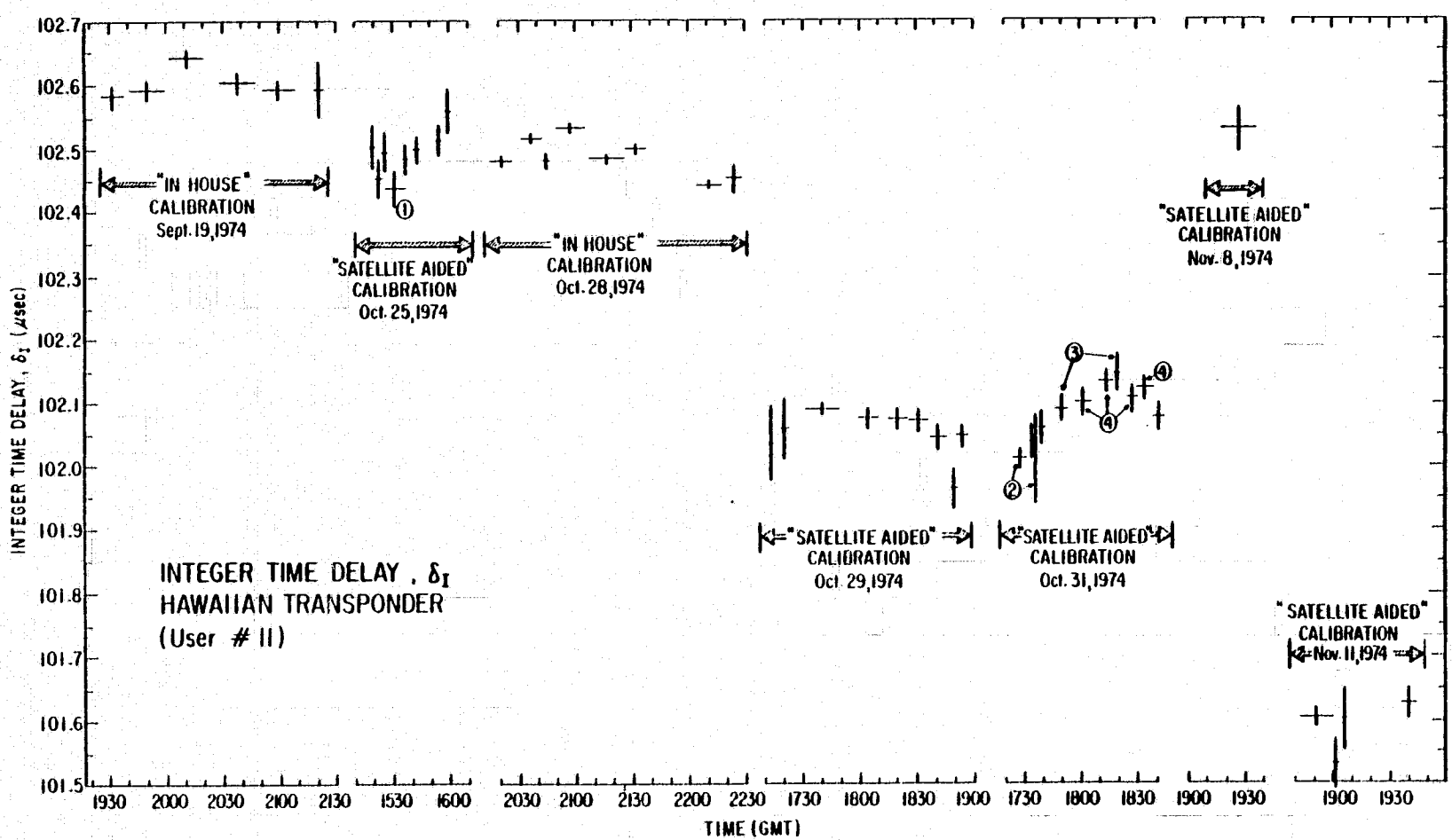

FIGURE 6.11 MEASUREMENTS OF HAWAIIAN TRANSPONDER INTERNAL TIME DELAY

The lack of a second proper L-band mixer required the use of a relay for the "in house" calibrations of the Hawaiian transponder. The new calibration measurement circuit depicted in Figure 6.12 also contained approximately 16 feet of cable between the transponder self calibration taps and the mixer simulating the satellite, yielding a cable delay, δ_M, of 0.020 μsec. One feature, however, gives the new technique a distinct advantage over that used for the calibration of the Buenos Aires transponder; the Observatory interrogator-RF-correlator internal time delay can be measured on every interrogation of the remote transponder, eliminating the need to interpolate the Observatory's randomly varying time delay. The Observatory transmitter keying circuit closes the switch shown in Figure 6.12.

The "in house" calibration of Sept. 19, 1974, was specifically designed to demonstrate the variation of the transponder logic time delay as a function of the frequency of the 10 MHz responder oscillator. The frequency of the 10 MHz oscillator was adjusted to several different values and measured to better than 1 part in 10^{10} while the responder was being interrogated. Figure 6.13 shows the uncorrected values of the responder integer time delay as a function of the 10 MHz oscillator frequency. The value of the integer time delay changed because the logic time delay had been temporarily assumed to be a constant. During these tests, the total "logic" delay of the ranging interrogation signal within the responder was approximately 521 msec. For each cycle that the frequency of the 10 MHz oscillator is high, the logic time delay of the responder will be low by 0.052 μsec. Correcting the integer time delay data of Figure 6.13 for the appropriate frequency change resulted in a constant value for the integer time delay, δ_I, at 102.602 $\pm$ 0.002 μsec. As a value of 102.4 μsec had been expected, it can only be concluded that the responder unit has an additional logic time delay of approximately two cycles of the 10 MHz oscillator. This additional delay may occur in switching from the correlation mode to the transmit mode.

Continuous adjustments of the 10 MHz oscillator during the test of Sept. 19, 1974 damaged the oscillator trimming coil. The entire oscillator was removed from card #1 of the responder and a new oscillator was installed and set to 10 MHz. The new oscillator has a frequency stability of $\pm$ 2 parts in 10^7. No further simultaneous measurements of the oscillator frequency and integer time delay were conducted.

The "satellite aided" calibration of Oct. 25, 1974 demonstrated the long term stability of the 10 MHz oscillator in the responder by yielding in a mean integer time delay of 102.477 $\pm$ 0.009 μsec, representing a drift in oscillator frequency of 2.4 Hz. The data point labeled with the number 1 represents the mean integer time delay of 19 samples, each sample having been taken with a different setting of the remote transponder thumbwheels. Different thumbwheel settings generate different logic time delays in the responder. This adjustment allows anticipation of the ranging time and subsequent passage of the response to the ranging interrogation through the "window" of the spinning ATS-5

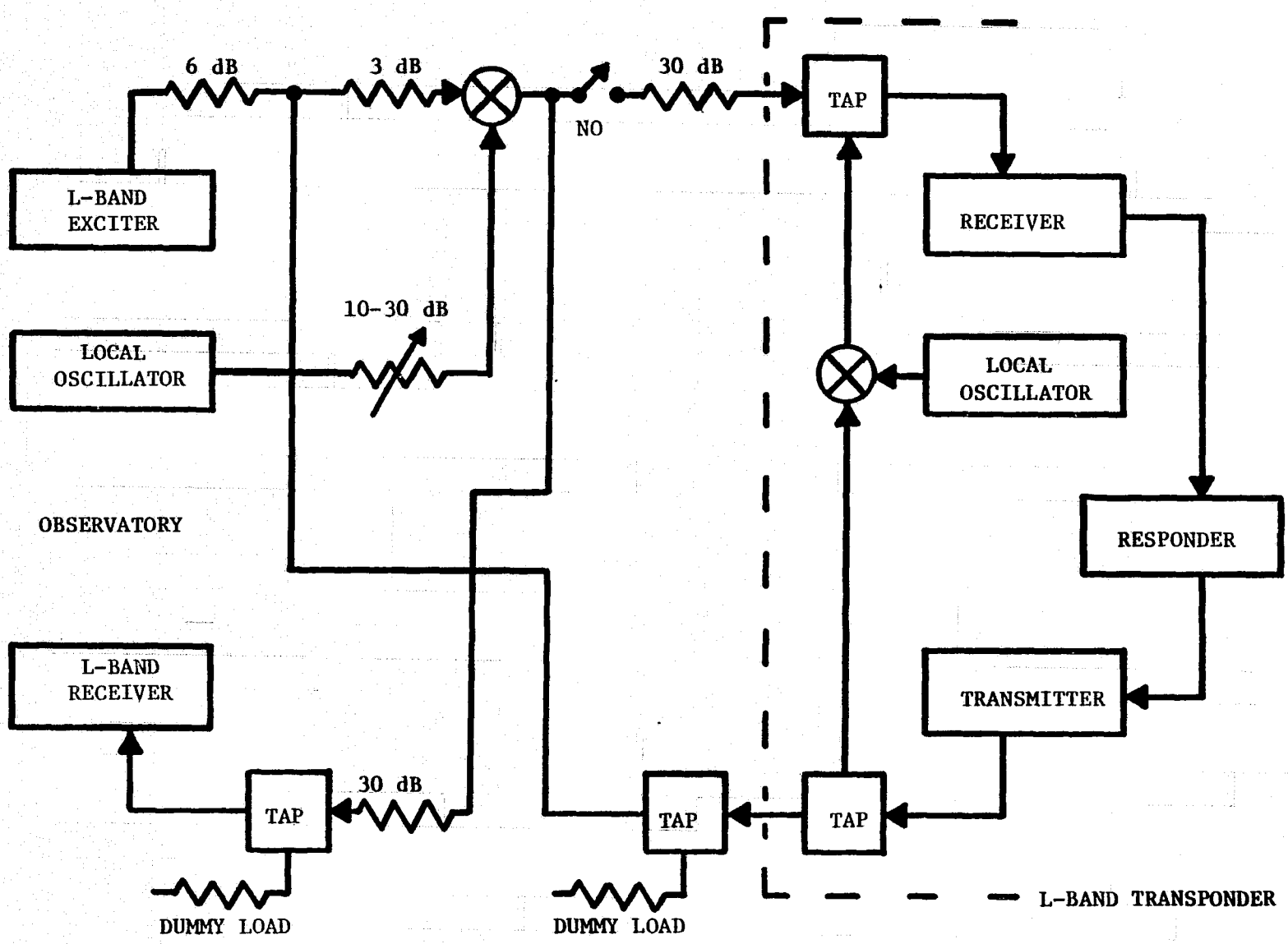

FIGURE 6.12 "IN HOUSE" CALIBRATION TO SIMULTANEOUSLY DETERMINE REMOTE TRANSPONDER INTEGER TIME DELAY AND OBSERVATORY INTERNAL TIME DELAY.

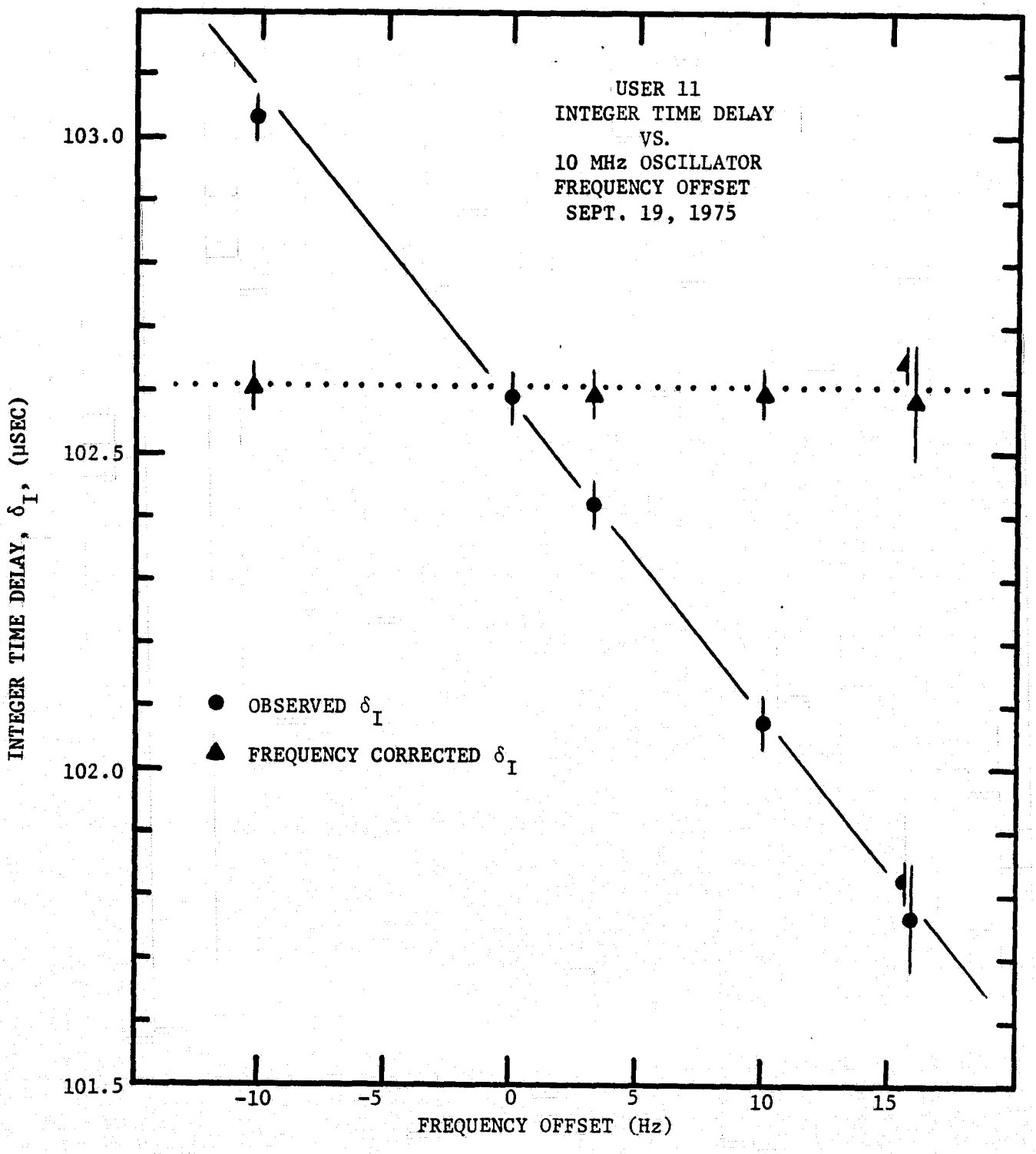

FIGURE 6.13 INTEGER TIME DELAYS VS. RESPONDER 10 MHz OSCILLATOR FREQUENCY

satellite. Figure 6.14 demonstrates the linearity of the thumbwheel setting with respect to logic time delay. If the logic time delay were other than predicted by Equation 6.10, the computed integer time delay would not remain constant. In Figure 6.14, each digit of the three digit numbers refers to the particular setting of each responder thumbwheel. Standard deviations on individual measurements are typically 0.1 μsec.

The "in house" calibration of Oct. 28, 1974, again verified the long term stability of the 10 MHz responder oscillator by yielding a mean integer time delay of 102.491 ± 0.003 μsec, in excellent agreement with the test of Oct. 25, 1974. The transponder was operated with the thumbwheels set to 460 during this entire test and during all subsequent calibration experiments.

The "satellite aided" calibration of Oct. 29, 1974 showed a sharp disagreement in the measurement of the integer time delay. The mean value of the integer time delay was found to be 102.066 ± 0.006 μsec and implies that the frequency of the 10 MHz responder oscillator went approximately 10 Hz high. It is conceivable that this change resulted from mechanical stress on the oscillator brought about by twisting card #1 of the responder and by pushing it in and out of its slot. In all other respects, this test was identical to the "in house" calibration conducted on Oct. 28, 1974.

The "satellite aided" calibration of Oct. 31, 1974 confirmed the apparent frequency change of the 10 MHz oscillator, yielding a mean integer time delay of 102.082 ± 0.007 μsec. The first and third data points on Figure 6.11 labeled with number 2 were taken with the Observatory L-band receiver tuned away from center frequency by approximately 2 kHz. No apparent change in the true value of the integer time delay results from this offset. The data points labeled with number 3 were taken while the responder tuned circuits were subjected to intense heat; data points labeled with number 4 were taken while the tuned circuits were cooled with a spray of freon. Throughout this temperature cycling, no significant variation in the integer time delay was observed. Figure 6.15 depicts the individual ranging interrogations during one hot and one cold cycle. The top trace represents the Observatory-satellite-remote transponder ranging time less twice the Observatory-satellite ranging time and thus differs from the integer time delay by only a constant. During heating and cooling, the transponder internal time delay and self calibration response matched each others variations through approximately 5.0 and 3.0 μsec, respectively. In both the hot and cold cycles, the integer time delay (middle trace) maintained its integrity. Throughout the calibration on Oct. 31, 1974, the integer time delay drifted through approximately 0.12 μsec, corresponding to a 10 MHz oscillator drift of approximately 2.5 Hz.

Before the "satellite aided" calibration of Nov. 8, 1974, the 10 MHz oscillator was set back onto center frequency, and the responder showed an integer time delay of 102.530 ± 0.032 μsec, consistent with the

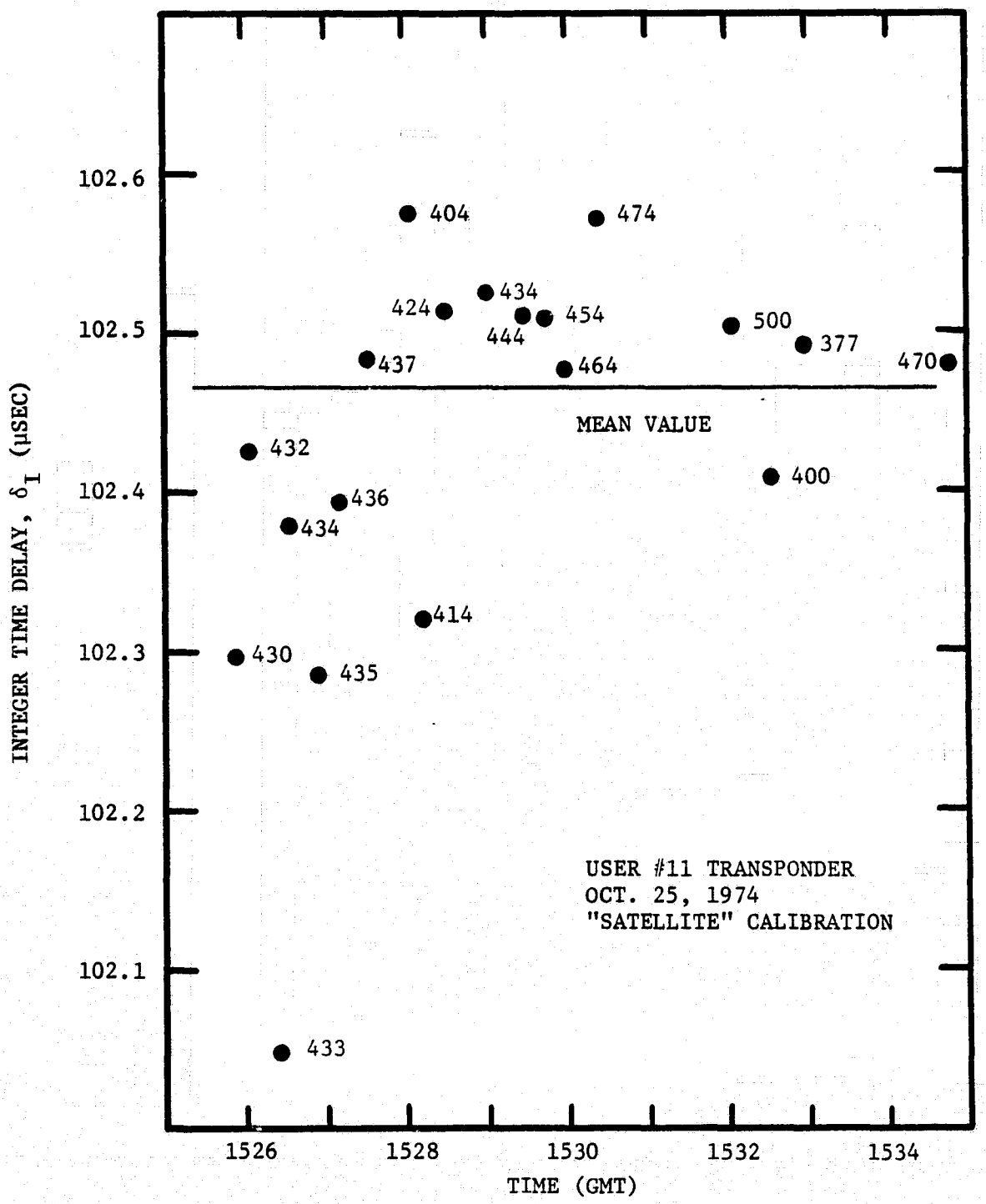

FIGURE 6.14 VARIATION OF USER #11 INTEGER TIME DELAY VS. SETTING OF TIME DELAY THUMBWHEELS

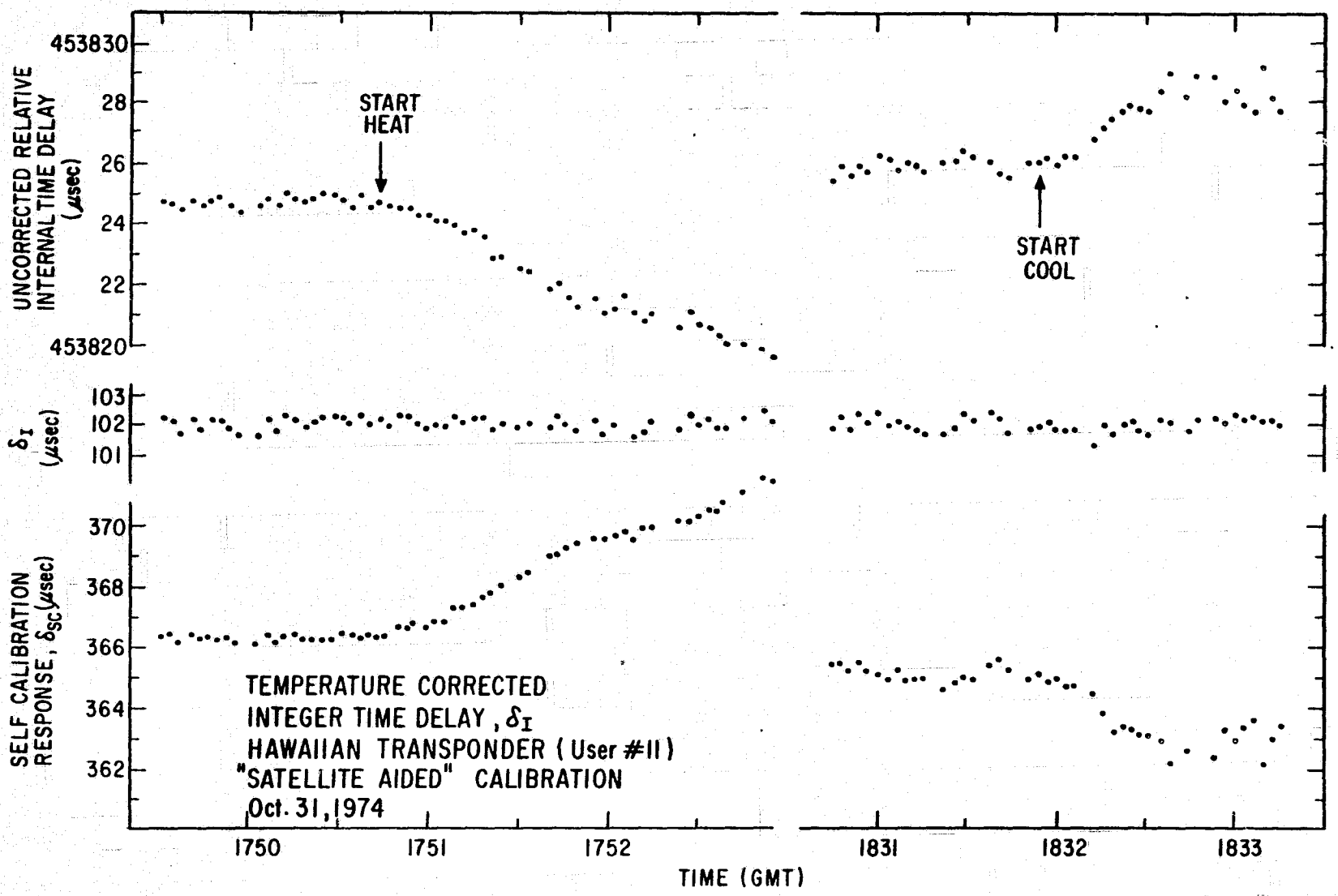

FIGURE 6.15 SELF CALIBRATION CORRECTION OF HAWAIIAN TRANSPONDER INTERNAL TIME DELAY, "SATELLITE AIDED" TEST

first three calibration tests depicted in Figure 6.11.

As a precaution against possible short circuits should the IC cards of the responder bend, the 10 MHz oscillator was removed and reinstalled with more adequate insulation prior to the "satellite aided" calibration of Nov. 11, 1974. The oscillator frequency was not checked for accuracy after this operation. The calibration test resulted in the measurement of a mean integer time delay of 101.605 $\pm$ 0.012 μsec, suggesting a frequency change in the 10 MHz oscillator of approximately 19 Hz. The transponder was shipped to Hawaii following this test without a final check on the frequency of the oscillator.

6.5 MEASUREMENT OF RESPONDER OSCILLATOR FREQUENCY

The VHF communication channels of the remote transponders can be employed to accurately and precisely yield a measurement of the frequency of the responders' 10 MHz oscillator. Figure 6.16 depicts the equipment configuration for such a test. The responder clock divides the frequency of the 10 MHz oscillator to generate the 2.4414 kHz audio frequency tone utilized for VHF ranging. Operating the VHF transponder in the continuous keying mode causes the responder to continuously modulate the carrier with this audio tone. Disconnecting the input to the responder from the VHF receiver prevents the phase matching circuits of the responder from adjusting the transmitted phase of the 2.4414 kHz tone to agree with that received through the VHF self calibration loop.

The frequency of the audio tone which leaves the transponder can be defined as f_s. If the satellite is moving away from the transponder with velocity v_r, the satellite will see a Doppler shifted frequency, f'_s, where

$$f'_s = f_s(1 - \frac{v_r}{c}), \tag{6.20}$$

and where c is the speed of light. The frequency seen at the Observatory, f_o, will again be Doppler shifted, such that f_o is given by

$$f_o \cong f_s(1 - \frac{v_o + v_r}{c}). \tag{6.21}$$

where v_o is the velocity of the satellite moving away from the Observatory. The motion of the satellite with respect to the transponder or Observatory is such that only the longitudinal Doppler shift need be considered.[13] The tranverse (relativistic) Doppler shift contributes only 1 part in 10^{13} to 10^{14}. Normal VHF ranging to the satellite and to the remote transponder before and after the frequency determinations measured changes in slant ranges which were directly converted into satellite velocities with respect to the ground stations.

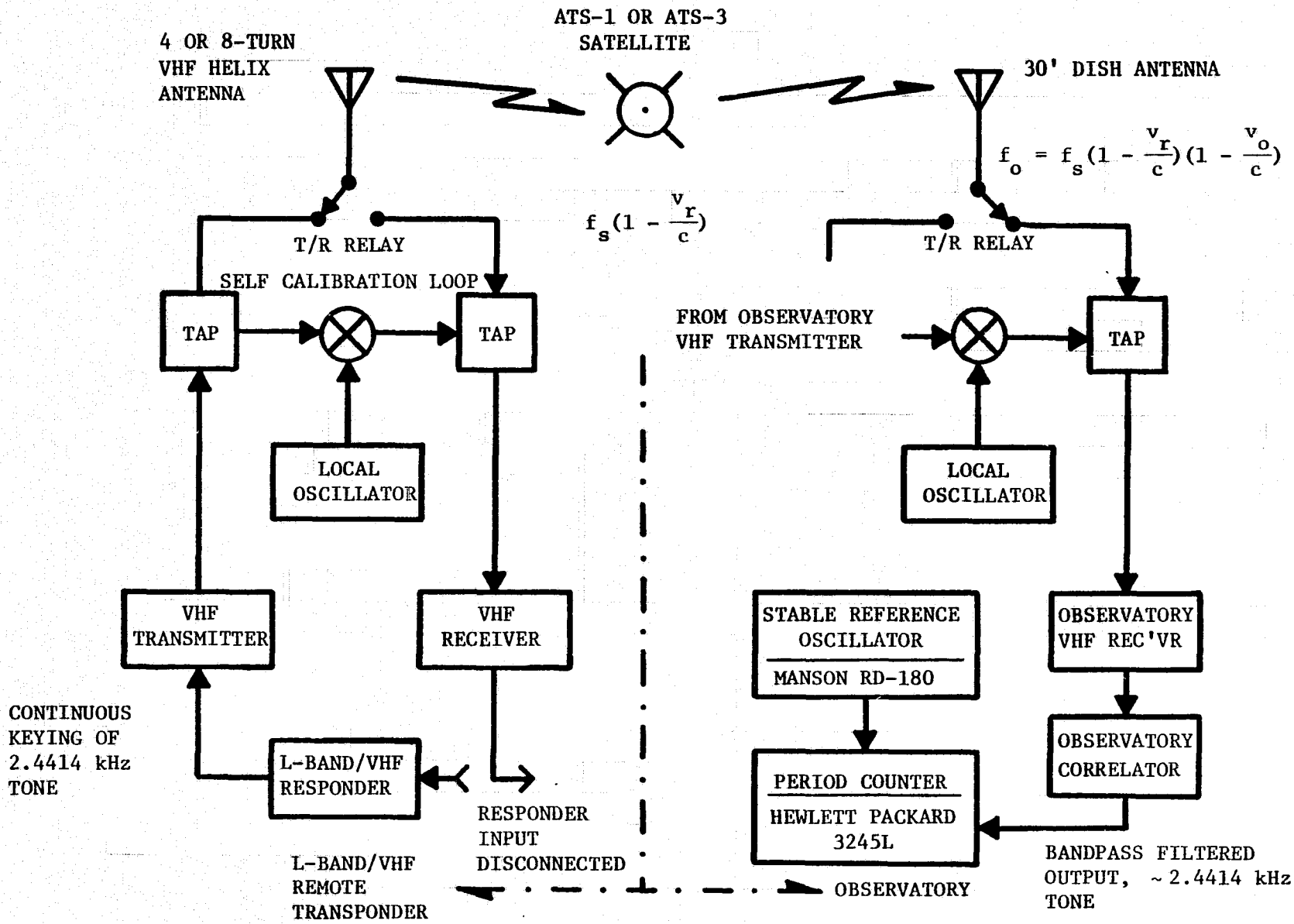

FIGURE 6.16 EQUIPMENT CONFIGURATION TO MEASURE FREQUENCY OF REMOTE TRANSPONDER 10 MHz OSCILLATOR

The VHF signal received at the Observatory is demodulated and bandpass filtered. The received 2.4414 kHz audio frequency tone drives a period counter referenced to a 1 MHz frequency standard. Ten thousand cycles of audio tone result in the counting of approximately 4.096×10^6 cycles of the standard frequency.

The results of several tests to measure the responders's 10 MHz oscillator frequency are listed in Table 6.1. This calibration technique was evaluated in two steps. First, the 2.4414 kHz audio frequency tone generated by the Observatory interrogator was directly connected to the period counter and showed the 10 MHz oscillator of the interrogator to be low by 0.05 ± 0.09 Hz. Since the period counter and the interrogator reference the same frequency standard, no frequency difference had been anticipated. Second, the Observatory interrogator tone continuously modulated the Observatory VHF transmitter. After a round trip to the satellite, the demodulated tone at the output of the Observatory correlator was applied to the period counter. The measured frequencies were corrected for the Doppler shift and the weighted mean frequency of the interrogator 10 MHz oscillator was found to be high by 0.86 ± 0.16 Hz. This includes five tests through two satellites. Again, no frequency change had been anticipated.

Two measurements of the 10 MHz responder oscillator in Buenos Aires were taken. Both show the oscillator frequency to be lower than 10 MHz. However, since the oscillator was assumed to be on frequency and since no simultaneous measurements of its frequency and the integer time delay were made, this frequency difference is only of academic interest. Continued tests over a long period of time under differing operating conditions can verify whether the oscillator is performing according to specifications, i.e., operating within $\pm$ 1 part in 10^6 of some unknown frequency near 10 MHz.

Four measurements of the 10 MHz responder oscillator in Hawaii were conducted. They show the weighted mean frequency 17.12 ± 0.24 Hz higher than nominal. This frequency difference is consistent with transponder calibrations while the transponder was still at the Observatory. If the 10 MHz oscillator is 17.12 Hz higher in frequency, the responder logic time delay is correspondingly low by 0.900 μsec. During the "in house" calibration of Sept. 19, 1974, simultaneous measurements of the oscillator frequency and the responder integer time delay allowed the integer time delay to be fixed at 102.605 μsec while the 10 MHz oscillator was directly on center frequency. Mechanical disturbance of the oscillator between Nov. 8 and Nov. 11, 1974 apparently caused the oscillator to change frequency, reducing the logic time delay and implying an apparent integer time delay of 101.605 μsec. An oscillator frequency shift of approximately 19 Hz could account for this change in integer time delay. The "in house" calibration of Sept. 19, 1974, the "satellite aided" calibration of Nov. 11, 1974 and VHF measurements of oscillator frequency thus become consistent to within the $\pm$ 2 parts in 10^7 specification of the oscillator frequency, if it is assumed that the frequency changed abruptly before Nov. 11, 1974.

TABLE 6.1

VHF SATELLITE MEASUREMENT OF RESPONDER
10 MHz OSCILLATOR FREQUENCY

Date (1975)	Time (GMT)	Satellite	Source	Frequency Error (Hz)
2/13	1554	ATS-3	Observatory	- 0.91 ± 0.68
		ATS-3	Buenos Aires	- 9.21 ± 0.50
		ATS-1	Hawaii	+17.26 ± 1.21
2/18	1554	ATS-3	Observatory	+ 0.27 ± 0.66
		ATS-3	Buenos Aires	- 6.97 ± 0.41
2/20	1549	ATS-1	Observatory	+ 0.59 ± 1.96
		ATS-1	Hawaii	+18.14 ± 1.02
3/4	1420	ATS-1	Hawaii	+17.79 ± 1.68
		ATS-1	Observatory	+ 1.35 ± 1.51
		ATS-1	Observatory	+ 2.17 ± 0.51
		ATS-1	Hawaii	+16.66 ± 0.59
3/6	-	Direct Connection	Observatory	- 0.05 ± 0.09
Mean Value		ATS-1 and ATS-3	Observatory	+ 0.86 ± 0.16
Mean Value		ATS-3	Buenos Aires	- 8.09 ± 0.32
Mean Value		ATS-1	Hawaii	+17.12 ± 0.24

6.6 OPERATIONAL CONFIGURATION OF BUENOS AIRES TRANSPONDER (USER #8)

The L-band transponder in Buenos Aires is configured as sketched in Figure 6.17. The diplexer is connected directly to the output of the L-band power amplifier, with 8 feet of RG8 cable feeding the L-band receiver. 8 feet of ½" flexible foam dielectric coaxial cable connects the diplexer to the 7/8" air dielectric coaxial cable. The air dielectric coaxial cable is heavy and not readily set in place.

The components which contribute to the effective transponder internal time delay for USER #8 are listed in Table 6.2. While no simultaneous measurements of the 10 MHz oscillator frequency and integer time delay were made, it is interesting to note that the measurement of the 10 MHz oscillator frequency via the VHF communication channel suggests the oscillator frequency to be approximately 8 Hz low. Correcting the integer time delay for this frequency difference would yield a value of approximately 102.4 μsec, 0.2 μsec different from that observed for the Hawaiian transponder's integer time delay on Sept. 19, 1974. As both responders are the same, the same integer time delays are expected.

6.7 OPERATIONAL CONFIGURATION OF HAWAIIAN TRANSPONDER (USER #11)

The L-band transponder in Hawaii is configured as sketched in Figure 6.18. The diplexer is mounted on the back surface of the 10-foot antenna dish. 100-foot sections of 7/8 inch air dielectric and ½ inch foam dielectric coaxial cables connect the L-band power amplifier with the diplexer and the diplexer with the L-band receiver, respectively.

The various components which contribute to the effective transponder internal time delay are listed in Table 6.3. The value of 101.705 μsec for the integer time delay is based on the simultaneous measurement of integer time delay and 10 MHz oscillator frequency on Sept. 19, 1974 and the measurements of the 10 MHz oscillator frequency via the VHF communication channel. This disagrees by less than 0.1 μsec with the integer time delay measured on Nov. 11, 1974, at which time the 10 MHz oscillator is assumed to have had the same frequency as measured via the VHF communication channel.

6.8 INTERNAL TIME DELAY VARIATION VS. RADIO FREQUENCY

The two separate remote transponders transmitting to the Observatory via ATS-5 may not be received on exactly the same radio frequency. The Observatory L-band receiver is tunable but with two remote transponders and the Observatory self calibration response, tuning to each signal during ranging becomes impractical and one or all of the signals will be received slightly off frequency.

Apparent changes in the Observatory and remote transponder internal time delays are generated by detuning the L-band receivers. This was observed on Aug. 13, 1974 and on Jan. 8, 1975 by measuring the Observatory internal time delay with the Observatory L-band receiver alternately

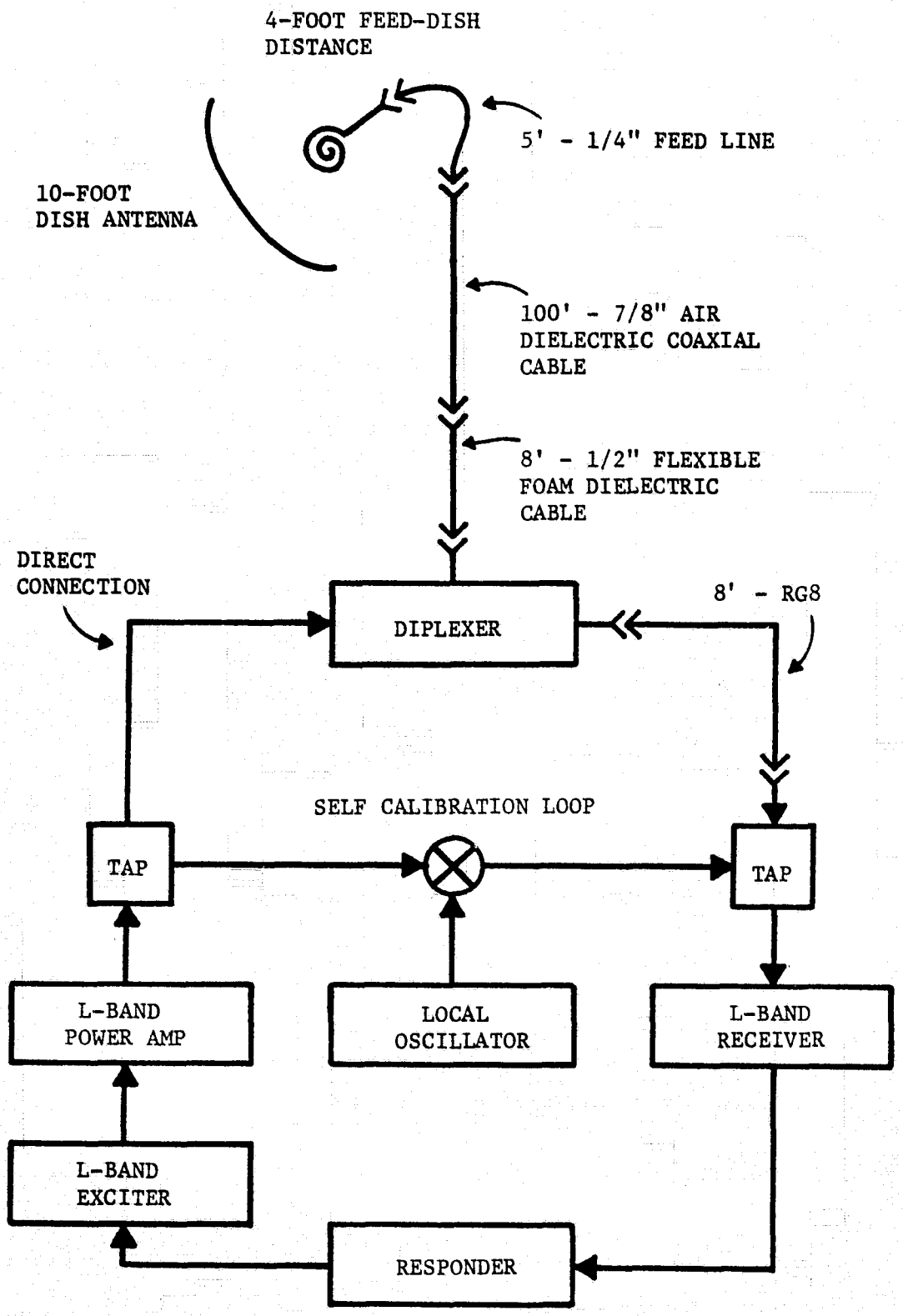

FIGURE 6.17 L-BAND TRANSPONDER CONFIGURATION IN BUENOS AIRES, ARGENTINA: USER #8

TABLE 6.2

EFFECTIVE TRANSPONDER DELAY

USER #8, BUENOS AIRES

(All units are microseconds)

δ_I		102.8
$-\delta_T$		-39334.300
$-S_T$		-36454.400
$S_R(370)$		101580.800
δ_{DR}		0.084
δ_{DT}		0.016
$2\delta_W$		0.263
δ_{CR}		0.010
δ_{CT}		0.000
Constant		405504.000
$\delta_R - \delta_S$*	=	431399.273

* δ_S is the ATS-5 L-L NBFM internal time delay.

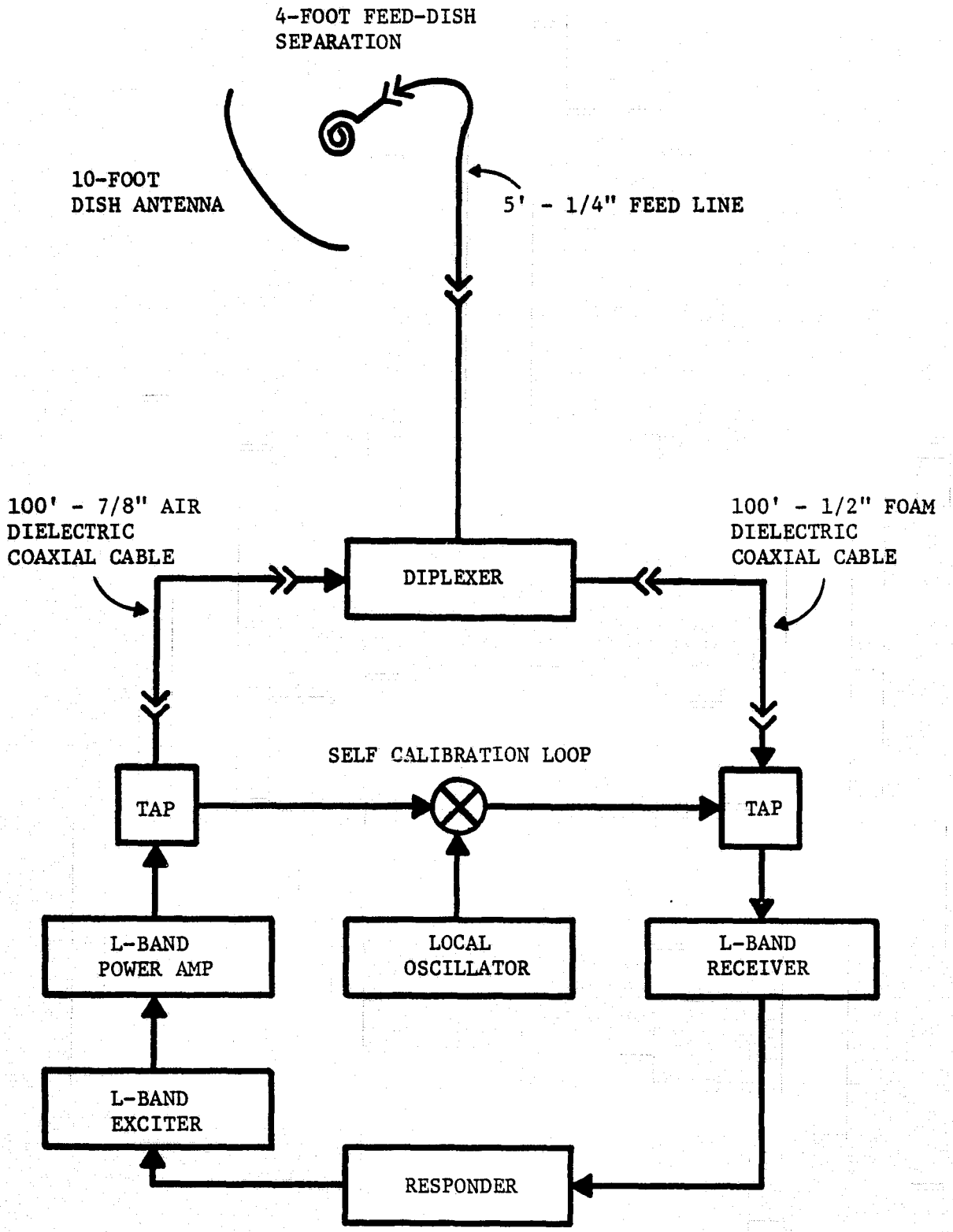

FIGURE 6.18 L-BAND TRANSPONDER CONFIGURATION AT THE U.S. COAST GUARD COMMUNICATION STATION NEAR WAIHIAWA, HAWAII: USER #11

TABLE 6.3

EFFECTIVE TRANSPONDER DELAY

USER #11, HAWAII

(All units in microseconds)

δ_I		101.705
$-\delta_T$		-39334.300
$-S_T$		-36454.400
$S_R(450)$		121241.600
δ_{DR}		0.084
δ_{DT}		0.016
$2\delta_W$		0.021
δ_{CR}		0.129
δ_{CT}		0.111
Constant		405504.000
$\delta_R - \delta_S$*	=	451058.966

*δ_S is ATS-5 L-L NBFM internal time delay.

tuned and untuned. Figure 6.19 presents the reduction in internal time delay as a function of frequency offset, with neglibible standard deviations on all data points. In a second experiment on Aug. 13, 1974, the Observatory L-band receiver was alternately on and off center frequency for the "in house" response from the Buenos Aires transponder. Inasmuch as all of these experiments were conducted over a short period of time with the receiver alternately on and off center frequency, the exciter and receiver frequencies are assumed to remain stable such that the relative frequency offsets are precise.

The RF crystals in the remote transponder and Observatory exciters are rated at 2 parts in 10^6 over an operating range from -30°C to +60°C. In a laboratory environment, they may be considered accurate to 1 part in 10^6, or approximately $\pm$ 1.7 kHz variation at the exciter output. Under the same operating conditions, the self calibration oscillator may vary at most by $\pm$ 500 Hz. Assuming a maximum $\pm$ 2 kHz variation in the remote transponder transmit and Observatory self calibration frequencies, the data of Figure 6.19 suggest that range measurement errors of less than 0.1 μsec, or roughly 15 meters in slant range, are achievable. Following warm-up, the Observatory L-band receiver can be tuned to within $\pm$ 200 Hz of any desired frequency.

The first and second local oscillators at 1520 MHz and 30 MHz, respectively, fix the receive frequencies of the remote transponders. Again assuming the frequency error in a laboratory environment to be half that given in oscillator specifications, the remote transponders may see signals from the Observatory and their own self calibration loop as much as $\pm$ 2 kHz from center frequency.

A less extensive test conducted on Sept. 20, 1974 with the Hawaiian transponder demonstrated that the apparent variation of the internal time delay due to changes in the frequency received at the transponder is no worse than that for the Observatory. During this test, the frequency of the 1520 MHz oscillator was adjusted to simulate changes in the received frequency. For the data of Figure 6.20, the off center frequencies in the first local oscillator were measured to within $\pm$ 0.1 Hz, but no measurement was made of the transmit frequency or the frequency of the second local oscillator. Although the two data points for the offset frequencies contain large uncertainties in absolute frequency, their relative frequency is accurately known, as they were taken within 5 minutes of each other. The slope of these two data points suggests a maximum change of 0.04 μsec/kHz, an error rate slightly better than that for the Observatory receiver.

6.9 ANALYSIS OF L-BAND RANGING PRECISION

Of the several factors affecting the precision achievable with the tone code ranging technique, the most severe is that due to noise accompanying the ranging tone. A theoretical analysis of this effect as reported by Milton[11] shows that for a frequency modulated carrier,

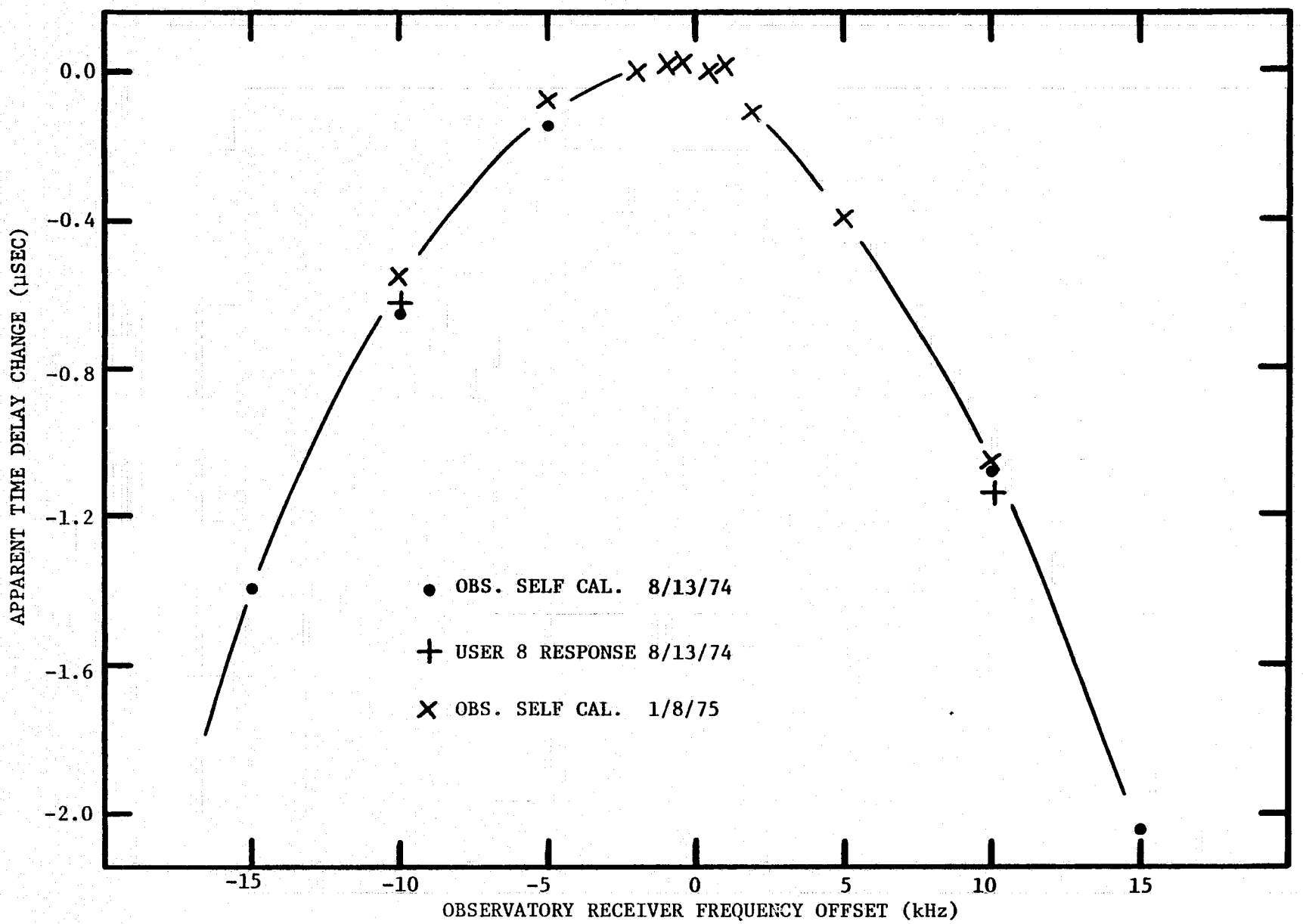

FIGURE 6.19 APPARENT TIME DELAY CHANGE VS. OBSERVATORY RECEIVER FREQUENCY OFFSET

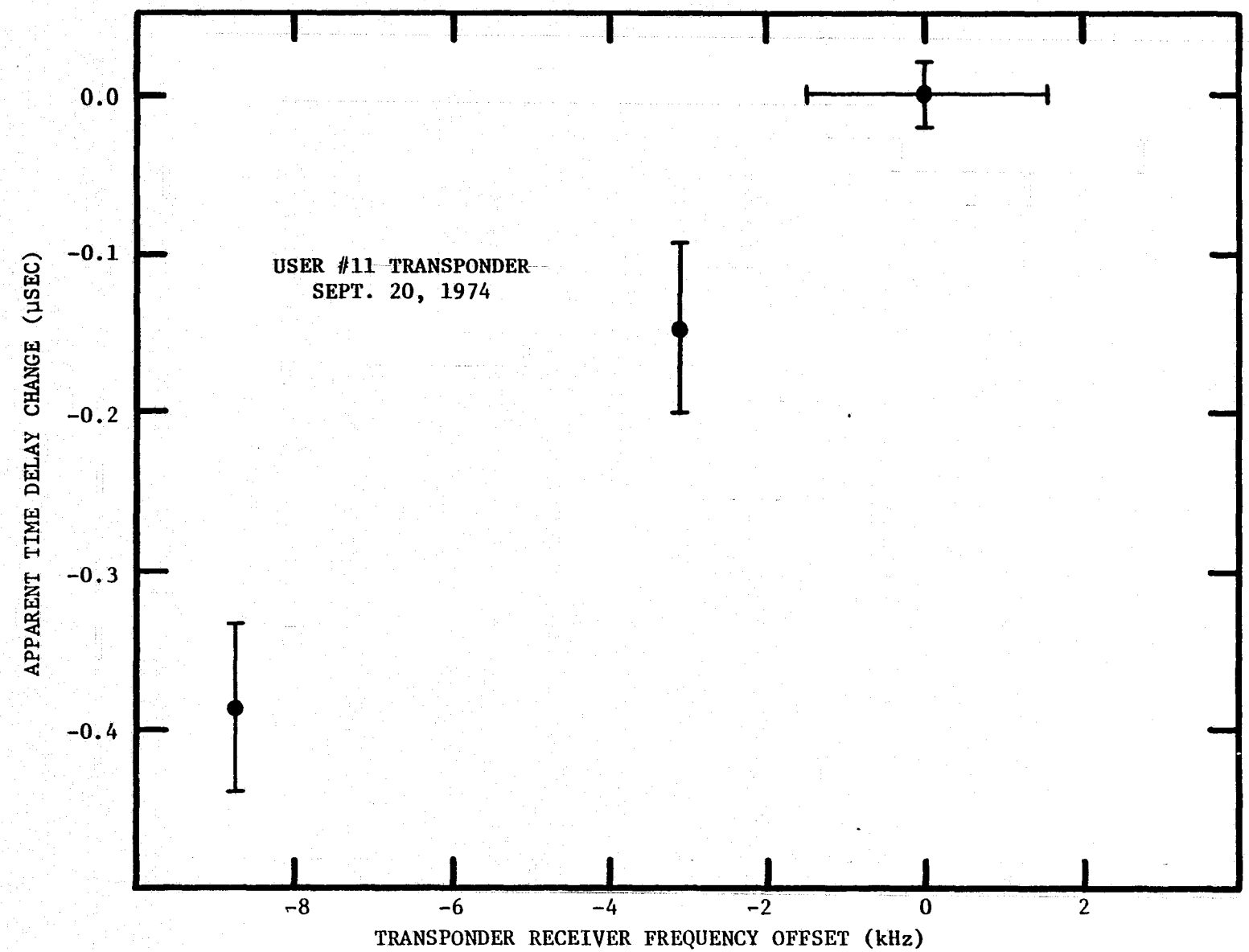

FIGURE 6.20 APPARENT TIME DELAY VARIATION VS. TRANSPONDER RECEIVER FREQUENCY OFFSET

the lower limt on the range measurement standard deviation is given by

$$\sigma_{RF} = \frac{1}{2\pi\Delta F}\left[T(C/N_o)\right]^{-\frac{1}{2}} \qquad (6.22)$$

where

ΔF = peak frequency deviation,

T = ranging tone duration,

C/N_o = carrier-to-noise density at IF.

The above equation assumes ideal demodulation of the signal. A modulation index of approximately 2 yields a value of 20 kHz for ΔF, given a modulating tone frequency of 9.7656 kHz. The 256 cycles of the ranging tone used to phase match the clock of the responder result in an effective tone duration of 26.2 msec. The theoretical ranging resolutions presented in Table 6.4 consider several values of carrier signal-to-noise ratio.

All correlators in the remote transponders and at the Observatory round off the time of arrival of the tone burst to the nearest 0.1 μsec, yielding a maximum error of ± 0.05 μsec. As the satellite is always moving with respect to a remote transponder or the Observatory, ranging errors from -0.05 μsec to +0.05 μsec are equally probable, resulting in a correlator generated range measurement standard deviation, σ_{CR}, of 0.029 μsec. This round off error occurs for every passage of the ranging tone through a correlator. Thus, for the Observatory-satellite link, the round off ranging error is 0.029 μsec; for the remote transponder-satellite-Observatory link, the two correlators result in a 0.041 μsec contribution to the standard deviation.

The data acquisition hardware reads the Observatory clock 0.1 seconds after correlation on the satellite return of the ranging interrogation. Recorded times are accurate to within plus one second and minus zero seconds. With two-way Observatory-satellite ranging times of approximately 0.25 seconds, reinterpretation of the recorded time as the interrogation time yields event times accurate to within plus 0.65 seconds and minus 0.35 seconds (0.15 second bias). Due to the spinning nature of ATS-5, interrogations are made on every third rotation, or approximately every 2.3 seconds. The random interrogation time within the one second time bin of the Observatory clock generates an interrogation time standard deviation of approximately 0.34 seconds.

If the satellite is not moving toward or away from the remote transponder or Observatory, slant ranges remain constant and a bias in the interrogation time will not introduce an inaccuracy. However, the two-way Observatory-ATS-5 slant range has been observed to change by as much as 0.09 μsec per second. A 0.34 second interrogation time standard deviation thus generates a "time recording" range measure-

TABLE 6.4

THEORETICAL RANGING RESOLUTION AT L-BAND

DUE TO RF NOISE

Signal-to-Noise (dB)	C/N_o in 60 kHz Bandwidth (dBHz)	σ_{RF} (μsec)
4.8	52.6	0.115
6.0	53.8	0.100
10.0	57.8	0.063
15.0	62.8	0.036
20.0	67.8	0.020

ment standard deviation, σ_{TR}, of 0.031 μsec. On the Observatory-satellite-remote transponder link, a maximum two-way slant range rate of change of 0.15 μsec per second has been observed, contributing 0.051 μsec to the range measurement standard deviation.

At L-band frequencies and with antenna elevation angles between 26 to 32 degrees, the ionospheric propagation time delay varies between approximately 0.007 and 0.030 μsec, night to day. Severe unpredictable solar disturbances may generate changes in the ionosphere which can cause the above time delays to fluctuate by more than 50 percent over periods of tens of minutes. As the maximum contribution due to the ionosphere corresponds to a two-way range measurement error of approximately 0.06 μsec, a negligible contribution is assumed for the range measurement standard deviation.

The maximum radio propagation time delay due to the troposphere varies between 0.012 and 0.015 μsec for all ground stations of the trilateration network. Since the tropospheric delay varies only approximately 20 percent over the range from 100 percent to zero percent relative humidity, no tropospheric contribution to the range measurement standard deviation will be considered.

Many range measurements were made from the Observatory to the satellite and to the remote transponders while they were temporarily installed at the Observatory. A 6-foot parabolic antenna was used instead of the 10-foot parabolic antenna used at the remote sites. The data shown in Figure 6.21 were taken with the Buenos Aires transponder on July 24, 1974 and are typical of all the data received, showing standard deviations of 0.067 μsec for the Observatory-satellite link and 0.15 μsec for the Observatory-satellite-remote transponder link. Taking a measured (and estimated on Table 4.3) signal-to-noise ratio of 4.8 dB (C/N_o = 52.6 dBHz) for the ranging interrogation in the remote transponder receiver and an estimated signal-to-noise ratio of 10.5 dB (C/N_o = 58.3 dBHz) for the ranging response in the Observatory receiver, a minimum standard deviation of 0.14 μsec is anticipated for the two-way ranging time to the remote transponder. Taking an estimated signal-to-noise ratio of 10.9 dB (C/N_o = 58.7 dBHz) for the satellite return of the interrogation in the Observatory receiver, a minimum standard deviation of 0.057 μsec is anticipated for the two-way Observatory-satellite ranging time. Both anticipated values are in excellent agreement with observation.

Following the installation of the transponders at their remote sites, range measurements were made approximately twice per week. Figure 6.22 contains ranging data taken on Nov. 26, 1974, with the Hawaiian transponder. Several differences exist between the presentation of this data and that contained in Figure 6.21. First, for the Observatory-satellite link, the ranging data has been corrected for variations in the Observatory internal time delay by subtracting the response of the Observatory self calibration circuit from the raw

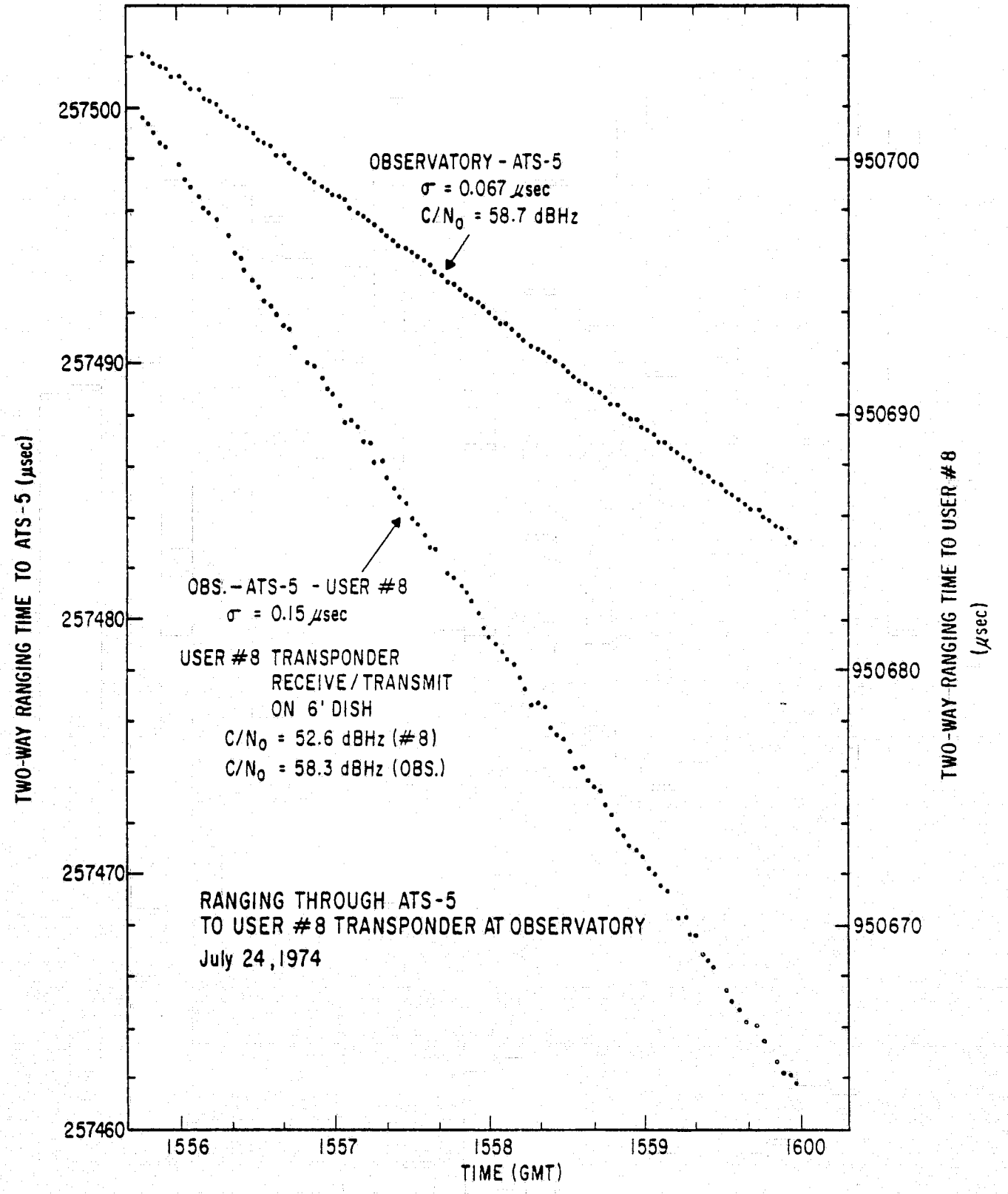

FIGURE 6.21 RANGING TO BUENOS AIRES TRANSPONDER WHILE AT OBSERVATORY

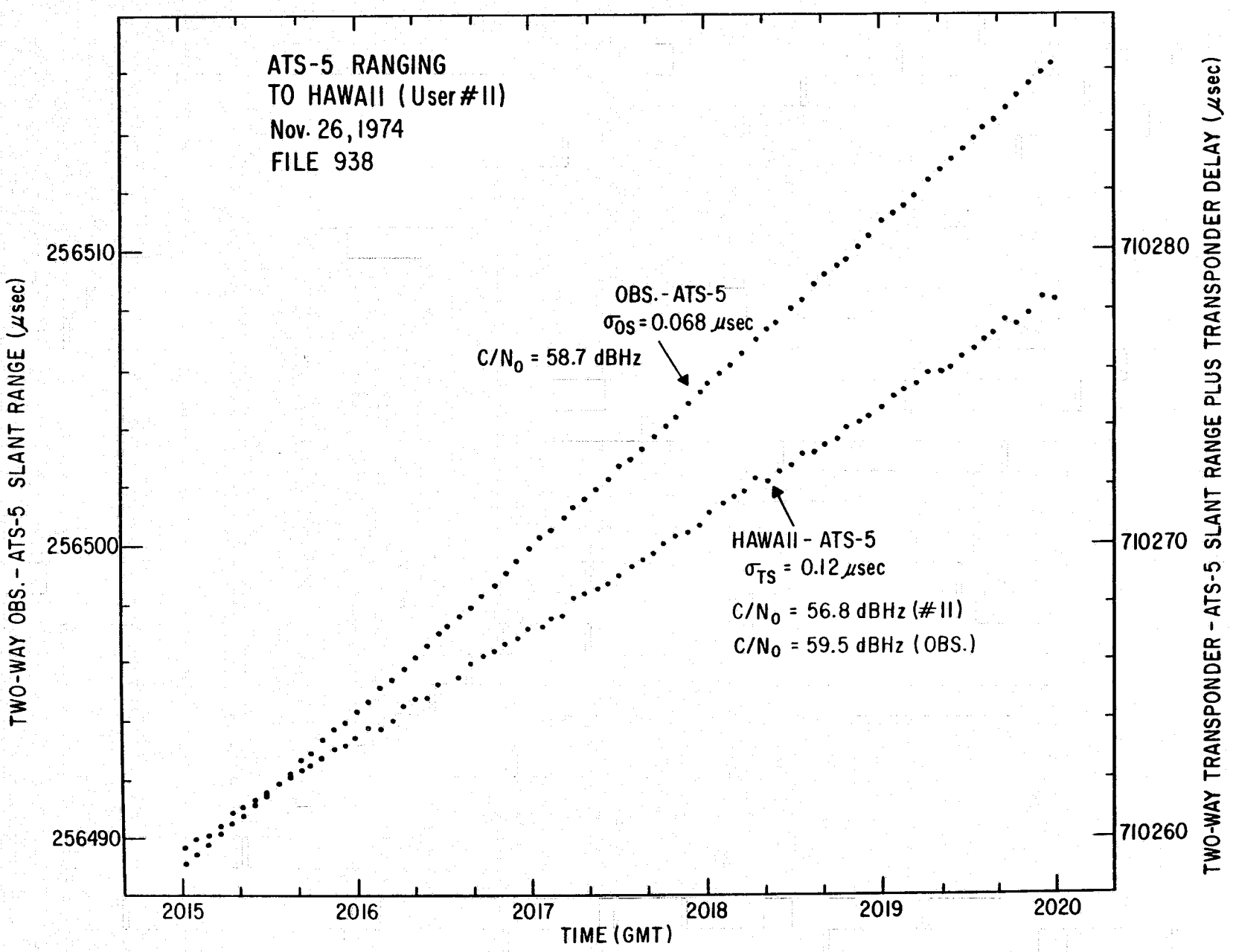

FIGURE 6.22 RANGE MEASUREMENTS TO HAWAIIAN TRANSPONDER

ranging data. The resultant thus corresponds to the two-way Observatory-satellite slant range. The range measurements to the Hawaiian transponder have also been corrected for all variable components by subtracting the Observatory-satellite ranging times and adding the output from the remote transponder self calibration circuit. Only the remote transponder's constant internal time delay need be subtracted from the resultant to yield the two-way transponder-satellite slant range.

The standard deviations quoted in Figure 6.22 reflect these corrections to the range measurements and give the precision of the two-way slant ranges inasmuch as further correction factors are constants and only affect the slant range accuracy. The observed standard deviations for both slant ranges are in excellent agreement with estimates, as indicated on Table 6.5. The estimated standard deviations were computed by taking into consideration the signal-to-noise ratio in the RF link, the round-off error in the correlators, and the inaccuracy in the recording of the event. Table 6.6 itemizes these various contributions which must be taken into account, for the data taken on Nov. 26, 1974. The self calibration signals are adjusted in strength to be slightly stronger than the signal strength from the satellite and consequently, they have improved precisions. The ranging interrogation in the Hawaiian receiver is estimated to have a signal-to-noise power density (C/N_o) of approximately 56.8 dBHz; for the remote transponder response into the Observatory receiver, 59.5 dBHz. The satellite return of the ranging interrogation in the Observatory receiver is estimated at a C/N_o = 58.7 dBHz.

Figure 6.22 also shows that ranging interrogations were made approximately every 3.9 seconds, or every fifth rotation of the ATS-5 satellite, as compared to 2.3 seconds (every third rotation) for the data of Figure 6.21. The Observatory interrogator is capable of initiating range measurements from every three rotations to every several hundred rotations.

The ranging data shown in Figure 6.23 were taken on Dec. 12, 1974, with the remote transponder in Buenos Aires. During this test, both transponders in Hawaii and Buenos Aires were interrogated, alternately, on every third rotation of the satellite. After approximately two minutes, the interrogation rate was slowed to once every seven rotations of the satellite.

In Table 6.5, the observed precision for the Buenos Aires transponder on two occasions is better than estimated. The largest contributions to the standard deviations are due to low signal-to-noise ratios in the RF links, estimated in the power budgets of Table 4.3. It is possible that the receive condition at Buenos Aires is significantly better than expected. It will be noted from Table 6.5 that if conditions in Buenos Aires were similar to those in Hawaii, the computed and observed precisions would be in agreement.

TABLE 6.5

SINGLE DATA POINT PRECISION
OF TWO-WAY SLANT RANGES

Date	Remote Transponder	Observatory-ATS-5 Observatory		Observatory-ATS-5-Remote Transponder-ATS-5-Observatory	
		Computed* (μsec)	Observed (μsec)	Computed* (μsec)	Observed (μsec)
Nov. 22, '74	Hawaii	0.077	0.067	0.13	0.16
Nov. 23, '74	Hawaii	0.078	0.082	0.13	0.17
Nov. 26, '74	Hawaii	0.081	0.068	0.14	0.12
Dec. 12, '74	Buenos Aires	0.080	0.072	0.15	0.11
Dec. 16, '74	Buenos Aires	0.077	0.084	0.15	0.12

* Computed precisions assume estimated signal-to-noise power densities (C/No) in units of dBHz as follows:

Observatory-ATS-5 and return	58.7
Observatory-Hawaii	56.8
Observatory-Buenos Aires	54.4
Hawaii-Observatory	59.6
Buenos Aires-Observatory	59.2

TABLE 6.6

CONTRIBUTIONS TO TWO-WAY SLANT RANGE
STANDARD DEVIATION
HAWAIIAN TRANSPONDER (USER #11)
NOV. 26, 1974

Observatory-ATS-5 Link	Standard Deviation (μsec)
Interrogation time, σ_{TR}	0.031
FM demodulation, σ_{RF}	0.057
Correlator round-off, σ_{CR}	0.029
FM demodulation, σ_{RF}, Self calibration response	0.032
Correlator round-off, σ_{CR}, Self calibration response	0.029
Net two-way, Obs.-Sat. Standard deviation, σ_{OS}	0.083
Observatory-ATS-5-Remote Transponder Link	
Interrogation time σ_{TR}	0.051
Remote FM demodulation, σ_{RF}	0.071
Remote correlator round-off, σ_{CR}	0.029
Remote FM demodulation, σ_{RF}, Self calibration response	0.050
Remote correlator round-off, σ_{CR}, Self calibration response	0.029
Obs. FM demodulation, σ_{RF}	0.052
Obs. correlator, σ_{CR}	0.029
Obs.-Sat. two-way (no self calibration response)	0.071
Net two-way, Transponder-Satellite standard deviation, σ_{TS}	0.143

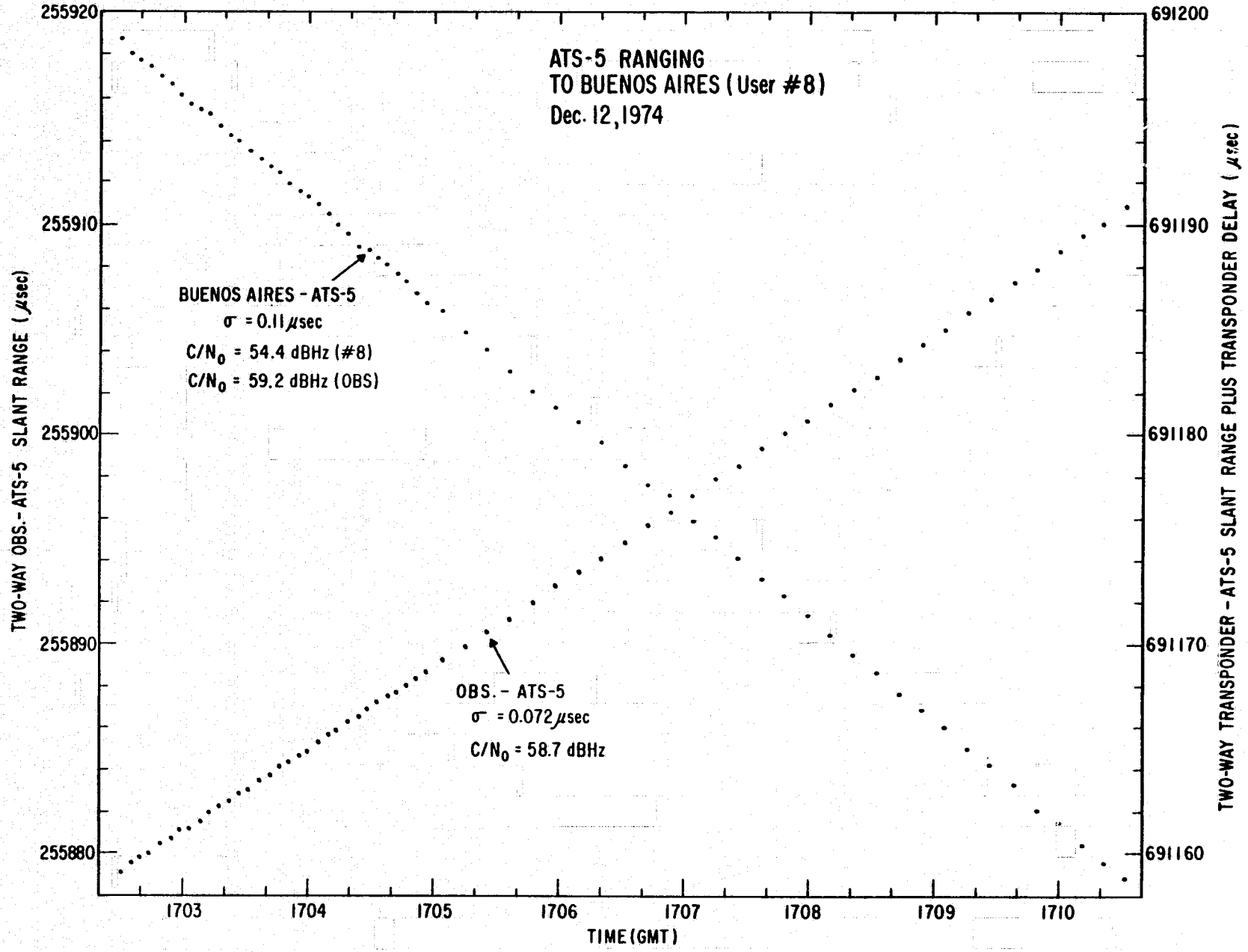

FIGURE 6.23 RANGE MEASUREMENTS TO BUENOS AIRES TRANSPONDER

Assuming standard deviations of 0.08 μsec and 0.15 μsec for the two-way Observatory-satellite and transponder-satellite slant ranges, respectively, the one-way slant range precision on a single measurement becomes 12 meters and 22 meters. The precision improves by the inverse square root of the number of measurements. In 5 minutes of ranging at one interrogation every three rotations of the satellite, the expected Observatory-satellite slant range standard deviation is one meter and the expected remote transponder-satellite slant range standard deviation is three meters.

SECTION 7

OPERATIONAL PROCEDURES

7.1 RANGING PROCEDURES

The equipment configuration used at the General Electric Radio-Optical Observatory in the operation of the L-band trilateration network is shown in Figure 7.1. The automatic address code sequencer determines the order of remote transponder interrogation and whether the interrogation is to be transmitted at L-band or at VHF. Any number from one to twelve stations can be sequentially addressed. With fewer stations on line, several may be repeatedly interrogated within the sequence.

All timing and synchronization circuits, clocks, and time interval counters at the Observatory are referenced to a Manson RD180 frequency standard with a stability better than 5 parts in 10^{10}.

The synchronizer triggers range measurement interrogations by the tone-code generator at times such that the interrogations pass through the "window" of the spinning ATS-5 satellite. Adjustable thumbwheels set the synchronizer period to match the rotational period of the satellite to within 0.8 μsec. A series of three push buttons advance or retard the synchronizer phase in 100 msec, 10 msec, or 1 msec steps. The synchronizer can be set into phase with the ATS-5 satellite "window" in one of two ways. First, the remainder of the Observatory system can be set to conduct range measurements. The two least significant push buttons are then depressed until the Observatory correlates on the satellite return of its own interrogation. The second technique utilizes CW transmissions from the Observatory and an oscilloscope to monitor the output of the L-band receiver. The push buttons are depressed until full quieting of the L-band receiver is centered at the anticipated two-way ranging time. This second technique is faster since the oscilloscope trace displays the full satellite "window" allowing all three push buttons to be used in order of significance. Without the oscilloscope display, the ranging interrogation must find the 50 msec "window" with non-optimum phase change rates and with a maximum sample rate of one interrogation every three spin cycles of the satellite. Interrogations can be made for every integer number of satellite spin cycles above two.

On command from the synchronizer, the tone-code generator sends approximately 768 cycles of audio tone followed by the 15-bit synchronization word and the 15-bit digital address code. The interrogation drives the Observatory exciter and L-band power amplifier for a tone-code transmission to the satellite. When the last complete cycle of address code has left the tone-code generator, the generator starts the time interval counters which measure the Observatory-satellite-Observatory ranging time and the Observatory self calibration time. The time interval counter which measures the Observatory-satellite-remote transponder-satellite-Observatory ranging

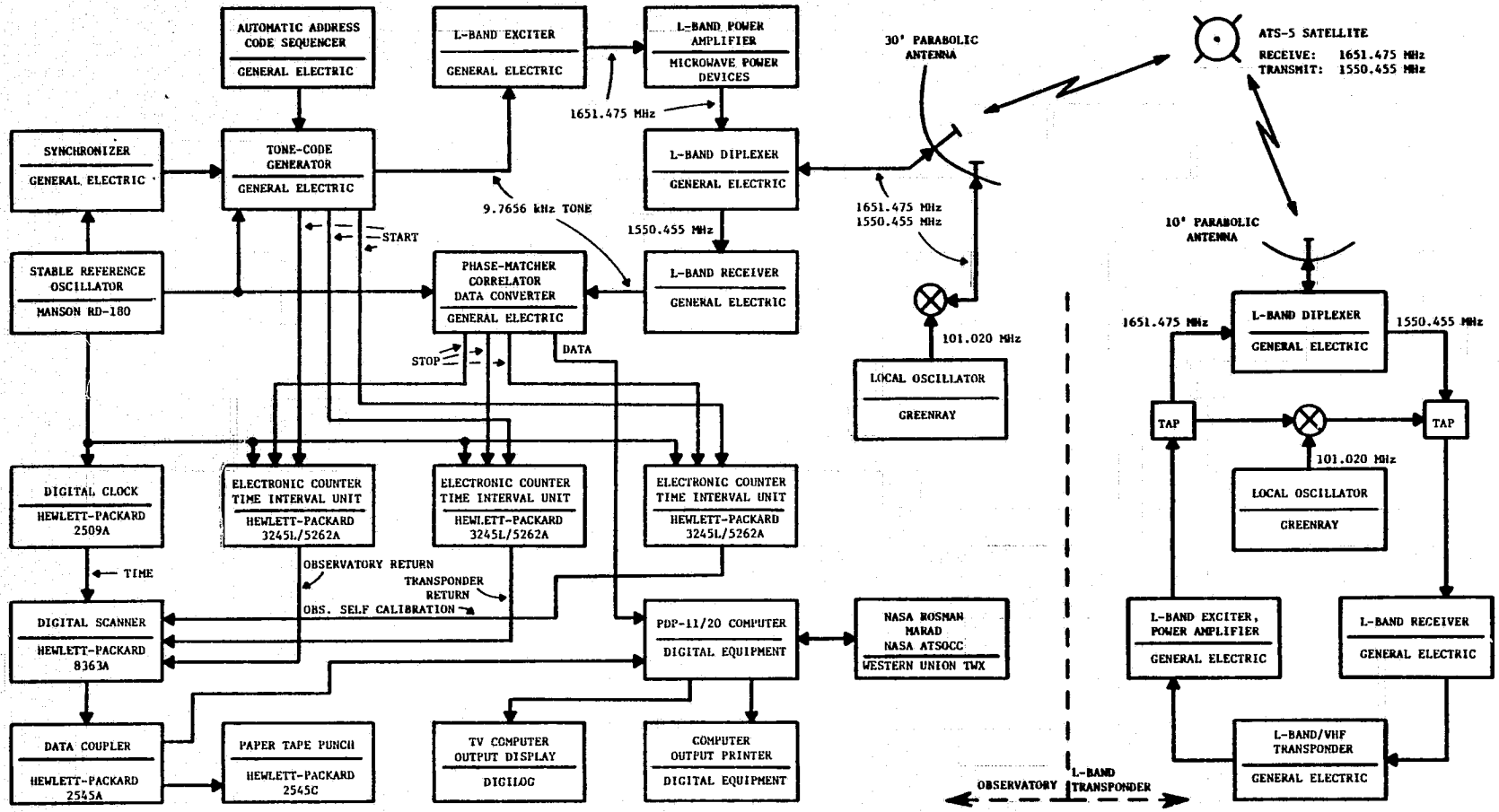

FIGURE 7.1 EQUIPMENT CONFIGURATION FOR L-BAND RANGING

time is started 0.039 to 0.248 seconds later, depending on the setting of manually adjustable tone-code generator thumbwheel switches. Without this delay, ranging times to the remote transponder would exceed one second.

L-band transmissions from the Observatory to ATS-5 are made with a 100 watt solid-state L-band power amplifier and a 30-foot parabolic antenna with a circularly polarized feed. A diplexer removes the need for an antenna transmit/receive relay switch. The signal-to-noise ratio at the satellite within the narrow band frequency translation mode receiver bandwidth is approximately 2.0 dB. The L-band trilateration network does not saturate the satellite receiver. If the satellite had a 60 kHz RF bandwidth similar to that used by the L-band trilateration receivers, the signal-to-noise ratio would be 18.2 dB (see Table 4.4). The signals from the satellite are received on the same 30-foot dish antenna. A low noise solid state preamplifier located within the diplexer housing behind the antenna feed essentially determines the sensitivity of the entire receive system. Figure 7.2 is a representation of the signal strengths from the ATS-5 satellite in 16 and 60 kHz bandwidths. During this test, ranging interrogations were initiated on every third rotation of the satellite. Transponders in Buenos Aires and Hawaii were alternately addressed. The Observatory's transmitted interrogation appears as a slight desensitization of the L-band receiver approximately 0.25 seconds before the satellite return. The Observatory self calibration oscillator was disabled during this experiment.

The Observatory phase matcher/correlator operates in much the same manner as the phase matching and correlation circuits of the responders. Phase matching occurs over 256 tone cycles and the unit correlates on the same address code selected by the interrogator. During a typical ranging experiment, address codes for the transponders in Buenos Aires and Hawaii are alternatively selected and the Observatory correlator responds to three tone-code sequences. The first phase match/correlation process starts before the complete tone-code interrogation has left the Observatory. The self calibration loop at the surface of the 30-foot dish antenna injects the translated interrogation into the L-band receiver. Typical Observatory internal time delays range from 144 to 147 μsec. The second phase match/correlation occurs on the satellite return of the interrogation, approximately 0.25 seconds after the ranging interrogation left the Observatory. The third phase match/correlation occurs on the satellite return of the remote transponder's response, approximately 1.02 seconds after interrogation. The delayed start of the time interval counter results in an apparent ranging time of approximately 0.97 seconds.

Disabling the Observatory self calibration loop results in the accumulation of the Observatory-satellite-Observatory range time in the time interval counter assigned to measure the Observatory internal time delay. The Observatory correlator is wired to show an Observatory-satellite-Observatory "range time" of approximately 0.35 seconds if the satellite return contained a tone-code sequence which did not result in correlation. A "range time" of approximately 0.40 seconds indicates absence of both tone and correlation. If tone is detected but correlation

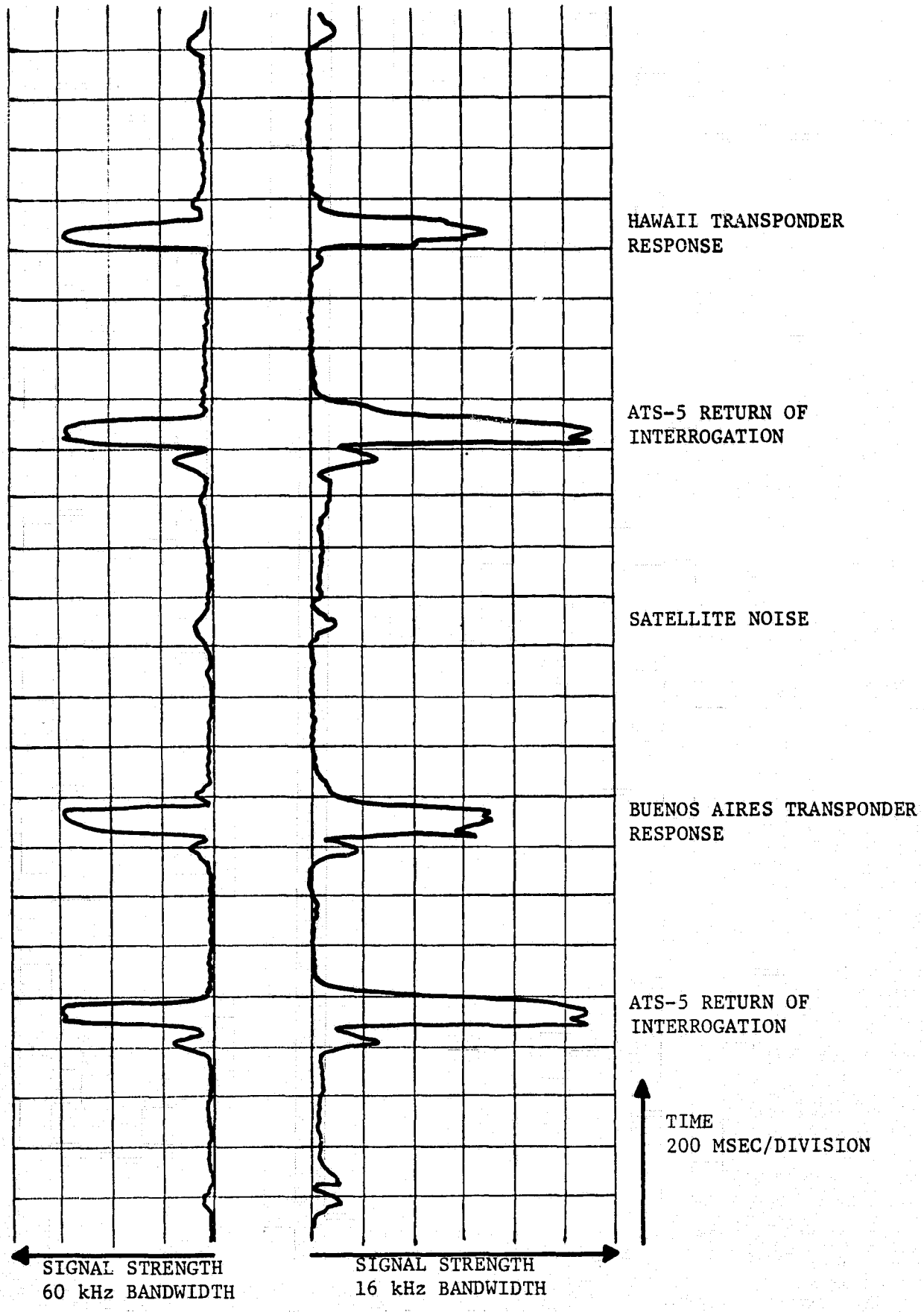

FIGURE 7.2 TRACING OF CHART RECORDING SHOWING RANGING INTERROGATIONS AND RESPONSES

does not occur, the Observatory correlator will pass a "range time" of approximately 1.00 seconds for the Observatory-satellite-remote transponder-satellite-Observatory range measurement. A "range time" of approximately 1.09 seconds indicates absence of response tone and correlation. The start pulse from the interrogator resets all time interval counters at the ranging interrogation.

A separate circuit in the Observatory correlator decodes the data stream following the address code in the responses from remote transponders. This digital data stream contains the setting of the adjustable responder thumbwheel switches which define the transponder "logic" time delay, the number of bits in error during transponder correlation, and a digital representation of the transponder self calibration response.

The outputs of the three time interval counters and the output of a digital clock pass automatically through a digital scanner and data coupler to a high speed paper tape punch. Adjustment of thumbwheel switches on the digital scanner causes the appropriate month, day, year, and file number identifying each ranging experiment to be punched on paper tape following each line of ranging data. The data coupler also automatically passes the outputs of the time interval counters and the output of the digital clock directly to the Observatory's PDP-11/20 computer. In addition, the PDP-11/20 computer receives digital data from the correlator relating the setting of the responder internal time delay thumbwheel switches, the number of bits in error during transponder correlation, and the response of the transponder self calibration circuits. A paper tape and printout of the ranging data can be generated by an ASR 33 teletype machine tied directly to the PDP-11/20 computer. The computer formats the data as shown in Figure 7.3. The data identification numbers are alternately printed several times near the beginning of each data file. This format is identical to that generated by the high speed paper tape punch with one exception; only the PDP-11/20 computer has the facility to add the remote transponder self calibration data. All tapes are punched in ASCII code.

Following completion of data processing by the Observatory's PDP-11/20 computer, ATS-5 satellite positions are printed on the computer's DECwriter. Position predictions follow if three periods of ranging had been successfully completed. Position predicts in the form of Greenwich Mean Time and ATS-5 longitude, geocentric latitude, and earth center distance are relayed to the NASA Rosman Tracking Station, to the MARAD Kings Point National Maritime Research Center, and to the NASA-Goddard Space Flight Center ATS Operations and Control Center via commercial TWX lines in ASCII even parity code.

7.2 SATELLITE POSITION/POSITION PREDICTION CALCULATION

During the transmission of data from the time interval counters to the computer, individual bits of range measurement data may be lost or altered. The first action of the computer software is to scan each data

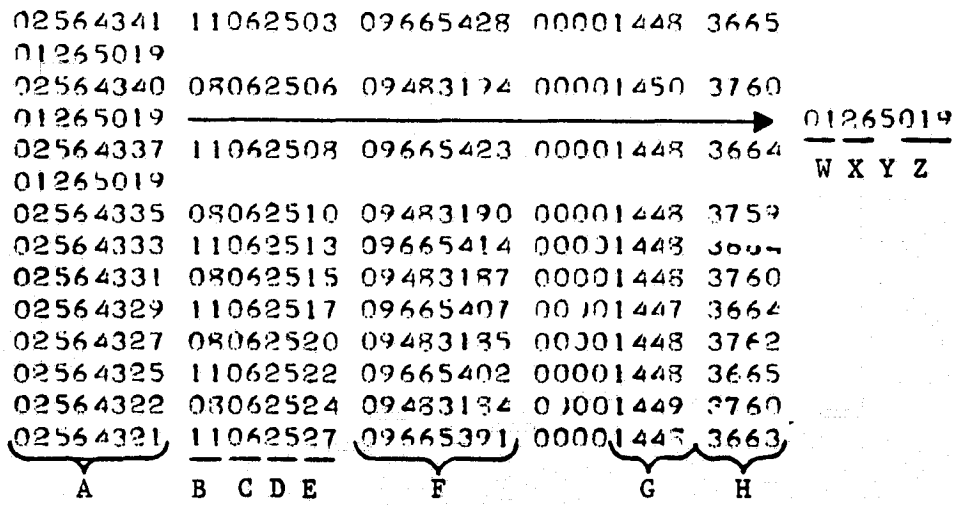

SYMBOL DESCRIPTION

A Two-way Observatory-satellite ranging time (tenths of μsec)

B Transponder address code (08 = Buenos Aires; 11 = Hawaii)

C Interrogation time in hours (GMT)

D Minutes,

E Seconds,

F Two-way Observatory-satellite-remote transponder ranging time (tenths of μsec)

G Observatory internal time delay (tenths of μsec)

H Transponder self calibration response (tenths of μsec)

W Month

X Day

Y Year

Z File Identification Number

FIGURE 7.3 FORMAT OF RECORDED RANGING DATA

character. Any line containing non decimal number characters is deleted.

Due to the geosynchronous nature of the ATS-5 satellite, range measurements are bounded by the extremes of the satellite orbit. Following a reading of acceptable data characters, all range measurements are screened for unacceptably high or low values. Only range measurements between anticipated limits are retained. A final check on data quality involves filtering of range measurements. Second order polynomials are fit to range measurements for all three legs of the triad. Individual range measurements disagreeing with the resultant fit by more than a predetermined amount are deleted.

Second order polynomials again represent the remaining range measurements, for two specific reasons. First, for every minute during which slant ranges were measured, a smoothed position of the satellite is computed and listed. Second, for a time midway between the beginning and end of the ranging period a single satellite position is computed. This position is one of three to be used in computing the orbital elements and consequently, the satellite ephemerides.

If data from two previous ranging periods had been processed in the above manner, three smoothed satellite positions exist and six Kepler orbital elements are computed by the method of Gibbs.

In the first section of the program, all acceptable ranging data were saved in the form of slant ranges to the satellite. The orbital elements generated for the ephemeris are used to compute a satellite position corresponding to each measured slant range. All observed slant ranges are compared with the computed slant ranges in the form of a standard deviation. A listing of the standard deviation on the satellite position prediction table allows a rapid assessment of data quality.

The total number of position predictions plus the time interval between them on the ATS-5 ephemeris must be specified before the computer program is started. Caution must be exercised in accepting position predictions a long time from the last range measurement as the prediction error increases approximately as the square of time. Position prediction data are stored in a separate data file on the computer for rapid retrieval and transmission to NASA and MARAD.

All satellite positions are quoted as a function of Greenwich Mean Time. The units of satellite longitude and geocentric latitude are degrees; satellite earth center distance is given in meters.

Details of the computer software are documented separately in the appendicies to this report[12].

7.3 ATS-5 SATELLITE RANGING SEQUENCES

Two interrogations, one to each remote transponder, generate a triad

of slant ranges which uniquely define the position of the satellite. Repeated interrogations improve the position precision roughly as the inverse square root of the number of measurements. During most ATS-5 position fixing experiments, slant ranges were measured over ten minute periods with interrogation rates of once every 2.3 seconds, generating approximately 256 Observatory-satellite, 128 satellite-Hawaii, and 128 satellite-Buenos Aires slant ranges. Smoothing the measurements over this time frame improves the precision of the Observatory-satellite and remote transponder-satellite slant ranges by factors of approximately 16 and 10, respectively.

During tests in support of the two satellite position fixing experiments of NASA and MARAD, General Electric conducted trilateration position fixing measurements to the ATS-5 satellite for ten-minute periods every hour. Following three periods of trilateration range measurements, ATS-5 ephemerides covering two hours in one minute increments were generated and sent to NASA and MARAD. The remaining 50 minutes of every hour during the combined GE/NASA/MARAD tests were used to convert the ATS-5 satellite to the C-to-L frequency translation mode, to pass ranging signals through ATS-5 from the NASA Rosman Tracking Station to remote vehicles, and to reconfigure the ATS-5 satellite back to the L-to-L frequency translation mode. The failure of the L-band receiver on ATS-5 in early March, 1975 brought the combined experiments to a premature termination. No facilities existed for the C-band trilateration of ATS-5.

SECTION 8

VERIFICATION OF TRILATERATION POSITION MEASUREMENT AND PREDICTED POSITION ACCURACIES

8.1 NETWORK OPERATION

The L-band transponder in Hawaii became operational on Nov. 22, 1974. Since that time, the transponder was interrogated approximately twice per week until the failure of the L-band receiver on ATS-5 in early March, 1975. Only two problems developed in the transponder since deployment. First, it was noted almost immediately that the responder unit packaged inside the VHF receiver/transmitter base station was overheating. The self calibration response changed through several microseconds. A new responder back panel with cooling fans was sent to Hawaii and kept the responder at nominal temperatures. The second problem concerned the failure of the transponder to respond properly during a regular test on Jan. 14, 1975. The VHF communications link was used to discuss the performance of the transponder with the attending U.S. Coast Guard electronics technician. No cause for the failure could be found. Acting on the report that the area had been hit by a severe wind storm, the 10-foot dish antenna was repointed toward ATS-5 as the satellite crossed the equator; the transponder immediately returned to normal operation.

The L-band transponder in Buenos Aires became operational on Dec. 9, 1974 and was also interrogated approximately twice per week. This transponder exhibited only one major problem. On Jan. 9, 1975, the L-band transponder failed to respond at approximately 1930 GMT after having operated perfectly since 1500 GMT that same day. During the next scheduled test on Jan. 14, 1975, the unit operated perfectly and diagnostics of the responder showed no malfunctioning components. On Jan. 26, the transponder again failed to respond, this time at 1830 GMT, after successful operation since 0630 GMT on the same day. The transponder came back to normal operation at 0130 GMT on Jan. 27. A VHF voice contact from Buenos Aires through ATS-3 the following day indicated that the temperature in Buenos Aires had risen to 99^{o}F on Jan. 26. Furthermore, the transponder is in a non air-conditioned office on the sun side of a building in downtown Buenos Aires. It is assumed that the transponder failed because excessive heat changed the electrical properties of a component in some timing circuit of the responder.

Both transponders suffered from an intermittent problem in the self calibration circuits. Approximately one percent of the self calibration responses were in error, containing values which differed slightly from the expected response to values which were in error by as much as can be represented in four octal digits. It is believed that intermittent broad band noise generated by the L-band solid state power amplifiers passed through the self calibration loop and made it impossible for the responder to measure the phase of the audio tone. This was not a disabling problem but merely an inconvenience as sufficient excellent self calibration data existed to generate accurate interpolations over the bad responses.

Table 8.1 summarizes the dates and times when both remote transponders were in operation and used to locate the ATS-5 satellite. The tests from Dec. 10, 1974 to Jan. 7, 1975 represent the regular Tuesday/Thursday schedule designed specifically to assure the continued availability and performance of the transponders. During some tests, ranging was conducted continuously and the data were later separated into several sections with no more than 300 ranging interrogations per section, limiting each section to no more than approximately 15 minutes duration. The tests of Jan. 17, 28, and 30 were conducted for the same reason and their data were grouped in a similar manner.

The test of Jan. 9 was intended to provide an extended period of ranging to allow a comparison of predicted satellite positions with measured satellite positions. Range measurements were conducted every half hour on the half hour.

The tests of Jan. 21 and 31 and Feb. 24, 25, and 26 were conducted in support of NASA's two satellite position fixing experiments. Table 8.2 itemizes the ranging periods for each test and details the number of completed slant range measurements. As a measurement of the Observatory-satellite slant range is accomplished on every interrogation of a remote transponder, the sum of Observatory-ATS-5-Hawaii and Observatory-ATS-5-Buenos Aires range measurements should equal the number of Observatory-ATS-5 range measurements, under ideal conditions. The data of Table 8.2 indicates a 96 percent remote transponder response rate.

The most significant test was conducted on Jan. 26-27, 1975 in conjunction with NASA. Trilateration range measurements were made every hour on the half hour for periods of 10 minutes, with the exception of 1530 and from 1830 to 0030 GMT. NASA conducted range and range-rate measurements from its Rosman and Mojave tracking stations to ATS-5 during this same 24-hour period. The range and range rate measurements were used by NASA to generate the ATS-5 position predictions for the next month. The simultaneous tracking of ATS-5 allowed a direct comparison of the two systems and provides experimental verification of the trilateration system accuracy.

Each section of ranging data from Dec. 10, 1974 to Feb. 26, 1975 contains from 40 to 300 ranging interrogations with durations from approximately 3 to 15 minutes. Over any small section of satellite orbit, a second order polynomial is assumed to provide an accurate representation of the satellite-ground station slant ranges. The computed slant ranges at the midpoints of the ranging periods are used in the software routines to determine the six Kepler orbital elements. The second order polynomials are also used to compute satellite positions on every minute for the duration of the ranging period. If excellent ranging data existed for the entire ranging period, the second order polynomials yield accurate slant ranges for the computation of the satellite position. If one transponder failed to respond to ranging interrogations except perhaps near the beginning or near the end of the ranging period or if a transponder responded only once, a poor fit and subsequent inaccurate satellite positions result. Figure 8.1 depicts a computer print out of trilateration positions of the ATS-5 satellite corresponding to the ranging period from 06:25:03 to 06:34:58 GMT on Jan. 26, 1975.

TABLE 8.1

TWO TRANSPONDER RANGING EXPERIMENTS

Date	File	Satellite Contact Time (GMT) Start	Stop	Sections of Ranging Data	Comments
12/10/74	F956	1800	2000	5	User 11 responder overheat; Self calibration data lost.
12/12/74	F960	1700	1730	4	
12/17/74	F964	1500	1600	5	
12/19/74	F967	1500	1600	4	
1/2/75	F001	1500	1600	2	
1/7/75	F005	1500	1645	9	
1/9/75	F008	1500	2110	10	User 8 responder overheat; No responses after 1930.
1/17/75	F015	1330	1530	7	
1/21/75	F016	1100	1610	9	ATS-5 Trilateration Support.
1/26/75	F019	0625	2400	11	24 hour test with NASA;
1/27/75	F020	0000	0635	6	No responses from User 8 from 1800 to 0100.
1/28/75	F021	1530	1635	4	
1/30/75	F023	1530	1635	3	
1/31/75	F025	0900	1410	6	ATS-5 Trilateration Support.
2/24/75	F037	0930	1245	3	ATS-5 Trilateration Support.
2/25/75	F038	1125	1440	4	ATS-5 Trilateration Support.
2/26/75	F040	0815	1225	4	ATS-5 Trilateration Support.

TABLE 8.2

ATS-5 TRILATERATION SUPPORT

Date	File	Ranging Period Time (GMT) (Hours, Minutes, Seconds) Start	Stop	Range Measurements OBS.-ATS-5	OBS.-ATS-5-HAW	OBS.-ATS-5-BA
1/21/75	F016P0	110317	111457	158	75	66
	1	112022	112759	193	96	92
	2	115048	115830	198	99	94
	3	122452	123200	183	92	87
	4	125538	130227	175	85	86
	5	132538	133159	163	81	80
	6	153725	154024	77	38	32
	7	154040	154832	203	102	95
	8	160107	160434	89	45	44
1/31/75	F025P2	090847	091738	200	69	99
	3	095800	100802	257	106	128
	4	105834	110600	191	94	96
	5	120242	121023	197	98	99
	6	125700	130504	207	104	102
	7	135500	140527	268	133	134
2/24/75	F037P1	093919	094356	119	56	59
	2	102200	103058	230	115	114
	4	123656	124500	207	91	93
2/25/75	F038P1	112500	113459	256	128	126
	2	122500	123459	256	128	121
	3	132506	133458	253	123	113
	4	142602	143631	269	134	123
2/26/75	F040P1	081537	082559	266	127	98
	2	092301	093258	255	128	121
	3	101500	102501	257	128	123
	4	121500	122459	256	128	128

```
ATS-5 TRILATERATION POSITIONS
FROM  26  6 25  3 TO  26  6 34 58
          2183103.          2183698.
   26    6  25 -105.55031    1.50341   42213276
   26    6  26 -105.55087    1.51094   42213068
   26    6  27 -105.55143    1.51843   42212864
   26    6  28 -105.55199    1.52589   42212656
   26    6  29 -105.55257    1.53330   42212444
   26    6  30 -105.55314    1.54069   42212236
   26    6  31 -105.55372    1.54803   42212020
   26    6  32 -105.55430    1.55533   42211808
   26    6  33 -105.55489    1.56260   42211592
   26    6  34 -105.55547    1.56984   42211372
   26    6  35 -105.55607    1.57703   42211152
   26    6  36 -105.55666    1.58419   42210932
```

A B C D E

Symbol Definitions:

- A Day of year,
- B Greenwich Mean Time in hours and minutes,
- C Satellite longitude in degrees,
- D Satellite geocentric latitude in degrees,
- E Satellite earth center distance in meters.

FIGURE 8.1 COMPUTER LISTING OF TRILATERATION POSITION OF ATS-5 SATELLITE

8.2 TRILATERATION POSITION ACCURACY

Accuracy of the General Electric trilateration positions of ATS-5 were experimentally verified by comparison with NASA's range and range rate measurements from the Rosman Tracking Station, Rosman, NC, and the Mojave Tracking Station, Goldstone, CA.

NASA conducts range and range rate measurements from Rosman and Mojave every two weeks. The slant range and velocity of each Advanced Technology Satellite are measured every second during 2.5-minute periods, every two hours during the 24-hour day. These data plus the tracking antenna azimuth and elevation angles are sent to the NASA-Goddard Space Flight Center via teletype. Following the accumulation of twelve sets of data for each satellite and from each ground station, the data for each tracking period are smoothed and four or five representative values of range, velocity, and tracking antenna azimuth and elevation are produced per tracking period, as a function of time. Approximately, 48 sets of observations for each ground station are passed to an iterative program which infers the set of orbital elements displaying the minimum residuals when the observations are compared with computed slant ranges, velocities, and look angles from both tracking stations. After four iterations, slant range residuals are typically 0.04 meters with standard deviations of 0.6 meters; range rate residuals are 0.4 ± 2.5 m/sec. It may be assumed, therefore, that the inferred satellite positions are accurate over the time that tracking measurements are made.

In light of the NASA capability to determine accurately the satellite positions, a simultaneous NASA range and range rate and GE trilateration experiment was scheduled for the 24-hour period from 0630 GMT on January 26, 1975, to 0630 GMT on January 27, 1975. General Electric conducted ATS-5 trilateration range measurements from approximately 25 minutes after every hour until approximately 35 minutes after every hour. An operational error resulted in the loss of trilateration data from the 1530 GMT ranging period and the temporary outage of the Buenos Aires transponder prevented accumulation of trilateration data from 1830 to 0030 GMT. The NASA Rosman Tracking Station conducted range and range rate measurements to the ATS-5 satellite for 150 second periods at approximately 28 minutes after every even hour from January 26, 0800 GMT until January 27, 0600 GMT. The NASA Mojave Tracking Station conducted similar range and range rate measurements at approximately 22 minutes after every even hour during the same time period.

Figure 8.2 displays the differences between the NASA and GE positions of the ATS-5 satellite as observed from the NASA C-band range and range rate and the GE L-band trilateration measurements on January 26-27, 1975. The differences represent the NASA position less the GE position and have mean values as follows:

0.00014 ± 0.00012	degrees longitude,
0.00003 ± 0.00023	degrees latitude,
18 ± 19	meters earth center distance.

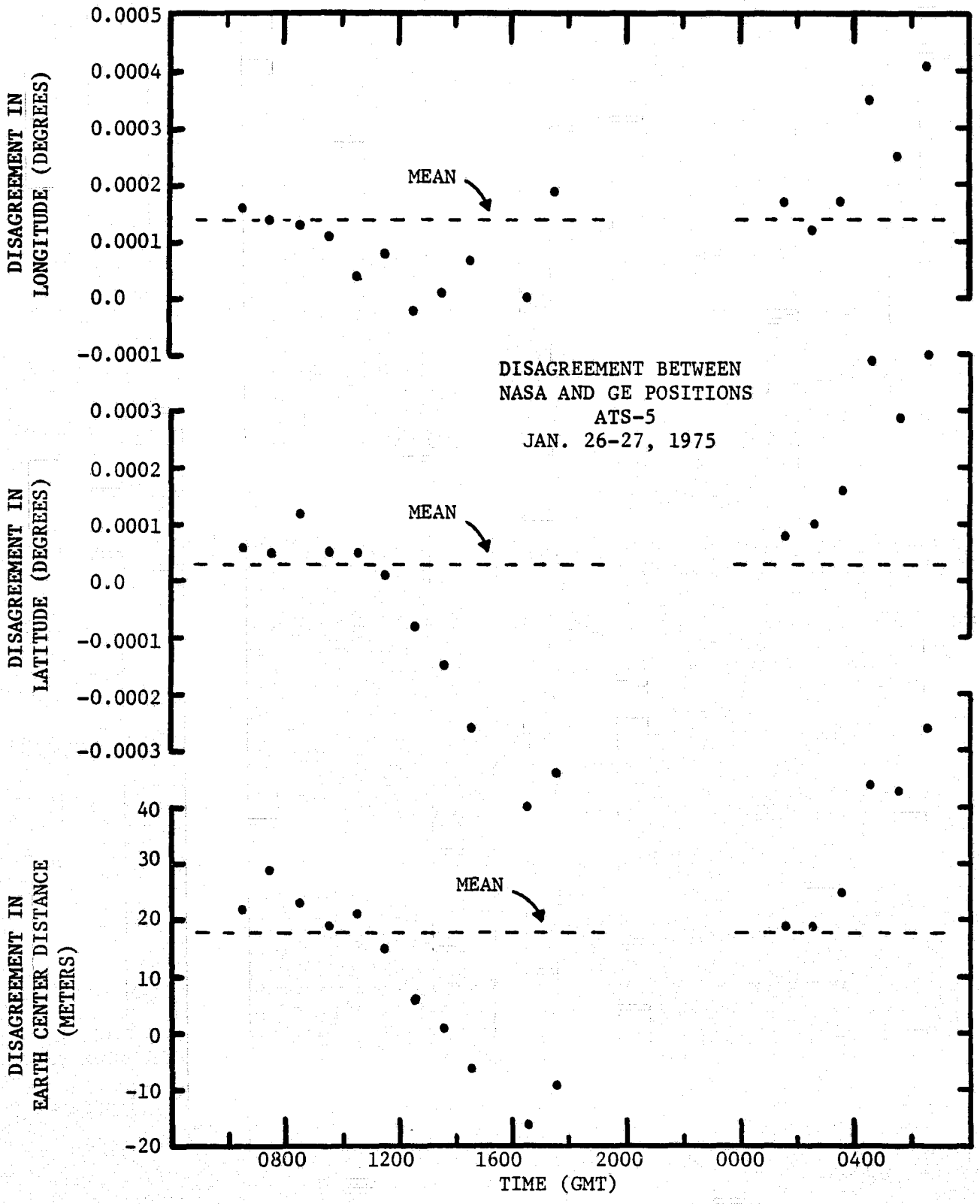

FIGURE 8.2 DIFFERENCES BETWEEN THE NASA AND GE POSITIONS OF THE ATS-5 SATELLITE

The above mean values represent differences over one entire orbit of the satellite. Although stationary to the casual observer, the ATS-5 satellite traces a figure "8" in space through approximately 0.4 degrees longitude, 4.6 degrees latitude, and 1.4 X 10^5 meters altitude about its mean geo-synchronous location on the equator at 105 degrees west longitude and 3.6 X 10^7 meters altitude.

The close agreement of the two completely independent systems suggests that the absolute accuracy of the L-band trilateration is approximately the magnitude of the disagreement with the NASA positions.

The primary contribution to the standard deviations about the mean disagreement between the GE and NASA positions results from the sinusoidal characteristic with an apparent 24-hour periodicity displayed in Figure 8.2. The variations about the mean disagreement cannot be ascribed to inaccuracies in the NASA position of the satellite; slant ranges to the NASA ground stations computed from the NASA positions agree with NASA measurements to within approximately $\pm$ 0.6 meters, one sigma standard deviation. A one meter slant range error between ATS-5 and Rosman may generate a 0.000026 degree longitude error, a 0.000014 degree latitude error, and 1.0 meter earth center distance error in the position of the satellite. The variations on Figure 8.2 thus far exceed the error contribution due to the NASA position uncertainty.

The variations on Figure 8.2 are interpreted to be due primarily to the drift in the internal time delays of the remote transponders in Buenos Aires and Hawaii and secondarily due to the technique for smoothing raw ranging data. The 10 MHz oscillators in the remote transponders in Buenos Aires and Hawaii are stable to within one part in 10^6 and two parts in 10^7, respectively. Assuming maximum oscillator excursions within these specifications and a 520000.0 μsec transponder internal time delay, the Buenos Aires transponder time delay may change through $\pm$ 0.52 μsec, generating satellite position errors of $\pm$ 0.00014 degrees longitude, $\pm$ 0.00049 degrees latitude, and $\pm$ 35 meters earth center distance. Likewise, the Hawaiian transponder may show a change in internal time delay of 0.10 μsec, generating satellite position errors of $\pm$ 0.00011 degrees longitude, $\pm$ 0.00002 degrees latitude, and $\pm$ 7 meters earth center distance.

This hypothesis was tested by computing the differences between the mean and observed disagreements of Figure 8.2. Appropriate drifts in Observatory and remote transponder internal time delays necessary to generate the observed variations in longitude, latitude, and earth center distance were then computed for each ranging period. The data of Table 4.3 defined the error contributions as a function of time delay change in the solution of the three linear simultaneous equations. Figure 8.3 depicts the results of this computation, showing the unique drifts required of the Observatory and remote transponder internal time delays to account for the observed variations of Figure 8.2. The Buenos Aires transponder internal time delay is inferred to vary between -0.40 and +0.25 μsec, well within specifi-

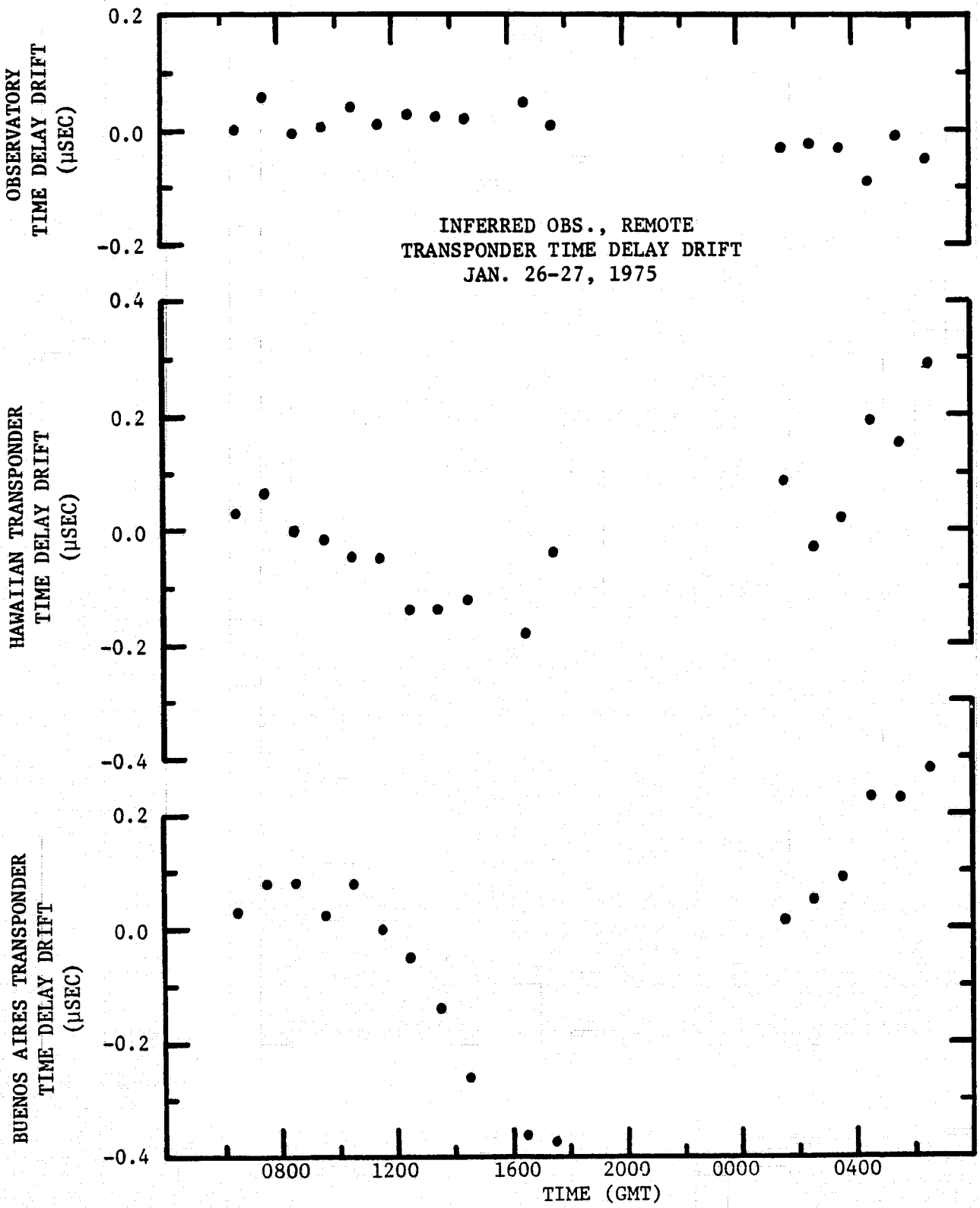

FIGURE 8.3 VARIATION IN OBSERVATORY AND REMOTE TRANSPONDER TIME DELAYS RESULTING FROM TIMING OSCILLATOR DRIFT

cations; the Hawaiian transponder internal time delay varies between -0.20 and +0.25 μsec, more than a factor of two beyond specifications. Finally, the Observatory internal time delay varies between -0.1 and +0.1 μsec with a mean value of 0.00 ± 0.04 μsec. No error in the Observatory internal time delay had been anticipated as the delay is measured with respect to the Observatory frequency standard, accurate to within one part in 10^9. The apparent variation in the Observatory internal time delay is interpreted to result from errors in the technique for smoothing ranging data.

The second contribution to the variations observed in Figure 8.2 is believed to result from the technique for smoothing slant ranges for each ranging period. As the satellite follows an elliptical orbit, second order polynomials (conic sections) had been assumed to provide accurate representations of the satellite-ground station slant ranges for the durations of the individual ranging periods, in spite of the spatial separation between the ground stations and the focus of the ellipse. Figures 8.4 and 8.5 show the disagreement between the NASA positions and the smoothed GE positions for three smoothing techniques during two representative ranging periods. The solid curves represent smoothing by second order polynomials while the dashed lines indicate smoothing over three ranging periods by the assumption of a Kepler orbit (the same orbital elements are used to generate satellite position predictions). The near constant position disagreement suggests that the Kepler orbit represents more closely the position of the satellite than a triad of slant ranges smoothed by second order polynomials.

A linear fit to the slant ranges generates satellite position errors approximately an order of magnitude greater than the second order polynomials or the Kepler model. The greatest error appears near the beginning and end of the ranging period. Table 8.3 itemizes the difference between the second order polynomial and Kepler model smoothing techniques over five ranging periods.

The intersection of the two models at the midpoint of the ranging period results from the a priori decision to assume the midpoint position as representative of the ranging period.

Assuming the mean disagreement of Table 8.3 to be due to identical smoothing errors on all legs of the triad yields a value of 0.014 ± 0.033 μsec for the variation on each triad leg. The inferred variation at the Observatory as shown in Figure 8.3 was 0.00 ± 0.04 μsec, slightly greater than estimated. The same effect degrades the satellite slant ranges to Hawaii and Buenos Aires. This effect, however, cannot be separated from the larger variation due to oscillator drift for the Hawaiian and Buenos Aires sites.

Computed slant ranges from the General Electric L-band trilateration positions of the ATS-5 satellite to the NASA Rosman and Mojave ground stations may be compared directly with the NASA measured slant ranges. Range measurements to the NASA ground stations were smoothed by second order polynomials over the 150-second tracking periods. Individual NASA range measurements have a precision better than 2 meters, such

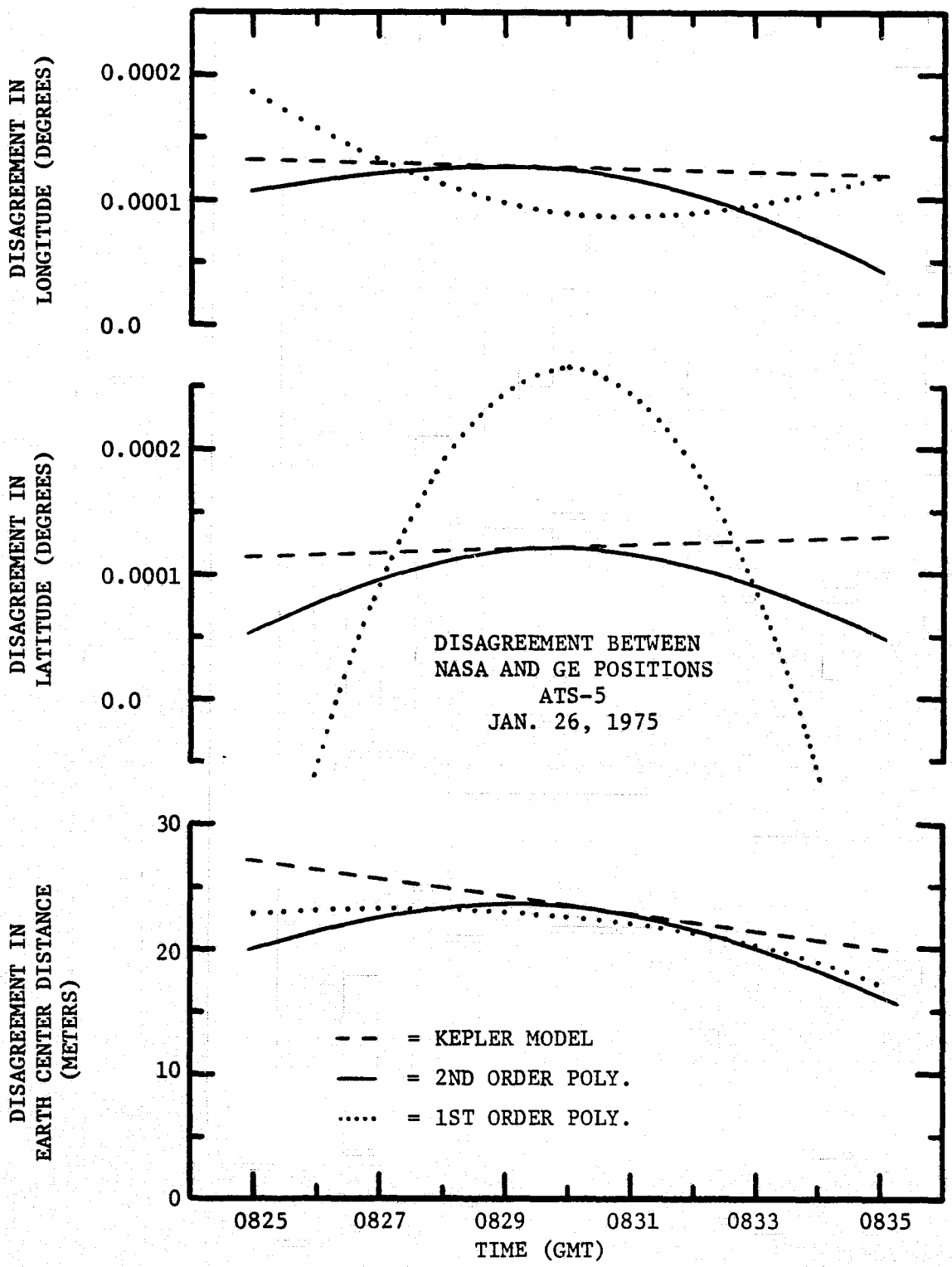

FIGURE 8.4 COMPARISON OF GENERAL ELECTRIC SMOOTHED SATELLITE POSITIONS FOR RANGING PERIOD AT 0830 GMT, JAN. 26, 1975

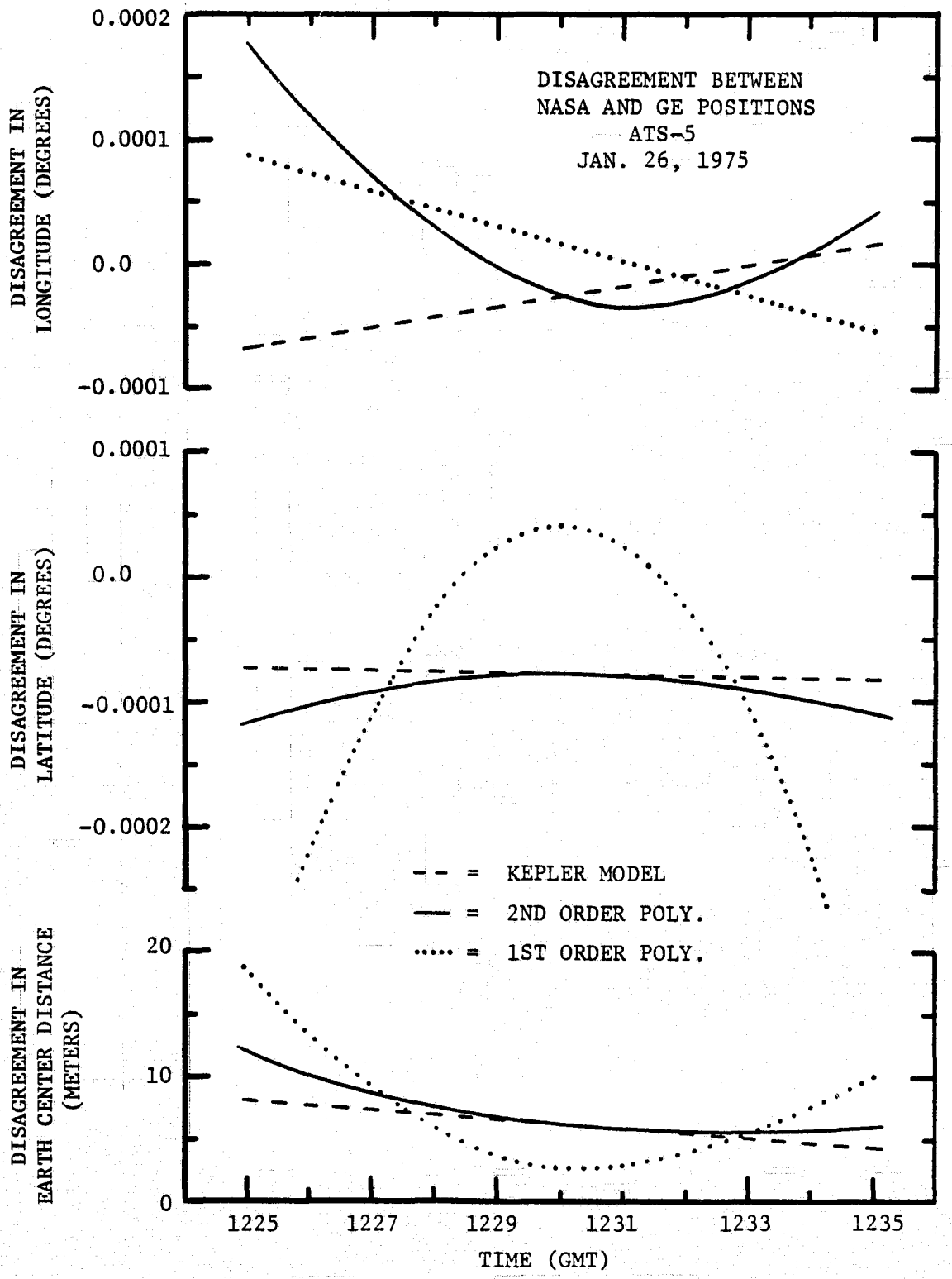

FIGURE 8.5 COMPARISON OF GENERAL ELECTRIC SMOOTHED SATELLITE POSITIONS FOR RANGING PERIOD AT 1230 GMT, JAN. 26, 1975

TABLE 8.3

DISAGREEMENT BETWEEN KEPLER ORBIT

AND SECOND ORDER POLYNOMIAL SMOOTHED

RANGING DATA

JAN. 26-27, 1975

RANGING PERIOD	MEAN DISAGREEMENT		
TIME (GMT)	LONGITUDE (10^{-5} DEGREES)	LATITUDE (10^{-5} DEGREES)	EARTH CENTER DISTANCE (METERS)
0830	1.8 ± 2.9	3.0 ± 2.8	2.3 ± 3.3
1030	4.2 ± 4.8	1.9 ± 2.5	3.1 ± 3.7
1230	-5.0 ± 7.3	1.5 ± 1.6	-0.5 ± 2.8
1430	3.5 ± 5.0	0.9 ± 3.9	2.2 ± 4.1
0630	12.8 ± 15.2	0.2 ± 0.9	7.0 ± 8.4
MEAN	3.5 ± 9.8	1.5 ± 2.6	2.8 ± 5.3

that smoothed slant ranges should be precise on the order of 0.1 meters.

For most tracking periods, range measurements from NASA Rosman were made during trilateration ranging periods; this occurred only once for ranging from the NASA Mojave station. Extrapolations of the trilateration slant ranges beyond the ranging period may generate significant errors, as suggested by Figures 8.4 and 8.5. Consequently, NASA slant ranges must be compared against slant ranges derived from Kepler smoothed satellite positions. Table 8.4 itemizes the range measurement differences with the second order polynomial smoothed trilateration data and with the Kepler smoothed data. In comparing the Mojave data, extrapolations based on the second order polynomial smoothing up to six minutes resulted in a range difference standard deviation a factor of three greater than that based on Kepler smoothed data. No disagreement of this magnitude exists for the range differences to Rosman. Table 8.4 also itemizes the disagreement between the NASA measured slant ranges and slant ranges computed from the NASA predictions. Standard deviations on the order of 2.0 meters most probably result from errors associated with interpolating the NASA data and with truncation in the calculations at the eighth significant decimal digit; the NASA predictions list satellite positions on the minute while the interative program which determined orbital elements computed slant ranges for the exact measurement time. Figures 8.6 and 8.7 depict the range differences to the Rosman and Mojave sites, respectively.

The General Electric computed vs. NASA measured slant range differences to the Rosman and Mojave ground stations show decreases near 1600 GMT on Jan. 26, 1975 and increases near 0600 GMT on Jan. 27, 1975. These variations are consistent with the diurnal variations observed in the satellite position differences shown in Figure 8.2. The slant range differences which result from the position differences of Figure 8.2 disagree with the observed slant range differences of Figure 8.6 (Rosman slant ranges) by 0.3 ± 3.3 meters; the disagreement with the observed slant range differences of Figure 8.7 (Mojave slant ranges) is 6.2 ± 7.8 meters. Successive smoothings and truncations are only partially responsible for these disagreements. The primary cause results from comparing satellite positions and slant ranges at two different times and using poorly fitting polynomials to represent the trilateration data.

8.3 LONG TERM TRILATERATION ACCURACY

The simultaneous GE trilateration-NASA range and range rate tracking of ATS-5 on Jan. 26-27, 1975 demonstrated trilateration accuracy based on NASA positions of ATS-5 unaffected by the degradation of NASA positions as a function of time since epoch date. The NASA computer algorithms which deduce an orbit and subsequently generate the satellite ephemeris consider the effects of the earth with harmonic coefficients of order 15 and degree 15, the moon, the sun, and solar radiation pressure[13]. Numerical integration step sizes of 150 seconds are employed. While the algorithms have been shown in Section 8.2 to generate an excellent orbit model with respect to measured range and range rate data on the day of the measurements, predicted satellite positions will not exhibit the same

TABLE 8.4

NASA RANGE MEASUREMENT LESS COMPUTED

RANGE ASSUMING GE TRILATERATION POSITION

ATS-5

JAN. 26-27, 1975

ROSMAN RANGE DIFFERENCE					MOJAVE RANGE DIFFERENCE				
TIME (GMT)	SLANT RANGE (METERS)	NASA ORBIT (METERS)	2nd ORDER POLYNOMIAL (METERS)	KEPLER ORBIT (METERS)	TIME (GMT)	SLANT RANGE (METERS)	NASA ORBIT (METERS)	2nd ORDER POLYNOMIAL (METERS)	KEPLER ORBIT (METERS)
836	37445434.6	1.5	14.8	8.1	824	37116865.9	-0.6	18.7	21.8
1024	37410175.0	-0.7	14.5	20.2	1020	37077512.1	-1.8	-10.2	2.0
1225	37413000.9	-2.0	12.2	14.6	1220	37082385.0	-1.5	52.1	8.9
1424	37459764.5	-2.7	9.4	8.7	1419	37132476.8	-2.6	- 9.9	8.7
1626	37541357.6	-2.2	9.7	7.0	1622	37219420.8	-2.0	64.0	- 3.3
1826	37632959.1	-1.5			1820	37314916.1	-0.6		
2027	37710196.0	0.6			2022	37398476.4	1.6		
2231	37750316.3	2.6			2220	37441224.0	2.0		
0025	37742393.3	3.5			0020	37433614.9	2.3		
0234	37685580.7	3.6	9.8		0230	37370777.0	3.2	16.0	
0426	37609222.3	1.8	0.4	2.9	0422	37287325.2	2.9	12.8	17.1
0625	37521539.4	0.3	8.7	8.3	0619	37194419.9	2.3	-58.3	31.8
MEAN		0.4± 2.2	9.9 ± 4.5	10.0 ± 5.7			0.4 ± 2.1	10.6 ± 38.3	12.4 ± 12.0

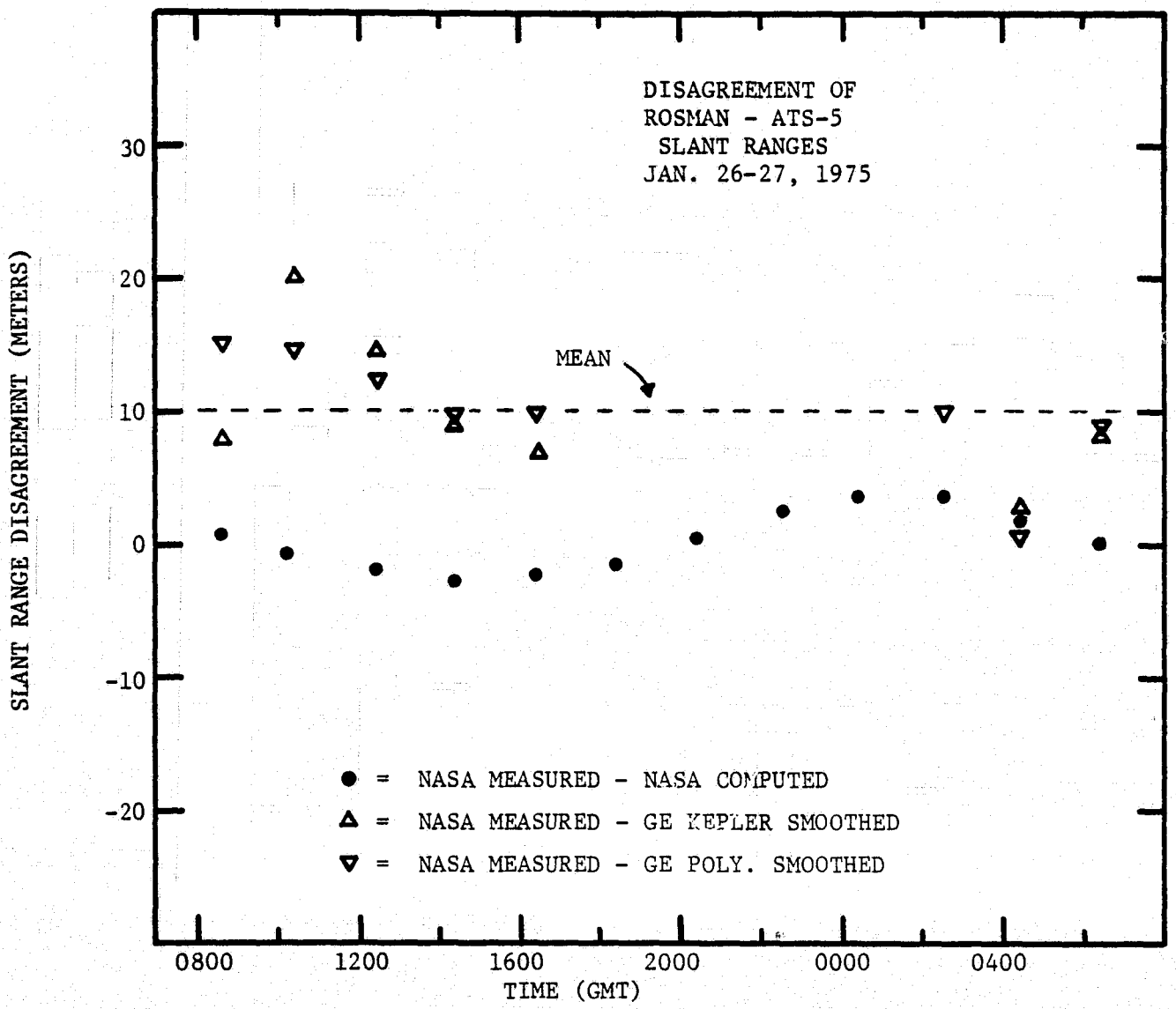

FIGURE 8.6 NASA MEASURED ATS-5-ROSMAN RANGES LESS GE COMPUTED RANGE

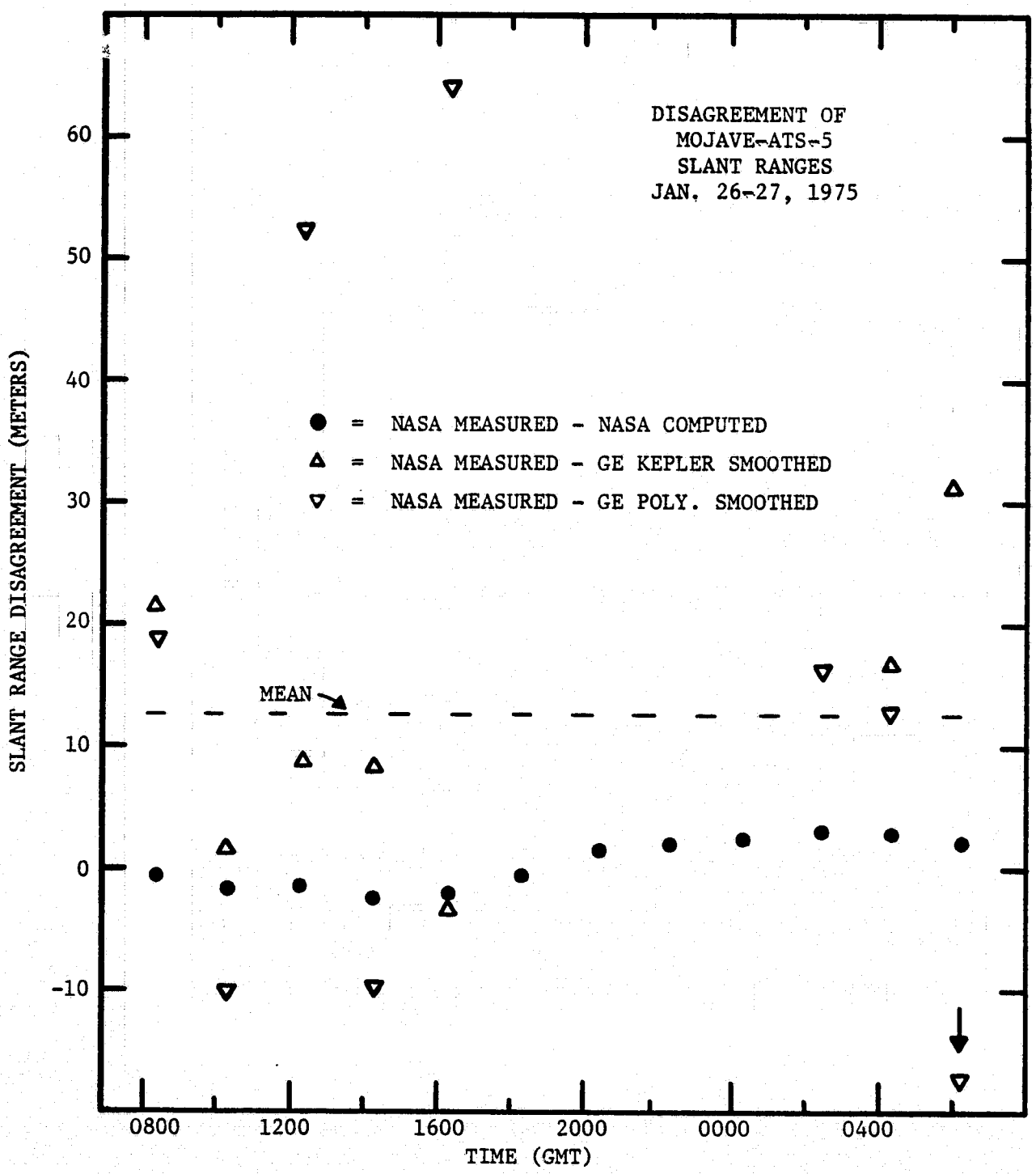

FIGURE 8.7 NASA MEASURED ATS-5-MOJAVE RANGES LESS GE COMPUTED RANGE

degree of accuracy. Comparison of the L-band trilateration positions with those predicted on the basis of C-band range and range rate data may only yield an upper bound on the accuracy of the trilateration.

The accuracy of the NASA satellite position predictions may be evaluated by predicting satellite positions from one epoch date to the next, and comparing positions of the first epoch date with those from the second epoch date. Figure 8.8 presents such a comparison for data of Jan. 12, 1975. Satellite positions predicted on the basis of range and range rate tracking on Dec. 29, 1974 less satellite positions predicted from the Jan. 12, 1975 tracking data disagree by maximum values of 0.0011 degrees longitude, 0.0001 degrees latitude, and 66 meters earth center distance. Comparing satellite positions at every hour, the data from the two different epoch dates show mean disagreements of -0.00090 ± 0.00015 degrees longitude, 0.00001 ± 0.00007 degrees latitude, and 14 ± 36 meters earth center distance. As no further comparisons of this type have been made, it will be assumed that the degradation of ephemeris accuracy as observed for Jan. 12, 1975 is typical of all NASA satellite position predictions. The slight sinusoidal variations with a 24-hour period observed on Figures 8.6 and 8.7 represent an initial misalignment between the true orbit and the NASA computed orbit. This initial sinusoidal variation is assumed to increase linearly to the variations of the type as shown in Figure 8.8.

Table 8.2 presents a complete summary of all ATS-5 data taken during Dec., 1974, Jan., 1975, and Feb., 1975, while both remote transponders were in operation. Table 8.5 supplements this summary, giving the mean disagreements between the NASA predicted positions of the satellite and the General Electric trilateration positions. These position differences are plotted in Figure 8.9 as a function of day of year and in Figure 8.10 as a function of time since epoch date.

On Figure 8.10, the horizontal dashed lines represent the mean disagreements while the diverging dotted lines represent the envelope of degradation in the NASA predictions. If one were to assume that the degradation of the NASA predictions were due to unaccountable gravitational fields, the position predictions should show a degradation as the square of time. However, the degradation is assumed to be due to a tilt or misalignment of the model orbit with the true orbit, generating errors linear as a function of time.

While some GE-NASA position disagreements on Figure 8.9 appear significantly larger than the mean of the Jan. 26-27, 1975 experiment, the addition of the envelope defining the degradation of NASA predictions as a function of time since epoch date clearly identifies the larger disagreements as being due to the inaccuracy of the NASA predictions. The longitude and earth center distance disagreements all lie within the degradation envelope after three days since epoch date. The NASA algorithms produce exceptionally excellent satellite latitudes such that the NASA latitude degradation is smaller than most individual disagreements. The data of Figure 8.10 suggest that 24-hour range and range rate tracking should be conducted every four days if accuracies equal to the trilateration accuracy are to be maintained.

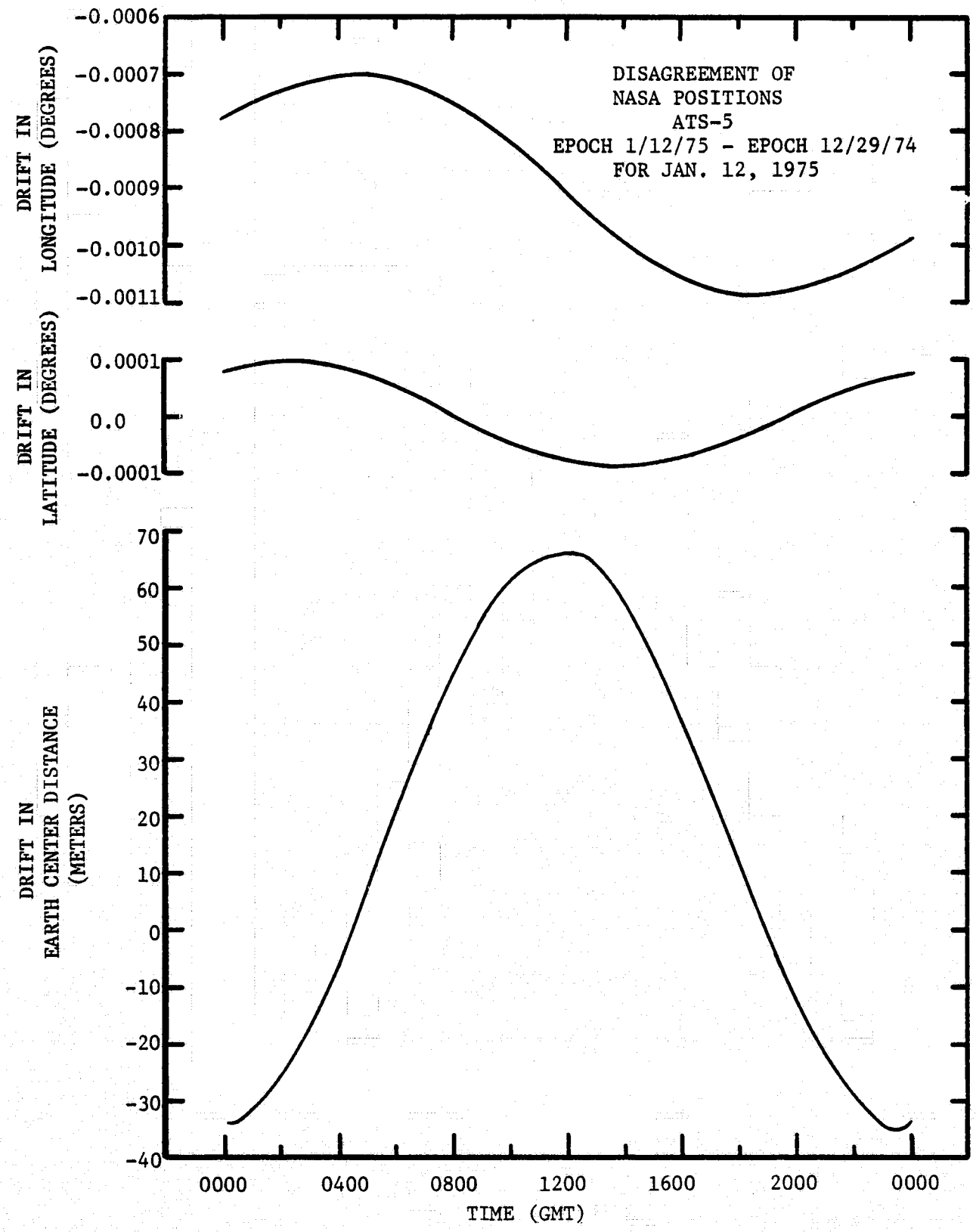

FIGURE 8.8 COMPARISON OF NASA SATELLITE EPHEMERIDES FROM TWO DIFFERENT EPOCH DATES

TABLE 8.5

SUMMARY OF DISAGREEMENTS BETWEEN

NASA AND GE POSITIONS OF ATS-5

Date	File	Sections of Ranging Data	NASA Epoch	Disagreement in Longitude (10^{-5} degrees)	Disagreement in Latitude (10^{-5} degrees)	Disagreement in Earth Center Distance (meters)
12/10/74	F956	5	12/8/74	10.8 ± 49.8	-43.2 ± 25.8	- 2.2 ± 38.9
12/12/74	F960	4	12/8/74	19.5 ± 7.4	-27.5 ± 3.3	- 3.0 ± 2.9
12/17/74	F964	5	12/8/74	44.8 ± 3.3	17.0 ± 11.7	-23.6 ± 6.9
12/19/74	F967	4	12/8/74	81.0 ± 4.8	14.2 ± 4.5	-32.7 ± 5.3
1/2/75	F001	2	12/29/74	0.0 ± 5.6	-39.0 ± 0.0	-24.5 ± 0.7
1/7/75	F005	9	12/29/74	56.2 ± 8.4	-22.9 ± 10.5	-28.8 ± 9.7
1/9/75	F008	10	12/29/74	72.4 ± 14.8	-20.2 ± 9.9	-10.0 ± 18.1
1/17/75	F015	7	1/12/75	-27.3 ± 16.0	-26.7 ± 11.1	-22.1 ± 15.3
1/21/75	F016	9	1/12/75	31.8 ± 10.6	-18.0 ± 21.6	-20.0 ± 8.4
1/26-27/75	F019-F020	17	1/26/75	14.0 ± 11.6	3.1 ± 22.6	18.2 ± 18.9
1/28/75	F021	4	1/26/75	- 9.7 ± 11.4	- 3.0 ± 15.1	1.0 ± 13.8
1/30/75	F023	3	1/26/75	3.0 ± 5.0	- 8.7 ± 7.1	- 6.3 ± 6.1
1/31/75	F025	6	1/26/75	15.0 ± 7.4	16.3 ± 12.4	11.8 ± 12.1
2/24/75	F037	3	2/23/75	5.8 ± 5.7	34.9 ± 5.1	35.5 ± 5.2
2/25/75	F038	4	2/23/75	-15.2 ± 9.0	17.7 ± 11.2	16.0 ± 12.7
2/26/75	F040	4	2/23/75	2.2 ± 10.4	11.5 ± 16.7	16.7 ± 10.1
OVERALL		96		23.6 ± 33.2	- 7.1 ± 24.6	- 4.3 ± 24.0

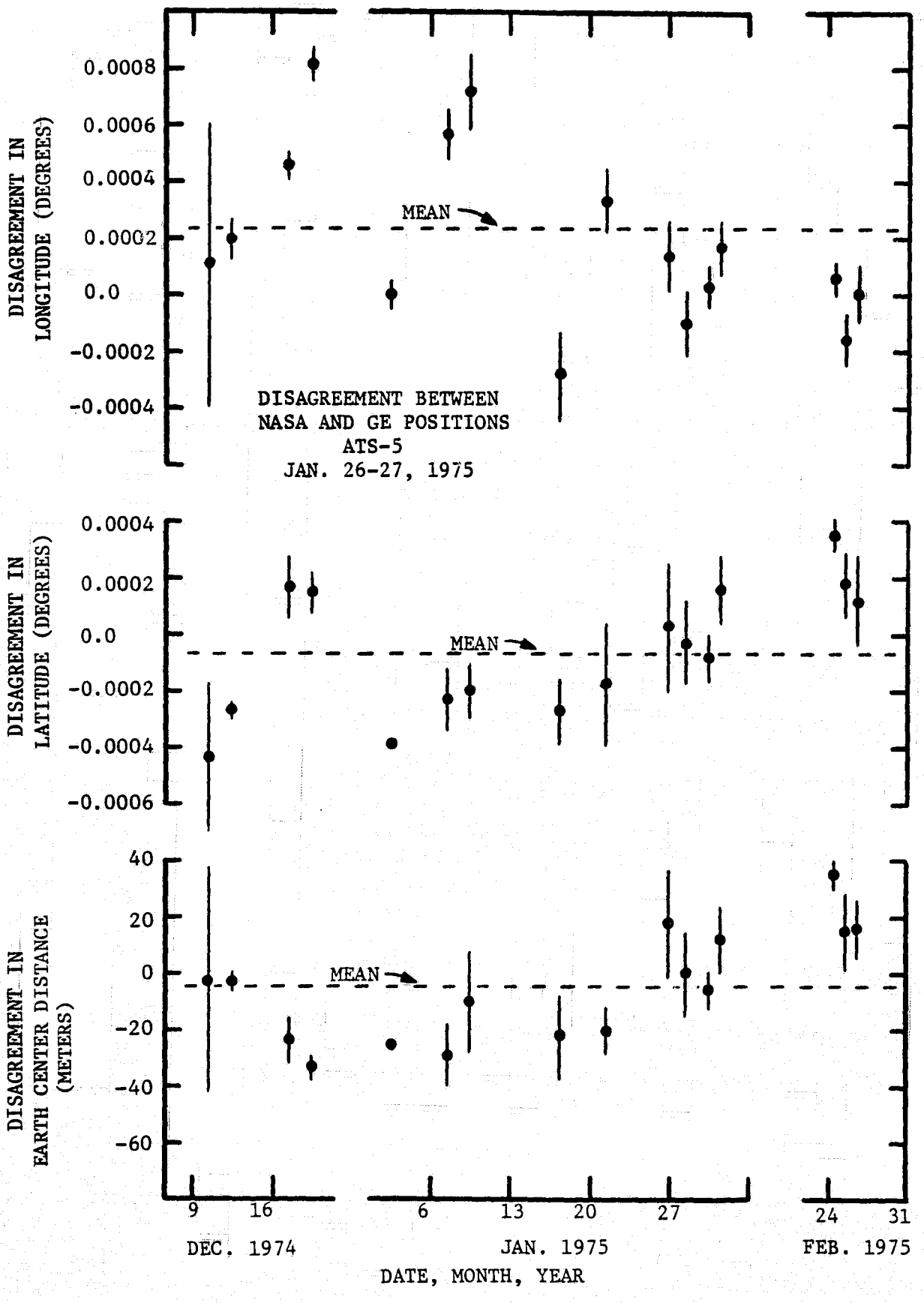

FIGURE 8.9 DIFFERENCES BETWEEN NASA AND GE POSITIONS OF THE ATS-5 SATELLITE, DEC. 1974 TO FEB. 1975

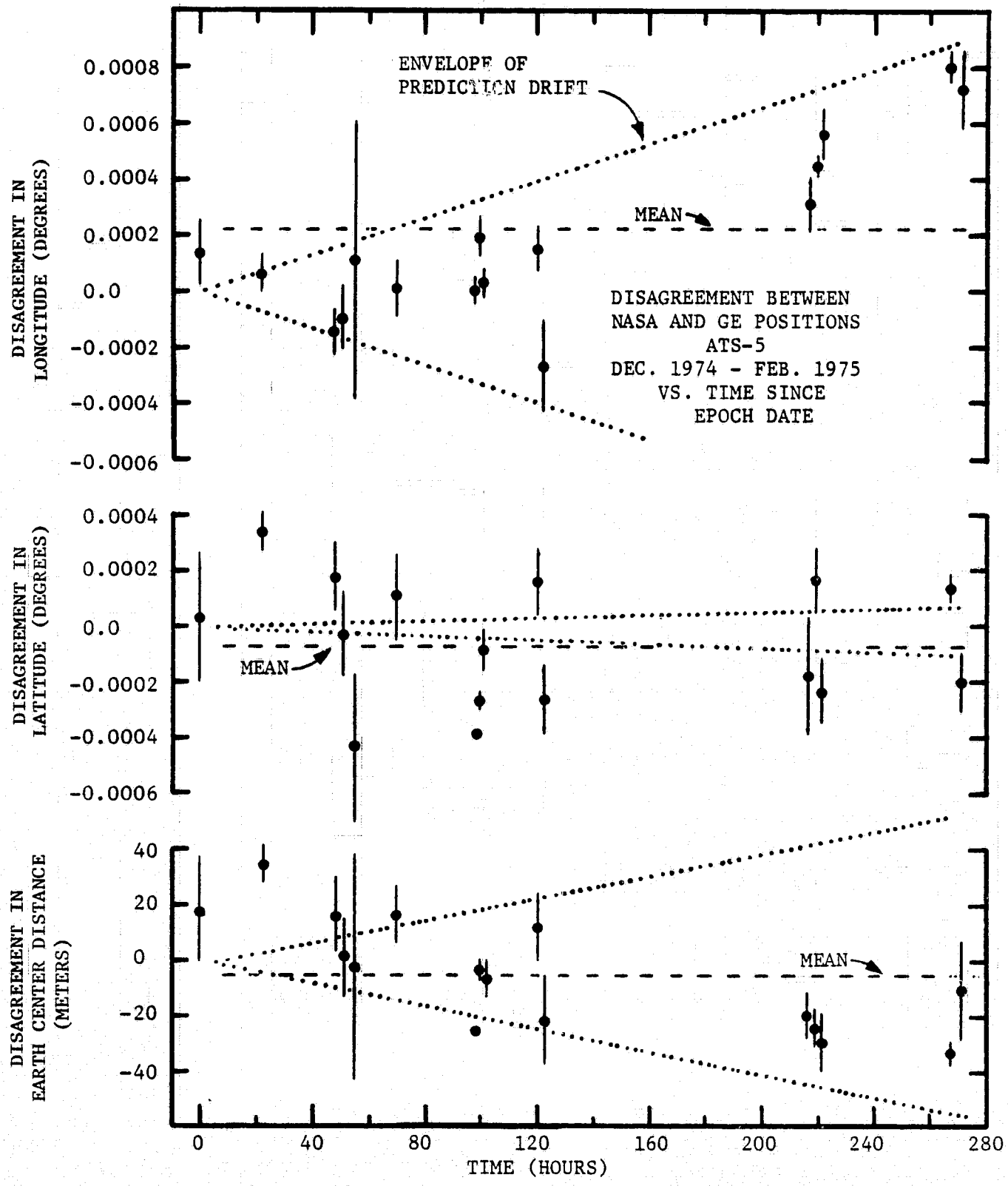

FIGURE 8.10 DIFFERENCES BETWEEN NASA AND GE POSITIONS OF THE ATS-5 SATELLITE AS FUNCTION OF TIME SINCE EPOCH DATE, DEC. 1974 to FEB. 1975

Table 8.5 lists the mean disagreement between the General Electric and NASA positions of ATS-5 during the three operational months of the experiment. Five experiments were conducted explicitly in support of NASA's and MARAD's two satellite vehicle location experiments. The mean disagreements between the General Electric and NASA positions of ATS-5 for these five tests were 0.00013 $\pm$ 0.00019 degrees longitude, 0.00006 $\pm$ 0.00024 degrees latitude, and 5 $\pm$ 22 meters earth center distance. The mean time since epoch date during these experiments was 3.5 days.

8.4 ACCURACY OF PREDICTED SATELLITE POSITIONS

A simple model was specified for the computer algorithm that determines the near real-time position predictions of the ATS-5 satellite. Simple models such as the six element Kepler model produce large position errors for predictions extending more than a few hours. The largest perturbations stem from the relative motions of the sun and moon. Due to the relatively small excursions of a geostationary satellite, an excellent long term six parameter orbit model would be possible if the sun and moon were to remain fixed. An effective gravitational field nonconcentric with the earth's gravitational field would be assumed.

Figure 8.11 presents a comparison between predictions based on three previous ranging periods and positions determined at the subsequent plotted times, for the Jan. 26-27, 1975 24-hour tracking experiment. The predicted satellite longitudes and earth center distances disagree with measured values with an apparent 12-hour periodicity, an effect very much like ocean tides; the predicted latitudes disagree with observed latitudes with an apparent 24-hour periodicity.

The data points in Figure 8.11 represent the predicted positions less the observed positions. Straight lines connect three dots for clarity of presentation; the dots centered on zero position error represent the disagreement between the predicted and observed positions at the last ranging period, and consequently, show no error; the second dots represent predicted position errors after one hour; the third dots represent predicted position errors after two hours. Dashed lines represent interpolations or extrapolations where an absence of data prevented a comparison. All the curves of Figure 8.11 with the exception of the two starting at 1630 and 1730 GMT are based on ranging periods separated by one hour; the two exceptions contain ranging periods one and two hours apart.

At approximately 1900 and 0700 GMT (1200 and 0000 local time), the simple Kepler model predicted the satellite to move closer to the earth than measurements verified. During this particular ranging experiment, the sun and moon were at opposite sides of the earth resulting in a maximun pull away from the earth at local noon and local midnight, represented by the symbols "||" in Figure 8.11. Correspondingly, at $\pm$ 6 hours from local noon (symbol "$\perp$" in Figure 8.11), the satellite passed closer to the earth than predicted. The orthogonality of the longitude and earth center distance coordinates causes the longitude distortions to be three hours out of phase with earth center distance distortions, as observed in Figure 8.11.

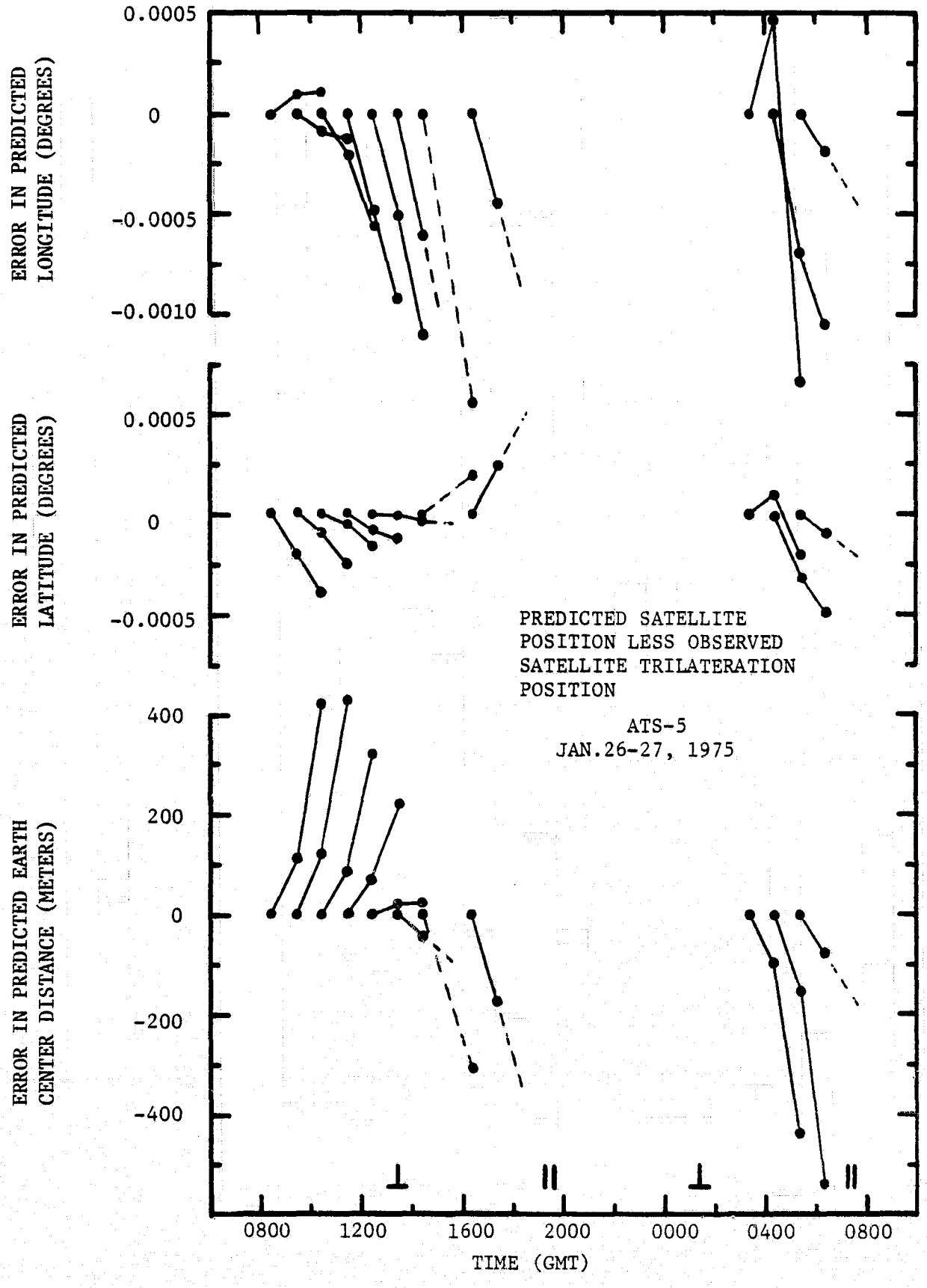

FIGURE 8.11 DEGRADATION OF PREDICTED SATELLITE POSITION VS. TIME OF DAY

The magnitudes of the predicted position errors are roughly consistent with the maximum estimated errors shown on Table 5.1.

The predicted and observed latitudes disagree with an apparent 24-hour periodicity. As the satellite moved south across the equator, its relatively constant velocity away from the ecliptic plane resulted in low prediction errors. Slight inaccuracies in the computation of the orbit inclination angle due to the varying gravitational effects from the moon and the sun result in maximum latitude errors at the northern and southern extremes of the orbit. The inclination of the earth with respect to the ecliptic plane causes a bias which draws the satellite to a continuously increasing inclination, up to 23 degrees after several tens of years.

The tidal effect on the accuracy of predicted satellite positions is more clearly seen in Figure 8.12. This figure contains the same data of Figure 8.11 plus the distortions to predicted satellite positions from the tests on Jan. 9, 21, 26, 27, and 31 and Feb. 25 and 26, where predicted positions could be compared with trilateration positions. In Figure 8.12, the solid lines connect data points for clarity of presentation and represent the growing error in predicted satellite position from zero hours after the last range measurement (zero error) to two hours after the last range measurement. Continuous smooth curves cannot be drawn as trilateration positions were determined once every hour in most cases; the kink represents a comparison at one hour after the last range measurement. Solid lines which change to dashed lines represent comparisons at zero hours and one hour since the last range measurement and an extrapolation to two hours. Fully dashed lines represent comparisons at zero hours and two hours; lack of data prevented a comparison at one hour.

The abscissa of Figure 8.12 corresponds to hours of effective local time, adjusted to reflect the vector sum of the gravitational fields of the sun and the moon. When the gravitational vector sum points parallel to the earth-satellite axis, the compensated local time is 12 hours.

The data of Figure 8.12 reflect position predictions generated from three ranging periods spaced one hour apart, one half hour apart, and one and two hours apart. Insufficient data exists to make any significant observation with regard to the spacing of ranging periods to yield optimum position predictions. Table 8.6 lists the maximum observed inaccuracies in predicted satellite positions as a function of time since the last range measurements.

Predicted satellite ephemerides containing 120 positions of ATS-5 at one minute intervals were sent to NASA and MARAD in support of the two satellite remote vehicle position fixing experiments. Figure 8.13 lists a typical ephemeris. The header contains the answerback and number of the Observatory TWX machine, the date and time, and the numbers, addresses, and names of recipients of the data. A sequence of four ampersands signals the beginning of the ephemeris list to the NASA and MARAD computers. The first line of the ephemeris lists the date and time; the second line lists the one sigma single range measurement standard deviation of all slant ranges with respect to the orbit model and the total number of trilateration slant ranges. Predicted satellite positions follow in the form of time

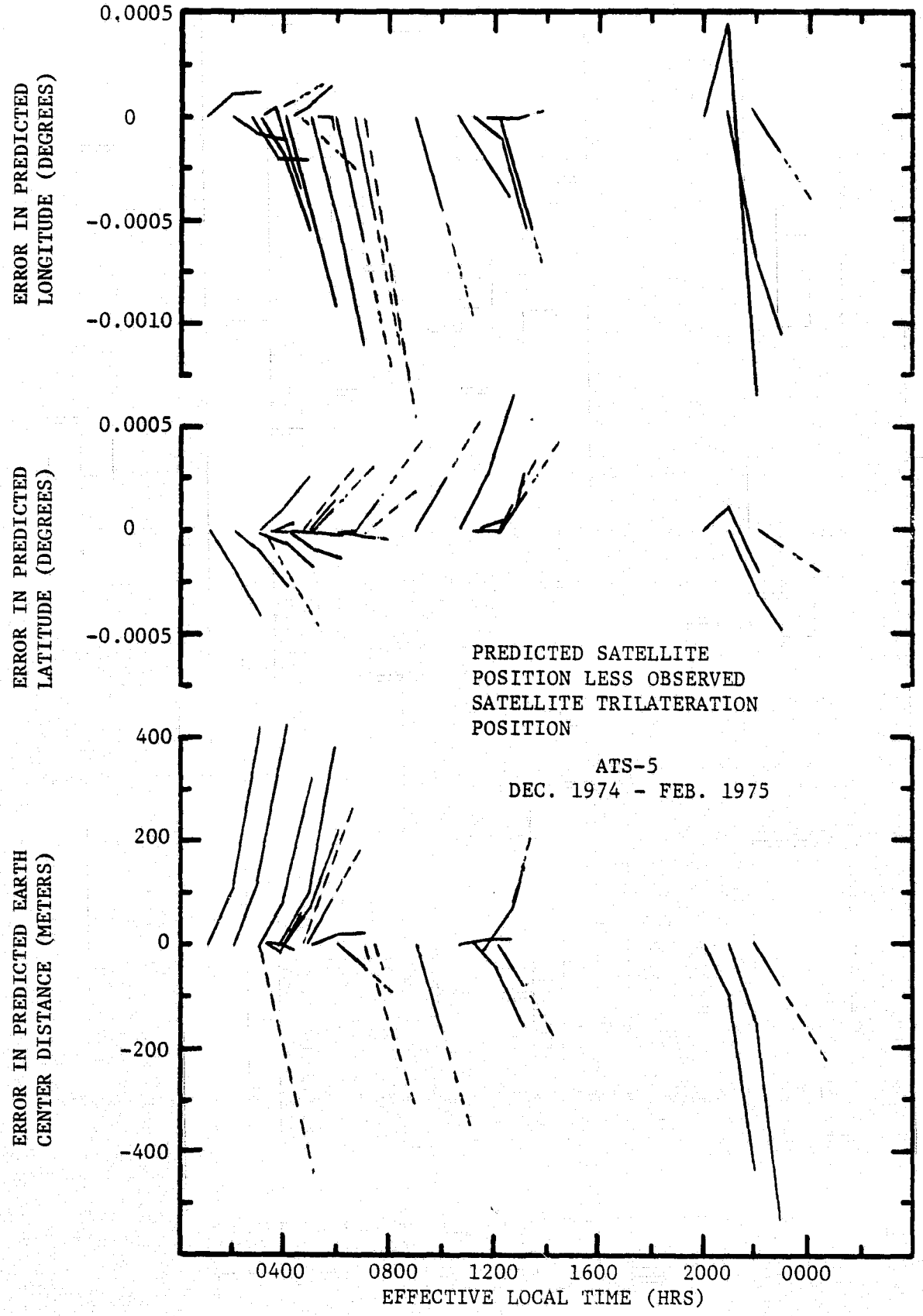

FIGURE 8.12 DEGRADATION OF PREDICTED SATELLITE POSITION VS. ORIENTATION OF VECTOR SUM OF MOON AND SUN GRAVITATIONAL VECTORS

TABLE 8.6

OBSERVED MAXIMUM INACCURACIES

OF PREDICTED SATELLITE POSITIONS

TIME PERIOD (minutes)	LONGITUDE ERROR (degrees)	LATITUDE ERROR (degrees)	EARTH CENTER DISTANCE ERROR (meters)
60	0.0007	0.0003	180
120	0.0015	0.0007	540

```
DE G E. SCDY OBS TWX 710-442-2986
12-SEP-75  18:49:41
TWX 510-935-4089 RDS NASA STA ATTEN: PLACE
TWX 510-223-0845 MCC KP KGPT  ATTEN: J. PUGLISI
TWX 710-828-9716 NASA GSFC  ATTEN: ATSOCC SYSGER F  KISSEL
                 NASA GSFC  ATTEN: PLACE OPSMGR GALICINAO


$$$$
ATS-5 TRILATERATION 5 026 08 5 026 12
 0.732E-01 1511
030-105.59042   2.17753 42181756 37448292
035-105.59057   2.19205 42180336 37445896
040-105.59061   2.20552 42178912 37443560
045-105.59053   2.21794 42177480 37441288
050-105.59035   2.22930 42176044 37439080
055-105.59007   2.23960 42174604 37436932
060-105.58969   2.24882 42173160 37434852
065-105.58921   2.25697 42171712 37432
070-105.58862   2.26404 42170
075-105.58794   2.27003                 37407636
080-105.58717                 42127956 37408112
085-105                       42126792 37408672
    105.52702   1.89546 42125648 37409316
    105.52431   1.86709 42124524 37410040
245-105.52156   1.83782 42123420 37410844
250-105.51880   1.80767 42122336 37411726
255-105.51601   1.77665 42121276 37412704
260-105.51321   1.74477 42120236 37413756
265-105.51038   1.71205 42119220 37414892
270-105.50754   1.67851 42118224 37416104
$$$$
```

A B C D E

Symbol Definitions:

- A Time in minutes,
- B Longitude of satellite, in degrees,
- C Geocentric latitude of satellite, in degrees,
- D Satellite earth center distance, in meters,
- E Rosman-ATS-5 slant range, in meters

Predicted satellite positions for day 26, 1975, from 0830 to 1230 GMT. Single slant range standard deviation based on a comparison of 1511 slant ranges with respect to the orbit model is 0.073 μsec.

FIGURE 8.13 ATS-5 POSITION PREDICTION TABLE

in minutes, longitude and geocentric latitude in degrees, earth center distance in meters, and the ATS-5-Rosman slant range in meters. The sequence of four ampersands signals the end of data to the NASA and MARAD computers.

8.5 ESTIMATED CONTRIBUTIONS OF FACTORS THAT LIMIT ACCURACY

The accuracy of the L-band trilateration satellite positions may be evaluated by considering the error contribution of each factor that affects accuracy. The absolute satellite position inaccuracy has two components, a relative inaccuracy and a bias inaccuracy. The relative inaccuracy reflects factors such as the day-to-day variations in the ionospheric and tropospheric propagation time delay and responder oscillator frequency. The bias inaccuracy on the other hand encompasses effects due to the uncertainty in the absolute location of the remote transponders and the Observatory, the mean frequency of the timing oscillators in the transponders, and the internal time delay of the satellite in the narrowband L-L frequency translation mode. Tables 8.7 and 8.8 itemize individual contributing factors to satellite position uncertainty and their estimated effects. Values for the factors were selected as described in the following paragraphs.

The 10 MHz oscillator in the Buenos Aires transponder has a frequency stability of one part in 10^6 over a 0°C to 50°C temperature range. The specified stability leaves a $\pm$ 0.52 μsec uncertainty in the internal time delay of the transponder. The calibration experiments (Figure 6.5) and measurements of the responder oscillator frequency via the VHF communication channel (Table 6.1) suggest a $\pm$ 0.2 μsec uncertainty. The data of Figure 8.3 infer a variation from -0.4 μsec to +0.3 μsec over a 24-hour period. With the realization that the drift of the internal time delay to a value of -0.4 μsec below nominal occurred because of a temperature extreme, an uncertainty of $\pm$ 0.3 μsec is assumed for the Buenos Aires transponder internal time delay.

The 10 MHz oscillator in the Hawaiian transponder has a frequency stability of two parts in 10^7 over a 0°C to 50°C temperature range. Neglecting the step jumps in transponder internal time delay, the individual calibration experiments (Figure 6.11) showed variations through approximately 0.15 μsec. Measurements of the transponder oscillator frequency via the VHF communication channel (Table 6.1) show maximum variations through 1.5 Hz, suggesting a maximum variation in internal time delay of 0.08 μsec. The data of Figure 8.3 infer variations of the internal time delay from -0.2 to +0.3 μsec. The transponder in Hawaii is operated in an air conditioned room and cooling fans draw an adequate volume of air through the responder; before the installation of the cooling fans, this transponder had experienced overheating problems which generated significantly larger fluctuations in internal time delay. An uncertainty of $\pm$ 0.2 μsec is assumed for the Hawaiian transponder internal time delay.

Unusual variations in the electron content of the ionosphere can increase the radio propagation time delay by a factor of two. The contribution listed in Table 8.7 assumes a maximum variation from the simplified

TABLE 8.7

RELATIVE INACCURACY OF SATELLITE

POSITION FROM L-BAND TRILATERATION

Effect	Magnitude of Effect	Longitude (degrees)	Latitude (degrees)	Earth Center Distance (meters)
Estimated variation in Buenos Aires 10 MHz responder oscillator.	± 0.3 μsec	0.00008	0.00029	20
Estimated variation in Hawaii 10 MHz responder oscillator.	± 0.2 μsec	0.00021	0.00004	13
Uncorrectable daily variation in the ionosphere.	± 0.01 μsec	0.00003	0.00003	2
Uncorrectable daily variation in the troposphere.	± 0.002μsec	0.00001	0.00001	-
Variation in transponder time delay external to the self calibration loop.	negligible	-	-	-
RF components off center frequency.	± 0.1 μsec	0.00015	0.00013	9
Error due to satellite motion during ranging time interval.	negligible	-	-	-
Smoothing of slant range data.	-	0.00012	0.00004	8
RMS Relative Inaccuracy		0.00030	0.00032	27

RELATIVE SLANT RANGE INACCURACIES

Ground Station	Slant Range (meters)
NASA-Rosman	37
NASA-Mojave	36

TABLE 8.8

BIAS INACCURACY OF SATELLITE

POSITION FROM L-BAND TRILATERATION

Effect	Magnitude of Effect	Longitude (degrees)	Latitude (degrees)	Earth Center Distance (meters)
Internal time delay of ATS-5 satellite in narrowband L-L frequency translation mode.	unknown	-	-	-
Integer time delay in Buenos Aires transponder.	± 0.05 μsec	0.00001	0.00005	3
Integer time delay in Hawaiian transponder.	± 0.05 μsec	0.00005	0.00001	3
Location of Buenos Aires transponder with respect to local reference.	See Table 4.3	0.00002	0.00009	6
Location of Hawaiian transponder with respect to local reference.	See Table 4.3	0.00001	-	1
Location of Observatory with respect to local reference.	See	0.00001	0.00002	-
Net bias inaccuracy (less unknowns)		0.00006	0.00011	7

BIAS SLANT RANGE INACCURACIES

Ground Station	Slant Range (meters)
NASA-Rosman	11
NASA-Mojave	11

ionospheric model of 40 percent. Variations in the tropospheric propagation time delay are negligible. The quoted amount represents a change from zero percent relative humidity to 100 percent relative humidity.

At both remote transponders, cables between the L-band power amplifier and the antenna feed and between the antenna feed and the L-band receiver are external to the self calibration loop. The total time delay through this cable system and the diplexer is on the order of 0.4 μsec. Neither the diplexer nor the RF cables are expected to exhibit a variable time delay as a function of environmental conditions.

Proper tuning of all RF oscillators and operation of the transponders in a room environment justifies a $\pm$ 0.1 μsec estimate on the inaccuracy generated by L-band receivers or transmitters being off center frequency. This estimate is considered high as the specifications on the oscillators cover operation over a broad temperature range with no warm-up time. Furthermore, partial correction for components being off center frequency is accomplished by the self calibration circuit.

The time of every ranging interrogation is recorded approximately 0.1 seconds after correlation at the Observatory on the satellite return. The data acquisition system reads the Observatory clock to the nearest second such that recorded times are accurate to within plus one second and minus zero seconds. As the signal passes through the satellite approximately 0.125 seconds before correlation, the recorded time may thus be considered the satellite transpond time, accurate to within plus 0.775 seconds and minus 0.225 seconds (0.275 second bias). Neglecting this bias, ground station satellite velocities on the order of 15 meters per second would generate slant range errors of four meters. A first order correction of slant ranges in the software algorithms reduces this four meter error to negligible amounts.

The a priori assumption to represent slant ranges between the satellite and ground station with second order polynomials has been shown in Section 8.2 to be slightly inadequate. Satellite positions computed from slant ranges based on second order polynomials show the greatest inaccuracies at the beginning and end of the ranging period. The position errors quoted in Table 8.7 reflect values of the mean plus a standard deviation from Table 8.3.

The inaccuracies mentioned above represent conservative estimates. The inaccuracy of most individual measurements will be less than stated values. As a result of these, the General Electric L-band trilateration satellite positions can be expected to change from day to day within 0.00030 degrees in longitude, 0.00032 degrees in latitude, and 27 meters in earth center distance. Table 8.7 also lists the slant range inaccuracies to the NASA Rosman and Mojave tracking stations which correspond to the RMS relative inaccuracy.

The above mentioned inaccuracies are inherent in the design of the trilateration network and are not expected to improve without changes in system parameters or system software. The bias errors, however, are

due primarily to a lack of information in two key areas, the internal time delay of the ATS-5 satellite and the absolute locations of the three ground stations. The internal time delay of the ATS-5 satellite in the narrowband L-L frequency translation mode was measured by the spacecraft manufacturer prior to launch at 0.520 μsec[14]. NASA remeasured this same time delay at 0.610 μsec after two years in orbit. A value of 0.610 μsec has been used for all data of this report. An uncertainty of 0.1 μsec in the satellite internal time delay would generate a 0.00015 degree errors in satellite latitude and longitude and 9 meter errors in earth center distance.

The best estimates of effective remote transponder internal time delays quoted in Tables 6.2 and 6.3 are assumed to be accurate to within ± 0.05 μsec. The results of individual calibration experiments show time delay variations exceeding this uncertainty. Most effects, however, are considered as variables with daily fluctuations and as such, affect the relative inaccuracy. The ± 0.05 μsec uncertainty represents the correlator round-off error on a single range measurement.

No error in the Observatory internal time delay is anticipated as the Observatory clocks are referenced to a highly stable frequency standard. Averaging several measurements of Observatory internal time delay eliminates correlator round-off as a source of inaccuracy.

None of the three ground stations constituting the L-band trilateration network have been located by an accurate survey. The inaccuracies quoted on Table 4.1 result from general surveys conducted in the area of the ground stations prior to the deployment of the network. Errors relating the local reference to the datum origin and the datum origin to the common geocentric coordinate system are assumed negligible. Ground station position errors of up to three meters generate insignificant satellite position errors.

The disagreement between earth models and the uncertainty in the absolute location of datums creates a problem in defining the accuracy of any worldwide satellite navigation or surveillance system. The system may be very accurate according to its own references, but if the craft using the system employs charts that are based on other references, the useful accuracy for the user may be degraded.

The trilateration positions of the satellite are expected to have an absolute accuracy (neglecting relative inaccuracies) of 0.00006 degrees longitude, 0.00011 degrees latitude, and 7 meters earth center distance. The corresponding uncertainties in the slant ranges for ATS-5 to the NASA Rosman and Mojave tracking stations are 11 meters.

8.6 SLANT RANGE STANDARD DEVIATIONS

It has been shown in Section 6.9 that one sigma range measurement standard deviations of 0.08 μsec are routinely achievable on the Observatory-satellite link and 0.15 μsec on the Observatory-satellite-remote

transponder link. These standard deviations relate, however, only to a second order polynomial fit to the raw ranging data. They do not reflect a standard deviation with respect to an orbit model.

In an operational sequence, each ranging period has a duration of approximately 10 minutes and contains approximately 256 interrogations, 128 to each remote transponder. This defines a total of approximately 512 slant ranges from the satellite to the three ground stations. Second order polynomial fits to each set of slant ranges are used to compute slant ranges to the satellite for a single time midway between the beginning and end of the ranging period. The mean slant ranges are then used to compute a mean satellite position. Three periods of ranging thus produce three mean satellite positions which are used to calculate the six Kepler orbital elements by the method of Gibbs.

The prediction section of the computer software uses the six Kepler orbital elements to compute the position of the satellite. The first predicted satellite position is calculated for a time near the end of the third ranging period. The remaining predicted satellite positions follow according to a specified temporal spacing and total specified number. The same six Kepler orbital elements are also used to compute the position of the satellite for every time a ranging interrogation took place during the three ranging periods. Slant ranges from the satellite to the appropriate ground stations are computed and compared with measured slant ranges in the form of a standard deviation. Consequently, with three periods of ranging of roughly 512 slant ranges each, each standard deviation will reflect approximately 1536 data points.

The total number of slant ranges in three ranging periods and the range measurement standard deviation are printed at the top of each ATS-5 trilateration position prediction table. These two numbers are also sent to NASA and MARAD to provide an immediate indication as to the quality of the ranging data and consequently, the predicted positions. Table 8.9 lists the numbers of slant ranges and the one sigma range measurement standard deviations for the data taken during the 24-hour test of Jan. 26-27, 1975. The first column of the table lists the mean times of the three ranging periods used to generate the satellite orbit model.

The range measurement standard deviations do not appear to be correlated to satellite latitude. An effect of this type could be anticipated due to the narrow beamwidth of the 10-foot dish antennas at both remote transponder sites. At the extremes of the satellite orbit, the remote transponder antenna gains are down by 3 dB. This results in a 3 dB reduction in signal-to-noise ratio in the remote transponder receivers and an approximately 0.7 dB reduction in the Observatory receiver on the transponder return. The reduced signal-to-noise ratio in the remote transponder receivers increases the theoretical ranging resolution, σ_{RF}, by approximately 0.020 μsec. As this factor is the leading contributor to the overall range measurement standard deviation, some variation as a function of satellite position could have been anticipated.

TABLE 8.9

RANGE MEASUREMENT STANDARD DEVIATION
WITH RESPECT TO KEPLER ORBIT MODEL
JAN. 26-27, 1975

Mean Time of Ranging Periods (Times in GMT)	Satellite Latitude (degrees)	No. Slant Ranges	Single Range Measurement Standard Deviation (μsec)
0630-0730-0830	1.9	1511	0.074
0730-0830-0930	2.2	1531	0.084
0830-0930-1030	2.3	1537	0.115
0930-1030-1130	2.2	1544	0.127
1030-1130-1230	2.0	1529	0.159
1130-1230-1330	1.7	1528	0.167
1230-1330-1430	1.2	1517	0.141
1330-1430-1630	0.4	1508	0.188
1430-1630-1730	-0.2	1471	0.109
0130-0230-0330	-0.7	1494	0.154
0230-0330-0430	-0.1	1580	0.107
0330-0430-0530	0.5	1582	0.083
0430-0530-0630	1.1	1576	0.208
MEAN			0.132

The standard deviations quoted in Table 8.9 refer to single range measurements. One should not assume, however, that simple division by the square root of the total number of slant ranges yields the standard deviation of the mean. The stated standard deviation is based on three periods of ranging, each ranging period having roughly twice as many Observatory-satellite slant ranges as Buenos Aires-satellite or Hawaii-satellite slant ranges. An estimate of the precision of the satellite position from each ranging period can be made by first assuming the standard deviation of a single transponder-satellite slant range to be a factor of two greater than a single Observatory-satellite slant range. Second, consider the mean single range measurement standard deviation from Table 8.9 to be 0.13 μsec. These assumptions result in a one sigma Observatory-satellite single range measurement standard deviation of 0.082 μsec; the one sigma transponder-satellite single range measurement standard deviation becomes 0.164 μsec. Both values are in excellent agreement with the standard deviations of Section 6.9, based on data smoothed by second order polynomials. With 256 Observatory-satellite slant ranges per ranging period, the mean slant range standard deviation becomes 0.0051 μsec for each ranging period; with 128 transponder-satellite slant ranges, 0.015 μsec. Translating the mean slant range precisions into mean satellite location precisions, the mean satellite position for each ranging period is determined to within 0.00002 degrees in latitude and longitude and 1 meter in earth center distance. Due to the relatively small satellite position uncertainty resulting from ranging precision, mean satellite positions based on 10 minute ranging periods suffer position errors due only to the relative and bias inaccuracies.

Similar range measurement standard deviation data from the experiment on Jan. 9, 1975 is presented in Table 8.10. The standard deviations appear to be approximately a factor of two less than those from Table 8.9, possibly due to the 4 minute ranging periods as compared to the 10 minute periods. The shorter ranging periods yield mean satellite positions with uncertainties due to ranging precision only slightly greater than those for the 10 minute ranging periods of Jan. 26-27, 1975.

The first six lines of data in Table 8.10 reflect the determination of an orbit model based on ranging periods separated by 30 minutes. The last two sets of two lines each represent a recomputation of the orbit model using alternate periods of ranging, separated by 60 minutes. No degradation in the associated single range measurement standard deviations is observed.

The above quoted precisions apply only to the mean satellite position midway between the beginning and end of a ranging period. At the end points, the satellite position accuracy will be degraded by errors in computing coefficients for the second order polynomial fit. These degraded positions, however, are well within the precision of a single range measurement. For ten minute ranging periods, this implies differences in precision between the middle and ends of ranging periods by less than a factor of ten.

TABLE 8.10

RANGE MEASUREMENT STANDARD DEVIATIONS
WITH RESPECT TO KEPLER ORBIT MODEL
JAN. 9, 1975

Mean Time of Ranging Periods (Times in GMT)	Satellite Latitude (degrees)	No. Slant Ranges	Single Range Measurement Standard Deviation (μsec)
1600-1630-1700	0.1	644	0.060
1630-1700-1730	-0.2	540	0.071
1700-1730-1800	-0.5	542	0.072
1730-1800-1830	-0.7	519	0.075
1800-1830-1900	-1.0	596	0.072
1830-1900-1930	-1.3	594	0.073
1600-1700-1800	-0.2	646	0.072
1700-1800-1900	-0.7	619	0.070
1630-1730-1830	-0.5	517	0.076
1730-1830-1930	-1.0	517	0.072

8.7 SYNCHRONIZATION OF RANGING INTERROGATOR WITH PHASE OF SATELLITE "WINDOW"

The L-band antenna on ATS-5 spins with the body of the satellite at a rate of one revolution every 780 msec. The beam width of the antenna as it sweeps past a ground station provides a "window" with an approximately 50 msec duration between the -3 dB points. Consequently, all ranging interrogations and responses must be timed to pass through the satellite while its antenna is pointed toward the earth.

In a typical ranging experiment, the Observatory interrogator is "synchronized" with the satellite prior to commencement of the transmission of ranging interrogations. While the Observatory transmits a CW L-band signal to the satellite, the interrogation synchronizer triggers a delayed sweep oscilloscope. The sweep delay corresponds exactly to the anticipated two-way ranging time to the satellite. Consequently, when full "quieting" is observed centered in the oscilloscope display, the synchronizer is in phase with the satellite and ranging interrogations will pass through the satellite while the satellite antenna is pointed toward the earth. The synchronizer frequency and phase are manually adjustable and can be incremented during ranging to maintain phase with the satellite.

Following synchronization, the two remote transponders are sequentially addressed on every third rotation of ATS-5. Table 8.11 lists the number of responses and failures to respond (no responses) during the Jan. 26-27, 1975 ranging experiment. The Observatory return from the satellite has a higher signal-to-noise ratio than the returns from the remote transponders. The Observatory thus correlates on its own transmission close to the edges of the ATS-5 "window" where correlation on the return from the remote transponders is impossible. Table 8.11 points out that the Observatory correlated on every interrogation without fail.

Both the Buenos Aires and Hawaiian transponder failed to correlate on a few interrogations during several periods of ranging. A low signal-to-noise ratio in the remote transponders could cause the responders to misinterpret bits in the 15-bit synchronization word and 15-bit address code. More than 3 bits in error result in a failure to correlate. This problem, however, is primarily associated with operations through much smaller antennas, typically a 6-foot dish antenna. The signal-to-noise ratio attainable in the transponders when using the 6-foot dish antenna is just above the FM detection threshold. While both transponders were operated at the Observatory with the 6-foot dish antenna, one and two bits were frequently in error. On occasions, the transponders correlated on less than 25 percent of the interrogations.

The remote transponders did not fail to respond, however, due to low antenna gains. The synchronization of the Observatory interrogator frequently drifted far enough to place the interrogation into the edge of the ATS-5 antenna "window". The ATS-5 "window" is approximately 50 msec wide at the -3 dB points and approximately 90 msec at -10 dB. The Observatory with its 30-foot dish antenna can tolerate a greater reduction

TABLE 8.11

RESPONSES/NO RESPONSES
TO RANGING INTERROGATIONS
JAN. 26-27, 1974

Time (GMT)	File	Observatory	Buenos Aires	Hawaii
0630	F19P01	253/0	127/0	125/1
0730	02	255/0	128/0	122/5
0830	03	256/0	126/2	119/9
0930	04	263/0	132/1	130/0
1030	05	256/0	128/1	127/0
1130	06	256/0	124/4	128/0
1230	07	255/0	127/0	128/0
1330	08	256/0	127/1	127/1
1430	09	251/0	121/4	125/1
1530+				
1630	11	255/0	119/9	127/0
1730	12	244/0	107/15	122/0
1830*				
1930*				
2030*				
2130*				
2230*				
2330*				
0030*				
0130	F20P02	256/0	91/37	127/1
0230	03	256/0	125/3	128/0
0330	04	256/0	127/1	128/0
0430	05	281/0	140/1	139/1
0530	06	256/0	128/0	127/1
0630	07	256/0	125/3	124/4

\+ All data lost due to operational error at Observatory.

* Buenos Aires transponder temporarily out of service.

in signal-to-noise ratio than the remote transponders with their 10-foot dish antennas. Consequently, the Observatory will correlate further from the center of the satellite antenna "window" than will the remote transponders. When the remote transponders failed to respond, the Observatory synchronizer was brought back into phase with the satellite "window" in preselected step sizes.

The remote L-band transponders need not be continuously adjusted to maintain phase with the "window" of the spinning ATS-5 satellite. Following their installation at the remote sites, the manually adjustable time delay thumbwheels on the responders are adjusted until the transponders response to a ranging interrogation passes through the center of the ATS-5 satellite antenna "window". This single adjustment need never be altered as the satellite-transponder slant range changes by less than 0.5 percent. On all subsequent ranging interrogations, the transponder will transmit its ranging response after precisely the same time delay, and all responses will pass through the satellite within $\pm$ 1 msec of the center of the 50 msec "window".

Ranging interrogations conducted between 1330 and 1730 GMT on Jan. 26, 1975 show increasing rates of no response from the Buenos Aires transponder and between 0130 and 0330 on Jan. 27, decreasing rates of no response. Extreme temperatures in Buenos Aires most probably caused a component in a timing circuit of the responder to change its electrical characteristics. This failure manifested itself as an apparent narrowing of the "window" through which interrogations would be accepted.

The date of Table 8.11 show that under normal operating conditions, all Observatory returns from the satellite resulted in correlation. Approximately one to two percent of the ranging interrogations of remote transponders failed to yield a response due to inadequate monitoring of the phase drift between the satellite "window" and the Observatory synchronizer.

SECTION 9

CONCLUSIONS

9.1 PROGRAM GOALS

All objectives of the ATS-5 Trilateration Support contract were achieved. Specifically,

1. An investigation on the manner in which the contract was to be carried out was completed and sent to NASA during February, 1974.

2. The remote L-band transponder developed under NASA contract NAS5-11634 was installed near Honolulu, Hawaii, and became operational on November 22, 1974.

3. A second remote transponder was designed, manufactured, and installed in Buenos Aires, Argentina, and became operational on December 9, 1974.

4. An L-band exciter and power amplifier were installed at the General Electric Radio-Optical Observatory near Schenectady, New York, and became operational during July, 1974.

5. Computer software developed to compute real-time positions of the ATS-5 satellite, orbital elements, range measurement standard deviation, and predictions of satellite position was completed during June, 1974.

6. Cooperative experiments with NASA exercising the near real-time trilateration position fixing of the ATS-5 satellite, establishing a basis for predicting satellite positions up to several hours, and verifying trilateration position and predicted position accuracy were completed during January, 1975.

9.2 L-BAND TRILATERATION ACCURACY AND PRECISION

The cooperative tests with NASA and additional ATS-5 position fixing experiments from Dec. 1974 to Feb. 1975 yielded several significant results:

1. Transponder Self Calibration: The self calibration circuits installed in the Observatory and the remote transponders eliminated transponder internal time delay uncertainty as a source of range measurement inaccuracy. Self calibration responses from the Observatory and remote transponders allow for the correction temperature and tuning related time delay variations of typically $\pm$ 1.5 μsec. Without this correction, internal time delay changes would result in satellite position errors of $\pm$ 0.003 degrees in latitude and longitude and $\pm$ 200 meters in earth center distance.

2. Simultaneous NASA/GE Tracking of ATS-5: Positions of the ATS-5 satellite determined by the simultaneous 24-hour NASA range and range rate and General Electric trilateration tracking on Jan. 26-27, 1975 agree to within 0.00014 $\pm$ 0.00012 degrees longitude, 0.00003 $\pm$ 0.00023 degrees latitude, and 18 $\pm$ 19 meters earth center distance. Computing the slant ranges from the General Electric position of the satellite to NASA's Rosman and Mojave ground stations and comparing these with NASA's measurements shows a disagreement of 10.0 $\pm$ 5.7 meters to the Rosman site and 12.4 $\pm$ 12.0 meters to the Mojave site. This excellent agreement with the positions and slant ranges determined by the completely independent NASA system operating through a different transponder on ATS-5 and at a different frequency suggests that the absolute inaccuracy in trilateration positions may be approximately the value of the disagreement with the NASA positions.

3. Long Term Trilateration Accuracy: The gradual degradation as a function of time since epoch date of the bi-weekly generated NASA ATS-5 ephemerides limits the precision of the comparison between the NASA and GE positions. Yet, the results from 17 separate days of trilateration tracking of ATS-5 from Dec. 1974 to Feb. 1975 show agreement with NASA positions to within 0.00024 $\pm$ 0.00033 degrees longitude, 0.00007 $\pm$ 0.00025 degrees latitude, and 4 $\pm$ 24 meters earth center distance. A comparison of NASA position predictions from epoch dates two weeks apart indicates a degradation rate which produces position inaccuracies at three days following the epoch date equivalent to the NASA/GE position disagreement on an epoch date.

4. Bias Uncertainty: Bias uncertainties in the internal time delay of the ATS-5 satellite and in the local control of the remote transponders' and Observatory's locations limit the absolute accuracy of the satellite position to within 0.00006 degrees longitude, 0.00011 degrees latitude, and 7 meters earth center distance. All ground stations of the General Electric L-band trilateration and the NASA C-band range and range rate tracking networks have been referenced to the Modified Mercury Geoid of 1968 thus eliminating differences in earth models and datum orientations as a source of satellite position error.

5. Relative Uncertainty: The relative accuracy of trilateration positions are limited by day-to-day variations in the remote transponder internal time delays and in the atmospheric propagation time delay. All uncertainties have been studied and evaluated; the primary uncertainty lies in the instability of the 10 MHz responder oscillators as a function of temperature. The oscillator in Buenos Aires has a specified accuracy of one part in 10^6 over a narrow temperature range and has been inferred to generate approximately ± 0.3 μsec errors in the transponder internal time delay. Relative uncertainties bound satellite positions within 0.0003 degrees longitude and latitude, and 30 meters earth center distance.

6. Ionospheric Model: The trilateration software assumes ionospheric propagation time delays to vary sinusoidally throughout the day, with a peak delay approximately one hour after local noon. No trilateration position errors resulting from this simplified model can be isolated.

7. Data Smoothing: The use of second order polynomials to represent the satellite-ground station slant ranges for ten minute ranging periods generates minimal but detectable satellite position errors.

8. Position Prediction Accuracy: The inaccuracies in predicted satellite positions one hour after the last trilateration range measurement have been observed not to exceed 0.0007 degrees longitude, 0.0003 degrees latitude, and 80 meters earth center distance. Three ranging periods typically one hour apart generated the six Kepler orbital elements. The gravitational influences of the moon, sun, and non-spherical components of the earth have been neglected. Real-time operations and short term position predictions do not require the consideration of these effects.

9. Range Measurement Precision: The precision routinely achieved on individual two-way range measurements from the Observatory to the satellite is 0.08 μsec (12 meters); from the Observatory through the satellite to the remote transponders, 0.15 μsec (23 meters). Based on 10-minute ranging periods, mean slant ranges from the Observatory to the satellite are estimated to have a precision of 0.005 μsec (1 meter); from the remote transponders to the satellite, 0.015 μsec (2 meters). Slant ranges with this precision generate satellite positions with a precision of 0.00002 degrees in latitude and longitude and one meter in earth center distance. Narrow bandwidth, short duration tone code ranging produces range measurements that do not significantly affect satellite position accuracy.

9.3 L-BAND TRILATERATION CAPABILITIES

The remote L-band transponders are automatic and have been shown to be inexpensive, reliable, and accurate. They can be used at unmanned remote sites; the only manual operations performed during ranging exercises were the functions of power-on and power-off.

While the results presented in this report are excellent, a factor of approximately four improvement in satellite position accuracy may be achieved by equipping the remote transponders with oscillators stable to within one part in 10^8 instead of the present one and 0.2 parts in 10^6 and by conducting accurate local surveys of the ground station locations. The present demonstrated accuracy (one sigma standard deviation) of approximately $\pm$ 0.0002 degrees in latitude and longitude and $\pm$ 20 meters in earth center distance will contribute less than $\pm$ 40 meters error to the line-of-position of a remote vehicle 45 degrees from the sub-satellite point.

A trilateration network which contributes only ± 10 meters error to a remote vehicle's line-of-position may form the basis of a vehicle surveillance system. The network of inexpensive, automatic transponders would allow the real-time determination of vehicle positions at a shore base for traffic control applications. A minor hardware addition will suffice for vehicles with existing satellite communications equipment.

The L-band trilateration network achieved its high precision and accuracy within a total RF bandwidth of 60 kHz, roughly compatible with narrow bandwidth communication channels. The tone-code durations of 30 msec are insignificantly short compared to durations of typical communications. Received signal-to-noise power densities at the Observatory and remote transponders ranged between 55 and 60 dBHz.

The tone-code ranging technique utilized in the trilateration experiments could be used to track any vehicle and do not require additional equipment on satellites with an existing communications transponder. The 15-bit unique digital address codes of the transponders could be expanded to accommodate any number of remote transponders and mobile craft.

SECTION 10

RECOMMENDATIONS

10.1 NETWORK IMPROVEMENTS

The cooperative tracking of the ATS-5 satellite by NASA and General Electric made possible the isolation of several factors which degrade trilateration position accuracy. Satellite position uncertainties may be reduced by approximately a factor of four by implementing the following:

1. Return the remote transponders from Buenos Aires and Hawaii to Schenectady; replace the existing 10 MHz timing oscillators with units having stabilities on the order of one part in 10^8; recalibrate the remote transponders.

2. Improve computer algorithms which process ranging data to eliminate random position errors due to inadequacy of second order polynomial smoothing technique.

The improved L-band transponders should be redeployed under the "footprint" of the ATS-6 L-band fan beam antenna after the return of ATS-6 from India; the best sites will most probably be in the south eastern and in the western parts of the continental United States. Repetition of simultaneous NASA C-band range and range rate and General Electric L-band trilateration experiments over 24-hour periods will verify the trilateration accuracy.

10.2 FURTHER EXPERIMENTS

The excellent results achieved with the trilateration of ATS-5 justify the reduction of the present trilateration technique to operational status and the development of the next generation remote transponders. Specifically, the maritime community may have at its disposal a technique for determining ship lines-of-position and position fixes. Tasks required for the implementation of maritime satellite ranging experiments are as follows:

1. Fabricate additional L-band transponders and ground support equipment to locate the MARISAT satellite by trilateration.

2. Modify several L-band shipborne satellite communications terminals to transpond ranging signals from MARISAT to MARISAT and ATS-6.

3. Improve trilateration computer software to determine satellite positions and remote vehicle lines-of-position and position fixes in real-time.

4. Add software algorithms to consider the gravitational fields of the moon, sun, and non-spherical components of the earth to extend predicted satellite positions.

Two satellite L-band maritime position fixing experiments are anticipated to demonstrate a 0.1 nautical mile position accuracy. In addition to providing cost effectiveness data on ship navigation, the impact to operational safety and fleet management may be evaluated.

Remote transponders with increased accuracy and precision may assume responsibility for tasks presently being accomplished at significantly greater costs. C-band trilateration, for example, may simplify and improve NASA's satellite position determination operations by providing frequent range measurements from unmanned equipment at remote sites. Furthermore the capability for accurate position fixing may encourage applications in areas such as:

1. Earthquake prediction,
2. World-wide survey,
3. Geodesy,
4. Time and frequency dissemination.

SECTION 11

PUBLICATIONS

A paper entitled

"L-Band Trilateration of ATS-5"

was presented at the 31st Annual Meeting of the Institute of Navigation in Washington, D.C. on June 25, 1975. This paper described the L-band trilateration network and presented preliminary results on the simultaneous General Electric/NASA ranging experiment of Jan. 26-27, 1975.

SECTION 12

REFERENCES

1. Anderson, Roy E., "Final Report on Phases 1 and 2 - VHF Ranging and Position Fixing Experiment Using ATS Satellites", General Electric Company Report S-71-1109 on NASA contract NAS5-11634, 1971.

2. Anderson, Roy E., "Final Report on Phase 3 - ATS Ranging and Position Fixing Experiment", General Electric Company Report SRD-73-062 on NASA contract NAS5-11634, 1973.

3. Anderson, Roy E., et. al., "Experimental Evaluation of Satellite Communications and Position Fixing for Maritime Users", Joint Final Report, Exxon Corporation and General Electric Company, June 1974.

4. "NASA Directory of Observation Station Locations", Computer Sciences Corporation for NASA-GSFC, Third Edition, Nov. 1973.

5. Gurther, Thor, Computer Sciences Corporation, Silver Spring, Maryland, Private Communication, 1975.

6. "Integrated Test Plan for ATS-F L-Band Experiment", Vol. 1, NASA-GSFC, TP-750-73-1, Sept. 1973.

7. "Operation and Maintenance Manual, L-Band/VHF Transponder", General Electric Company Report, under preparation.

8. Goldstein, H., "Classical Mechanics", Addison-Wesley Pub. Co. Inc., Reading, Mass., 1965.

9. Baker, R.M.L. and Makemson, M.W., "An Introduction to Astrodynamics", Academic Press, New York, 1960.

10. Millman, George H., "A Survey of Tropospheric, Ionospheric, and Extraterrestrial Effects on Radio Propagation Between the Earth and Space Vehicles", General Electric Company Report TIS R66EMH1, 1966.

11. Milton, Robert T., "Tone Code Ranging Precision", Memorandum, 1971, see Reference 2.

12. Brisken, Axel F., "Final Report, ATS-5 Trilateration Support, Appendices", General Electric Company Report for NASA Contract NAS5-20034, SRD-76-004, 1975.

13. Doll, Edward, NASA-Goddard Space Flight Center, Private Communication, 1975.

14. Galicinao, I., NASA-Goddard Space Flight Center, Private Communication, 1975.